In those years (the 17th, 18th and 19th centuries) science was a liberating force, not because it had found the truth, or the right method, but because it restricted the influence of other ideologies and thus gave the individual room for thought.

Paul Feyerabend, Science in a free society

Ίσως να φτάσεις στον σκοπό, κι αν όχι, πάλι τράβα.
Αυτό το ίσως αδερφέ, είναι μεγάλο πράγμα.

Mode Plagal, Ta Paidia tis geitonias sou

Promoters

Prof. dr. ir. Korneel Rabaey

Department of Biotechnology, Faculty of Bioscience Engineering, Ghent University, Gent, Belgium

Dr. Jan Arends

Department of Biotechnology, Faculty of Bioscience Engineering, Ghent University, Gent, Belgium

Dr. Erika Fiset

BOSAQ, Technologiepark Zwijnaarde, Belgium

Members of the examination committee

Prof. dr. ir. Veerle Fievez

Chair

Department of Animal Sciences and Aquatic Ecology, Faculty of Bioscience Engineering, Ghent University, Gent, Belgium

Prof. dr. ir. Arne Verliefde

Secretary

Department of Green Chemistry and Technology, Faculty of Bioscience Engineering, Ghent University Gent, Belgium

Prof. dr. ir. Marjan De Mey

Department of Biotechnology, Faculty of Bioscience Engineering, Ghent University, Gent, Belgium

Prof. Dr. Piet Lens

Department of Environmental Engineering and Water Technology of IHE Delft, Delft, The Netherlands

Dr. dipl.-ing. Jelena Radjenovic

Department of Technology and Evaluation Area, Catalan Institution Water Research (ICRA), Girona, Spain

Dean:

Prof. dr. ir. Marc Van Meirvenne

Rector:

Prof. dr. Rik Van De Walle

Waste gas valorisation via electrochemical sulfide (H_2S) oxidation and biological carbon fixation

Eleftheria Ntagia

Thesis submitted in fulfillment of the requirements for the degree of Doctor (PhD) in Bioscience Engineering: Environmental Sciences and Technology

Cover artwork by Ioanna Florou (Ιωάννα Φλώρου)

Titel van het doctoraat in het Nederlands:

Elektrochemische sulfide verwijdering en biologische koolstoffixatie voor de valorizatie van gasstromen

ISBN: 978-94-6357-407-5

This work was funded by Ghent University (Assistant – 2016-2021).

The author and the promoters give the authorisation to consult and to copy parts of this work for personal use only. Every other use is subject to the copyright laws. Permission to reproduce any material contained in this work should be obtained from the author.

Στη μάνα και στον πατέρα

Notation Index & Terminology

List of Abbreviations

AEM	Anion Exchange Membrane
AP	Acidification Potential
BES	Bioelectrochemical Systems
CEM	Cation Exchange Membrane
CCU	Carbon Capture and Utilization
CDW	Cell Dry Weight
CI	Current Interrupt
CGC	Compact Gas Chromatography
COD	Chemical Oxygen Demand
CP	Chronopotentiometry
CV	Cyclic Voltammetry or Voltammogram
DAC	Direct Air Capture
DIC	Dissolved Inorganic Carbon
ECSA	Electrochemical Surface Area
EDX	Energy dispersive X-ray spectroscopy
EEA	Estimated Absolute Abundance
FCM	Flow Cytometry
GHG	Greenhouse Gas
HRT	Hydraulic Retention Time
IC	Ion Chromatography
IEM	Ion Exchange Membrane
IUPAC	International Union of Pure and Applied Chemistry
LCA	Life Cycle Assessment
MEC	Microbial Electrolysis Cell

MFC	Microbial Fuel Cell
MMO	Mixed Metal Oxide
NCG	Non-condensable Gas
OCP	Open Circuit Potential
OD_{600}	Optical Density at 600 nm wavelength
RE	Reference Electrode
SAOB	Sulfide Antioxidant Buffer
SCE	Standard Calomel Electrode
SCS	Spent Caustic Streams
SEM	Scanning Electron Microscopy
SHE	Standard Hydrogen Electrode
SOB	Sulfide Oxidizing Bacteria
TDS	Total Dissolved Sulfide
TSS	Total Suspended Solids
VFA	Volatile Fatty Acids
VSS	Volatile Suspended Solids
WLP	Wood-Ljungdahl Pathway
WWTP	Wastewater Treatment Plant
XRF	X-Ray Fluorescence

Symbols

α_O	Activity of the oxidized form of a redox couple (dimensionless)
α_R	Activity of the reduced form of a redox couple (dimensionless)
ΔG_r^0	Standard Gibbs free energy (J mol^{-1})
η	Overpotential (V)
μ_{max}	Maximum growth rate (h^{-1})
C_{app}	Apparent geometric capacitance (mF cm^{-2})

C_O	Interfacial concentration of the oxidized form of redox couple (mol L^{-1})
C_R	Interfacial concentration of the reduced form of redox couple (mol L^{-1})
CE_{HS-}	Coulombic efficiency for sulfide oxidation to S^0 (%)
CE_{SO4}	Coulombic efficiency for sulfide oxidation to SO_4^{2-} (%)
E	Electrode potential (V)
E^0	Standard redox potential (V)
$E^{0'}$	Formal potential (V)
Ea	Activation energy (kcal mol^{-1})
E^0_{app}	Apparent standard redox potential at pH 7 (V)
E_{cell}	Cell voltage (V)
E_{WE}	Working electrode potential (V)
F	Faraday constant (96,485 C mol^{-1})
I	Current (A)
IC_{50}	Half maximal inhibitory concentration (mol L^{-1})
j	Current density (A m^{-2})
n (or z)	Number of electrons (dimensionless) involved in a reaction
r_{Ac}	Volumetric acetate production rate (mol L^{-1} h^{-1})
r_{Ac}^{max}	Maximum volumetric acetate production rate (mol L^{-1} h^{-1})
R	Universal gas constant (8.314 J mol^{-1} K^{-1})
R_{int}	Internal ohmic resistance (Ω)
R_u	Uncompensated resistance (Ω)
v	Surface reaction rate (mol s^{-1} m^{-2})

ABSTRACT

Industrial waste gas fermentation can pave the way for the de-fossilization of the chemical industry. The oil refinery, the pulp and paper and the geothermal power production industries are key sectors where carbon dioxide (CO_2) and hydrogen sulfide (H_2S) are concomitantly emitted. The first can serve as a carbon source for commodity chemicals production through fermentation, whereas the second is a potential inhibitor of such bioproduction processes, as well as a corrosive agent. To enable efficient H_2S removal while unlocking the full potential of CO_2, this thesis places electrochemical treatment at the core of a three process treatment train, with alkaline gas absorption and H_2/CO_2 fermentation acting as upstream and downstream processes.

Absorption in concentrated sodium hydroxide (NaOH, caustic soda) followed by oxidation to elemental sulfur (S^0), through a series of high temperature and high pressure oxidation steps, is commonly applied in industry to avoid H_2S emissions. Here we propose replacement of the chemical oxidation with electrochemical sulfide (HS^-) oxidation. Selective absorption of H_2S over CO_2 in a liquid NaOH stream, will allow for maximum CO_2 output, minimum contamination of the CO_2 with H_2S, while minimizing the consumption of NaOH required for absorption. In Chapter 2, the connection of an H_2S absorption unit with an electrolysis unit for simultaneous HS^- removal and continuous NaOH recovery, was explored. First, a large-scale gas absorption column treating 0.4 kg gas s^{-1} was simulated using the Aspen Plus software and next, the resulting liquid stream was effectively downsized to examine continuous electrochemical treatment in a lab-scale system. Electrolysis was conducted continuously for 10 h at 300 A m^{-2} current density. HS^- was removed with 90% efficiency and with 4.96 ± 0.11 kWh kg^{-1} S energy investment. Concurrently, a continuous flow of 46 g d^{-1} NaOH was obtained as effluent of the cathodic compartment of the electrochemical cell. The system demonstrated a continuous, energy efficient recovery of 60% of the initial scrubbing liquid and further large-scale application should consider optimization to increase NaOH recovery to 100% and effectively remove the S^0 formed to avoid clogging of the electrochemical reactor.

The electrochemical reactions conducted in the electrolysis unit take place at the interface between the electrode surface and the electrolyte, therefore, maintaining an active electrode (anode) surface area is of utmost importance to ensure high operational efficiency. Electrochemical HS^- oxidation often suffers from low efficiencies, as the product, S^0, covers the electroactive sites of the anode acting as an insulator and can eventually induce passivation. In Chapter 3, the impact of the anode catalyst choice on the catalytic activity towards HS^- oxidation and the robustness against passivation under high sulfide concentrations (50 mM Na_2S) and high alkalinity (pH>12) was investigated. Six commercially available electrode materials were tested: Ir Mixed Metal Oxide (MMO), Ru MMO, Pt/IrO_x, Pt, PbO_x and $TiO_2/IrTaO_2$ coated titanium-based electrodes. The results suggest that Ru MMO and Ir MMO are equally active towards HS^- oxidation, but Ir MMO should be considered as the most stable electrode as no catalyst loss and only a small increase in potential (< 0.5 V) were observed

during the stability tests. Ultimately, it was confirmed that high alkaline, sulfidic and oxidative conditions deteriorate the electrocatalyst and a good trade-off between activity, stability and cost was proposed as a prerequisite for a future educated selection of the suitable electrocatalyst to treat sulfur pollution.

In Chapter 4, the industrial relevance and the scalability of electrochemical HS^- removal with simultaneous NaOH recovery were verified by treating an industrial sulfidic spent caustic stream (SCS) for 20 consecutive days at 300 A m^{-2} current density. Operational and energy efficiency were reflected through the 38 ± 8 % S removal, the recovery of a 12 wt.% NaOH solution, as well as through the low energy investment of 3.7 ± 0.6 kWh per kg sulfur removed and of 6.3 ± 0.4 kWh per kg NaOH recovered. The costs for purchasing and transporting NaOH at the industrial site hold the lion's share in the total costs of alkaline gas absorption units. Hence, the on-site NaOH recovery in the proposed configuration illustrates a great future potential in decreasing the costs associated with this commodity chemical, as well as improves the overall sustainability profile of the total process.

Understanding the effect of gaseous pollutants, such as H_2S, on the microbial communities involved in reductive acetogenesis will allow for identification of the extent of gas pre-treatment required prior to fermentation. In Chapter 5, the H_2S toxicity effect on the aforementioned communities was studied in batch experiments, using a mixed homoacetogenic culture that was cultivated under total dissolved sulfide (TDS) concentrations between 0 and 5 mM and pH between 5 and 7. Key finding was the identification of the sulfide inhibitory concentrations for the homoacetogens, with IC_{50}^{rAc} values between 0.86 and 1.36 mM [TDS]. It was found that a [TDS] above 3.33 mM completely inhibits acetate production and microbial growth at the tested pH window. Higher tolerance levels were exhibited at pH 5, possibly due to higher community robustness developed already due to initial cultivation with a pH lower than the physiological pH of the community. Whilst correlations highlighting the sulfide impact on key community members could be demonstrated, definitive statements on key homoacetogens in these communities could not be made. Ultimately, it is suggested here that sulfide and pH combinations will determine the microbiological landscape in a gas fermenter performing acetogenesis, as different tolerance levels are exhibited by the bacterial genera constituting a mixed microbial community.

Continuous operation of a process unit is a desired deliverable when commercialization is considered. Therefore, in Chapter 6, continuous fermentation hindered by H_2S and boosted by electrolytically-produced H_2 was examined. A 10-L scale gas fermenter was operated for a total experimental period of 168 days. Three cycles of inhibition (1.3 mM TDS) and recovery were applied, then the fermenter was operated at 0.5 mM TDS for 35 days. Upon sulfide addition, methanogenesis and acetogenesis were instantly inhibited, whilst upon removal of the inhibitor, methanogenesis presented a 7 days lag-phase of recovery, compared to acetogenesis that resumed within 48 h. During final operation at 0.5 mM TDS, the volumetric acetate production rate reached 7.1 ± 1.5 mmol $C_{acetate}$ L^{-1} d^{-1}, whereas methanogenesis appeared continuously suppressed. Up to 44 ± 16 % of the electrons provided as H_2

and 52 ± 19 % of the carbon provided as CO_2 were distributed to acetate and 8 ± 4 % of the electrons and 7 ± 4 % of the carbon to butyrate, as the second most abundant fermentation product. The microbial community was dominated by an unclassified member of the *Eggerthellaceae* family and by the genera *Eubacterium* and *Proteiniphilum*. The taxonomic diversity of the community decreased and conversely, the phenotypic diversity increased during operation.

The much preached and expected increase in renewable energy the coming decade will create opportunities for electrochemical solutions that are fit for waste treatment. Electrochemical treatment has the potential to not only enable bioproduction from fouler industrial gas emissions, but to additionally provide the treatment concept with on-site recovery of NaOH and H_2, that can be reused in the upstream and downstream processes. In the closing chapter of this thesis, the recovery prospects of electrochemical sulfide oxidation are discussed and the scene for future applications of the proposed treatment train is set, within the general notions of electrification and sustainability.

SAMENVATTING

Gas fermentatie uit industriële afvalstromen kan een belangrijke schakel worden in de chemische industrie bij de transitie naar hernieuwbare energie. Olieraffinaderijen, pulp en papier productie en het opwekken stroom vanuit geothermische bronnen behoren tot essentiële sectoren waar simultaan hoge emissies koolstofdioxide (CO_2) en waterstof sulfide (H_2S) plaatsvinden. Hierbij kan CO_2 als koolstofbron dienen voor productie van basis-chemicaliën middels fermentatie, terwijl H_2S corrosief is en een mogelijke inhibitor is in biologische productieprocessen. Om H_2S efficiënt te verwijderen en zo het volledige potentieel van CO_2 in deze gasstromen te benutten, staat een elektrochemische behandeling centraal in deze thesis. De volledige behandeling bestaat verder uit een upstream alkalische gas absorptie en downstream een H_2/CO_2 fermentatie.

Doorgaans wordt in de industrie emissie van H_2S vermeden door absorptie in geconcentreerd natrium hydroxide (NaOH) gevolgd door een reeks oxidatiestappen tot elementair zwavel (S^0) onder hoge temperatuur en druk. In dit onderzoek wordt de chemische oxidatie vervangen door een elektrochemische sulfide (HS^-) oxidatie. Een selectieve absorptie van H_2S ten opzichte van CO_2 beperkt het gebruik van de NaOH oplossing terwijl het een maximale CO_2 output garandeert met een minimum aan H_2S verontreiniging. In Hoofdstuk 2 wordt onderzocht hoe de H_2S absorptie gekoppeld kan worden met een elektrolyse cel voor de simultane verwijdering van HS^- gas en productie van NaOH. Hiervoor werd eerst een simulatie van een volwaardige absorptiekolom die 0.4 kg gas s^{-1} behandelt uitgevoerd in Aspen Plus software. Vervolgens werd de elektrochemische behandeling getest op kleinere schaal in een laboratorium opstelling. De elektrolyse verliep voor 10 uur bij een stroomdichtheid van 300 A m^{-2} waarbij HS^- voor 90 % verwijderd met behulp van 4.96 ± 0.11 kWh kg S^{-1} elektrische energie. Tegelijk werd een constante stroom van 46 g d^{-1} NaOH gemaakt als effluent van de kathode van de elektrochemische cel. Het systeem toonde aan dat op een efficiënte wijze tot 60 % van de initiële was-oplossing herwonnen kan worden. Verdere optimalisaties kunnen de hergebruikte fractie van NaOH doen toenemen tot 100 % en dienen ervoor te zorgen dat de gevormde S^0 efficiënt verwijdert wordt om verstopping in de reactor te vermijden.

De elektrochemische reacties vinden plaats op de interfase tussen het elektrode oppervlak en de elektrolytoplossing. Daarom is het behoud van een actief oppervlak op de elektrode (anode) van cruciaal belang om een hoge efficiëntie te garanderen. De elektrochemische HS^- oxidatie verloopt soms bij erg lage efficiënties doordat S^0 een isolerende laag vormt op de anode, wat finaal leidt tot passivatie van het materiaal. In Hoofdstuk 3 wordt het effect van het anode oppervlak nagegaan op de katalytische conversie van HS^-. De robuustheid ten opzichte van de passivatie wordt onderzocht bij hoge sulfide concentraties (50 mM Na_2S) en hoge alkaliniteit (pH > 12). Zes commerciële elektrodes werden getest: Ir Mix Metaal Oxide (MMO), Ru MMO, Pt/IrO_x, Pt, PbO_x en $TiO_2/IrTaO_2$ gecoat titanium elektrodes. Resultaten tonen aan dat Ru MMO en Ir MMO en gelijkaardige activiteit hebben in HS- oxidatie, maar dat Ir MMO beschouwd wordt als het meest stabiel gezien er geen

verlies van elektrodemateriaal optrad en slechts een geringe toename in potentiaal (< 0.5 V) werd geobserveerd doorheen de stabiliteitstesten. Uiteindelijk daalde alsnog de activiteit van de elektrokatalysator onder invloed van de sterk alkalische, oxidatieve condities in aanwezigheid van sulfides. Selectie van een geschikte elektrokatalystor voor zwavel decontaminatie dient dan ook rekening te houden met een overwogen afweging tussen de activiteit, stabiliteit en kost ervan.

In Hoofdstuk 4 wordt de industriële relevantie en schaalbaarheid van elektrochemische HS^- verwijdering met simultane NaOH terugwinning nagegaan door een echte corrosieve afvalstroom met sulfides te behandelen voor 20 opeenvolgende dagen bij 300 300 A m^{-2} stroomdichtheid. Zwavel kon worden verwijderd tot 38 ± 8 % bij een energieconsumptie van 3.7 ± 0.6 kWh per kg S en NaOH kon gerecupereerd worden in een 12 wt.% oplossing bij een energieconsumptie van 6.3 ± 0.4 kWh per kg NaOH. Het leeuwendeel van de kosten voor alkalische gas absorptie omvat de aankoop en transport van NaOH naar de industriële site. Daarom kan de *on-site* productie van NaOH in de voorgestelde configuratie een groot perspectief bieden om de totale kosten die gerelateerd zijn aan deze basis grondstof te verminderen en tegelijk bij te dragen aan een verduurzaming van het gehele proces.

Het beter begrijpen van de invloed van contaminanten zoals H_2S in de gasstroom op de microbiële gemeenschappen die betrokken zijn in reductieve acetogenese laat toe om de vereiste eigenschappen en dus de behandeling van de gasstromen beter te identificeren. In Hoofdstuk 5 wordt de toxiciteit van H_2S op de genoemde microbiële gemeenschappen getest door middel van batch experimenten en een homoacetogene cultuur gekweekt onder totale opgeloste zwavelconcentraties (TDS) tussen 0 en 5 mM en tussen pH 5 en 7. Als belangrijkste resultaat geldt, voor de eerste keer, de identificatie van de limiterende sulfide concentraties met IC_{50}^{rAc} waarden tussen 0.86 en 1.36 mM. Bij TDS groter dan 3.33 mM treedt volledige inhibitie van acetaatproductie en stopt de microbiële groei, binnen het geteste pH gebied. Hogere tolerantie vond plaats bij pH 5, mogelijk doordat de microbiële gemeenschap reeds een grotere robuustheid vertoonde door de kweek bij niet-fysiologische condities. Correlatie tussen de sulfide concentratie en de belangrijkste microbiële species onderstreept de impact van TDS, hoewel geen definitieve uitspraak over de homoacetogenen in de gemeenschap kon gedaan worden. Finaal wordt geponeerd dat de combinatie van de sulfide concentratie en de pH het microbiëel landschap bepalen in gas fermentatie voor acetaatproductie vermits elk bacterieel species een verschillende tolerantie bezit.

Commerciële exploitatie van eenheidsprocessen is gebaat bij een continue operatie. Daarom werd in Hoofdstuk 6 de continue CO_2-fermentatie onder invloed van H_2S onzuiverheden en ondersteund door elektrolytisch geproduceerd H_2 gas onderzocht. Een 10-L gas fermentor werd gedurende 168 dagen bediend in 3 opeenvolgende cycli met toevoeging en verwijdering van (1.3 mM TDS), vooraleer gedurende 35 dagen 0.5 mM TDS toegediend werd. Door de aanwezigheid van sulfide werd de methanogenese en acetogenese verstoord. Bij het wegnemen van de sulfide inhibitie, vertoonde het herstel van methanogenese een vertraging van 7 dagen vergeleken met acetogenese dat binnen 48

uur werd hervat. Onder de finale condities (0.5 mM TDS) bereikte de acetaat productie 7.1 ± 1.5 mmol $C_{acetate}$ L^{-1} d^{-1}, terwijl de methanogenese constant onderdrukt werd. Tot 44 ± 16 % van de toegediende elektronen als H_2 en 52 ± 19 % van de koolstof als CO_2 werden omgevormd tot acetaat en 8 ± 4 % van de elektronen en 7 ± 4 % van de CO_2 tot butyraat, als tweede meest voorkomende fermentatieproduct. De microbiële gemeenschap werd gedomineerd door een ongeclassificeerde *Eggerthellaceae*, *Eubacterium* en *Proteiniphilum*. De taxonomische diversiteit van de gemeenschap daalde terwijl de fenotypische diversiteit toe nam gedurende de werking van de reactor.

De geanticipeerde toename in hernieuwbare energie komend decennium plaatst elektrochemische oplossingen in de schijnwerper die in staat zijn om afvalstromen te behandelen. Elektrochemische technologie heeft niet enkel het potentieel voor bioproductie vanuit rest-emissies uit de industrie, maar biedt bovendien ook een concept om NaOH en H_2 ter plaatse te genereren, die vervolgens ingezet kunnen worden in de verschillende onderdelen van het proces. In het laatste Hoofdstuk van deze thesis worden de herwinningsmogelijkheden van elektrochemische sulfide oxidatie toegelicht. Daarnaast wordt een beeld geschetst voor toekomstige toepassingen van de voorgestelde behandelingstrein binnen de algemene concepten van elektrificatie en duurzaamheid.

ΠΕΡΙΛΗΨΗ

Η βιοκαταλυτική μετατροπή (ζύμωση) αέριων ρύπων της βιομηχανίας μπορεί να συμβάλλει στην απεξαρτητοποίηση της χημικής βιομηχανίας από τα ορυκτά καύσιμα. Η πετρελαιοβιομηχανία, η βιομηχανία χαρτοπολτού και χαρτιού καθώς και η παραγωγή ενέργειας από γεωθερμικές πηγές, αποτελούν κύριους παραγωγούς εκπομπών διοξειδίου του άνθρακα (CO_2) και υδρόθειου (H_2S). Το πρώτο μπορεί να αποτελέσει πηγή άνθρακα για την παραγωγή χημικών πρώτων υλών, ενώ το δεύτερο μπορεί να αναχαιτίσει τη βιοπαραγωγή λόγω της τοξικότητάς του καθώς και της δράσης του ως διαβρωτικού παράγοντα. Για να επιτευχθεί πλήρης απομάκρυνση του H_2S με παράλληλη ολική εκμετάλλευση του CO_2, η παρούσα διπλωματική εργασία τοποθετεί την ηλεκτροχημική επεξεργασία στο κέντρο μιας αλληλουχίας διεργασιών, συνδέοντας έτσι την απορρόφηση αερίων σε αλκαλικό διάλυμα με τη ζύμωση υδρογόνου και διοξειδίου του άνθρακα (H_2/CO_2), ως ανάντη και κατάντη διεργασίες.

Η απορρόφηση αερίων σε αλκαλικό διάλυμα (NaOH, καυστική σόδα) και κατόπιν, η οξείδωση προς παραγωγή στοιχειακού θείου (S^0), μέσω μιας σειράς σταδίων οξείδωσης σε υψηλή θερμοκρασία και πίεση, είναι η κατεξοχήν μέθοδος που εφαρμόζεται στη βιομηχανία για την αποφυγή εκπομπών H_2S. Στο παρούσα εργασία προτείνεται η αντικατάσταση της χημικής οξείδωσης με ηλεκτροχημική οξείδωση του υδρόθειου (HS^-). Η επιλεκτική απορρόφηση του H_2S έναντι του CO_2 σε ένα αλκαλικό διάλυμα, αναμένεται να οδηγήσει στη μέγιστη εκμετάλλευση του CO_2, καθώς και στην ελαχιστοποίηση της επιμόλυνσης του CO_2 από H_2S και της κατανάλωσης του NaOH, αναγκαίου για το αρχικό στάδιο της απορρόφησης. Στο Κεφάλαιο 2, διερευνάται η σύνδεση μιας μονάδας απορρόφησης H_2S με μια μονάδα ηλεκτόλυσης για ταυτόχρονη απομάκρυνση HS^- και ανάκτηση NaOH.

Πρώτα, μια στήλη απορρόφησης αερίου για επεξεργασία 0,4 kg αερίου s^{-1} προσομοιώθηκε χρησιμοποιώντας το λογισμικό Aspen Plus και στη συνέχεια εξετάστηκε η δυνατότητα ηλεκτροχημικής επεξεργασίας του προκύπτοντος διαλύματος σε ένα σύστημα εργαστηριακής κλίμακας. Η ηλεκτρόλυση διεξήχθη συνεχόμενα για 10 ώρες σε πυκνότητα ρεύματος 300 A m^{-2}. Το HS^- απομακρύνθηκε αποτελεσματικά με απόδοση 90% και με 4,96 ± 0,11 kWh kg^{-1} S ενεργειακή επένδυση. Ταυτόχρονα, επιτεύχθηκε ανάκτηση ενός διαλύματος ροής 46 g d^{-1} NaOH. Το σύστημα επέδειξε συνεχή, ενεργειακά αποδοτική ανάκτηση του 60% του αρχικού διαλύματος προς απορρόφηση. Για μια επιτυχή μελλοντική εφαρμογή μεγάλης κλίμακας θα πρέπει να εξεταστεί βελτιστοποίηση για αύξηση της ανάκτησης του NaOH στο 100% και για την αποτελεσματική απομάκρυνση το σχηματιζόμενου S^0, έτσι ώστε να αποφευχθεί η παρεμπόδιση της ανακυκλοφορίας του ηλεκτροχημικού αντιδραστήρα.

Οι ηλεκτροχημικές αντιδράσεις που πραγματοποιούνται στη μονάδα ηλεκτρόλυσης λαμβάνουν χώρα στη διεπαφή μεταξύ της επιφάνειας του ηλεκτροδίου και του ηλεκτρολύτη, επομένως, η διατήρηση μιας ενεργού επιφάνειας ηλεκτροδίου (της ανόδου) είναι ύψιστης σημασίας για να εξασφαλιστεί υψηλή λειτουργική απόδοση. Η ηλεκτροχημική οξείδωση του HS^- συχνά υποφέρει από χαμηλή απόδοση, καθώς το S^0 είναι μονωτικό και μπορεί να καλύψει τις ενεργές θέσεις της

ανόδου, προκαλώντας τελικά παθητικοποίηση. Στο Κεφάλαιο 3, διερευνήθηκε ο αντίκτυπος της επιλογής καταλύτη ανόδου στην ηλεκτροκαταλυτική δραστικότητα προς την οξείδωση του HS^- και η ανθεκτικότητα έναντι παθητικοποίησης υπό υψηλές συγκεντρώσεις HS^- (50 mM Na_2S) και υψηλή αλκαλικότητα (pH > 12). Έξι διαφορετικά ηλεκτρόδια με μέταλλο βάσης το τιτάνιο (Ti) δοκιμάστηκαν: Ir Mixed Metal Oxide (MMO), Ru MMO, Pt/IrOx, Pt, PbOx και $TiO_2/IrTaO_2$. Τα αποτελέσματα δείχνουν ότι τα Ru MMO και Ir MMO είναι εξίσου ενεργά στην οξείδωση του HS^-, αλλά το Ir MMO πρέπει να θεωρηθεί ως το πιο σταθερό ηλεκτρόδιο καθώς δεν παρατηρήθηκε απώλεια καταλύτη και μόνο μικρή αύξηση του δυναμικού (<0,5 V) κατά τη διάρκεια των δοκιμών σταθερότητας. Συμπερασματικά, επιβεβαιώθηκε ότι οι υψηλές αλκαλικές, θειικές και οξειδωτικές συνθήκες επιδεινώνουν τον ηλεκτροκαταλύτη και προϋπόθεση για για μια μελλοντική επιλογή του κατάλληλου ηλεκτροκαταλύτη για την αντιμετώπιση της ρύπανσης από θείο, θα πρέπει να είναι μια σωστή ανταλλαγή μεταξύ ηλεκτροκαταλυτικής δραστικότητας , σταθερότητας και κόστους.

Στο Κεφάλαιο 4, εξετάστηκε η επεκτασιμότητα σε βιομηχανική έκταση της ηλεκτροχημικής απομάκρυνσης HS^- με ταυτόχρονη ανάκτηση NaOH, μέσω της επεξεργασίας ενός βιομηχανικού αποβλήτου ξοδευμένης καυστικής με θειούχα συστατικά (SCS) για 20 συνεχόμενες ημέρες σε πυκνότητα ρεύματος 300 A m^{-2}. Η λειτουργική απόδοση και η ενεργειακή απόδοση αντικατοπτρίστηκαν μέσω της αφαίρεσης 38 ± 8% S και της ανάκτησης ενός καθαρού διαλύματος NaOH 12% κ.β, καθώς και της χαμηλής ενεργειακής επένδυσης της τάξης των 3,7 ± 0,6 kWh ανά kg θείο που απομακρύνθηκε και 6,3 ± 0,4 kWh ανά κιλό NaOH που ανακτήθηκε. Το κόστος αγοράς και μεταφοράς NaOH στη βιομηχανική περιοχή κατέχει τη μερίδα του λέοντος στο συνολικό κόστος των μονάδων απορρόφησης αερίων. Ως εκ τούτου, η επιτόπια ανάκτηση NaOH από την προτεινόμενη διεργασία έχει μεγάλο ενδιαφέρον για τη μείωση του κόστους που σχετίζεται με αυτό το χημικό προϊόν, καθώς επίσης και βελτιώνει το συνολικό προφίλ βιωσιμότητας της συνολικής διαδικασίας.

Η κατανόηση της επίδρασης των αερίων ρύπων, όπως το H2S στις μικροβιακές κοινότητες που εμπλέκονται στην αναγωγική οξικογένεση θα βοηθήσει στο να τεθούν σαφή όρια στις ανάγκες προεπεξεργασίας των αερίων ρύπων, πριν τα τελευταία οδηγηθούν προς ζύμωση. Στο Κεφάλαιο 5, η επίδραση της τοξικότητας του H2S στις προαναφερθείσες κοινότητες μελετήθηκε χρησιμοποιώντας μια μικτή οξικογενή μικροβιακή καλλιέργεια που καλλιεργήθηκε υπό ολικές συγκεντρώσεις διαλυμένου υδρόθειου (TDS) μεταξύ 0 και 5 mM και pH μεταξύ 5 και 7. Βασικό εύρημα αυτού του κεφαλαίου η αποτελεί η εύρεση των συγκεντρώσεων υδρόθειου που αναχαιτίζουν τη μικροβιακή ανάπτυξη και τη βιοπαραγωγή, με τιμές IC_{50}^{rAc} μεταξύ 0,86 και 1,36 mM [TDS]. Διαπιστώθηκε ότι μια συγκέντρωση [TDS] άνω των 3,33 mM αναστέλλει πλήρως την παραγωγή οξικού οξέος και τη μικροβιακή ανάπτυξη, στα πλαίσια του εξεταζόμενου pH. Υψηλότερα επίπεδα ανοχής παρουσιάστηκαν στο pH 5, πιθανώς λόγω της μεγαλύτερης αντοχής της κοινότητας που αναπτύχθηκε ήδη σε προγενέστερη καλλιέργεια σε pH χαμηλότερο του φυσιολογικού. Ενώ θα μπορούσαν να αποδειχθούν συσχετισμοί που να επισημαίνουν την επίδραση του υδρόθειου στα βασικά μέλη της κοινότητας, δεν κατέστη δυνατό ένα απόλυτο συμπέρασμα για αυτό το συσχετισμό. Τελικά, προτείνεται εδώ ότι ο συνδυασμός υδρόθειου και pH αναμένεται να καθορίσει το

μικροβιολογικό τοπίο στη διεργασία ζύμωσης αερίων για οξικογένεση, καθώς διαφορετικά επίπεδα ανοχής παρουσιάζονται από τα βακτηριακά γένη που αποτέλεσαν εδώ τη μικτή μικροβιακή κοινότητα.

Η συνεχής λειτουργία μιας μονάδας επεξεργασίας είναι το επιθυμητό παραδοτέο όταν εξετάζεται η εμπορευματοποίηση της προτεινόμενης επεξεργασίας. Επομένως, στο Κεφάλαιο 6, εξετάστηκε η συνεχής ζύμωση, αναχαιτισμένη από H2S και ενισχυμένη από ηλεκτρολυτικά παραγόμενο H2, σε έναν αντιδραστήρα ζύμωσης αερίων κλίμακας 10-L για συνολική πειραματική περίοδο 168 ημερών. Εφαρμόστηκαν τρεις κύκλοι αναστολής (1,3 mM TDS) και μικροβιακής ανάκτησης, και στη συνέχεια ο αντιδραστήρας λειτούργησε στα 0,5 mM TDS για 35 ημέρες. Κατά την προσθήκη υδρόθειου, η μεθανογένεση και η οξικογένεση αναστάλθηκαν άμεσα, ενώ κατά την απομάκρυνση του αναστολέα, η μεθανογένεση παρουσίασε μια φάση υστέρησης 5 ημερών της ανάκτησης, σε σύγκριση με την οξικογένεση που ανακτήθηκε εντός 48 ωρών. Κατά τη διάρκεια της τελικής λειτουργίας στα 0,5 mM TDS, ο ρυθμός παραγωγής οξικού οξέος έφτασε τα 7,1 ± 1,5 mmol $C_{οξικού}$ L^{-1} d^{-1}, ενώ η μεθανογένεση ήταν συνεχώς κατασταλμένη. Μέχρι 44 ± 16% των ηλεκτρονίων που παρέχονταν ως H2 και 52 ± 19% του άνθρακα που παρέχονταν ως CO2 χρησιμοποιήθηκαν για τη βιοπαραγωγή οξικού οξέος, ενώ 8 ± 4% των ηλεκτρονίων και 7 ± 4% του άνθρακα για την παραγωγή βουτυρικού, ως το δεύτερο κατά σειρά προϊόν ζύμωσης. Στη μικροβιακή κοινότητα κυριάρχησε ένα μη ταξινομημένο μέλος της οικογένειας *Eggerthellaceae*, καθώς και τα βακτηριακά γένη *Eubacterium* και *Proteiniphilum*. Η ταξινομική ποικιλομορφία της κοινότητας μειώθηκε και αντιστρόφως, η φαινοτυπική ποικιλομορφία αυξήθηκε κατά τη διάρκεια της λειτουργίας.

Η πολυσυζητημένη και αναμενόμενη αύξηση της παραγωγής ανανεώσιμης ενέργειας την επόμενη δεκαετία αναμένεται να φέρει την ηλεκτροχημική επεξεργασία αποβλήτων στο προσκήνιο. Η ηλεκτροχημική επεξεργασία έχει τη δυνατότητα όχι μόνο να επιτρέψει τη βιοπαραγωγή από βιομηχανικές εκπομπές αερίων ρύπων, αλλά και να συμβάλλει επιπρόσθετα στην επιτόπια ανάκτηση NaOH και H2, τα οποία μπορούν να επαναχρησιμοποιηθούν στις διαδικασίες επεξεργασίας ανάντη και κατάντη της ηλεκτροχημικής. Στο τελευταίο κεφάλαιο αυτής της διατριβής, συζητούνται οι προοπτικές ανάκτησης που μπορεί να προσφέρει η ηλεκτροχημική οξείδωση του υδρόθειου και στήνεται η σκηνή για μελλοντικές εφαρμογές της προτεινόμενης αλληλουχίας διεργασιών, στο γενικότερο πλαίσιο των εννοιών της ηλεκτροδότησης και της αειφορίας.

Table of Contents

CHAPTER 1

Introduction

Adapted from:

Eleftheria Ntagia, Antonin Prévoteau and Korneel Rabaey. Electrochemical removal of sulfur pollution, in: P.N.L. Lens (Ed.), Environ. Technol. to Treat Sulfur Pollut. Princ. Eng., 2nd ed., IWA Publishing, *2020*: pp. 247–276.

Eleftheria Ntagia, Ioanna Chatzigiannidou, Adam J Williamson, Jan B A Arends, and Korneel Rabaey. Homoacetogenesis and microbial community composition are shaped by pH and total sulfide concentration. Microbial Biotechnology, *2020*, 13(4), 1026–1038. https://doi.org/10.1111/1751-7915.13546

1.1 Waste gas emissions and valorisation opportunities

Anthropogenic global greenhouse gas (GHG) emissions, directly linked to climate change, rose sharply after the industrial revolution and keep increasing, reaching an annual average of 57.4 Gt CO_2eq in 2019, with Europe being responsible for ~9% (EEA 2020) and Belgium ~0.3% (EEA 2020; Olivier and J.A.H.W 2020). Although CO_2 is a gas emitted largely by industrial activities, it is rarely emitted as pure CO_2 but rather accompanied by other polluting gases. These gaseous pollutants, however not always GHG and thus not contributing to climate change, still pose an environmental hazard. An example is hydrogen sulfide gas (H_2S), known for its toxicity to humans already at ppm levels.

H_2S is a gas naturally produced in the full gamut of anoxic and anaerobic environments, as sulfate (SO_4^{2-}) reducing bacteria, respondible for its production, are ubiquitous in the natural environment. However, industrial intensification and the use of petrochemical feedstocks for industrial activities has led to additional anthropogenic H_2S emissions. Natural H_2S emissions reach 4.4 Mt yearly, with geothermal activities holding the lion's share of them (Rubright et al. 2017), while additionally 3 Mt H_2S are emitted from industrial point sources (Ausma and De Kok 2019). Mainly natural gas plants, petrochemical refineries, geothermal power production and pulp and paper industries are responsible for anthropogenic H_2S emissions and secondarily sewage treatment plants and biogas installations (Habeeb et al. 2018; Pikaar et al. 2015; Rubright et al. 2017). H_2S has a short residence time in atmosphere (15 days), as it gets rapidly oxidized to sulfur dioxide (SO_2) and further to sulfuric acid (H_2SO_4) by hydroxyl radicals (Steudel 2020), ultimately resulting in acid rain or precipitation. The latter concerns a human activities induced environmental phenomenon that was prominent in the 1970s and already disappeared since the 90s in Europe and the US, owing to stronger environmental regulations (Rafferty 2020; Weiss 2012). Therefore in rural areas, H_2S concentrations are ranging between 0.02 and 0.3 nl L^{-1}. However, in proximity to volcanic areas or areas of intensified industrial activity, atmospheric H_2S concentrations may even exceed 0.1 µl L^{-1} (Ausma and De Kok 2019; Burstyn et al. 2007)

Aside from their polluting nature, both CO_2 and H_2S present potential for valuable products recovery. More stringent environmental regulations call for their removal, but the current gas abatement methods, among them the alkali scrubbers, require high expenditure and are often missing the opportunity for recovery of valuable constituents (Georgiadis et al. 2020; Huertas et al. 2020; Rodríguez et al. 2014). To fully capitalise on carbon, H_2S needs to be efficiently removed from waste gas streams, to render them safe for the living organisms employed for bioproduction or avoid fouling of catalysts. Electrochemical treatment could aid unlocking of this potential through gas clean-up, recovery of potentially valuable chemicals, as well as, in certain applications, electrical power generation (Feng et al. 2016; M. Sun et al. 2016). It is a highly modular technology, easily adjustable to different waste sources and needs. Additionally, electrochemical treatment comes through as a

green process compared to conventional chemical treatment. The latter lies within the main principle of electrochemistry, which is that the driving force for chemical reactions essential for pollutants removal and products recovery, is an electron flux commonly generated by an external power source (Bockris 1972; Feng et al. 2016). Electrons are commonly considered as a clean reagent, particularly when they are sourced from renewable electricity, hence electrochemical treatment can be considered as potentially more sustainable than conventional chemical treatment (Katsounaros et al. 2014; Radjenovic and Sedlak 2015).

In parallel, gas fermentations have gained substantial ground the last decade, as they offer a reroute of chemical industry gas exhaust to production of new chemicals. An example is the production of ethanol from industrial CO/CO_2 off-gases, already demonstrated in large scale by Lanzatech (Handler et al. 2016; Liew et al. 2016). Hydrogen gas (H_2) is a common byproduct of electrolysis applied for waste removal or chlorine production, resulting from the water reduction reaction performed at the cathode of the electrochemical cell. Thus naturally, electrolysis can boost gas fermentations for carbon valorisation, by providing the required electron donor in the form of H_2.

To unravel the full sustainability potential of electrochemical interlinked with gas fermentation techonologies and manage to provide a sound economic argument, renewable electricity in abundance is rudimental. Despite the fact that the global COVID-19 pandemic restrictions resulted in an energy demand decrease which has principally hurt the biofuels sector, a close to 7% growth in renewable electricity was recorded for 2020 (IEA 2020). Renewable electricity resilience has been proven throughout 2020, where after a decrease in production in the first semester, compared to 2019, recovered, scoring an additional 200 GW installed capacity, an almost double capacity addition since 2013. Ultimately, the global installed renewable electricity from solar PV and wind is projected to reach 2400 GW by 2025, overtaking coal and natural gas as the primary electricity production sources (IEA 2020).

This thesis explores an integrated system for the production of essential chemicals in electrochemical and microbial reactors, to initiate new production processes driven by industrial off-gases rather than fossil resources. This work centers around sulfide (H_2S) as the compound of interest, presenting a challenge for both electrochemistry and fermentations, due to its intrinsic corrosive and toxic properties.

1.2 Sulfur, the burning element

Sulfur constitutes the tenth most abundant element in nature, found mainly in sulfur-containing mineral deposits and, by only 0.07 wt%, in the Earth's crust. It was already known and used in most of the ancient civilisations where its combustion fumes were used as antiparacitics. The practice of burning sulfur gave to the element its greek name, 'θείο' (theio; etymology: θεειον: arizing from the

verb to fume) (Βάρβογλης 2014) as well as its name in the Bible, brimstone (Lide 2004). It is an essential element of life, being present in amino acids, (poly-)peptides, enzyme cofactors, sulfolipids and carbohydrates, essentially representing 2g per kg of the human body (Dahl 2020; Steudel 2020). Sulfur has an average atomic weight of 32.066. It comes with a high chemistry complexity, as a result of the variety in oxidation states that is found and the vast array of chains and rings that sulfur in the zero oxidation state forms, through the catenation process (Lide 2004). The most commonly reported, and thermodynamically most stable at ambient conditions, form of elemental sulfur (S^0) is the orthorhombic α-S_8. Upon dissolution in alkaline sulfide solutions, sulfur forms a series of homoatomic polysulfide dianions (S_n^{2-}, n = 2 – 9) of variable chain lengths (Steudel and Chivers 2019; Teder 1971). The size of the polysulfides obtained will be dictated by the alkalinity and the total sulfur concentration. Polysulfides are dominating higher pH regions (pH>6), as lower than neutral pH favors the formation of H_2S and S^0 precipitation (Steudel 2020).

Hydrogen sulfide (H_2S) is the most reduced form of sulfur whereas sulfate (SO_4^{2-}) is the most oxidized form. Both compounds, along with several sulfur oxyanions and organosulfur compounds, are common contaminants in gaseous and aqueous waste streams such as sour gases, sewage and industrial wastewaters. Sulfur pollution treatment today comprises a wide range of biological (Alcántara et al. 2004; Buisman et al. 1989, 1999; Janssen et al. 2009; Lens et al. 1998) and physicochemical (Pikaar et al. 2015; L. Zhang et al. 2008) processes. The selection of treatment strategies will depend upon the targeted pollutant, the total sulfur concentration, the pH range and the presence of additional contaminants, e.g. organic compounds or trace metals. The present thesis centers around sulfide (H_2S/HS^-).

Sulfide in its gaseous form ($H_2S_{(g)}$) is a colorless, heavier than air (1.19 specific gravity at 15 °), corrosive and poisonous gas (more on its toxic properties on paragraph 1.2.2). It is also highly flammable (260 °C ignition temperature) and when at concentrations between 4 and 44 vol%, H_2S forms exposive mixtures with atmospheric air (Rubright et al. 2017; Steudel 2020). At room temperature and standard pressure the solubility of H_2S in water is 0.40 g/100 g H_2O (0.12 M) and decreases with increasing temperature. It is a weak acid and deprotonates in aqueous solutions, with the deprotonation extent depending on the pH and according to the following H_2S dissociation reactions:

$$H_2S + H_2O \rightleftarrows [H_3O]^+ + HS^- \qquad K_1 = 10^{-7} \quad (20°C)$$

$$HS^- + H_2O \rightleftarrows [H_3O]^+ + S^{2-} \qquad K_2 = 10^{-14} \text{ to } 10^{-17} \quad (20°C)$$

The dissociation constants K_1 and K_2 will depend on the salt concentration and the ionic strength of

the aqueous solution (Hartle and Pluth 2016; Steudel 2020). It should be mentioned here that although values between 10^{-14} and 10^{-17} have consistently been reported in literature for the second dissociation constant (K_2), an average value of 10^{-16} would practically mean that sulfide ions S^{2-} do not exist in solutions of pH ≤ 12. Based on also spectroscopic data, May and coworkers have recently ruled out the presence of S^{2-} in aqueous solutions in general, suggesting that it should be abolished by chemical literature, in favour of clarity (May et al. 2018). As it is concluded from the acid dissociation constants, at pH 7 the molar ratio of H_2S over HS^- will be 1 and therefore, in most of the wastewater streams that an environmental engineer will be called to treat, sulfide will be present as a mix of H_2S/HS^-.

Sulfide (H_2S/HS^-) in this thesis is of interest for both of the two main technologies combined: electrochemistry and gas fermentation. Therefore in the two following paragraphs, first, the toxic properties of sulfide are outlined and second, the electrochemical properties of sulfur compounds. The first is fundamental to understant how sulfide will affect a biological process, in this case the gas fermentation, in terms of energy input and efficiency. In the same way, the second, is fundamental to understand the energetic aspects of the electrochemical cell used for sulfide pollution treatment and likewise, how the operational conditions selected will affect the energy revenue and the efficiency of the treatment.

1.2.1 Sulfide induces toxicity to prokaryotic and eukaryotic organisms

A foul, rotten-egg smell is the hallmark of hydrogen sulfide gas ($H_2S_{(g)}$) at ambient levels (< 1 ppm), where it can easily get picked up by the human nose, however the sense of smell is lost already at 100 ppm (Guidotti 2010). In higher concentrations H_2S becomes highly toxic, scoring only second after carbon monoxide in inhalation deaths (Jingjing Jiang et al. 2016; Rubright et al. 2017). Several inhalation deaths at occupational settings such as natural gas extraction wells, sewage piping networks and while handling manure in farming or anaerobic digesters are attributed to H_2S and therefore the maximum allowed concentration in working places has been set to 10 ppm for an 8-hour long exposure (NIOSH 2011; Shutske et al. 2017). Upon inhalation H_2S irritates the olfactory tract and subsequently the pulmonary function, with the symptoms experienced ranging from eye and lung irritation at 20 ppm to acute death at 700 ppm or higher (Hartle and Pluth 2016). Inhibitory intracellular concentrations between 0.1 and 1 ppm have been reported and the mechanism of inhibition includes sulfide binding and inhibition of cytochrome C oxidase in the complex IV of the mitochondrial electron trasport chain, ultimately inhibiting ATP synthesis. Detoxification mechanisms reported so far include oxidation in the liver, methylation and mitochondrial sulfide oxidation (Jingjing Jiang et al. 2016; Rubright et al. 2017).

Sulfide inhibition of biological processes is an ever-occuring nuisance for reactor engineers, as

concluded by studies on its toxicity properties and reactor engineering approaches for its alleviation, from the early 80s till today (Isa et al. 1986; Yuan et al. 2020). It has been extensively studied in anaerobic digesters, where usually a mixed anaerobic microbial community, containing SO_4^{2-} reducers and methanogenic archaea, is present, with the two communities often competing for H_2 as an energy source (Y. Chen et al. 2008). The methods for sulfide inhibition alleviaton in anaerobic digesters range from simply applying operational conditions that will not allow SO_4^{2-} reducers to thrive over other hydrogenotrophs, to more sophisticated approaches, such as addition of catalytic materials to supress SO_4^{2-} reduction (Yin et al. 2020) or to aid H_2S removal (Choudhury and Lansing 2020; T. Wang et al. 2018).

Sulfide toxicity has been reported for both mammalian and bacterial cells, and the mechanisms of toxicity may range from a general inhibition of respiratory activity (Chen et al., 2008; Bouillaud and Blachier, 2011), DNA damage and protein denaturation (Wu et al., 2015) to inhibition of specific activities, unique for specific organisms. Sulfide impairs a number of specific metabolic activities such as anammox, denitrification and SO_4^{2-} reduction, by decreasing the heme c content (Jin et al., 2013), by inhibiting the N_2O reductase activity (Pan et al., 2013) and by inhibiting the sulfur reductase activity of cytochrome c3 (Reis et al., 1992), respectively. In the case of homoacetogenic bacteria little is known and the information provided includes either studies on CO-utilizing acetogens, usually employed in synthesis gas conversion (Vega et al., 1990; Grethlein et al., 1992), or homoacetogens as part of a general anaerobic community active during anaerobic digestion (Colleran et al., 1998; O'Flaherty et al., 1998b; Dar et al., 2008). Whatever the mechanism of inhibition, it is generally reported that pollutants contained in gaseous emissions, are expected to hinder bioproduction and the extent of inhibition will be dicated by the operational conditions applied as well as the microbial communities employed in the process.

1.2.2 The electrochemical properties of sulfur compounds

Extensive research on electrochemical equilibria and electrochemical oxidative and reductive processes of sulfur species took place in the last 40 years, mainly because of the complexity of the sulfur chemistry (Levillain et al. 2006). Considerable inconsistency exists in the sulfur literature regarding the final products of sulfide oxidation and S^0 reduction, respectively, due to a lack of suitable analytical techniques to study many of the different sulfur forms in existence (Levillain et al. 2006). The well discussed complexity of sulfur chemistry is a result of the many oxidation states that the sulfur atoms present, ranging from −2 to +6. The most common sulfur compounds found in electrochemical sulfur pollution treatment systems are presented in Table 1.1, with their respective oxidation numbers.

In order to study and predict the thermodynamic stability area of aqueous and solid sulfur compounds, one can use the Pourbaix diagrams. The Pourbaix diagrams, or potential (Eh)-pH equilibrium

diagrams, allow to study which redox species are predominant at thermodynamic equilibrium, expressed as functions of the pH and the redox potential of the solution (Pourbaix 1966). These, however, only describe the situation under equilibrium conditions, the ultimate understanding and prediction of electrochemical reactions requires the knowledge of kinetics and of the actual concentrations in solution as well (Bouroushian 2010).

Table 1.1 – Sulfur compounds considered in electrochemical sulfur pollution treatment systems with their respective oxidation numbers (Pourbaix 1966)

Compound name	Formula	Oxidation number
Hydrogen sulfide	H_2S	− 2
Bisulfide (or hydrogen sulfide ion)	HS^-	− 2
Elemental sulfur	S^0	0
Polysulfides	S_n^{2-}	− 1 to − 0.40
Thiosulfate	$S_2O_3^{2-}$	+ 2
Sulfite	SO_3^{2-}	+ 4
Sulfate	SO_4^{2-}	+ 6

Only H_2S, HS^-, S^0, HSO_4^- and SO_4^{2-} will be found in solution in equilibrium (Dutta et al. 2010; Pourbaix 1966). Thiosulfate ($S_2O_3^{2-}$), sulfite (SO_3^{2-}), dithionate ($S_2O_4^{2-}$) and polythionates ($S_n(SO_3)_2^{2-}$) are excluded from the potential-pH diagram for aqueous sulfur compounds (Figure 1.1) as they are thermodynamically unstable and tend to decompose in aqueous solutions (Pourbaix 1966). Zero-valent sulfur is stable in the presence of water and acid solutions (pH<6), but unstable in alkaline regions (pH>6), where it disproportionates to HS^-, polysulfides and SO_4^{2-}. Sulfate is stable in the presence of water and aqueous solutions at all pH values and the same applies for sulfide (Pourbaix 1966). Table 1.2, overviews the most common reversible electrochemical reactions taking place in electrochemical cells treating sulfur containing electrolytes.

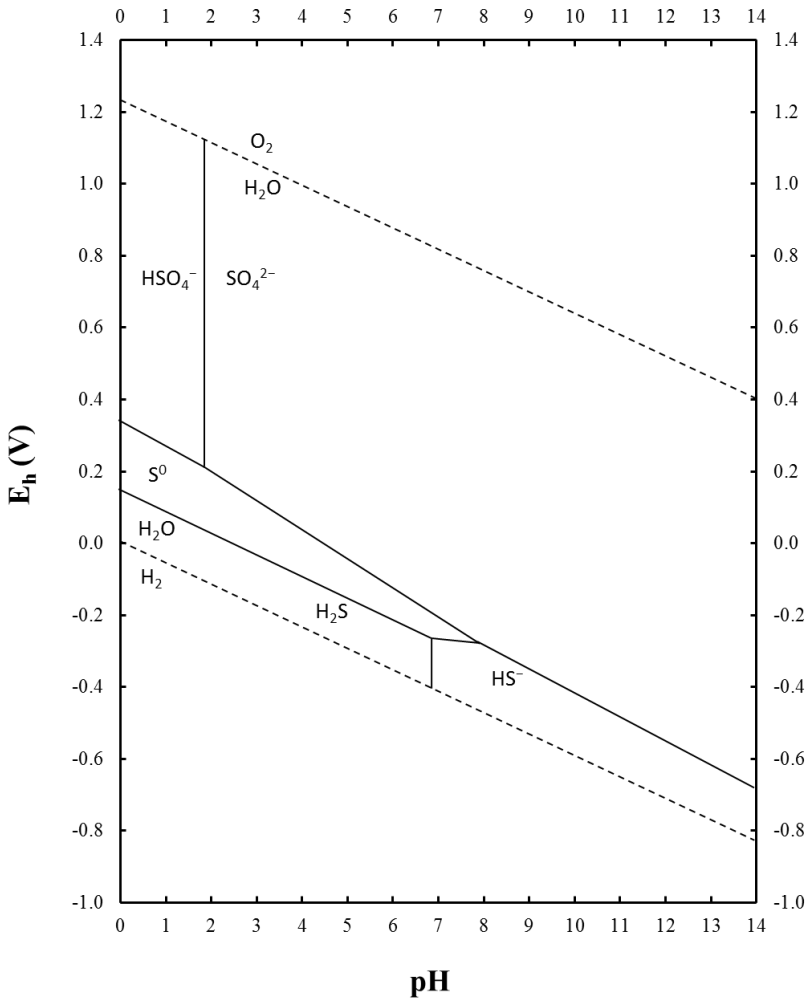

Figure 1.1 – Potential (Eh)/pH diagram for the system sulfur-water, including predominance regions at equilibrium for H_2O, O_2, H_2, S^0, H_2S, HS^-, HSO_4^- and SO_4^{2-} at standard temperature (0 °C) and pressure (1 atm) (STP) and [S] = 1 M, produced based on (Dutta et al. 2010; Pourbaix 1966). *Potentials are expressed with respect to the Standard Hydrogen Electrode (SHE), which corresponds to the standard potential of the H^+/H_2 couple, i.e. the corresponding equilibrium potential between the redox couple and an inert electrode for all reagent activities equal to 1 (pH 0 and 1 atm partial pressure of H_2).*

Table 1.2 – Standard redox potentials (E^0, pH 0) and apparent standard redox potentials at pH 7 (E^0_{app}) of the most common sulfur involving half-reactions (Bouroushian 2010; Dutta et al. 2010; Levillain et al. 2006; Mao et al. 1991; Pourbaix 1966)

Half-Reaction	E^0 (V vs. SHE, at 25 °C)	E^0_{app} (V vs. SHE, at 25 °C and pH=7)
$nS(s) + 2e- \rightarrow Sn^{2-}$, $4 \leq n \leq 5$	− 0.340 to − 0.315	− 0.340 to − 0.315

$S(s) + H^+ + 2e^- \rightarrow HS^-$	− 0.065	− 0.272
$Sn^{2-} + nH^+ + (2n-2)e^- \rightarrow nHS^-$, $2 \leq n \leq 5$	+ 0.007 to + 0.298	− 0.251 to − 0.116
$S(s) + 2H^+ + 2e^- \rightarrow H_2S(aq)$	+ 0.142	− 0.272
$S_2O_3^{2-} + 8H^+ + 8e^- \rightarrow 2HS^- + 3H_2O$	+ 0.200	− 0.214
$SO_4^{2-} + 9H^+ + 8e^- \rightarrow HS^- + 4H_2O$	+ 0.252	− 0.214
$SO_4^{2-} + 8H^+ + 6e^- \rightarrow S(s) + 4H_2O$	+ 0.357	− 0.194

Having already presented the chemical and electrochemical properties of sulfide, it becomes clear that many waste gases, however excellent candidates might be for bioproduction, they might bring along toxicity to the microbial communities employed for their valorisation. Below, the process potential for waste carbon valorisation will be overviewed (paragraph 1.3) and further on, proposals on how to do that in an efficient and sustainable way, by electrochemistry will be outlined (paragraph 1.4).

1.3 Carbon valorisation via gas fermentation

This thesis explores the contribution of electrochemical technologies for the advancement of the emerging field of gas fermentation. The latter focusses on steering the human society from a carbon emitting, to a carbon recycling one and principally, away from a fossil-based carbon production processes. In that scenario, carbon originally consumed to fuel industrial and agricultural activities, is prevented from emission to the atmosphere and is instead used to produce chemical building blocks via a biological process. The emerging field of waste gas fermentations is one of the paths to realize that aspiration. Gas fermentations employ anaerobic, acetogenic bacterial single strains or communities, where CO_2 emitted from point industrial sources can be fixed to produce chemical building blocks, including a wide array of acids and alcohols (Ragsdale and Pierce 2008). Applying the suitable upgrading or downstream processes, these can be transformed to commodity chemicals fit to specific purity levels required by the chemical industry (Figure 1.2).

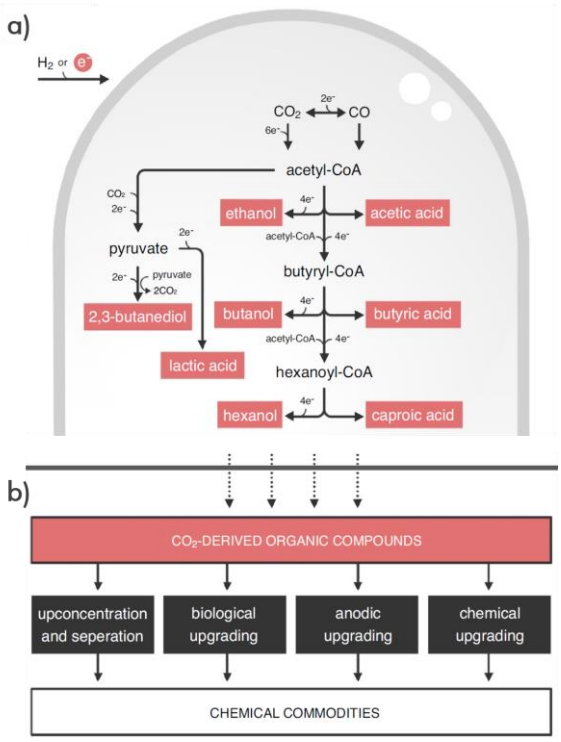

Figure 1.2 – Simplified reductive acetyl-CoA (Wood-Ljungdahl) pathway for CO_2 fixation into organic products and b) Upgrading and downstream processing routes for the production of commodity chemicals from the organic products (adapted from (Prévoteau et al. 2020))

1.3.1 Acetogens, the workforce of gas fermentations

Drake and colleagues in their book chapter in 2013 have pointed out the systematic inconsistency in the definition of acetogens in the literature. Therefore, the definition of an acetogen, given by them, is presented here, in order to clarify the group of microorganisms that this thesis focuses on:

"Acetogen: An anaerobe *that can use the acetyl-CoA pathway as a (1) mechanism for the reductive synthesis of acetyl-CoA from CO_2, (2) terminal-electron-accepting, energy-conserving process, and (3) mechanism for the fixation (assimilation) of CO_2 in the synthesis of cell carbon*." (Drake et al. 2013).

An acetogen needs to abide by all three cell processes in order to live up to the name. In literature, often also the term "homoacetogen" is used, which simply refers to the production of acetate as the single product of CO_2 reduction. This is mainly a result of bacterial cultivation under certain conditions, for example, usually when H_2/CO_2 are provided as energy and carbon sources to the cultivation system (Drake et al. 2013; Müller 2019). Acetogenic bacteria conduct linear CO_2 fixation, using hydrogen (H_2) as electron donor by exploiting the Wood-Ljungdahl pathway (WLP), thereby coupling CO_2 fixation with ATP synthesis (Drake et al. 2008; Müller 2019). They conserve energy by reducing two moles of CO_2 first to one mol of acetyl coenzyme A (acetyl-CoA) and then to acetate (Figure 1.3), at the expense of the reaction:

$$2CO_2 + 4H_2 \rightleftarrows CH_3COO^- + H^+ + H_2O \qquad \Delta G^0 = -55.8 \text{ KJ mol}^{-1}$$

When physiological conditions, usually applied in bioreactors, are considered (pH = 7) a higher energetic gain is expected, with $\Delta G^{0\prime} = -95.6$ KJ mol^{-1} (Philips 2020). This pathway holds the highest theoretical thermodynamic efficiency among the carbon fixation pathways, as it links endergonic reactions with non-ATP consuming exergonic reactions, thus avoiding most of the ATP-consuming reactions (Heffernan et al. 2020; Prévoteau et al. 2020). This becomes possible by the coupling mechanism known as electron bifurcation where 2 electrons arising from the same electron donor are split to two different electron acceptors, higher and lower than the electron donor energetically, respectively (Figure 1.3). This ultimately requires 0.27 ATP energy investment, which is the lowest among the coupling mechanisms (ATP hydrolysis requires 1ATP and reverse electron transport 0.58 ATP) and allows for bacterial growth even in thermodynamically unfavourable conditions (Buckel and Thauer 2018; Müller et al. 2018).

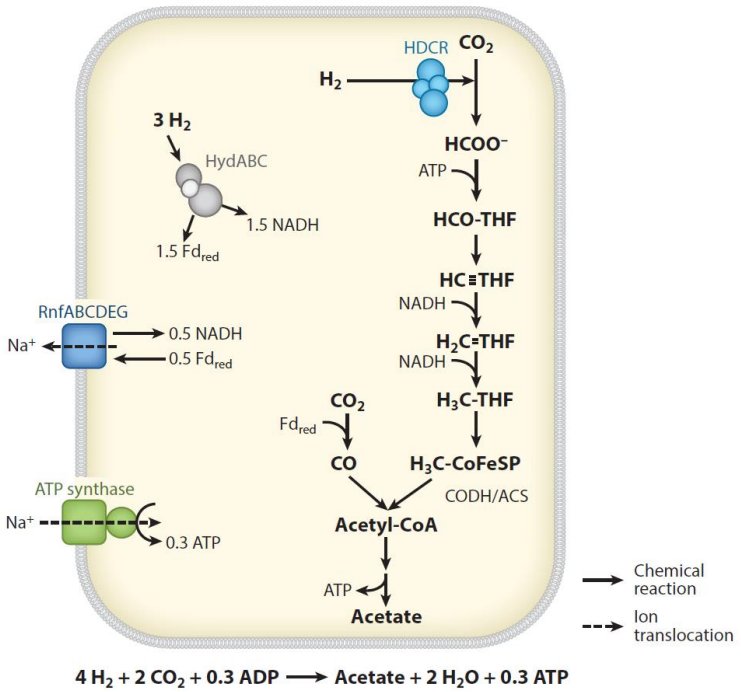

Figure 1.3 – Detailed Wood-Ljungdahl pathway for acetogenesis as carried out by Acetobacterium woodii, showcasing electron bifurcation. (CODH/ACS: carbon monoxide dehydrogenase/acetyl-CoA synthase, CoFeSP: corrinoid–iron-sulfur protein, Fd: ferredoxin, HDCR: hydrogen-dependent carbon dioxide reductase, THF: tetrahydrofolate) (from (Müller et al. 2018))

Moorella thermoacetica, initially named *Clostridium themoaceticum* when isolated in 1942, has been

studied as the model acetogen, after the temporary loss of isolates of *Clostridium aceticum* (Drake et al. 2013). That was the first bacterium to produce acetate from H_2/CO_2, isolated by Wieringa in 1939 (Wieringa 1939). Next in isolation sequence was *Acetobacterium woodii* and up to date, 100 different acetogenic species have been isolated. A list of all the 100 acetogenic species is given in the "Acetogenic Prokaryotes'' book chapter by Drake and colleagues, along with a detailed description of the WLP (Drake et al. 2013) as well as in the gas fermentation review paper of Liew et al. (Liew et al. 2016). Although most acetogens are classified within the *Firmicutes* phylum, various acetogenic species have been classified as *Spirochaetes*, *δ-Proteobacteria* and *Acidobacteria* (Ragsdale and Pierce 2008). Recently, even *Actinobacteria* harbouring the WLP have been discovered (Merino et al. 2020). Acetogens are ubiquitous in anoxic environments, thereby contributing to the production of 10% of a total 10^{13} kg acetic acid produced yearly in terrestrial habitats and they are also responsible for the annual production of 10^{10} kg acetic acid in the human colon (Drake et al. 2013). They constitute a phylogenetically versatile group of bacteria that thrive in both acidic and alkaline pH environments (Drake et al. 2008) with a growth optimum between pH 5.5 (Grimalt-Alemany et al. 2018) and neutral (Ayudthaya et al. 2018; Braun and Gottschalk 1982; Grimalt-Alemany et al. 2018).

1.3.2 Continuous H_2/CO_2 acetogenesis with biomass retention

The first and most extensively studied applications of gas fermentations were batch operated reactor studies (Demler and Weuster-Botz 2011) as a means to fundamentally understand acetogenesis and the metabolic pathways involved. However, recently the focus has shifted towards continuous operation which allows for maintaining an active culture for longer times, decreasing in this way potential operational costs invested for microbial regrowth in the case of batch operation (Richter et al. 2013). Additionally, lab-studies on continuous gas fermentation are seen as a way to provide steady-state operational performance data but also to provide a more realistic approach of the technology, heading towards commercialization. Gas, and specifically syngas, fermentation have been studied thoroughly for ethanol production, due to the importance of ethanol as a fuel. Acetate however, is another industrially significant commodity chemical, with global size market expected to reach almost 12 million tonnes by 2026, that is used in the food and paint industry, but is also a precursor for the production of butyric acid and ethanol (Expert Market Research 2020). Most commonly, pure cultures of *Clostridium*, *Acetobacterium* or *Moorella* species (Kantzow et al. 2015; Steger et al. 2017; Riegler et al. 2019) have been studied so far for continuous acetate production, as they allow for a more defined product spectrum. Nevertheless, mixed culture fermentations are gaining momentum as they are applicable to a wider range of substrates, owing to microbial diversity. Additional advantages of mixed microbial communities compared with single strain fermentation within the industrial biotechnology scope include the avoidance of sterilization processes and intensive control of the process and therefore the lower operational cost (Agler et al. 2011; Kleerebezem and

van Loosdrecht 2007), as well as process robustness.

One challenge that continuous fermentations have to tackle, is the low growth rates of acetogens, thus possible wash-out of the microbial community from the bioreactor and subsequently loss of the productivity. In particular, maximum growth rates (μ_{max}) between 0.024 and 0.195 h^{-1} have been reported for H_2 consuming acetogens. In an attempt to maintain high biomass density in the fermentation reactor and thereby sustain a higher activity, reactors with different approaches for cell retention have been engineered (recent work see Table 1.3). The volumetric acetate production rate is the parameter used to evaluate activity performance of a continuous gas fermenter. The highest productivity achieved so far for acetate is 147 g L^{-1} d^{-1}, by Kantzow and colleagues, which is also by far the highest achieved in H_2/CO_2 acetogenic bioproduction in general.

Table 1.3 – Continuous H_2/CO_2 acetate production in bioreactors with cell retention

Microbial community	Cell retention method	Gas mixture[1]	Volumetric production rate ($g_{acetate}$ L^{-1} d^{-1})	Reference
Clostridium aceticum	Packed-bed and trickle-bed	CO_2:H_2:N_2 (3:12:10)	19.9	(Riegler et al. 2019)
Mixed anaerobic community	Submerged hollow fiber membrane	H_2:CO_2 (60:40)	10.5	(Y. Q. Wang et al. 2017)
Acetobacterium woodii	Submerged linen cylinder	H_2:CO_2 (80:20)	1.21	(Steger et al. 2017)
Acetobacterium woodii	Submerged microfiltration unit	H_2:CO_2:N_2 (60:25:15)	147	(Kantzow et al. 2015)
Mixed anaerobic community	Hollow fiber membrane biofilm reactor	H_2:CO_2 (60:40)	0.4	(F. Zhang et al. 2013)
Mixed anaerobic community	Hollow fiber connected in the liquid recirculation line	H_2:CO_2 (70:30)	0.7[2]	This work, Chapter 6

[1] All gas mixtures are synthetic, clean gas mixtures

[2] Maximum reported during uninhibited, devoid of H_2S, fermentation

A few full-scale gas fermentation applications have been realized in the last decade and some of the

most successful of them, commissioned by LanzaTech, are based on the fermentation of steel mill off-gases for the production of ethanol (Handler et al. 2016; Liew et al. 2016). Nevertheless, financial competitiveness has still not been proven, as the majority of scaled-up demonstrations of gas fermentations have suspended their operations in 2016 (Heijstra et al. 2017), even though biotechnological approaches for carbon utilization are more sustainable compared to intensive chemical routes. Even if in some cases waste gas fermentations are boosted by electrolytically produced H_2, a theoretically green chemical, however most of this H_2 is still produced by natural gas, thus counteracting the sustainability argument. On the other hand, the increase in affordable renewable electricity distributed to electrolysis has the potential to render waste gas fermentations a competitive and sustainable route for bioproduction. Additionally, electrolysis does not only serve as the H_2 producer, but can also aid upstream desulfurization and recover relevant to the processes commodity chemicals, thus the overall process gains in circularity and sustainability. This could potentially be achieved with electrochemical desulfurization of the industrial off-gasses.

1.4 Electrochemical sulfur conversions: adding circularity and sustainability credits to desulfurization

Desulfurization of H_2S containing waste gases, when H_2S is not flared or stripped with N_2, proceeds via a series of absorption and oxidation steps. Absorption is commonly conducted via alkanolamine, ammonia or alkaline salts solutions. When NaOH is the alkaline salt solution employed, the liquid product arising from the absorption process is commonly referred to as spent caustic stream (SCS), or more specifically sulfidic SCS (Hawari et al. 2015). Further processing of SCS is conducted via physicochemical, thermal and biological processes, or a combination of those when needed, in order to meet the locally applied environmental regulations. The most commonly applied chemical approaches include neutralization, wet air oxidation (WAO) and the Claus process. The first case, although simple, involving just a drop in pH and taking advantage of the H_2S dissociation properties, is unsustainable as the H_2S previously absorbed is just released back in the atmosphere. The latter two include a series of treatment steps conducted at temperatures and pressures well above the ambient values. In particular the Claus process, majorly applied in sour and natural gas desulfurization, requires the use of expensive catalysts, such as alumina and titania, that reportedly get rapidly deactivated, thereby increasing the overall costs of the process (Carlos and Clayton B. Maugans 2000; Eow 2002; Kohl and Nielsen 1997).

Evidently, the majority of the physicochemical approaches applied so far are chemical and energy intensive. In an effort to reduce the costs, while offering an environmentally more benign approach, biological approaches involving sulfide oxidizing bacteria (SOB) have been developed (L. Zhang et al. 2008). Biological desulfurization is conducted under ambient temperature and pressure and the

microbial community conducted the required reactions, is readily available and costless. However, a source of organic carbon, as well as a relevant electron acceptor, O_2 or NO_3^- according to the microbial community conducting sulfide oxidation, is required to sustain biological activity, hence, desulfurization. Usually the industrial SCS do not contain NO_3^- and the organic compounds that come along are complex organic molecules, difficult to be degraded. Therefore the addition of these compounds will add to the total operational costs of the unit (Khanongnuch et al. 2019; L. Zhang et al. 2008). Additionally, the increased pH of the SCS (pH>12) as well as the increased H_2S content (2 – 3 wt%) (Hawari et al. 2015), hinder biological treatment, if the latter is applied without pre-treatment steps or after extensive dilution steps that will ensure biocompatibility.

Electrochemical technologies rely on electrical energy as the driver for the reactions needed for pollutant removal and product recovery, rather than on chemicals, which makes them more sustainable, in particular when renewable energy can be locally sourced. The ability to easily control the parameters (current or voltage) controlling the performance of the cell with a virtually non-limited electron source is considerably advantageous when compared to the safety, environmental and logistic issues generally accompanying chemical-intensive processes. The versatility of electrochemistry has now led to many different approaches to treat sulfur-containing streams, ranging from, direct or indirect, abiotic electro-oxidation or electro-reduction of the sulfur compounds, electrodialysis, electrocoagulation and electroflotation to microbial fuel cells and microbial electrolysis cells. Electrochemical treatment centers around the electrochemical cell, which is principally a reactor, connected to an external electron source, where the electro-oxidation and electro-reduction reactions that are used in physicochemical waste treatment are realized. In the paragraphs that follow, the fundamentals of electrochemical treatment (1.4.1), followed by an overview of the electrochemical sulfide oxidation concept (1.4.2) and electrochemical sulfide treatment studies (1.4.3) will be outlined.

1.4.1 The basics of electrochemical treatment

Electrochemical treatment lies in the interface between engineering and electrochemistry, therefore, both the fundamental concepts of electrochemical reactions and the reactor configuration need to be studied thoroughly and designed carefully, in order to achieve optimal operation. The latter translates into optimal pollutant removal efficiencies or products recovery with in parallel cost minimization. Key aspects that need to be considered when assessing electrochemical processes are: i) the design of the electrochemical cell or electrochemical reactor, ii) the thermodynamics of the electrochemical reactions possibly involved iii) the electron transfer kinetics at the electrode/electrolyte interface, iv) certain losses taking place in an electrochemical cell and v) the performance of the processes such as current efficiency and electric power investment.

1.4.1.1 The electrochemical cell – facilitating the electrochemical reactions

The core of electrochemical treatment is the electrochemical reactor, or simply the electrochemical cell. An electrochemical cell is usually comprised of: 1) two electrodes: an anode and a cathode on which oxidation and reduction reactions are conducted, respectively; 2) one or several electrolytes, which are conductive solutions containing the chemical reagents taking part in the reactions as well as supporting (i.e. non-electroactive) ions allowing sufficient conductivity; 3) one or several solid separators, which are typically ion-exchange membranes which can be permselective or not, depending on the desired process (Figure 1.4).

The electrodes are connected to a power supply or potentiostat/galvanostat through an electrical circuit, that enables electron flow from the anode to the cathode. The electron flow translates into a current (I), however, in electrochemical engineering applications the current density (j) is most commonly reported, which is the current applied per surface area (A) (usually the projected or geometric surface area) of the electrode. Simultaneously, an ion flow takes place in the electrolyte, where anions migrate towards the anode and cations towards the cathode to ensure charge balance in the overall system. The ion-exchange membrane allows for selective passage of negatively (anion-exchange membrane) or positively (cation-exchange membrane) charged ions. Using a membrane results in the formation of two electrolyte chambers (Juyuan Jiang et al. 2012). This separation provides specific process advantages, such as product recovery in the separate electrolyte chambers, pH gradient, and separation of toxic products in the case of bioelectrochemical systems.

A third electrode with a well-defined equilibrium potential is placed close to the electrode of interest (anode or cathode) in the electrochemical cell, in order to allow for continuous monitoring of the absolute potential, developed under varying experimental conditions. This electrode is known as reference electrode. The reference electrode is an electrode that is immersed in a defined electrolyte (and maintains a constant potential during the experimental period (Smith and Stevenson 2007). A number of different reference electrodes exist and the most commonly used in environmental electrochemistry are the Silver/Silver Chloride (Ag/AgCl / 3 M KCl/NaCl) and the Standard Calomel Electrode (SCE / Saturated KCl) with potentials at + 0.209 and + 0.241 vs. SHE, respectively, at 25 °C. In this work all potentials are reported as SHE unless stated otherwise (e.g. in Chapter 2 they are reported in SCE).

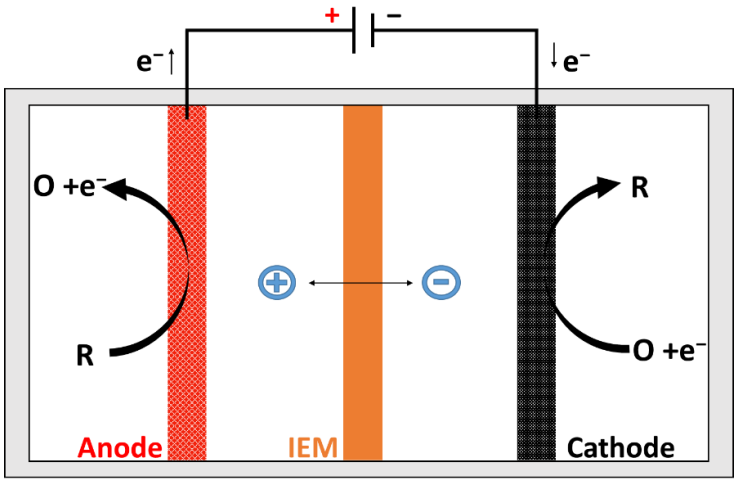

Figure 1.4 – Schematic drawing of a two-compartment electrochemical cell controlled with an external power source (electrolytic cell) that enables electron flow from the anode to the cathode. The two electrodes, anode and cathode, are separated with an ion exchange membrane (IEM), that allows for (selective) passage of positively or negatively charged ions. An oxidation reaction occurs at the anode (positively charged electrode) and a reduction reaction occurs at the cathode (negatively charged electrode).

Electrochemical cells are divided in galvanic and electrolytic cells. The cell is considered as galvanic when the overall cell reaction (i.e. considering both anodic and cathodic reactions as a single redox process) is thermodynamically favourable ($\Delta G < 0$), allowing for spontaneous reactions to occur on both electrodes and possibly for generation of electricity, if the cell is not under short circuit (i.e. inducing a non-zero voltage). The anode of a galvanic cell is the negative electrode, whereas the cathode is positive. Conversely, an electrolytic cell requires the addition of external electric power to drive a non-spontaneous reaction ($\Delta G \geq 0$), i.e. to translate electric energy into chemical energy (Ciobanu et al. 2007; Pourbaix 1966). The corresponding electrode polarity, due to the external power, is opposite to the galvanic cell, with a positive anode and a negative cathode.

1.4.1.2 Thermodynamics of electrochemical reactions and the electrode potential

Electrochemical reactions differ from homogeneous chemical reactions because they occur at the interface between the electrodes and their respective electrolyte, stressing the dramatic impact of electrode surface area and mass transfer parameters on the overall rate of reactions. An electrochemical reaction can be seen as a "delocalized" redox reaction, physically separating the two half-reactions that are the oxidation (at the anode/electrolyte interface) and the reduction (at the cathode/electrolyte interface) (Pourbaix 1966). As such, electrochemical studies generally focus on those half-reactions separately, considering they are specific, amongst others, to the redox couple(s) involved, the electrode material and the nature of the electrolyte.

In electrochemistry, the basic form of the Nernst equation characterizes the equilibrium for an electrochemical reaction involving an inert electrode and a single dissolved redox couple O/R (where O represents the oxidized form and R the reduced form of the redox couple). The Nernst equation links the electrode potential with the ratio of the interfacial concentration of the oxidized and reduced forms of the redox couple when the system is at equilibrium (Allen J. Bard and Faulkner 2001). For an electrochemical reaction involving a single redox couple O/R (without a proton coupled to the electron transfer):

$$O + ne^- \rightleftarrows R$$

the Nernst equation is:

$$E = E^0 + \frac{RT}{nF} ln \frac{a_O}{a_R} = E^{0'} + \frac{RT}{nF} ln \frac{C_O}{C_R} \quad (1.1)$$

where E is the electrode potential (V), E^0 is the standard potential of the considered redox couple (V), $E^{0'}$ is the formal potential, R is the universal gas constant (8.314 J mol^{-1} K^{-1}), T is the temperature (K), F is the Faraday constant (96,485 C mol^{-1}), n is the number of electrons (dimensionless) involved in the reaction, α_O and α_R are the activities (dimensionless) and C_O and C_R are the interfacial concentrations (mol L^{-1}) of, respectively, the oxidized and reduced form of the considered redox couple. Whereas E^0 is a thermodynamic constant for a specific redox couple at a specific T, $E^{0'}$ varies with the activity coefficients of the redox compounds, and therefore with their concentration as well as the ionic strength of the medium (Allen J. Bard and Faulkner 2001). The IUPAC (International Union of Pure and Applied Chemistry) convention hereby used, considers a positive electrode potential as the one favouring oxidation reactions (low energy electrons on electrode surface) and a negative electrode potential as the one favouring reductions (high energy electrons on electrode surface). It is often assumed that the redox compounds are at sufficiently low concentrations, thus the latter are considered to be equal to the activities, and the Nernst equation is commonly used with the standard potential and the concentrations (Ciobanu et al. 2007).

When wastewater is considered as an electrolyte in electrochemical treatment, it is expected that the pH will vary substantially from one case to another. To calculate the electrode potential E at different operational pH values, one can write an electrochemical reaction to include proton exchange coupled to electron transfer:

$$aA + cH_2O + ne^- \rightleftarrows bB + mH^+$$

where A is the acid form and B the alkaline form of a compound. E can then be calculated based on the Nernst equation taking into account the influence of the pH:

$$E = E^0 - \frac{0.0591 \times m}{n} \times pH + \frac{0.0591}{n} \times log\frac{(A)^a}{(B)^b} \quad (1.2)$$

with E and E^0 in V (Pourbaix 1966). This is a useful and fast tool to calculate the expected theoretical electrode potential in an electrochemical reactor, operated at pH ≠ 0.

The free energy change of the overall electrochemical reaction conducted in the cell is related to the cell voltage (electrode potential difference) according to:

$$\Delta G_r^0 = -nFE^0 \quad (1.3)$$

where ΔG_r^0 is the standard Gibbs free energy of the overall cell reaction (J mol^{-1}) (Ciobanu et al. 2007; Christos Comninellis and Chen 2010).

1.4.1.3 Overpotential and ohmic resistance

The relationship between current density and electrode potential is essential to define an electrochemical system (see Chapters 3 and 4). For a specific combination of electrode and redox couple, the reaction rate depends upon mass transfer to the electrode, kinetic variables and surface effects (Allen J. Bard and Faulkner 2001). Assuming all the electrons exchanged at the electrode interface are dedicated to a single electrochemical reaction, the relationship between the surface reaction rate (v) and the electric current (I) is described by Faraday's law of electrolysis:

$$v = \frac{I}{n \times F \times A} = \frac{j}{n \times F} \quad (1.4)$$

where v is given in mol s^{-1} m^{-2}.

When current is applied in an electrochemical cell, previously at equilibrium, both anode and cathode potentials are shifted from their equilibrium value. This shift in the electrode potential results in what is called overpotential (η), which is the difference between an electrode potential under a current density j and its equilibrium potential (j = 0):

$$\eta_{(j)} = E_{(j)} - E_{eq.} = E_{(j)} - E_{(j=0)} \quad (1.5)$$

where E(j) is the potential that the electrode acquires upon application of a specific current density (j). Reaction overpotentials are, therefore, a loss with respect to the thermodynamic potential and should be minimized in absolute value when possible. The overpotential at a specific current density depends on a series of different parameters, including the nature of the redox reaction and the reagents and

products concentration, the mass transfer parameters between the bulk electrolyte and the electrode interface, the nature of the electrode material, the electrolyte composition and the temperature.

An electrochemical cell necessarily exhibits an internal ohmic resistance (R_{int}) which is the sum of ionic resistances (electrolytes and ion exchange membrane(s) and electronic resistances (solid electrode, external circuit and the contact resistance from their respective connections). Consequently, a current flowing through the electrochemical cell causes an additional energy loss with a corresponding ohmic drop which increases the voltage of an electrolysis cell, or decreases the voltage of an electrochemical power source (fuel cell) (Allen J. Bard and Faulkner 2001). This ohmic drop (in Ω) is the product of the applied current and the internal resistance of the cell:

$$\text{Ohmic drop} = I \times R_{int} \tag{1.6}$$

The magnitude of the ohmic drop is particularly important since it can substantially impact the voltage and, therefore, the energy efficiency of the system. An internal resistance that is too high can considerably impede the development of an electrochemical process (Prévoteau et al. 2020). In reactions where a solid product is formed, for example in electrochemical sulfide oxidation with S^0 formation, the solid particles can insulate the active electrode surface area (see paragraph 1.4.2) or precipitate on the ion-exchange membrane, the electrochemical cell can suffer from a rapid increase in internal resistance (see Chapter 3). It is therefore important to quantify internal resistances, for example via the current interrupt method (Allen J. Bard and Faulkner 2001). Since the ionic resistance often represents a substantial fraction of R_{int}, the latter can be decreased by i) decreasing the distance between the anode and the cathode, ii) using more conductive membranes or iii) using more conductive electrolytes. In the latter lies the advantage of spent caustic streams (SCS), in contrast to domestic wastewater, when they act as electrolytes in electrochemical wastewater treatment (see paragraph 1.4.2 and Chapter 4). Whereas higher current densities allow for higher removal rates, they necessarily increase the ohmic drop proportionally (assuming R_{int} is invariant within the range of current considered).

The ohmic drop is also an important concept to consider when studying electrochemical reactions on a single electrode, i.e. when focusing on a half-cell of the electrochemical setup. The applied, or recorded, potential (E_{rec}) of the working electrode will include an ohmic drop contribution that is proportional to the uncompensated resistance R_u present between the working electrode and the reference electrode (due to the electrolyte present between them). Thus, the recorded potential can be corrected to obtain the real working electrode potential (E_{real}):

$$E_{real} = E_{rec} - i \times R_u \tag{1.7}$$

where the current follows the aforementioned convention, i.e. positive for an anode ($E_{real} \leq E_{rec}$) and negative for a cathode ($E_{real} \geq E_{rec}$). It is recommended to limit the amplitude of Ru by positioning the tip of a reference electrode in close vicinity to the working electrode, as long as the mass transfer properties from and towards the electrode surface are not substantially impacted.

1.4.1.4 Efficiencies of the electrochemical process

The efficiency of an electrochemical process is based on the efficiency with which charge is transported through the electrochemical cell and is facilitating the electrochemical reactions. This is described by Faraday's law, that relates the amount of electrochemical reactions conducted at an electrode to an amount of charges exchanged through the electrochemical cell (Allen J. Bard and Faulkner 2001). Based on Faraday's law of electrolysis, the coulombic efficiency (also called "faradaic efficiency" or "current efficiency") can be defined as the ratio of output charges of interest to the input charges. For electrolysis, it corresponds to the amount of charge actually involved in the electrochemical reaction(s) of interest divided by the amount of charges that actually crossed the electrolysis cell:

$$CE\ (\%) = \frac{n \times F \times \Delta m}{\int_0^t I(t) \times dt} \tag{1.8}$$

where CE (%) is the coulombic efficiency, Δ_m is the change in the number of moles (mol) of the redox compound of interest during the electrolysis time dt (s) and I is the applied current (1 A = 1 C s^{-1}) .

In the same way, in an electrochemical cell the energy efficiency is used to describe the energy output of the system compared to the energy input. The energy efficiency of the process will highly depend on the internal resistance of the cell, as explained in section 4.1.3, as the higher the losses in the electrochemical cell, the lower the energy efficiency of the process will be. The energy efficiency simply describes how much of the energy input, in an electrolysis cell for example, ends up in the desired reaction, rather than side reactions or ohmic losses in the system. The energy efficiency will thus be the product of the voltage and current efficiencies:

$$EE = \frac{E_{eq}}{E_{cell}} \times CE \tag{1.9}$$

Where E_{eq} is the cell voltage at equilibrium and E_{cell} the cell voltage obtained under operation at a specific current density (Klans Jüttner 2007).

The operational performance of the electrochemical cells is usually evaluated based on the removal rate (with respect to an electrode surface or a reactor volume), the removal efficiency or product recovery as well as on the power consumption by an electrolysis cell or the power output of a fuel cell.

As in electrochemical processes the addition of chemicals is limited to the minimum and the only actual input is the energy inpput, the energy efficiency of the process will determine the cost efficiency of the process. In both cases, the power input/output is given by a combination of Joule's law with Ohm's law (Allen J. Bard and Faulkner 2001; Logan et al. 2006):

$$P = I \times E_{cell} \tag{1.10}$$

where P is the power (W) and E_{cell} is the cell voltage (V). The operational costs of electrochemical treatment are directly related to the power consumption of the electrochemical cell. It is, therefore, of utmost importance to minimize this power consumption. In an electrolysis cell, this can be done by reducing the cell voltage, by decreasing the distance between the two electrodes, or by increasing the electrolyte conductivity, among other measures.

1.4.2 Electrochemical sulfide oxidation

Sulfide oxidation to S^0 readily occurs at a low potential ($E_{eq} = -0.419$ at pH 12, Table 1.2), possibly allowing for low operational voltages i.e. energetically attractive processes. In addition, most of the waste streams that contain high concentrations of sulfide, excluding domestic wastewater, come with a high conductivity, which promotes them as ideal candidates for electrochemical processing. These are probably two of the reasons that electrochemical treatment for hydrogen sulfide removal was introduced as an application of environmental technology, already in the early 80s (Nozaki 1982; Winnick et al. 1984). Studies on the effect of sulfide oxidation on different electrode materials, and vice versa, initiated the field of direct electrochemical desulfurization around 50 years ago (Hamilton and Woods 1983; Ramasubramanian 1975). The interest in this application for sulfide pollution treatment was boosted by the fact that electrochemical treatment allows for on-site recovery of sulfur compounds (e.g. S^0 and H_2SO_4), or electrolysis side-products (H_2 gas, caustic soda (NaOH) (Dutta et al. 2008; Rabaey et al. 2006; Vaiopoulou et al. 2016), ultimately resulting in the minimization of the operational costs (Chatzisymeon et al. 2013; Pikaar et al. 2015; Rankin et al. 2010).

Electrochemical sulfide treatment comprises a combination of oxidation processes that can be direct (i.e. at the electrode/electrolyte interface) and indirect (homogeneous redox process in solution). In the first case, the sulfide is electro-oxidized at the electrode surface. In the second case, the oxidation proceeds through anodic production of oxidative intermediates such as oxygen or chlorine which can further oxidize sulfide in solution (Bockris 1972; Feng et al. 2016; Pikaar et al. 2011a). The electrode material holds a crucial role in selecting for direct or indirect oxidation. Among the first materials tested for sulfide oxidation where carbon based electrodes, due to their high selectivity for direct sulfide oxidation towards S^0 and their low cost (Anani et al. 1990; Ateya et al. 2005). On the downside, S^0

particles are insulating and can cover the electroactive sites of the anode, ultimately inducing passivation (A. Chen and Miller 2004; Feng et al. 2016; Miller and Chen 2006). Therefore, later, studies with metallic electrodes emerged, in an attempt to tackle this hindrance of oxidation and thus of the overall process efficiency, by favouring indirect sulfide oxidation (Feng et al. 2016). Indirect oxidation enables maintaining a higher current density, as the mass transfer of sulfide to the anode surface may be diffusion-limited even under well-mixed conditions. However, O_2 and Cl_2 are generated at higher potentials compared to sulfide oxidation, resulting ultimately in a higher cell voltage and thus a lower energy efficiency. In addition, indirect oxidation can result in the formation of halogenated toxic byproducts, that can limit the application of this method for treatment of complex wastewaters. Extensive discussion has been conducted so far in literature on whether indirect or direct sulfide oxidation should be promoted (Pikaar et al. 2015), without however considering the fact that both processes can be simultaneously taking place in a galvanostatically operated cell, under a wide range of potentials (Table 1.2). Striking a balance between long-term, unpassivated operation and high sulfur recovery efficiency is still a challenge, as the distribution of the final sulfide oxidation products will depend upon a diverse set of parameters, such as the nature of the electrode and the electric input (current density or potential), the sulfide concentration, the convection and thus the reaction configuration, the pH and composition of the anolyte (S. Song et al. 2008; Vaiopoulou et al. 2016).

1.4.3 Electrochemical treatment of sulfide containing waste streams

Electrochemical sulfide treatment has been tested in a large spectrum of synthetic, and in some cases, real wastewater, however full-scale applications have not been yet applied, mainly due to the complexity that sulfur generation and precipitation brings along in the electrochemical cell operation. Lab-scale electrochemical desulfurization systems have been tested for a wide range of liquid waste streams, including tannery wastewater (Rajalo and Petrovskaya 1996; Szpyrkowicz et al. 2005), pulp and paper processed water and alkaline sulfidic streams (K. Kim and Han 2014; Vaiopoulou et al. 2016; Longyao Wang et al. 2015), geothermal brines (Ateya et al. 2003; Ateya and Al-Kharafi 2002; El-Sherif et al. 2010; Rankin et al. 2010), domestic wastewater (Pikaar et al. 2011a, 2011b, 2012) and mixed liquor of anaerobic digesters (H. Lin et al. 2016). The deterioration of the anode material as a result of sulfide oxidation is a common phenomenon reported in desulfurization studies (Al-Kharafi et al. 2010; Behm and Simonsson 1999; Miller and Chen 2006). Therefore, extensive research has been dedicated to selecting electrode materials that would exhibit both electrocatalytic activity towards sulfide oxidation (low overpotential), and high stability (Table 1.4).

Table 1.4 – Electrochemical sulfide removal performance when treating sulfur contaminated wastewaters, with different anode materials

Cell configuration	Anode material	Electrolyte (T / pH electrolysis)	Applied current density or potential / E_{AN} (vs SHE)	Reference
Undivided polarization cell	Graphite disk	Synthetic geothermal brines (25 °C / 12)	−0.8 to +1.4 V	Ateya et al. 2003
Undivided glass cell	Ti/RhO_x–TiO_2, Ti/PdO–Co_3O_4, Ti/PbO_2, Ti/Pt–Ir	Tannery wastewater (n.a. / ~8)	200 to 400 A m^{-2}	Szpyrkowicz et al. 2005
Pyrex beaker and glass cell	Boron Doped Diamond (BDD)	Synthetic sour brines (n.a. / ~13)	160 to 1300 A m^{-2}	Waterston et al. 2007
Two chamber (separated by CEM)	Carbon fibre brush	Synthetic (21 °C / 7)	11.9 A m^{-2}	Dutta et al. 2009b
Pyrex beaker	Ti_4O_7 (Ebonex®)	Synthetic sour brines (n.a. / ~13)	100 A m^{-2}	El-Sherif et al. 2010
Undivided polarization cell	Polycrystalline Pt	Synthetic (25 °C / 9 – 12)	−0.95 to +0.80 V	Al-Kharafi et al. 2010
Two chamber (separated by CEM)	Ta/Ir, Ru/Ir, Pt/Ir , PbO_2 and SnO_2 coated Ti	Domestic wastewater (~25 °C / 7.5)	100 A m^{-2}	Pikaar et al. 2011b
Two chamber (separated by microporous membrane)	Ti/RuO_2	Synthetic alkaline medium (20 °C / 13)	250 A m^{-2}	Wang et al. 2015
Two chamber (separated by CEM)	Ta/Ir coated Ti	Synthetic alkaline spent caustic streams (SCS) (25 °C	100 to 300 A m^{-2}	Vaiopoulou et al. 2016

		/ 14)		
Rotating cylinder reactor (separated by CEM*)	Pb coated Cu	Synthetic alkaline medium (80 °C / 10)	−0.6 to +1.0 V	Fornés and Bisang 2017
Undivided glass cell	GF-Mn_xO_y	Real sewage (24 °C / 8.2)	+0.4 V	(Sergienko and Radjenovic 2020)
Two chamber (separated by CEM)	Ir MMO	SCS produced in chemical industry (25 °C / >12)	300 A m^{-2}	This work, Chapter 4

CEM: Cation Exchange Membrane

Extensive research has been dedicated to the electrochemical treatment of alkaline sulfidic streams (SCS). Main reasons are their remarkably high sulfide content (0.5 – 4 wt% sulfide-S) and the fact that the current treatment methods are financially and environmentally (paragraphs 1.1 and 1.4) problematic, both of which are a hurdle for petrochemical refineries, the chemical manufacturing and the pulp and paper industry (Alnaizy 2008; Pokhrel and Viraraghavan 2004). Due to the high sulfidic content and the highly alkaline nature (pH > 13) of these streams, biological treatment is hindered, while the currently employed chemical methods require extreme operational conditions (125 < T < 320 °C and 0.5 < P < 20 MPa), such as for wet oxidation (Hawari et al. 2015; Zermeño-Montante et al. 2011). Moreover, the key component, caustic soda, is not recovered with the conventional methods. Instead, electrochemical treatment performs efficiently at ambient conditions, allows for recovery of chemicals and is highly adjustable to variable operational conditions (Chaplin 2019). At last, an additional motivation for the electrochemical treatment of industrial streams is their typically high conductivity (600-800 mS cm^{-1}) (Chapter 4), that makes them an attractive electrolyte, as it reduces the ohmic losses in the electrolysis cell and thus decreases the overall power input required to drive the process (Ateya et al. 2003).

1.5 Objectives and outline of the thesis

Pollutants are inherent to waste streams and a study of their nature, their effects on process efficiency and the financial success of waste valorisation applications is a prerequisite for future large-scale applications. This thesis centers around H_2S as the compound of interest, since its corrosive and toxic properties negatively affect the two technologies of interest here, electrochemical technology and gas fermentation. The objective of this thesis is to examine how electrochemical treatment can offer a sophisticated and potentially sustainable solution, not only for gas clean-up, but also for simultaneous recovery of chemicals, useful in upstream and downstream processing (Figure 1.5). That was studied by coupling two reactor concepts: 1) an electrochemical cell for simultaneous sulfide (HS^-) oxidation and sodium hydroxide (NaOH) and hydrogen gas (H_2) recovery and 2) a gas fermenter for carbon dioxide (CO_2) conversion to organic acids with H_2 gas serving as electron donor.

In **Chapter 2** the continuous absorption of an H_2S loaded gas stream in a NaOH liquid stream via a gas absorption column was simulated aiming to establish the operational limits for maximum H_2S absorption with minimum NaOH consumption. Next, the simulated liquid stream output, product of the gas absorption process, was treated in a lab-scale electrochemical system for continuous H_2S removal as S^0 with simultaneous recovery of NaOH. Ultimately, the aim was to suggest a gas absorption/electrochemical treatment train for continuous gas clean-up and chemicals production while limiting operational interference to the minimum. **Chapter 3** covers the study of certain limitations that electrochemical sulfide removal faces and focuses on the deterioration of the

electrochemical equipment due to the formation of S^0 during the process, but also due to the corrosive properties of sulfide (H_2S/HS^-). The electrode lifetime is especially limited by the accumulation of S^0 and the aggressive nature of H_2S/HS^-, therefore, six commercially available electrode materials (Ir Mixed Metal Oxide (MMO), Ru MMO, Pt/IrOx, Pt, PbOx and $TiO_2/IrTaO_2$ coated titanium-based electrodes) were tested for the impact of the electrocatalyst on sulfide removal and final product of sulfide oxidation, during the electrochemical treatment process. The stability of the electrocatalyst under high sulfide concentrations (50 mM Na_2S) and high alkalinity (pH>12) were also determined. In **Chapter 4**, the knowledge gained in the lab tests for electrochemical H_2S removal and NaOH recovery were verified using an industrial stream, to prove the industrial relevance and the scalability of the process. The electrochemical treatment of SCS from a chemical manufacturing industry was studied in an electrolysis cell, where anodic HS^- removal and cathodic NaOH, devoid of sulfide, recovery took place simultaneously as a function of the applied current density. The techno-economic viability of the process was proven, based on the low energy requirements for NaOH recovery and the avoidance of H_2O_2 otherwise used for sulfide oxidation.

In order to determine relevant pretreatment approaches for industrial off-gasses containing H_2S that allow for biological valorisation, the second section of this thesis focuses on determining the limits of bacteria exposed to H_2S containing gasses. In **Chapter 5**, the limits of the H_2S toxicity to bacterial cultures relevant for chemical building blocks production through gas fermentation were studied. The toxicity limits were tested in batch experiments using a mixed homoacetogenic culture studied under total dissolved sulfide concentrations ([TDS]) between 0 and 5 mM and pH between 5 and 7. The extent of inhibition was evaluated based on acetate production rates and microbial growth, while community composition transitions as a stress response were also examined. **Chapter 6** extends the investigation of the H_2S toxicity effects to a larger scale. A 10 L fermenter comprised of a robust acetogenic community was continuously sparged with a H_2/CO_2 gas stream and continuously produced acetic acid as the main metabolic product. Additionally, the study of long-term vs transient toxicity effects on the recovery of bioproduction and bacterial recovery time was studied as well as the differentiation of bacterial and archaeal response to the applied H_2S stress. Finally, a sustainable approach for electron donor supply in CO_2 fermenters was highlighted in this study, by electrolytically produced H_2 using an on-site, membrane divided, electrochemical cell. **Chapter 7** discusses the perspectives of the electrochemical technologies fit for gas clean-up and bioproduction, within the general concept of electrification and sustainability.

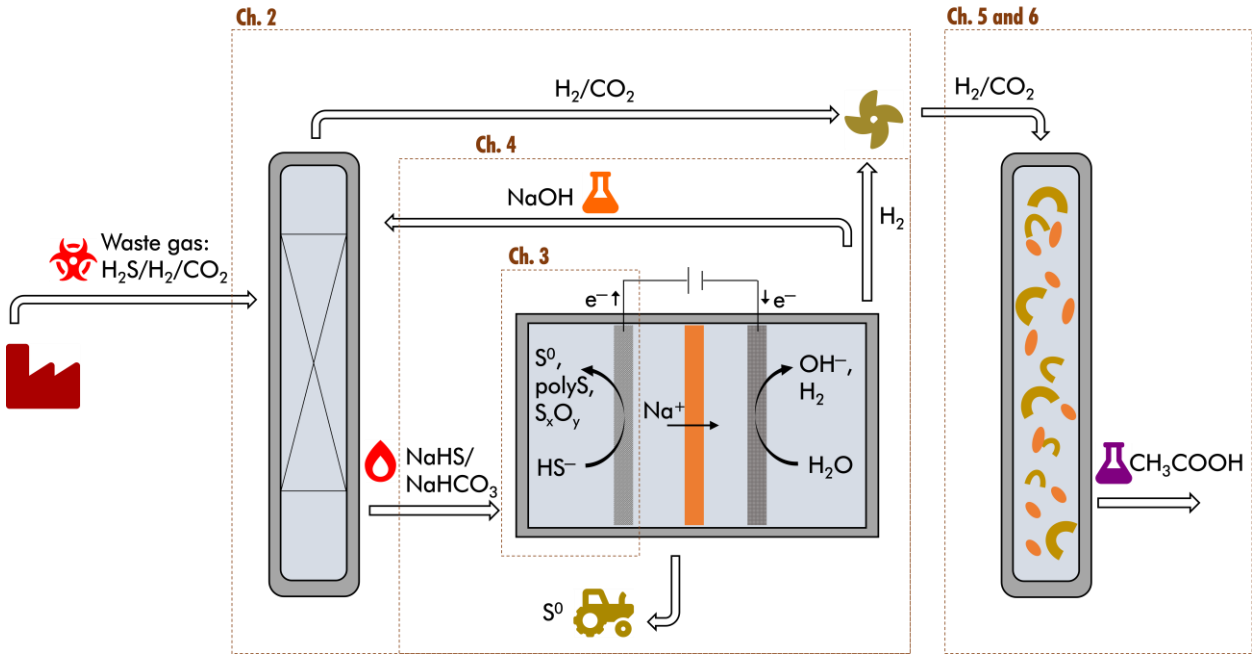

Figure 1.5 – General outline of this thesis, linking the six chapters and demonstrating the integration of the three processes for waste gas valorisation with electrochemical treatment as the main process

CHAPTER 2

Electrochemical control of gas absorption

Adapted from:

Eleftheria Ntagia and Korneel Rabaey. Electrochemical scrubbing liquid (NaOH) regeneration from scrubber derived sulfidic spent caustic streams (SCS) (Manuscript in preparation)

Abstract

The production of power with e.g. geothermal power plants can lead to the production of CO_2 and H_2S containing gas streams at million ton level. Both compounds have a negative environmental impact if emitted, but simultaneously represent a great interest for recovery. Commonly applied gas absorption in concentrated sodium hydroxide (NaOH) solutions entail high operational costs while lacking the opportunity for resource recovery. In this study, a combination of Aspen Plus V11 software simulation and lab-scale electrochemical treatment was studied to suggest a system for continuous gas absorption with simultaneous gas clean-up and NaOH regeneration which in principle should harvest the energy comprised in the H_2S via production of H_2, and to minimize the input of chemicals. The gas exhaust of a geothermal power plant was used as model stream, containing 48.5% v/v CO_2 and 25.5% v/v H_2S. The simulation results provided a scrubbing solution with 48 g H_2S d^{-1} and 23 g CO_2 d^{-1} mass flow (0.5 M NaHS + 0.16 M $NaHCO_3$) directed for electrochemical treatment. A 90% H_2S removal was achieved with an energy input of 5.0 ± 0.1 kWh kg S^{-1}. A caustic solution with 46 g NaOH d^{-1} NaOH mass flow was recovered, devoid of S^0 precipitates, which would represent 60% of the NaOH solution mass flow originally used for gas absorption. Ultimately the study suggests a gas absorption-electrochemical treatment setup, for continuous gas clean-up and chemicals production in an attempt to limit operational interference to the minimum.

2.1 Introduction

Power production activities hold the lion's share in greenhouse gases (GHG) global emissions with 15 billion tonnes CO_{2eq} being emitted annually worldwide from electricity and heat production (Ritchie and Roser 2016). Even geothermal power production, generally considered a green energy source, releases about 122 kgCO_2 and between 0.05 and 9800 kg H_2S per MWh, with a current world installed capacity of 12 $\times$ 10^3 MWe (Basosi et al. 2020; Uihlein 2014). Non-condensable gases (NCG) and in particular CO_2 and H_2S are naturally present in geothermal fluids and upon electricity production they are collected in the condenser of the steam turbines, from where they are most commonly released in the atmosphere (Aradóttir et al. 2015; Ingimundarson et al. 2015). The extent of carbon and sulfur emissions can be highly variable depending on the geology of the geothermal fluid extraction site (Anderson and Rezaie 2019; Karlsdottir et al. 2020; Tomasini-Montenegro et al. 2017). Carbon emitted into the atmosphere contributes to global warming, but it is also a valuable source, that if captured, can re-enter the production cycle and contribute to new chemical production while replacing fossil carbon extraction for chemical production (Liew et al. 2016). Accordingly, H_2S emissions may lead to acid rain, which is reflected through the high acidification potential (AP) scored by geothermal power production in Life Cycle Assessment (LCA) studies (Asdrubali et al. 2015; Basosi et al. 2020; Bravi and Basosi 2014), but if recovered as elemental sulfur (S^0) can also present a low value resource for the production of commodity chemicals and fertilizers or even cosmetics (Chung et al. 2013).

More stringent environmental regulations call for CO_2 and H_2S emissions decrease, but the current gas abatement methods, mainly gas exhaust absorption in concentrated sodium hydroxide (NaOH) solutions (scrubbing) (Mamrosh et al. 2014) or re-introduction into the extraction wells (current pump-down approach) (Karlsdottir et al. 2020), miss recovery opportunities and add to the total operational costs (Niknam et al. 2020). Electrochemical technology can unlock the full potential of the two gases through recovery of the energy present in the H_2S to generate H_2 and S^0, and redirection of the cleaned CO_2 and the electro-produced H_2 to biosynthesis. The method relies on the simultaneous anodic oxidization of sulfide ($H_2S_{(aq)}/HS^-$) coupled to cathodic H_2 gas generation in a two-compartment electrochemical cell. At the anode, $H_2S_{(aq)}/HS^-$ is oxidized to elemental sulfur (S^0) and other sulfur oxyanions, while at the cathode water is reduced to hydroxide ions (OH^-) and hydrogen gas (H_2) (Vaiopoulou et al. 2016). In order to maintain electroneutrality, OH^- migrates from the cathodic compartment to the anodic compartment through an anion exchange membrane (AEM), or otherwise, sodium ions (Na^+) or protons (H^+) migrate from the anodic to the cathodic compartment through a cation exchange membrane (CEM), serving as a separator between the two electrode compartments (Jüttner 2007) (Figure 2.1).

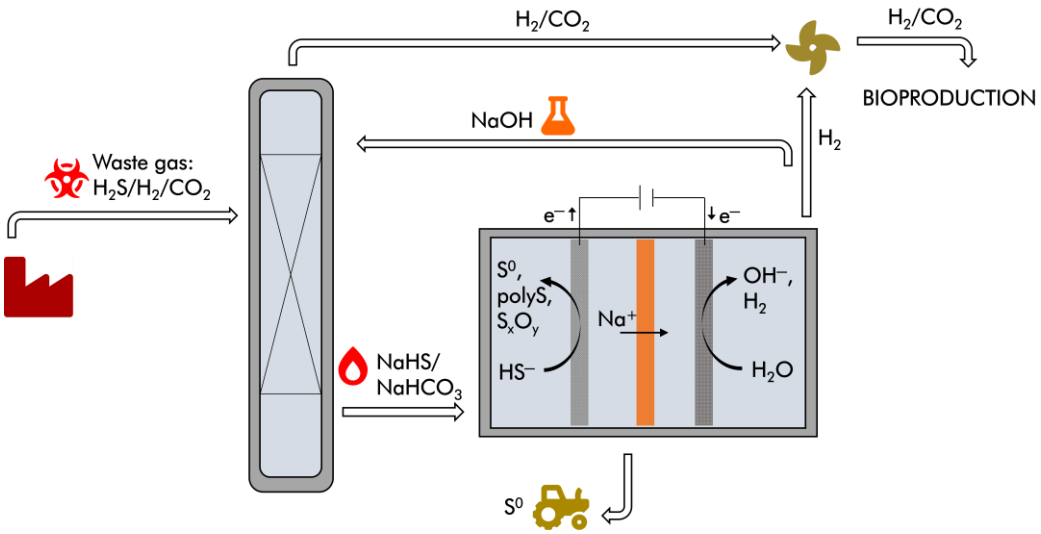

Figure 2.1 – Proposed process for waste gas clean-up and commodity chemicals recovery via electrochemistry, to enable boproduction downstream and sustain gas absorption upstream the electrochemical cell

A key-step in the attempt to valorise these gases is the selective absorption of H_2S over CO_2 in NaOH, which can be exploited with the selection of specific gas-liquid contact times and also with careful selection of the NaOH strength and temperature (Mamrosh et al. 2014; Niknam et al. 2020). The similar solubility of CO_2 and H_2S in aqueous NaOH solutions (Bontozoglou and Karabelas 1993; Lucile et al. 2012; J. Xia et al. 2000) still remains one of the key challenges in gas scrubbing, that raises concerns for production of carbonate salts and clogging of the installation. In addition, simultaneous CO_2 and H_2S absorption results in increased consumption of NaOH, a commodity chemical with a substantial contribution to the operational cost of gas abatement methods (Niknam et al. 2020).

In this study, the continuous absorption of a H_2S loaded gas stream in a NaOH liquid stream via gas absorption in a packed column was simulated with the Aspen Plus V11 software. The aim was to establish the operational limits for maximum H_2S absorption and minimum CO_2 absorption, combined with a minimum NaOH consumption and provide the basis for a synthetic SCS stream to be tested experimentally. Next, electrochemical treatment of the simulated liquid stream output was experimentally tested in a laboratory scale electrolysis cell, for simultaneous H_2S removal and NaOH regeneration. Aim was to study: 1) the sulfide removal efficiency and the products of sulfide oxidation, 2) the recovery of alkalinity (OH^-) and 3) the fate of CO_2 in the cell, along with 4) pH changes during electrolysis. Ultimately the study suggests a gas absorption/electrochemical treatment setup, for continuous gas clean-up and chemicals production while limiting operational interference to the minimum.

2.2 Materials and Methods

2.2.1 Aspen Plus Simulation

Prior to the electrochemical tests on sulfide oxidation, the Aspen Plus V11 software was used to simulate the spent caustic stream generated by a gas absorption column and serving as the electrolyte in the electrochemical cell. The exhaust of Hellisheidi power plant, the largest Icelandic geothermal power plant, with a 303 MWe and 267 MWth current capacity (Karlsdottir et al. 2020), mass flow rate 0.4 kg s^{-1} and increased H_2S content (Ingimundarson et al. 2015) was used as the model stream (Table 2.1).

Table 2.1 – Gas stream composition used in Aspen Plus simulation

Gas	CO_2	H_2S	H_2	H_2O
Volume concentration (% v/v)	48.5	25.5	24.4	rest

A structured packed column of 2 m packed height and 0.5 m diameter was used in the simulation for selective H_2S absorption in a concentrated NaOH stream (Bendall et al. 1983; Bontozoglou and Karabelas 1993). The column dimensions were selected as to allow for seamless absorption without column flooding. A rate-based calculation for a 5 stage column and -55 kW condenser duty were selected as inputs for the scrubbing process simulation. To describe the vapour-liquid equilibria, Aspen Plus uses the Electrolyte-NRTL (Non-random-two-liquid) model, that takes into account molecule-molecule, molecule-ion pair and ion pair-ion pair interactions to describe solutions that deviate from ideality (Moioli et al. 2013). A series of simulations with a 10 – 25 wt% NaOH solution, gas and liquid temperatures between 10 and 20 °C and liquid flows between 0.4 and 2 kg s^{-1} were tested. A list of reactions involved in the caustic scrubbing process were taken into account for the simulation (Table 2.2) , along with the coefficients based on vapour-liquid equilibria for weak electrolytes (A, B and C) (Edwards et al. 1978) and the kinetic parameters for the kinetic-controlled reactions (Cherif et al. 2016; Moioli and Pellegrini 2013) based on the equation relating the equilibrium constants dependency on temperature (Equation 2.1) and the power law expression used in Aspen Plus for the calculation of the kinetic-controlled reactions parameters (Equation 2.2). For reaction 3 the coefficients are not available in literature, therefore the equilibrium constant is automatically generated by Aspen Plus based on the Gibbs free energy (Cherif et al. 2016).

$$lnK_{eq} = A + \frac{B}{T} + C \times lnT \quad (2.1)$$

$$r = kT^n e^{(-\frac{E_a}{RT})}{}_{\iota=1}^{N} \Pi C_i^{a_i} \quad (2.2)$$

where r is the rate of reaction, k is a pre-exponential factor, T is the temperature, n is a temperature exponent, E_a is the activation energy, R is the universal gas constant, C_i is the concentration of component i and a_i is the stoichiometric coefficient of component i in the reaction (Cherif et al. 2016).

Table 2.2 – Equilibrium and kinetic-controlled reactions and the respective coefficents used in the Aspen Plus simulation

	Equilibrium reactions	A	B	C
1.	$2H_2O \leftrightarrow OH^- + H_3O^+$	132.899	-13445.9	-22.4773
2.	$H_2S + OH^- \leftrightarrow HS^- + H_2O$	147	-1930	-21.15
3.	$HS^- + OH^- \leftrightarrow S^{2-} + H_2O$	—	—	—
	Kinetic-controlled reactions	**k**		**Ea (kcal mol^{-1})**
4.	$CO_2 + OH^- \rightarrow HCO_3^-$	4.32×10^{13}		13.249
5.	$HCO_3^- \rightarrow CO_2 + OH^-$	2.83×10^{17}		29.451

2.2.2 Electrochemical cell configuration and operation

All electrochemical experiments were conducted with a two compartment electrochemical cell, with internal dimensions of 20 × 5 × 2 cm. A cation exchange membrane (CEM) (Fumasep© FKL-PK-130, Fumatech GmbH, Germany) was used to accommodate the two electrode compartments with internal volume of 200 mL each. An iridium mixed-metal oxide titanium-based (Ti) electrode (Ir MMO) (Magneto Special Anodes (an Evoqua brand), The Netherlands) was used as anode. A stainless steel thin mesh (Solana, Belgium) was used as a cathode. The two electrodes were planar with a projected surface area of 100 cm^2 (20 × 5 cm) and were positioned parallel to each other (distance between electrodes was ~8 mm). The current density is reported here with respect to the projected surface area of the anode (0.01 m^2).

The synthetic solution was first entering the anodic compartment, acting as anolyte. The anolyte outflow was directed to a 250 mL glass bottle, where the S^0 particles produced by oxidation in the anode were allowed to settle. Next, the solution was directed to the cathodic compartment, acting as

catholyte this time. Between the settling bottle and the cathodic compartment a non-woven cloth filter (Liplisse 3 Cloth, Libeltex, Belgium) was placed to separate colloidal S^0 particles from the electrolyte. Eventually the catholyte was directed to an outflow bottle (Figure 2.2).

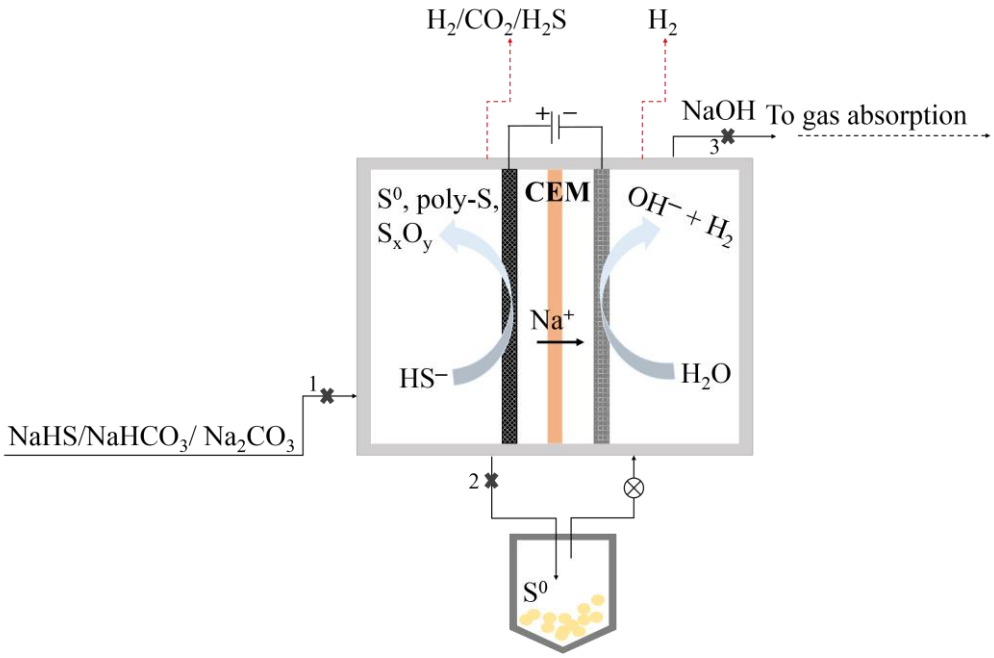

Figure 2.2 – The electrochemical cell setup used to treat synthetic scrubbing solution, the composition of which was dictated by the Aspen Plus simulation. The solution was entering the electrochemical cell from the bottom of the anodic compartment (sampling point 1), outflowing from the top (sampling point 2) and then was directed to the precipitation bottle. From there it was directed again to the bottom of the cathodic compartment. The recovered NaOH solution was outflowing from the top of the cathodic compartment (sampling point 3) and was directed to a collection bottle.

A DC power supply (Velleman LABPS3005 0−30 V, 0−5 A, Belgium) was used to control the electrochemical cell. The anode was selected as the working electrode and the anode potential is reported as the working electrode potential (E_{WE}). A saturated calomel electrode (SCE) (BAS Inc., Japan, +0.244 V vs. SHE at 25 °C) with a ceramic frit was used as reference electrode (RE) in the anodic compartment, in order to provide a frit more robust to the corrosive nature of HS^-. The anode potentials in this chapter are reported versus SCE. Prior to cell operation, the uncompensated resistance (R_u) between the anode and the reference electrode, and the cell resistance (R_{cell}) were measured with the current interrupt (CI) method (Allen J. Bard and Faulkner 2001) in 10 successive cycles (cycles of 50 ms at 100 mA followed by 50 ms open circuit with a recording period of 0.2 ms). The electrolyte used was synthetic SCS described in paragraph 2.2.3 and the resistances measured were lower than 1 Ω (Table A1.1). The anode potential (E_{WE}) and cell voltage (E_{cell}) were monitored

with the potentiostat by chronopotentiometry (CP). All electrochemical techniques were performed with a VSP potentiostat (Bio-Logic Science Instruments SAS, France).

2.2.3 Experimental procedure

A 0.5 M NaHS + 0.16 M $NaHCO_3$ solution with the pH adjusted at ~9 with NaOH was used as anolyte/catholyte, prepared according to the results of the Aspen Plus simulation, after downsizing the liquid mass flow by 5 orders of magnitude to accommodate to the experimental electrochemical cell. The synthetic solution was prepared in 4 L batches, after deaeration of the solution via N_2 gas sparging (~2 min for every 100 mL (Keller-Lehmann et al. 2006)). During the operation a 5 L gas bag filled with N_2 was connected to the anolyte/synthetic solution storage bottle, to ensure maintenance of anaerobic conditions. Both anodic and cathodic compartments were initially filled with 0.1 M NaOH (~ 25 mS cm^{-1}, to eliminate electrolyte resistance between the two electrode compartments) and at t=0 the synthetic solution was distributed in the anodic compartment. Experiments were conducted at 300 A m^{-2} current density, reported for 0.01 m^2 anode surface. The inflow rate was set to 2 mL min^{-1} to achieve 48 × 10^{-3} kg H_2S d^{-1} mass flow in the cell and the hydraulic retention time (HRT) was 5 h. Three experimental replicates were conducted based on which the averages and standard deviations of the values reported here were calculated. Each experimental period lasted 10 h, which was dictated by two initial experimental runs that were terminated at 10 h due to heavy production and precipitation of S^0 particles in the electrochemical cell and in the tubing connections (these tests are not included in the results presented here). Prior to the experiments an open circuit potential (OCP) test was conducted to evaluate the HS^- removal not induced by applied current. The results indicated no sulfide removal induced by chemical oxidation (contact of the anolyte with atmospheric air) and no further changes in the anolyte and catholyte during OCP conditions (Figure A1.1).

2.2.4 Analytical methods

The procedure that was followed for the CO_2 analysis was a commonly applied acidified headspace method (Åberg and Wallin 2014), in which the dissolved inorganic carbon (DIC) from an acidified liquid sample is completely released as CO_2 in the headspace of a vacutainer and is measured based on the constructed calibration curve (Figure A1.2) and the pH and temperature of the liquid sample. However, due to the additional presence of H_2S/HS^- in the samples the method was tested with both gases present in the liquid phase and the calibration curve was prepared with standards containing both HCO_3^- and HS^-. The samples were added in 12 mL Exetainer® Vials via a pierceable chlorobutyl septum (Labco Limited, United Kingdom), where 1mL of a 3 M H_2SO_4 solution was added prior to sample addition and next, the headspace was evacuated and further exchanged with helium (He) gas, through a headspace flushing process. The calibration curve was prepared with

0.16×10^{-3}, 0.8×10^{-3}, 4×10^{-3}, 20×10^{-3} and 100×10^{-3} M $NaHCO_3$ and NaHS standard solutions (Figure A1.2). The gas-phase composition in the vials of both the calibration curve standard samples, as well as the experimental samples was analysed with a Compact Gas Chromatograph (CGC) system (Global Analyser Solutions, Breda, The Netherlands) equipped with a Molsieve 5A pre-column, a Porabond column (CH_4, O_2, H_2 and N_2) and a Rt-Q-bond pre-column and column (CO_2, N_2O and H_2S). The concentrations of the gases were determined by a thermal conductivity detector. The total pressure of the vial headspace was measured with a UMS-Tensiometer (Infield 7) device.

The samples were analysed for pH, alkalinity and conductivity according to the standard APHA methods for water and wastewater sample analysis (APHA et al. 1999). The alkalinity of the samples was measured with 1 N HCl titration between the pH setpoints of 8.3 (carbonate alkalinity) and 4.5 (total alkalinity) and the bicarbonate alkalinity was calculated as the product of the total alkalinity minus the carbonate alkalinity (Greenberg et al. 1992). All alkalinity results are presented in eq L^{-1}.

2.2.4.1 Sulfur samples analysis

Samples for sulfur components were treated with Sulfide Antioxidant Buffer (SAOB) (Keller-Lehmann et al. 2006) by adding 10% buffer in the total sample volume. For the sulfur samples dilutions MQ water preciously sparged with Ar was used. Samples for sulfide (HS^-), sulfite (SO_3^{2-}) and thiosulfate ($S_2O_3^{2-}$) were analysed with a 930 Compact Ion Chromatograph Flex with Professional UV/VIS detector Vario (part of the Dual Channel IC), equipped with a Metrosep A Supp 15 – 150/4.0 column and a Metrosep A Supp 15 Guard/4.0 guard column (Metrohm, Switzerland). As eluent a 3.5mM Na_2CO_3 + 3mM $NaHCO_3$ solution was used. For sulfate (SO_4^{2-}) and anions analysis a 930 Compact IC Flex with chemical suppression and conductivity detector, equipped with a Metrosep A Supp 5-150/4.0 (61006520) column and a Metrosep A Supp 4/5 Guard/4.0 (61006500) guard column (Metrohm, Switzerland) was used, with 1.0 mM $NaHCO_3$ + 3.2mM Na_2CO_3 eluent. Samples for cations were analysed with a similar to the anions analysis IC, with a 1,7 mM HNO_3 and 1.7 mM DPCA (dipicolinic acid) eluent solution.

2.2.5 Calculations

The S^0 formed was calculated as the difference between the initial sulfide added in the electrochemical reactor (in moles) and the soluble sulfur species (i.e. sulfide, SO_3^{2-}, $S_2O_3^{2-}$ and SO_4^{2-}). The sulfide removal rates (R_{HS-}), the coulombic efficiencies (CE_{HS-}) and the energy input for sulfur removal were calculated based on the equations 2.3, 2.4 and 2.5, respectively:

$$R_{HS^-} = \frac{(n_{HS,to} - n_{HS,t})}{\Delta t} \quad (2.3)$$

where $n_{HS,t0}$ is the initial number of sulfide moles in the anolyte, $n_{HS,t}$ is the number of sulfide moles at each sampling time t and Δt the time of operation (s).

$$CE_{HS^-} = \frac{z*(n_{HS,to}-n_{HS,t})*F}{I*\Delta t} * 100 \quad (2.4)$$

where z = 2 is the number of electrons (e^-) involved in the reaction, F the Faraday constant (96,485 C mol^{-1}) and I the applied current (A). The CE_{HS-} here was calculated according to the direct oxidation of HS^- to S^0 that would give a recoverable product, which is a 2 e^- process. The coulombic efficiency for SO_4^{2-} production (CE_{SO4}) was calculated based on the SO_4^{2-} production, measured with IC, considering that the HS^- oxidation to SO_4^{2-} is an 8 e^- process (this thesis, paragraph 1.2.2).

$$Energy\ input\ for\ sulfur\ species\ removal = \frac{E_{cell} \times I \times \frac{\left(\frac{10^{-6}}{3.6}\right) kWh}{J}}{Q_{m\_S,removed}} \quad (2.5)$$

where E_{cell} is the averaged cell voltage (V), I the applied current (A = C s^{-1}) and $Q_{m\_S,removed}$ is the averaged mass flow of sulfide removed from the influent (kg S d^{-1}).

2.3 Results and discussion

2.3.1 Aspen Plus simulation results direct the production of a high S and low C containing synthetic stream for electrochemical treatment

The Aspen Plus software was used here to simulate a gas absorption column and provide an elegant way to design a realistic synthetic scrubber solution, without operating a large scale gas absorption column in a lab environment. After multiple simulations to allow for the minimum possible absorption of CO_2 and maximum H_2S absorption, the flow of liquid stream selected was 1.8 kg s^{-1}, with a 10 wt% NaOH solution at 10 °C and provided at 1 bar. The gas stream temperature was 20 °C and 1 bar pressure. The results of the simulation provided the daily flows of the components of interest for the electrochemical treatment (Table 2.3).

Table 2.3 – Aspen simulation results for the gaseous and liquids inputs and outputs of the absorption column, presented in molar flows (mol s^{-1})

Gas/ion/water molar flow (mol s^{-1})	Gaseous input	Gaseous output	Liquid input	Liquid output
H_2S	3.310	0.001	—	0.000
CO_2	6.295	5.249	—	0.000
H_2	3.167	3.167	—	—

OH^-	–	–	4.500	0.003
Na^+	–	–	4.500	4.500
HS^-	–	–	–	3.166
S^{2-}	–	–	–	0.143
HCO_3^-	–	–	–	1.046
CO_3^{2-}	–	–	–	0.000
H_2O	0.208	0.260	89.924	93.322

The H_2S was effectively removed from the gas stream with a 99.97% absorption efficiency while a 16.62% of the CO_2 was co-absorbed alongside the H_2S, according to the simulation (Table 2.3). This leads to an outflow CO_2 flow of 5 mol s^{-1}, suitable for a downstream bioproduction process. A selectivity index 6 for the absorption of H_2S over CO_2 was calculated based on the equation provided in Niknam et al. (Niknam et al. 2020), which indicates that further optimization would be needed to aim for a higher selectivity index, up to values of 10 as reported previously in optimization simulation studies (Niknam et al. 2020). It should be noted here however, that the content of H_2S in the aforementioned study was only 2%, which can allow for selection of a lower strength NaOH absorption solution and therefore potentially decrease the CO_2 co-absorption.

Furthermore, it should be mentioned that the standard Aspen Plus software presents a deviation from experimental data, when CO_2 absorption in alkaline solutions is considered. The rate-based model, that was also selected here, takes into account mass transfer limitations, however mass transfer is described based on the film-theory. The latter has reportedly led to overestimation of the amount of CO_2 absorbed and therefore also of the heat released by the whole process. In literature a few approaches have been studied to tackle this limitation, in an effort to describe more properly the absorption phenomenon, as well as to include in the simulation the effect of the density and the viscosity of the alkaline solution. In particular, Moioli et al. suggested an external simulation subroutine to describe absorption with the Eddy-diffusivity theory, with verified simulation results that were closer to the experimental data (Moioli et al. 2013).

The daily molar flow for sulfur contained in the scrubbing liquid as HS^- , was used to calculate the number of coulombs needed daily, thus the current, to remove this sulfur amount electrochemically, assuming an 80% coulombic efficiency for sulfide oxidation towards sulfur formation. Next, the current applied was downsized by 2×10^5 times, in order to be able to provide the required current within the limits of a lab scale experimental system (0 – 5 A current output range of the power source). Subsequently, the flow of sulfur and subsequently of carbon in the system, were downsized by the same ratios.

2.3.2 Sulfide is removed continuously and S^0 is recovered, at 300 A m^{-2} and 1.83 ± 0.08 mol S L^{-1} d^{-1} loading rate

Sulfide (HS^-) was continuously provided in the electrochemical setup with a 1.10 ± 0.05 mol S d^{-1} molar flow rate (corresponding to 1.83 ± 0.08 mol S $L_{reactor}^{-1}$ d^{-1} loading rate) (Figure 2.3A) and was first directed to the anodic compartment. During the 10 h (2×HRT) experiment a stable HS^- removal rate and HS^- removal efficiency were obtained, with averages of 0.99 ± 0.03 mol S d^{-1} (Figure 2.6A) and 89.77 ± 1.88 %. The main product of the HS^- oxidation was elemental sulfur (S^0), precipitated first on the electrode surface and afterwards in the different compartments of the electrochemical cell (Figure A1.3). The heavy precipitation of S^0 is reflected through the high coulombic efficiency calculated for S^0 production (CE_{HS-}), which averaged 78 ± 4 % in the 10 h experiment (Figure 2.3B) and highlighted S^0 dominance over the other possible HS^- oxidation products. Electrochemical oxidation of HS^- to S^0 is a 2 e^- process, therefore in a galvanostatically controlled cell it will be the first reaction conducted as the more energetically favourable (this thesis, paragraph 1.2.2).

The HS^- not converted, was then directed with the flow to the cathodic compartment and was eventually released with the cathodic effluent, redirected to the gas absorption as scrubbing liquid (Figure 2.1), with a 0.08 ± 0.05 mol S d^{-1} flow rate (Figure 2.3A). Concurrently, 0.06 ± 0.04 mol SO_4^{2-}–S d^{-1} and 0.01 ± 0.01 mol SO_3^-–S d^{-1} were released with the reactor effluent. The high standard deviations observed for both SO_4^{2-} and SO_3^- flow rates are a result of the hysteresis in their production compared to S^0. As highlighted by the increase in the molar flow rate of these two sulfur oxyanions with the experimental time, initially S^0 was mainly produced and eventually SO_4^{2-} was consuming 37 ± 6 % of the e^- provided to the system (Figure 2.3B, CE for SO_4^{2-}, CE_{SO4}). In the first 4 hours of the experiment 24 ± 1 % of the e^- were consumed for HS^- oxidation to SO_4^{2-}, a more oxidized product following an 8e^- electrochemical reaction (this thesis, paragraph 1.2.2). However, observing the 3 sampling times (Figure 2.3B) a steady increase in the CE_{SO4} can be seen, as a result of the SO_4^{2-} concentration increase in the electrochemical cell. This CE_{SO4} increase added to a higher than 100% total CE% at 10 h experimental time. Thus, a possible contribution to this higher than 100% total CE%, with the low pH in the anodic compartment (pH = 2.6 ± 0.5 established at 8 and 10 h) excluding the scenario of polysulfides formation (Mao et al. 1991; Pourbaix 1966), is indirect oxidation of sulfide to SO_4^{2-} via anodic O_2 production or further oxidation of S^0 deposited on the electrode surface to more oxidized products (Behm and Simonsson 1997).

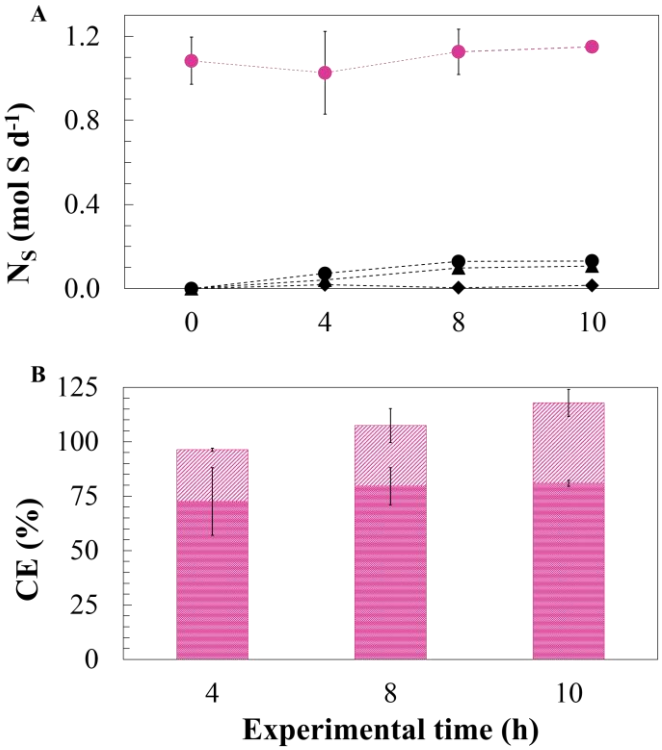

Figure 2.3 – Panel A: The sulfur molar flow rate (N_S in mol S d^{-1}) for HS^- in the inflow (pink circles) and HS^- (black circles), SO_4^{2-} (black triangles) and SO_3^- (black diamonds) in the outflow, cathodic effluent and Panel B: Coulombic efficiency (CE_{HS-} in (%) for S^0 production(trellis patterned pink bars) and CE_{SO4} in (%) for *SO_4^{2-} production (upward diagonal pink bars)), obtained during the 10 h of experimental cycle. The error bars represent the standard deviation of n=3 experimental replicates.*

A combination of pH < 7 and high current resulted in S^0 prevalence as the primary product of the HS^- oxidation and the increased S^0 precipitation (Figure A1.3B and A1.3C) (Behm and Simonsson 1997). The S^0 particles produced by anodic oxidation were precipitating partially in the bottom of the anodic compartment (Figure A1.3B) and then with the continuous electrolyte flow were directed to the connective bottle between anodic and cathodic compartment, and were precipitated (Figure A1.3C). The S^0 particles that remained suspended, were subsequently filtered through the filter cloth. The increased recovery of the removed H_2S in the form of S^0 except was for demonstrating the successful application of electrochemistry for waste gases treatment, also the main limitation of this experimental study due to clogging of the system. Therefore, it is suggested here that a scaled up application of electrochemical HS^- oxidation should abandon the regular channel flow cell design, commonly used in chloralkali industry and in lab-scale electrolysis cells and move towards a tank cell design (Arenas et al. 2020), that would allow for precipitation of the formed S^0 particles at the bottom of the tank, without interfering with the electrolyte recirculation flow.

Nevertheless, the decreased pH in the last experimental sampling times (pH < 3 at t= 8 and 10 h) raises concerns on the mechanism of HS^- removal. In order to comment on the mechanism, we attempted to set a sulfur balance across the electrochemical cell for the 10 h of the experimental period (in triplicate) (Figure A1.4), by collecting S^0 particles from the precipitation bottle, the filter connected to the outflow of the precipitation bottle, as well as partially, from the electrochemical reactor. Although in total average 13.5 ± 1.5 g of sulfur (HS – S) were removed in the 10 h, the solid sulfur collected was 5.2 ± 0.5 g. The total sulfur that would enter the reactor in the first 4 h was calculated at 5.9 ± 0.6 g. Therefore, we could not exclude the possibility that sulfide ($HS^-/H_2S(aq)$) was removed as S^0 mainly during the first 4 – 5 h (pH=6.3 ± 0.6 at t=4h) of the experimental period and then, due to the pH decrease in the anodic compartment (pH=2.7 ± 0.7), sulfide was also partially removed as H_2S gas from the reactor via volatilization. The aforementioned could also explain the higher than 100% total coulombic efficiency at 8 and 10 h sampling time (Figure 2.3 B). However, one should keep in mind that the collection of S^0 particles from the electrode surface or the tubing connections in the electrochemical cell was not possible, therefore the above described numbers and hypotheses for the sulfide removal should be considered with caution.

2.3.3 The electrochemical system recovers the alkalinity required for continuous gas absorption and CO_2 is completely removed from the system

Key contributor to the operational costs of gas absorption is the NaOH solution used as it is the single chemical input for the absorption and the electricity use for flows recirculation and heat exchange is limited (Mcintush et al. 2013). In the three experimental runs conducted here, NaOH was recovered through cathodic OH^- production, providing a clean, devoid of S^0 precipitates, NaOH solution (Figure A1.3D) for reuse in gas absorption. The total alkalinity (titration to pH 4.5) was used here to assess the effectiveness of the electrochemical cell in the recovery of NaOH used initially for the gas absorption and thus the recovery of sodium ions and the production of hydroxyl ions with cathodic water reduction (Figure 2.4A). The 2.26 ± 0.08 mol Na^+ d^{-1} flow entering the electrochemical cell were compensated at 8 h of operation, as the Na^+ outflow averaged 2.22 ± 0.22 and 2.25 ± 0.22 mol Na^+ d^{-1} at the 8 and 10 h sampling points (Figure 2.4A). The Na^+ were entering the electrochemical cell with the synthetic solution and the cathodic compartment through the CEM, to compensate for the flow of the electrons, used for sulfide oxidation. The total alkalinity of the scrubbing liquid entering the electrochemical system was at average 1.46 ± 0.01 eq d^{-1} and continuously 1.30 ± 0.07 eq d^{-1} of total alkalinity were outflowing from the cathodic compartment (Figure 2.4A). The lower total alkalinity outflowing the electrochemical cell is attributed to the partial removal of the absorbed CO_2 in the scrubbing liquid (Figure 2.5), by escaping the anodic compartment due to the decrease of pH to values lower than 4. The removal of CO_2 in this way resulted also in a minimum amount of CO_2 released with the produced NaOH solution, which averaged 0.01 ± 0.00 from the

0.53 ± 0.01 mol CO_2 d^{-1}, present in the CO_3^{2-} form considering the >12 pH of the cathodic effluent.

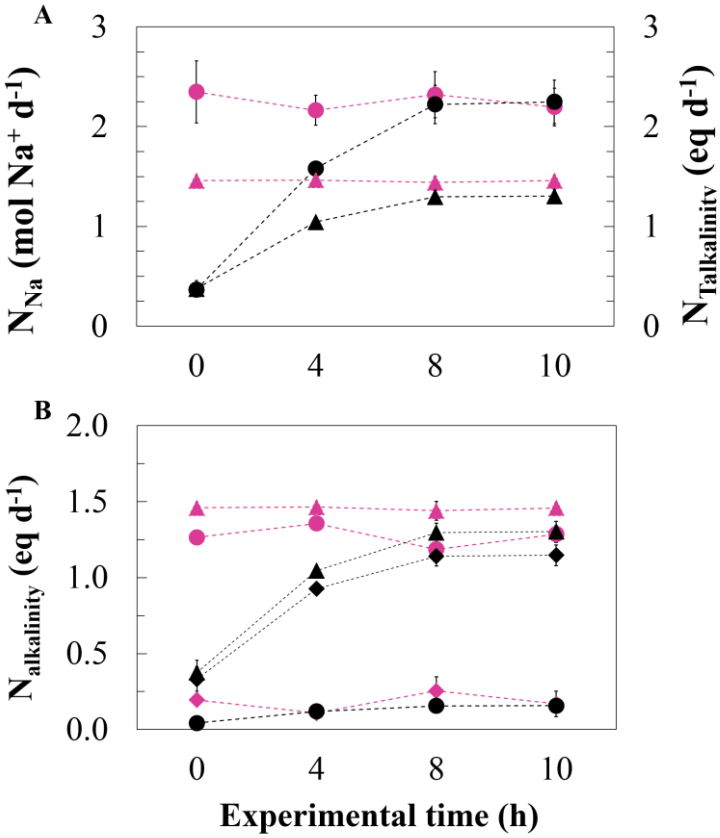

Figure 2.4 – Panel A: Sodium ions molar flow rate (N_{Na} in mol Na^+ d^{-1}) (circles, left axis) and total alkalinity flow rate ($N_{Talkalinity}$ in eq d^{-1}) (triangles) and Panel B: Alkalinity presented here as total alkalinity (in eq d^{-1}) (triangles), bicarbonate alkalinity (eq d^{-1}) (circles) and hydroxide alkalinity (in eq d^{-1}) (diamonds), evolution in the inflow (pink) and outflow (black) of the electrochemical reactor obtained during the 10 h of experimental cycle. The error bars represent the standard deviation of n=3 experimental replicates.

The synthetic solution containing carbonates, bicarbonates, hydroxides, but also sulfide ions is rather complex to distinguish the contribution of the individual alkalinities to the total with a titration at the two common alkalinity points (pH=8.3 and pH=4.5). Therefore, an attempt to calculate and present the two forms of alkalinity of interest for this system, bicarbonate and hydroxide alkalinity was calculated here (Figure 2.4B). In natural waters a number of factors can contribute to total alkalinity, one of them being sulfide ions (HS^-). Thus an interference with the bicarbonate analysis with the common titration method is expected (Lu Wang et al. 2014). This is demonstrated in the bicarbonate alkalinity result calculated for the synthetic solution, which averaged 1.27 ± 0.06 eq HCO_3^- d^{-1} for the 10 h of experiment for the three replicates (Figure 2.4B), although the result of the CO_2 headspace

analysis was 0.53 ± 0.01 mol CO_2 d^{-1} (equal to 0.53 ± 0.01 eq HCO_3^- d^{-1}) (Figure 2.5) which is in accordance with the HCO_3^- concentration in the synthetic solution.

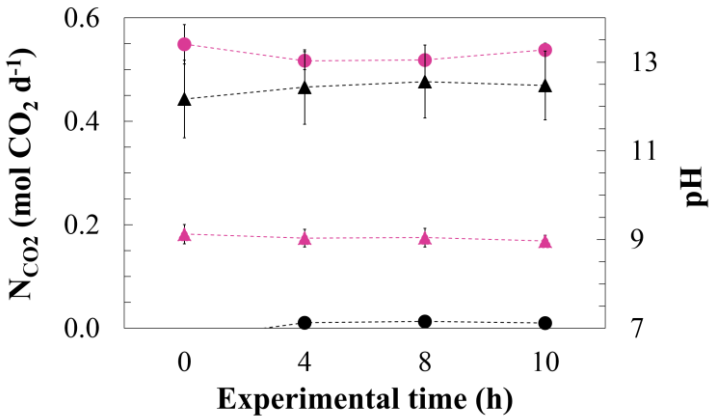

Figure 2.5 – Carbon dioxide molar flow rate (N_{CO2} in mol CO_2 d^{-1}) (circles, left axis) and pH (triangles, right axis) evolution in the inflow (pink) and outflow (black) of the electrochemical reactor obtained during the 10 h of experimental cycle. The error bars represent the standard deviation of n=3 experimental replicates.

The hydroxide alkalinity, calculated as the difference between the total and the bicarbonate alkalinity, outflowing from the cathodic compartment was at average 1.15 ± 0.07 eq d^{-1}, or differently, 1.15 mol NaOH d^{-1} could be distributed back to the gas absorption column. This is a more than 6 times higher NaOH flow compared to the inflow hydroxide alkalinity (Figure 2.4B), meaning that the electrochemical cell could successfully regenerate NaOH to be used on site for gas absorption. However, if this stream would be upsized by 2 × 10^5 times, the flow of produced NaOH would be 230 kmol d^{-1}, or, to be able to compare with Table 2.3, 2.66 mol s^{-1}. This means that with the electrochemical cell operated at the present mode, 60% of the NaOH initially used for gas absorption could be recovered. This lower than 100% recovery cannot be attributed to inefficiency of the electrochemical cell to recover NaOH, as from an incoming flow of 0.26 ± 0.01 mol OH^- d^{-1} the cell operation managed to provide 1.15 ± 0.07 mol OH^- d^{-1}, as outflow of the cathodic compartment. This lower, than initially used for absorption, resulting NaOH strength is mainly attributed to Na^+ consumed by non-converted HS^-, produced by oxidation SO_4^{2-} and HCO_3^-/CO_3^{2-} remaining in the electrolyte.

Therefore, a future system should be optimized towards minimizing even further the CO_2 absorption in the gas absorption unit, as well as increasing the residence time of the scrubber derived liquid in the electrochemical reactor to increase HS^- removal without increasing SO_4^{2-} production. The remaining CO_2 will end up in the regenerated NaOH as CO_3^{2-} since the pH of the electrochemical

cell outflow is 12.5 ± 0.8. The absorption of H_2S and CO_2 gases in Na_2CO_3, among other alkali solutions, has been studied and implemented as well. Both H_2S and CO_2 can be absorbed in Na_2CO_3 producing NaHS and $NaHCO_3$. Guo et al. (Q. Guo et al. 2018) have quantified the reaction rates of the two absorption reactions, commenting that the absorption of H_2S in Na_2CO_3 will take place 500 times faster than the CO_2. This difference, if exploited with a strategy similar to the one discussed in paragraph 2.3.1, can lead to further selective absorption of H_2S over CO_2. Further operation of the gas absorption column with the current, non-optimized system, would require a 40% compensation with a new NaOH solution, if the gas absorption column and the electrochemical cell were to run in parallel.

2.3.4 Stable operation at 6.51 ± 0.43 V cell voltage maintained during 10 h experiment

The electrochemical operation was stable during the 10 h experimental operation in tandem with the sulfide removal. The combination of the stability in these two parameters resulted also in a stable and relatively low energy input for the electrochemical sulfide removal achieved in the 3 experimental runs (Figure 2.6A). An average 6.51 ± 0.43 V cell voltage was obtained during operation under 300 A m^{-2} constant current density (Figure 2.5B). Accordingly, a stable anode potential (E_{WE}) was maintained during operation with an average 1.28 ± 0.07 V vs SCE. The ~10% increase of the E_{WE} between time 0 and 10 h (Figure 2.6B) can be attributed to the decrease of pH in the anodic compartment from an initial 12.05 ± 0.93, which quickly dropped to 6.34 ± 0.51 in 4 h of operation, to a final 2.57 ± 0.61 (Figure 2.5), which according to the Nernst equation would lead to an anode potential increase of 0.22 V (taking into account the difference between pH=6.34 and final pH=2.57) (Allen J. Bard and Faulkner 2001). The difference between the E_{WE} increase expected and the one recorded, can be attributed to pH differences between the bulk electrolyte and the electrode surface, temperature deviation in the lab environment and analytical errors. The stable anode potential and cell voltage during the operation suggest that no inactivation of the anode active surface or development of internal resistance differences due to membrane fouling from solids precipitation took place. Thus, a longer electrochemical operation could have been possible, was it not the blocking of the system with S^0 particles.

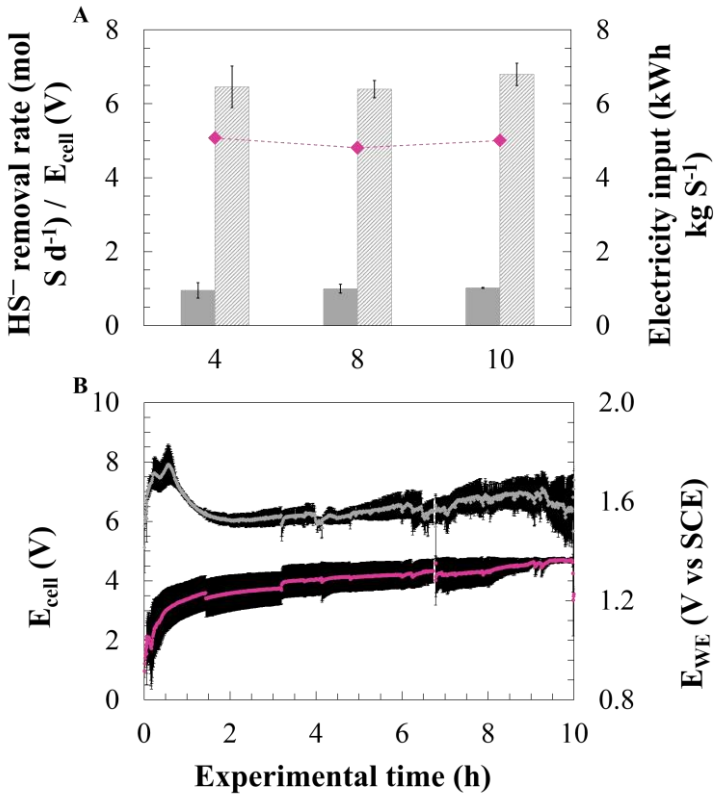

Figure 2.6 – Panel A: Sulfide removal rate (mol S d^{-1}) (full grey bars), cell voltage (V) (striped grey bars) and electricity input per sulfur removed (KWh kg S^{-1}) (black diamonds) and Panel B: Cell voltage (E_{cell}, in V) (grey line) and anode potential (E_{WE}, in V vs SCE) (pink line), averaged for the 10 h of experimental cycle. The error bars represent the standard deviation of n=3 experimental replicates.

An average 4.96 ± 0.11 kWh kg S^{-1} energy investment was required to remove sulfur efficiently from the electrochemical system for 10 h. Compared to similar previously tested systems, the cell voltage obtained here was higher (Vaiopoulou et al. 2016), due to the lower solution conductivity and due to the pH difference evolution between the anodic and cathodic compartments (Allen J. Bard and Faulkner 2001). The high sulfide content of this stream resulted in a continuous and increased electron donor availability in the system, leading to an energetically efficient process operation. Therefore, the only possibility for an efficient electrochemical sulfide treatment is continuous operation and well-designed S^0 precipitate separation system to establish a long-term operation.

2.4 Conclusion

This study was constructed aiming to simulate the selective H_2S absorption from a geothermal gas in NaOH and describe the role of electrochemical treatment in the recovery of the NaOH used for absorption, along with the recovery of the H_2S absorbed, as S^0. Using the Aspen Plus software a large-scale gas absorption column to treat 0.4 kg of gas per second was simulated and effectively downsized

to enable the recovery possibilities examination in a lab-scale electrochemical system. The electrochemical cell was operated continuously for 10 h with the main limitation of the experimental time being S^0 precipitation in the reactor and the connecting tubing. In the experimental time achieved here, the HS^- was removed from the scrubbing liquid (synthetic solution) with 90% efficiency, while producing 1.15 mol d^{-1} NaOH to be further used in continuous gas absorption. The electrochemical cell, controlled at 300 A m^{-2}, obtained and maintained a 6.5 V average cell voltage, which resulted in an average energy input of 5 kWh for the removal of 1 kg of sulfur entering the system. This value could be decreased with optimisation of the system and the environmental impact of the electricity provided could be compensated with renewable energy sources to power the electrochemical cell.

In this way, an up-scaled electrochemical system could continuously recover 60% of the NaOH solution used for gas absorption of an H_2S loaded gas stream. Key advantage of the tested system was also that no additional electrolytes, therefore chemicals, were needed for the operation of the electrochemical cell, as the scrubbing liquid was serving as both anolyte and catholyte. A future application of the proposed system should consider optimization of the gas absorption simulation for further minimization of the CO_2 absorbed, selection of an electrochemical cell design that would allow for efficient precipitation of S^0 without interference with the recirculation tubing, such as a tank cell design, and a sustainable solution for the compensation of the 40% of the NaOH flow still needed for continuous gas absorption. Finally, the effect of the remaining HS^- and CO_3^{2-} in the produced NaOH solution in the gas absorption process needs to be further studied, to verify whether the presence of CO_3^{2-} will aid further selectivity of H_2S absorption, or induce clogging upon accumulation of carbonate precipitates.

CHAPTER 3

Effect of sulfide on the electrode material

Adapted from:

Eleftheria Ntagia, Erika Fiset, Ligia da Silva Lima, Ilje Pikaar, Xu Zhang, Adriaan W. Jeremiasse, Antonin Prévoteau, Korneel Rabaey (2019). Anode materials for sulfide oxidation in alkaline wastewater: An activity and stability performance comparison. Water Res. 149, 111–119, doi.org/10.1016/j.watres.2018.11.004

Abstract

Electrochemical sulfide removal can be attractive as a zero-chemical-input approach for treatment of waste streams such as spent caustics coupled to caustic recovery. A key concern is possible decline in catalytic activity, due to passivation from deposited elemental sulfur (S^0) on the anode surface and stability limitation, due to sulfide oxidation under highly alkaline conditions. In this study, six commercially available electrode materials (Ir Mixed Metal Oxide (MMO), Ru MMO, Pt/IrOx, Pt, PbOx and TiO_2/$IrTaO_2$ coated titanium-based electrodes) were tested to investigate the impact of the electrocatalyst on the process efficiency in terms of sulfide removal and final product of sulfide oxidation, as well as to determine the stability of the electrocatalyst under high sulfide concentrations (50 mM Na_2S) and high alkalinity (pH>12). Short-term experiments showed that the catalyst type impacts the anode potential and the sulfide oxidation reaction products. Longer-term experiments under current densities up to 200 A m^{-2} showed a high differentiation in stability performance among the catalysts. Ru MMO was the most active towards sulfide oxidation with a coulombic efficiency of 63.2 ± 0.5% at an average anode potential of 0.92 ± 0.17 V vs SHE. Ir MMO was the most stable, preserving 100% of its original catalyst loading during the tests. The results demonstrated that Ru MMO and Ir MMO were the most suitable electrode materials for sulfide oxidation under highly alkaline conditions, while the need for establishing a good trade-off between activity, stability and cost still persists.

3.1 Introduction

Sulfide can be present in high concentrations in industrial wastewaters, such as geothermal brines (El-Sherif et al. 2010) and spent caustic streams (SCS) (Ateya et al. 2005; Dutta et al. 2008; Pikaar et al. 2015). The high alkalinity (5 – 12 wt% NaOH) and sulfidic content (0.1 – 4 wt% sulfide-S) of SCS limit the feasibility of biological treatment. Consequently, treatment of SCS mostly relies on chemical dosing, which incurs large caustic consumption and operational costs (Vaiopoulou et al. 2016). In this context, an interesting and chemical-free alternative method is electrochemical sulfide oxidation. In addition to its chemical-free nature, another advantage of the electrochemical method is the sulfide recovery in the form of elemental sulfur (S^0), along with the recovery of hydrogen gas (H_2), as potentially high value compound (Dutta et al. 2008; Rabaey et al. 2006; Vaiopoulou et al. 2016).

Electrochemical sulfide oxidation includes a variety of both direct and indirect sulfide oxidation reactions that can simultaneously take place under a wide potential range. In the case of indirect oxidation, sulfide is oxidized through intermediate oxidants ($OH\cdot$, O_2, Cl_2) that are anodically produced (Pikaar et al. 2011a). The final products of oxidation can be a mixture of S^0, polysulfides, sulfate (SO_4^{2-}) and thiosulfate ($S_2O_3^{2-}$) (Mao et al. 1991; Miller and Chen 2005; Pikaar et al. 2011b). The oxidation products depend on the electrode material used and the operational conditions, such as the sulfide concentration, the pH, the convection and the potential of the anode (Dutta et al. 2009; S. Song et al. 2008; Vaiopoulou et al. 2016). When S^0 is produced through direct sulfide oxidation (i.e. a 2-electron process), it is deposited on the anode surface (Vaiopoulou et al. 2016). As S^0 is an excellent insulator with a high resistivity ($\sim 10^{15}\ \Omega$ m), its deposition results in a decrease in the active electrode surface area (Fornés and Bisang 2017). This results in an increase of the anode potential, thus increasing the power requirements of the system, and ultimately results in complete anode passivation (Dutta et al. 2009). This phenomenon is typically illustrated during galvanostatic experiments, where a punctual and dramatic increase of the anodic potential reflects the start of O_2 evolution co-occurrence, after a threshold loss of the anode active surface area for sulfide oxidation.

A wide variety of electrode materials has been tested for anodic sulfide oxidation. Common carbon-based materials such as graphite plates (Anani et al. 1990) and carbon felt (Ateya et al. 2005) have low cost and although they mainly produce S^0, that can be recovered, suffer from electrode passivation, requiring surface regeneration (Dutta et al. 2009). A major disadvantage of carbon-based electrodes is that carbon can thermodynamically be oxidized to CO_2 from potentials as low as $E^0_{CO2/C} = 0.207$ V vs standard hydrogen electrode (SHE) (Fabbri et al. 2014). This can result in dissolution of the electrode itself, simultaneously with the onset of oxygen evolution at increasing levels of electrode passivation (Yi et al. 2017).

Non-carbon-based electrodes, such as titanium (Ti) oxide ceramic (El-Sherif et al. 2010), platinum (Kharafi et al. 2010; Ramasubramanian 1975) and nickel (Behm and Simonsson 1999) electrodes

have been investigated in industrial wastewater treatment applications, in particular for geothermal brines or white liquor from the pulp and paper industry. The reported drawbacks of the aforementioned electrodes include activity loss due to S^0 particles accumulation on the electrode surface, reduced kinetics towards sulfide oxidation (Lawrence et al. 2002; Waterston et al. 2007) and catalytic surface poisoning due to the formation of metal-sulfide films (Behm and Simonsson 1999; Kharafi et al. 2010; Miller and Chen 2006).

Considering the above limitations, Ti-based electrodes coated with a thin active layer of Mixed Metal Oxides (MMO) (Ch Comninellis and Vercesi 1991) have been proposed for treatment of sulfide containing sewage, since they possess high stability (Cherevko et al. 2016; Pikaar et al. 2011a) and a good performance towards sulfide oxidation (Pikaar et al. 2011b; Vaiopoulou et al. 2016). A consideration when using MMO electrodes is their high manufacturing costs as they employ rare metals as catalysts. Nevertheless, these electrodes present excellent electrocatalytic activity and stability compared to the so far examined carbon- and Pt-based electrodes (Katsounaros et al. 2014) in alkaline electrolytes and the alternative catalysts investigated at present have not yet been proven stable under real-life conditions (F. Song et al. 2018). So far, different noble metal coated and MMO electrodes, such as Pt/Ir, PbO_2, PdO/Co_3O_4 and $RhOx/TiO_2$ coated Ti-based electrodes, were tested for the electrochemical treatment of tannery wastewater with sulfide concentrations ranging between 5 and 10 mM (Szpyrkowicz et al. 2005). Depending on the electrode material, more than 90% sulfide removal was achieved in a 15-40 min electrolysis time, with indirect sulfide oxidation through oxygen being the most probable oxidation mechanism. The feasibility of electrochemical sulfide removal from sewage (i.e. ~ 0.3 mM sulfide) using 5 different MMO coated Ti-based electrodes, Ta/Ir, Ru/Ir, Pt/Ir, SnO_2 and PbO_2, was investigated at a current density of 100 A m^{-2}. Higher than 70% sulfide removal and coulombic efficiencies (CE) were achieved through indirect sulfide oxidation and without anode passivation (Pikaar et al. 2011b). Continuous sulfide oxidation in alkaline wastewater (~ 300 mM sulfide) was achieved at 200 A m^{-2} with Ir MMO anodes (Vaiopoulou et al. 2016). The sulfide removal reached 80% and the CE was higher than 68%, with SO_4^{2-} or $S_2O_3^{2-}$ as main products of indirect sulfide oxidation.

The above described studies highlight that several aspects drive the selection of the electrode material, including: (i) activity for sulfide oxidation in a specific alkaline stream; (ii) required electrode service life; (iii) concentration range of the sulfide and (iv) targeted product(s). While most studies on alkaline sulfidic waste streams have focused on proof of concepts for sulfide removal (Anani et al. 1990; Behm and Simonsson 1997; Mao et al. 1991; Selvaraj et al. 2016; Vaiopoulou et al. 2016) limited knowledge exists on the catalytic activity and stability of the proposed electrodes, certainly in relationship to each other. They do not provide a stability assessment or comparison of the performance of different electrodes. Monitoring of the sulfide oxidation side-products has not been conducted, except for the study of Vaiopoulou et al., but the electrochemical response to these (e.g.

anode potential shifts and evolution of anode coating) is not reported. A study on electrochemical sulfide oxidation from white liquor with high sulfidic content and high alkalinity was provided by Behm and Simonsson, where limited stability of an iridium-tantalum oxide coated titanium-based electrode was reported under operation at high current densities. Nevertheless, no surface analysis was conducted and only a single electrode material was tested.

Therefore, this study aimed to investigate the performance of different electrode materials under these harsh conditions. A series of batch and continuous tests were conducted to study the behaviour of the catalytic material (Ir MMO, Ru MMO, Pt/IrOx, Pt, PbOx and TiO_2/$IrTaO_2$), in highly alkaline (pH > 12) concentrated sulfidic solutions (50 mM). The electrodes were selected based on their high activity towards either the sulfide oxidation or the oxygen evolution reaction, depending on the catalyst employed, proven in previous studies. The different sulfide oxidation products were analysed to assess the activity of these materials. The stability of the electrodes was evaluated as the effect of operation at high current density (200 A m^{-2}), high alkalinity and sulfide concentration, on the catalyst loading of the electrodes. Through the combination of the above described tests, the impact of the catalyst choice on the sulfide oxidation and the impact of the sulfide oxidation in alkaline conditions on the catalytic layer were established.

3.2 Materials and methods

3.2.1 Electrochemical reactor setup

All electrochemical experiments were performed at ambient temperature (~ 25 °C) in a two-compartment custom-made glass reactor (Figure A2.1) (K. Guo et al. 2014). The reactor was closed by a circular Teflon cap (14 cm diameter, 1 cm thick), where influent and effluent connections enabled continuous inflow and outflow of the anolyte, and allowed for sampling. The cathode compartment was not sealed to avoid pressure build up due to the formation of H_2. Between the plastic cap and the glass anode compartment, a circular rubber sheet was used to seal the reactor and maintain anaerobic conditions.

The anodic chamber with a working volume of 700 mL accommodated three independent plate electrodes as working electrodes (WE). The cathodic compartment was equipped with a cylindrical stainless steel mesh counter electrode (Solana, Belgium, 2 cm diameter, 8 cm height). The anodic and cathodic compartments were separated by a PEEK-reinforced anion exchange membrane type Fumasep FAB-PK-130 with a thickness of 130 µm (FUMATECH BWT GmbH, Germany). All reported potentials refer to standard hydrogen electrode (SHE) but were measured with a Ag/AgCl (3 M KCl) reference electrode (ALS, Japan, + 0.210 V vs SHE at 25 °C) and a calomel (saturated KCl) reference electrode (Bio-Logic SAS, France, + 0.244 vs SHE at 25 °C), located in the anodic compartment. Uncompensated resistances between each WE and the reference electrode were assessed by a current

interrupt technique (CI) (see A2.2.1) (Allen J. Bard and Faulkner 2001). The uncompensated resistances are reported in Tables A2.1 and A2.2 for the activity and stability tests, respectively and were considered for the correction of the obtained anode potentials during the activity tests (Equation A2.1.1.3). The obtained potentials during the stability tests were not ohmic drop corrected, since continuous recording of changes in the ohmic drop during the long-term experiment was not possible. The anolyte was continuously mixed at a rotation speed of 100 rpm using a magnetic stirrer (Model F203A0160CR S/N 318450, Carl Roth, Italy) to create sufficient mixing.

3.2.2 Electrode materials

The Ir MMO, Ru MMO, Pt/IrOx, Pt, PbOx (Magneto Special Anodes (an Evoqua brand), The Netherlands) and $TiO_2/IrTaO_2$ by Yixing Entrustech Environmental Co., Ltd (China) were all made on Ti-based flat plates support with a surface area of 20 × 20 mm and 1 mm thickness. Since the catalyst loadings were all in the range of 5-15 g m^{-2} (except for PbOx, which had a loading of 150 g m^{-2}), we consider that the electrocatalytic properties are not affected by the loading but rather by the catalyst composition and electrochemical surface area (ECSA). The electrical connection of the electrodes was prepared for operational use as previously described (X. Zhang et al. 2017), by using an insulated copper wire as current collector. The wire (1.5 mm single core copper wire with PVC coating) was glued with silver paint (RS components Ltd, UK, Europe) to the one 20 × 20 mm side of the plate electrodes. The latter was subsequently completely insulated with water proof epoxy glue (TS10, THORLABS, Europe), as well as the 1 mm thick sides, thereby restricting the active electrode surface to only one 20 × 20 mm side. All parameters taking into account the surface area will be related to this 400 mm^2 geometric surface area.

3.2.3 Experimental procedures

3.2.3.1 Electrolyte preparation and sulfur species measurement

An aqueous solution of 50 mM Na_2S + 50 mM NaOH at a pH>12 and ~ 30 mS cm^{-1} conductivity was used as anolyte, and a 50 mM NaOH solution as catholyte. A gas bag filled with N_2 was connected to the anolyte storing bottle to preserve anaerobic conditions through the course of the experiment. Periodic anolyte samplings were performed every 2 h during operation and were treated and analysed as previously described (this thesis, paragraph 2.2.4.1). In the highly alkaline conditions (pH>12) preserved in this study, polysulfide formation occurring via chemical dissolution of S^0 in the sulfide containing solution, is expected. However, polysulfides arising from dissolution of the formed S^0 in the alkaline sulfidic anolyte (Mao et al. 1991) were not measured separately and the difference of the mole balance was regarded here as the sum of elemental sulfur (S^0) and polysulfides

(Vaiopoulou et al. 2016). The sulfide removal rates (R_{HS-}) and the coulombic efficiencies (CE_{HS-}) were calculated as previously described (this thesis, paragraph 2.2.5). CE_{HS-} higher than 100% observed for some of the materials of this study are attributed to the formation of polysulfides since the latter necessitates less than 2 e^- per sulfide removed (Behm and Simonsson 1997; Mao et al. 1991; Vaiopoulou et al. 2016).

3.2.3.2 Activity and stability tests design

Activity and stability tests were performed through electrochemical techniques with a galvanostat/potentiostat VSP-300 (Bio-logic SAS, France). Cyclic voltammetry (CV), linear sweep voltammetry (LSV) and CI were recorded for each electrode before and after the activity and stability tests. Fresh electrodes were used for both the activity and the stability tests. Prior to the activity tests, the apparent geometric capacitance (C_{app}) of the electrodes was measured by means of CV in a supporting electrolyte in absence of sulfide (Figure A2.2). A first CV allowed to quantify the geometric double-layer capacitance of each electrode in 50 mM NaOH solutions, in a potential window from 0 to 1.2 V vs SHE (− 0.2 to 1 V vs Ag/AgCl) at 5 mV s^{-1} scan rate (Figure A2.2). A second CV was recorded in a sulfide containing electrolyte (50 mM Na_2S, 50 mM NaOH) to identify the sulfide oxidation onset potential (an example for the Ir MMO electrode is given in Figure A2.3). Batch activity tests were performed over a period of 24 h for each electrode. The potential of the electrodes was recorded by chronopotentiommetry (CP) at a constant current density of 50 A m^{-2}. Specific focus was given to the WE potential since the anodic sulfide oxidation was the main interest in this study.

Stability tests were performed with a total duration of 305 h in a continuous mode, at a hydraulic retention time (HRT) of 4 h under continuous mixing of the electrolyte (i.e. 8.8 mmol S per h). The anolyte was prepared and kept anaerobic in a 5 L Schott bottle, from where it was pumped into the anodic compartment using a peristaltic pump of the type 520 S (Watson-Marlow, USA). A constant current density of 125 A m^{-2} was applied for a period of 278 h. This constant current density value was reached after a stepwise increase of 25 A m^{-2} increments every ~ 1 h time, starting from 50 A m^{-2} current density as a first step. This stepwise current density increase of 25 A m^{-2} increments was conducted a second time at t = 278 h starting from 50 A m^{-2} and increasing to 200 A m^{-2}. This 200 A m^{-2} step lasted 19 h, resulting in a total continuous test period of 305 h. The duration of the experiment was determined by the first apparent increase in the anode potential of one of the electrode materials tested. An electrode material was considered unstable when the WE potential experienced a fast increase (at least 3 V in less than 5 h), or when the cell voltage reached 10 V (Shao et al. 2014). The instability of the electroactivity of the electrodes was characterized by a relative mass loss of the catalyst from the electrode surface (*vide infra*).

3.2.4 Characterization of physical and chemical properties of the electrodes

The surface composition of the electrode catalyst was measured using scanning electron microscopy with energy dispersive X-ray spectroscopy (SEM/EDX) prior and after the stability tests by comparison of the initial catalyst to titanium (base material onto which the catalytic layer is coated) ratio with the final ratio. For each of the electrode materials provided by Magneto the catalytic layer of the electrodes was analysed using X-Ray Fluorescence (XRF) prior and after the long-term electrochemical oxidation process (stability tests). An XRF calibration curve was available for the catalyst loading. This calibration curve was used to express the remaining catalyst loading after the end of the stability tests as percentage of the initial loading. The calibration curve was adjusted for the different loadings. Therefore, a relative evolution of the catalyst loading of the electrodes was assessed, with an accuracy of $\sim$ 0.2 g/m^2 ($\sim$ 2%) dependent on the electrode coating. The SEM/EDX analysis was performed in a FEG SEM JSM-7600F (JEOL) and the XRF in a Fischerscope XRAY XAN (Fischer Technology Inc., US). Images before and after the experiments were taken at a magnification of 100 $\times$ and 400 $\times$ using 20 keV, in 3 points, 1 located at the centre and 2 at the edges of each electrode.

3.3 Results and Discussion

3.3.1 Activity analysis of the electrodes

Clear differences in surface roughness were observed between the electrode materials when the SEM/EDX images (Figure 3.1) were linked with the results of the capacitance measurements (Figure A2.2 and Table A2.3). The surface of the electrodes showed the characteristic "mud-cracked" structure, except for the TiO_2/$IrTaO_2$ electrode material. In the case of MMO electrodes the formation of mud-cracks is providing a large surface area available for direct electron donor oxidation and at the same time it provides a high durability under the oxidative environment of gases evolution (Takasu and Murakami 2000). Higher surface area has been reported to contribute to a higher double-layer capacitive current during potentiodynamic measurements, apart from the faradaic current arising from the sulfide used as electron donor and/or oxygen evolution (S. Song et al. 2008). The comparison of the capacitance between materials is an important aspect to consider for electrodes with the same projected surface area but differences in electron donor removal efficiencies. The double-layer capacitance has been proposed before as a possible method for estimation of the electrochemically active surface area of an electrode (Aromaa and Forsén 2006; McCrory et al. 2013).

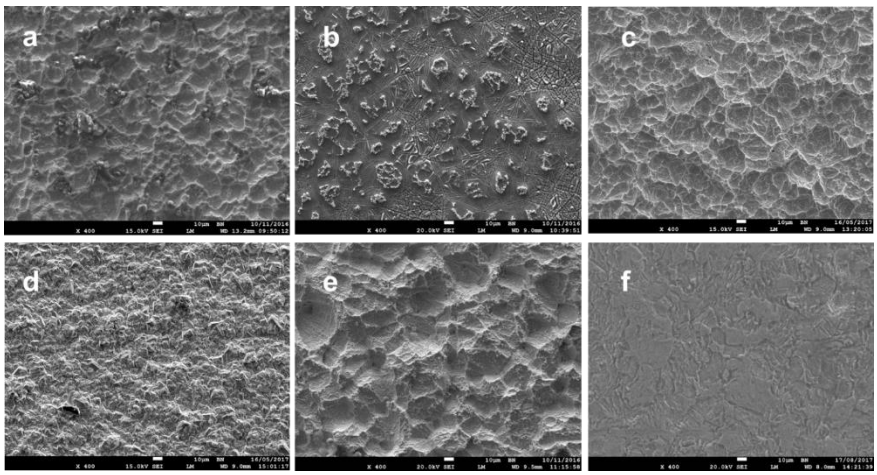

Figure 3.1 - SEM images of a) Ir MMO, b) Ru MMO, c) Pt/IrOx, d) PbOx, e) Pt and f) $TiO_2/IrTaO_2$. Magnification 400 X using 20 keV, before electrochemical sulfide oxidation. The white bars represent 10 μm.

The capacitance measured by CV (Table A2.3) is an apparent geometric capacitance (C_{app}) since it can simultaneously arise from two different processes: (i) the double layer capacitance and (ii) the pseudocapacitance from the oxidation/reduction cycle of some elements (faradaic process), such as the metal oxides in MMO anodes (Amatore et al. 1998). High C_{app} was calculated for the Ir MMO and Ru MMO, with values of 19.4 and 27.2 mF cm^{-2}, respectively, followed by the Pt/IrOx anode with 7.6 mF cm^{-2} (Table A2.3). The C_{app}, linked with the SEM images (Figure 3.1), can suggest a higher specific surface area for Ir MMO and Ru MMO, compared to the rest of the electrode materials tested in this study, related to the "mud-cracked" structure that these electrodes present. The lower C_{app} of 3.1 mF cm^{-2} calculated for the Pt anode can be linked to a low specific surface area, when compared to MMO anodes within the potential range tested (S. Song et al. 2008). The same C_{app} value with Pt/IrOx (7.6 mF cm^{-2}) was calculated for the $TiO_2/IrTaO_2$ anode. For the PbOx electrode, two oxidation peaks were observed, at 0.7 and 1.0 V vs SHE on the cyclic voltammogram (Figure A2.2). Two distinctive oxidation peaks have been reported n alkaline electrolytes (0.05 to 1.5 M NaOH), the first one attributed to PbO formation and the second to the oxidation of PbO to PbO_2 in a potential range from 0.8 to 1.0 V vs SHE (Rehim et al. 1997). In this light, due to the peak-shaped CV produced by the PbOx electrode the C_{app} was not calculated (N/A).

3.3.2 Catalyst choice impact on the final product of sulfide oxidation

During the 24 h activity tests the species formed varied from S^0 to other sulfur oxyanions and polysulfides, with an increase of products variation over time (Figure 3.2). The sulfur species produced from sulfide oxidation differed with the anode materials. Starting at a low anodic potential of ± 0.5 V vs SHE, direct sulfide oxidation to S^0 is typically the first reaction to take place (Miller and Chen 2005),

followed by $S_2O_3^{2-}$, SO_3^{2-} and SO_4^{2-} (Mao et al. 1991). This was reflected through the production of S^0 as main sulfide oxidation product within the first 10 hours of the experiments in the case of the Pt and PbOx electrodes (Figure 3.2). After 10 hours, either $S_2O_3^{2-}$ or SO_4^{2-}, depending on the catalytic coating, are the main sulfide oxidation products observed as final products within the electrode materials. The production of sulfur oxyanions during the sulfide oxidation can be associated to high anodic potentials reached in the activity tests, at different time points for each of the electrodes (Figure 3.3). The presence of SO_4^{2-} as final sulfide oxidation product can be explained by substitution of the produced SO_3^{2-} by the more thermodynamically stable SO_4^{2-} (Mao et al. 1991), with the ratio of SO_4^{2-} over SO_3^{2-} increasing after 6 h.

Different shifts of WE potential towards higher potential values were observed for all of the electrode materials during the 24 h activity tests (Figure 3.3). For all electrodes except for the TiO_2/$IrTaO_2$, the sulfide oxidation process started with direct sulfide oxidation to S^0 at anode potentials in the range of 0.2 to 0.8 V vs SHE. After initial direct sulfide oxidation to S^0 at the beginning of the activity tests, the anode potential increased for all the materials to values higher than ± 1 V vs SHE, where simultaneously oxygen evolution and sulfide oxidation are being conducted. A typical onset potential for electrochemical sulfide oxidation in alkaline wastewater is -0.065 V vs SHE (Mao et al. 1991; Vaiopoulou et al. 2016). Direct anodic sulfide oxidation results in formation of insulating S^0 on the surface of the electrode. The presence of S^0 leads to a decrease of the effective surface area of the anode available for sulfide oxidation, which, jointly with the consumption of the electron donor, will contribute to a certain increase of the anode potential (Longyao Wang et al. 2015). The increase in anode potential also leads to the formation of different products from sulfide oxidation (Miller and Chen 2006), either through direct sulfide oxidation towards more energetically demanding sulfur oxyanions or through indirect oxidation driven by oxygen evolution.

Potential oscillations were observed for Ru MMO and Ir MMO during the first 10 - 11 h of the activity tests (Figure 3.3). Oscillations during electrooxidation of sulfide on metal oxide electrodes have been reported as a result of a passivation layer formed by S^0 particles deposited at the surface of the catalytic layer of the electrode (A. Chen and Miller 2004; Fornés and Bisang 2017). This is followed by a deflaking of the S^0 and periodic evolution of oxygen (A. Chen and Miller 2004). For Ru MMO and Ir MMO, the oscillation amplitude varies with an average of 0.2 to 1.5 V vs SHE. Extensive study of potential oscillations in electrochemical sulfide oxidation on Pt electrodes has been conducted by Miller and Chen (Miller and Chen 2006). According to their findings the upper zone of the oscillation can be attributed to oxygen evolution reaction and oxidation of sulfide to sulfur oxyanions such as SO_4^{2-}, while the lower areas can be attributed to the oxidation of sulfide to S^0 or polysulfides, but without O_2 evolution. In this study, gas bubble formations coinciding with the upper part of the oscillations were visually observed, following after the deposition of S^0 particles on the surface of the electrode. After consumption of the sulfide as electron donor the production of S^0 is replaced by production of sulfur

oxyanions, which limits the oscillation phenomena and results in a stabilized ~ 1 V vs SHE anode potential, similar for both the Ir MMO and Ru MMO electrodes. The oscillatory behaviour of the potentials over time did not result in abrupt changes on the evolution of the sulfur products (Figure 3.2).

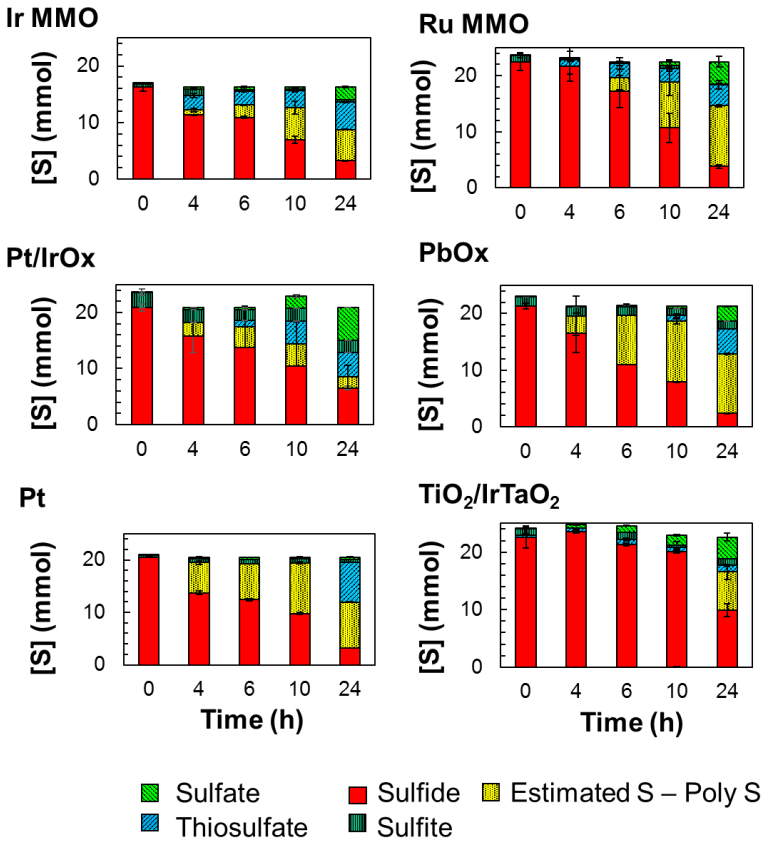

Figure 3.2 - Evolution over time of the sulfur species speciation during the activity tests of 24 h for all electrode materials. The electrode materials tested are stated by their name accordingly. Additional information on the evolution over time of the coulombic and removal efficiencies are given in Figure A2.4.

A sulfide removal rate of 0.5 ± 0.0 mmol h^{-1} was achieved by the Ir MMO electrode at a low average anode potential of 0.81 ± 0.30 V vs SHE and a CE_{HS^-} of 43.9 ± 0.2%. The change in the anode potential corresponds to the shift from an exclusive direct sulfide oxidation reaction to simultaneous sulfide oxidation and oxygen evolution reactions (Figure A2.2). Among all anodes tested, Ru MMO was the most energetically efficient material for sulfide oxidation, with a starting anode potential of 0.41 ± 0.04 V vs SHE to a final of 1.07 ± 0.03 V vs SHE after 24 h, and an average of 0.92 ± 0.17 V vs SHE (Table 3.1). The sulfide removal rate achieved by the Ru MMO electrode for the total 24 h

of the activity test was 0.8 ± 0.0 mmol h^{-1} with a CE_{HS^-} of 63.2 ± 0.5%. This is also depicted by the formation of more oxidized products such as $S_2O_3^{2-}$ in the final hours of the activity tests.

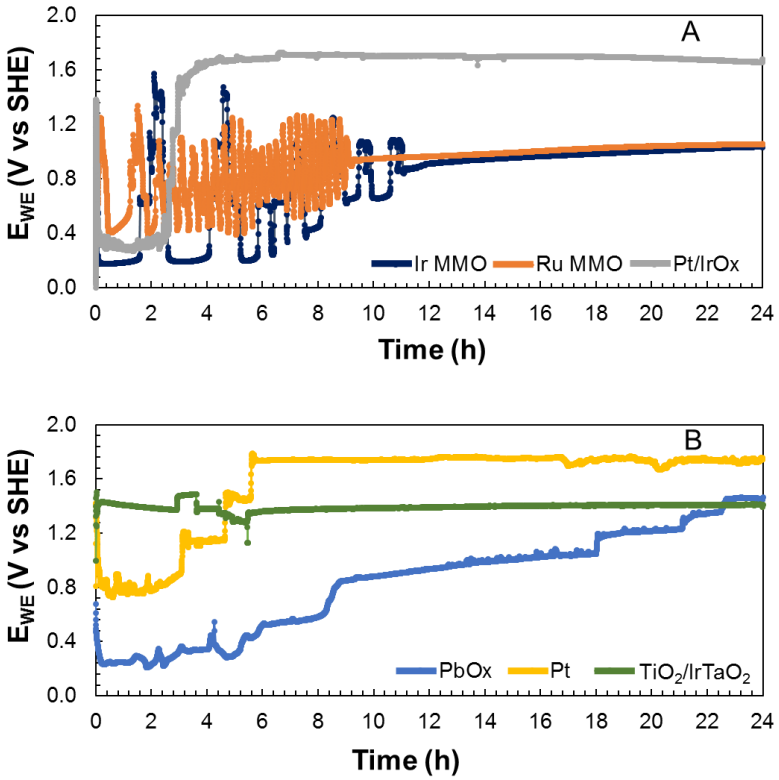

Figure 3.3 - Evolution of the ohmic drop corrected anode potential in the electrode materials (A: Ir MMO, Ru MMO, Pt/IrOx and B: PbOx, Pt, TiO_2/$IrTaO_2$) during the activity tests at constant current density of j = 50 A m^{-2}. The chronopotentiograms are representative of the triplicate experiments. The potential oscillation for Ir MMO and Ru MMO was observed in all independent recordings (Figure A2.5).

Table 3.1 - Activity performance of the electrode materials: the sulfide removal rate (R_{HS^-}, mmol h^{-1}); the coulombic efficiency (CE_{HS^-}, %); the initial potential (E_i), final potential (E_f) and averaged potential (E_{av}) recorded all along the experiment, of the anodes (V vs SHE). Values reported for the total experimental period of the activity tests. The potentials are reported after ohmic drop correction (Table A2.4 and A2.5). All experiments were conducted in triplicate.

Electrode material	R_{HS^-} (mmol h^{-1})	CE_{HS^-} (%)	E_i (V)	E_f (V)	E_{av} (V)
Ir MMO	0.5 ± 0.0	43.9 ± 0.2	0.18 ± 0.02	1.03 ± 0.01	0.81 ± 0.30
Ru MMO	0.8 ± 0.0	63.2 ± 0.5	0.41 ± 0.04	1.07 ± 0.03	0.92 ± 0.17

Pt/IrOx	0.6 ± 0.0	47.7 ± 1.3	0.34 ± 0.08	1.68 ± 0.10	1.26 ± 0.60
PbOx	0.8 ± 0.0	64.7 ± 0.3	0.25 ± 0.01	1.47 ± 0.01	0.86 ± 0.37
Pt	0.7 ± 0.0	58.9 ± 0.1	0.75 ± 0.07	1.74 ± 0.10	1.59 ± 0.32
$TiO_2/IrTaO_2$	0.5 ± 0.0	41.1 ± 4.2	1.42 ± 0.14	1.41 ± 0.13	1.39 ± 0.03

The Pt/IrOx, Pt and $TiO_2/IrTaO_2$ electrodes were considered the least suitable of the materials due to their high average anode potential. The high anode potential of 1.42 ± 0.14 V vs SHE observed in the beginning of the oxidation process for the $TiO_2/IrTaO_2$ electrode was attributed to the oxygen evolution reaction taking place for the most part, with limited sulfide oxidation. This high average anode potential was expected for the Pt electrode due to its relatively low catalytic activity towards oxygen evolution (S. Song et al. 2008), which contributes to the high final anode potential of 1.74 ± 0.10 V vs SHE obtained by this electrode. This also explains the low CE_{HS^-} of 41.1 ± 4.2% obtained for this material, the lowest obtained among all the materials tested. In the case of Pt and Ru MMO, the S^0 produced was visually observed either with deposition of the particles on the surface of the electrode (Figure A2.6) or with the changing of the electrolyte colour to yellow, which is associated with polysulfides formation after reaction of the produced S^0 with the remaining sulfide, in alkaline solutions (Moo et al. 2018; Selvaraj et al. 2016). The PbOx electrode achieved an apparent high sulfide removal rate (0.8 ± 0.0 mmol h^{-1}) with 64.7 ± 0.3% CE_{HS^-} and a low average (0.86 ± 0.37 V vs SHE) anode potential, but was not further considered as the most energetically efficient, due to the catalyst loss, that also raises concerns on the mechanism of sulfide removal. Overall, financial, as well as, environmental concerns raised by the fast dissolution of the catalytic layer of this electrode might hinder further application of this electrode for sulfide oxidation.

3.3.3 Continuous evaluation of material stability

3.3.3.1 Electrochemical measurements

Continuous tests for material stability evaluation were performed on the electrode materials for 305 h. The current density was increased stepwise from 50 to 200 A m^{-2} with 25 A m^{-2} increments to monitor the evolution of the anodic potentials in every current density step. To be able to compare the stability within the electrode materials, the tests were all stopped at the same time when one electrode (Pt/IrOx in this case) reached a cell voltage of 10 V (anode potential of > +5 V vs SHE).

At current densities of 50 – 200 A m^{-2} the Ir MMO anodic potential remained stable with an average of 1.82 ± 0.02 V vs SHE at the 200 A m^{-2} step. The Ru MMO showed stable and low operational

potentials, which were repeatable at the two stepwise increments of current density (up to 125 A m^{-2}) (Figure 3.4). At the last current density step of 200 A m^{-2}, the initial potential of Ru MMO anode was 1.54 V vs SHE and increased to a final potential of 1.59 V vs SHE, with an average of 1.56 ± 0.02 V vs SHE (Figure A2.7 and Table A2.4). This was the lowest average anode potential achieved among all the electrode materials. The PbOx electrode showed also a repeatable performance at the two stepwise increments of current density with an average potential of 2.04 ± 0.04 V vs SHE obtained during the 200 A m^{-2} step.

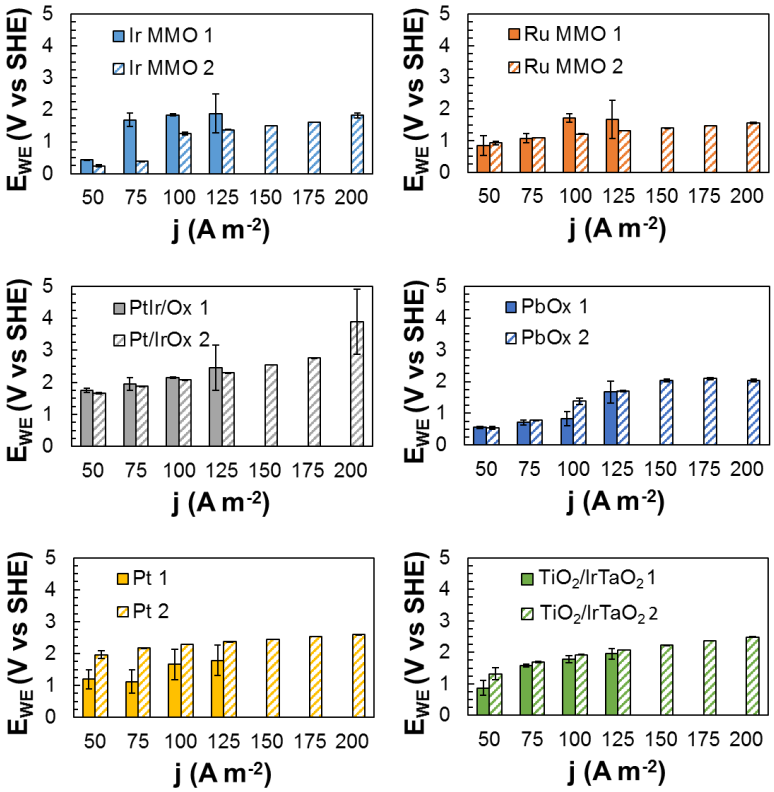

Figure 3.4 – Evolution of the anode potential with the current density recorded during the stability tests for all electrode materials. The stepwise increase in current density was performed twice at t = 0 (from 50 to 125 A m^{-2}; full bars, stated '1') and at t = 278 h (from 50 to 200 A m^{-2}, patterned bars, stated '2'). The stability tests were stopped for all electrodes once an electrode reached 5 V at the highest current density of 200 A m^{-2}, here Pt/IrOx electrode at t = 305 h (Figure A2.7 and Table A2.5).

Both Pt and TiO_2/$IrTaO_2$ catalysts showed an increase of their potential at the repeat of the current density stepwise increment. Among all the tested materials, Pt and TiO_2/$IrTaO_2$ exhibit a higher average potential at 200 A m^{-2} of 2.60 ± 0.01 and 2.48 ± 0.01 V vs SHE, respectively. Both materials preserved a stable anode potential in the last step. On the contrary, the potential of the Pt/IrOx anode was continuously increasing from 2.93 to 6.60 V vs SHE at 200 A m^{-2} (Figure A2.7 and Table A2.5).

This potential increase of more than 3 V over only 14 h suggested that the electrode either lost most of its catalytic layer or was largely – and increasingly – covered with insulating S^0.

3.3.3.2 Electrode surface characterization

The passivation or loss of the catalyst layer at the electrode surface was assessed using SEM/EDX, and compared with the results obtained from XRF analysis. In the first case the surface composition was determined, with a spectrum of the elements present on the electrode surface (in depth of a few µm). In this way remaining sulfur compounds on the electrode surface can also be detected, which indicates either S^0 that has permanently covered the catalytic surface of the electrode, presence of sulfur ions, or metal sulfide bonds created during sulfide oxidation (for the exact nature of sulfur X-Ray photoelectron spectroscopy can be conducted). In the case of XRF the catalyst loading before and after use of the electrodes was recorded, to give a relative percentage change with respect to the original coating (Table 3.2).

Table 3.2 – Catalyst to base metal ratio changes after the stability tests analyzed with SEM/EDX and XRF. The initial and the final ratio are presented, the wt% of sulfur (S) on the catalytic surface and the percentage of the original coating remaining intact after the stability tests. SEM images after the stability tests are presented in Figure A2.8 and compositional variations based on SEM-EDX in Table A2.6.

Electrode material	SEM/EDX				XRF
	Catalyst/ base metal ratio	Initial ratio	Final ratio	S (wt %)	Final catalyst loading (%)
Ir MMO	Ir/Ti	26.67 ± 0.53	19.73 ± 0.60	0.37 ± 0.19	100
Ru MMO	Ru/Ti	0.64 ± 0.01	0.55 ± 0.01	1.00 ± 0.14	92
Pt/IrOx	Pt, Ir/Ti	0.69, 0.22 ± 0.02	0.00 ± 0.00	0.73 ± 0.40	0
PbOx	N/A	N/A	N/A	0.20 ± 0.28	66
Pt	Pt/Ti	5.92 ± 0.23	6.07 ± 0.17	9.10 ± 0.78	89
TiO_2/IrTa O_2	Ti/Ir, Ta	*$IrTaO_2$	11.7, 32.2 ± 1.02	0.67 ± 0.09	N/A

* layer not exposed

Due to the complexity of the electrochemical phenomena taking place during sulfide oxidation, the catalytic surface changes can be attributed not only to S^0 deposition, but also to a selective leaching and metal dissolution (Cherevko et al. 2016; Hamilton and Woods 1983; Martelli et al. 1994). The XRF results showed 100% remaining coating for the Ir MMO while the SEM/EDX showed a decrease of the catalyst to base metal ratio from 26.67 ± 0.53 to 19.73 ± 0.60. This decrease of catalyst ratio could suggest S^0 deposition, that covers part of the catalytic surface of the Ir MMO, rather than a loss of catalyst. The Ru MMO catalyst layer change correlated well with the stability tests results. The XRF results suggested that after the stability tests 92% of the catalytic coating remained intact. Likewise, the SEM/EDX results showed a rather limited decrease of 17% of the initial Ru/Ti catalyst relative to total surface composition (Table 3.2). This reduced catalyst over base metal ratio can be explained by S^0 deposition, but in part also by the catalyst leaching due to corrosion (Table 3.2).

The XRF results for Pt and PbOx electrodes showed 89% and 66% of the catalyst loading, respectively, still coated on the Ti surface after the stability tests. In the literature, Pb or PbOx electrodes dissolution phenomena have been reported, where anodic Pb dissolution and film formation complex processes were taking place in alkaline wastewaters (Rehim et al. 1997; Rehim and Mohamed 1998; Van Hege et al. 2004; Y. Yang et al. 2016). A brown-reddish colour was observed in the anolyte after the batch and during the continuous sulfide oxidation test, (Figure A2.9), that can be associated with dissolved PbO_2 in the alkaline electrolyte (Vatistas and Cristofaro 2000). It is important to note that the mechanisms through which the PbOx electrode participates to sulfide removal can bring a negative rather than positive environmental effect on the industrial sulfide containing wastewater streams.

The results of SEM/EDX and XRF of the Pt/IrOx electrode showed no remaining catalytic layer, which is in good agreement with the fast and large increase in the anode potential at the end of the stability tests. The SEM/EDX combined with the XRF results can be associated with the potential changes during the stability tests. However, to establish a better view on the catalytic changes and verify the results of the combined XRF and SEM/EDX surface analyses, measurement of the leached, in the electrolyte, catalysts via inductively coupled plasma optical emission spectrometry (ICP/OES) could be proposed for future stability studies.

The full catalyst loss for the Pt/IrOx electrode corresponds to the decrease of the catalytic activity at high current density (increase of the anode potential of ~ 3 V in 14 h at 200 A m^{-2}) (Figure A2.7). On the contrary, the most stable electrode, Ir MMO, preserved intact catalyst coating during the stability tests.

3.3.4 Implications and future perspectives

One of the implications of this study is the unknown oxidation mechanisms that are governing the sulfide oxidation steps on the electrode surface. In Table A2.1 the oxygen evolution onset potential (OEP) and the sulfide oxidation onset potential (SOP) are given. It can be assumed that indirect sulfide oxidation (via O_2 evolution) will be favoured for the electrodes with low OEP, which was the case for the MMO electrodes, Ir MMO, Pt/IrOx and TiO_2/$IrTaO_2$ (OEP = 0.80, 0.77, 0.75 V vs SHE). The OEP differences, dictated by the morphological differences and the catalyst composition, will result in different operational sulfide oxidation performances. In contrary, the electrodes with high OEP, such as Pt and PbOx in our study (1.01, and 1.06 V vs SHE, respectively) will mainly undergo direct sulfide oxidation. This is supported by the high CE_{HS^-} achieved by the Pt and PbOx electrodes (58.9 and 64.7%, respectively) and the lower of the MMO electrodes. The Ru MMO constitutes an exception, which although presenting a low OEP (0.75 V vs SHE), achieved a high CE_{HS^-} of 63.2%. This indicates that the OEP cannot be considered as sole indicator of the oxidation mechanisms at different electrodes and both OEP and SOP, in combination with mechanistic studies are needed to determine the oxidation mechanisms at different electrodes.

Further research is needed to establish the impact of phenomena such as the oscillations produced by sulfide oxidation and provide a quantitative assessment of how they affect the products of the oxidation and also the electrode lifetime. Monitoring of metal leaching should be considered in further studies, in order to establish corrosion rates (e.g. amount of catalyst leaching per surface per time) with respect to the specific catalytic materials and current densities applied. The 8% catalyst loading loss of the Ru MMO electrode in these 305 h of continuous operation raises concerns about its performance on future long-term applications, considering the high price of this catalyst. On the contrary, the five times higher price of the more stable Ir MMO suggests that a determination of a good balance between activity and stability of the electrode materials will be key for a future scale-up of the system. Longer-term (field) studies of the electrode performance operated with real SCS are needed to quantify the electrode lifetime. Further work should be implemented to compare the sulfide removal efficiencies, lifetime and price of the different electrodes to assess practical application of electrochemical sulfide treatment with the Ir MMO and Ru MMO electrodes.

3.4 Conclusion

We investigated the impact of the catalyst choice on the activity of the Ir MMO, Ru MMO, Pt/IrOx, Pt, PbOx and TiO_2/$IrTaO_2$ electrodes towards sulfide oxidation and on their stability under operation at high sulfidic (i.e. 50 mM sulfide) and highly alkaline conditions (i.e. pH>12). Key finding of this work is that among all materials, the Ir MMO catalyst demonstrated excellent stability for sulfide oxidation , reflected through the conservation of the catalysts layer throughout the 305 h of stability test.

Subsequently, the Ru MMO was proven active towards sulfide oxidation with a CE% of 63.2 ± 0.5% and an average anode potential of 0.92 V ± 0.17 V vs SHE for a constant current density of 50 A m^{-2}. The Pt/IrOx electrode was proven unstable for sulfide oxidation under the experimental conditions applied in this study, by demonstrating an increase of 3 V and a total loss of the catalyst coating upon completion of the stability test. Finally, we concluded that the $TiO_2/IrTaO_2$ electrode, was not a suitable material towards sulfide oxidation, as it was unable to operate at the low anodic potential that is desired for direct sulfide oxidation.

CHAPTER 4

Electrochemical treatment of industrial, sulfide containing wastewater

Adapted from:

Eleftheria Ntagia, Erika Fiset, Linh Truong Cong Hong, Eleni Vaiopoulou, Korneel Rabaey (2020). Electrochemical treatment of industrial sulfidic spent caustic streams for sulfide removal and caustic recovery. Journal of Hazardous Materials, Volume 388, 15 April 2020, 121770, doi.org/10.1016/j.jhazmat.2019.121770

Abstract

Alkaline spent caustic streams (SCS) produced in the petrochemical and chemical manufacturing industry, contain high concentrations of reactive sulfide (HS^-) and caustic soda (NaOH). Common treatment methods entail high operational costs while not recovering the possible resources that SCS contain. Here we studied the electrochemical treatment of SCS from a chemical manufacturing industry in an electrolysis cell, aiming at anodic HS^- removal and cathodic NaOH, devoid of sulfide, recovery. Using a synthetic SCS we first evaluated the HS^- oxidation product distribution over time, as well as the HS^- removal and the NaOH recovery, as a function of current density. In a second step, we investigated the operational aspects of such treatment for the industrial SCS, under 300 A m^{-2} fixed current density. In an electrolysis cell receiving 205 ± 60 g S L^{-1} d^{-1} HS^- over 20 days of continuous operation, HS^- was removed with a 38.0 ± 7.7% removal and ~80% coulombic efficiency, with a concomitant recovery of a ~12 wt.% NaOH solution. The low cell voltage obtained (1.75 ± 0.12 V), resulted in low energy requirements of 3.7 ± 0.6 kWh kg^{-1} S and 6.3 ± 0.4 kWh kg^{-1} NaOH and suggests techno-economic viability of this process.

4.1 Introduction

Spent caustic streams (SCS) are generated in various industries, including petrochemical refineries, the chemical manufacturing and the pulp and paper industry (Alnaizy 2008; Pokhrel and Viraraghavan 2004; Stephenson and James B. Blackburn 1997) at thousands of cubic meters annually (Ben Hariz et al. 2013; Zermeño-Montante et al. 2011). Depending on the production site, SCS can contain hydrogen sulfide (HS^-), mercaptans, phenolic and hydrocarbon compounds, thus classified as sulfidic, naphthenic and cresylic SCS, respectively. The high alkalinity (5 – 12 wt.% NaOH), sulfide content (0.5 – 4 wt.% sulfide-S) and occasionally high temperature of the sulfidic SCS limit the feasibility of direct biological treatment. Therefore, chemical treatment is used in industry to treat SCS (Alnaizy 2008; Ben Hariz et al. 2013; S. H. Lin and Peng 1994; Zermeño-Montante et al. 2011). The methods followed include neutralization (Hawari et al. 2015), conventional (Alnaizy 2008; Carlos and Clayton B. Maugans 2000; Hawari et al. 2015) and advanced oxidation (Hawari et al. 2015; Zermeño-Montante et al. 2011), or a combination of the aforementioned (Sheu and Weng 2001). These methods are usually accompanied by high operational costs, due to high operational temperatures and pressures, the application of expensive chemicals and catalysts and the need for transport and storage of the chemicals (Alnaizy 2008; Vaiopoulou et al. 2016).

Electrochemical treatment is an interesting alternative to conventional methods as it provides a potentially more cost-efficient and more sustainable approach (Pikaar et al. 2015). For example, using sacrificial electrodes one can achieve an electrocoagulation process (Ben Hariz et al. 2013) or an electrochemically controlled Fenton process (Nuñez et al. 2009), where the coagulation is induced by electrolysis, instead of chemical addition. However, these approaches are limited by the regular need for electrode replacement and the lack of resource recovery. Another approach has been proposed by Zhai et al (Zhai et al. 2012), where, in a fuel-cell-assisted iron redox (FC-IR) process, sulfide is oxidized to elemental sulfur with concomitant regeneration of Fe(III) from Fe(II). This process included a Fe(III) sulfide oxidizing reactor, combined with a fuel cell for anodic Fe(III) regeneration. Elemental sulfur and power could be harvested from the system, however, in this case, as in the electrochemical Fenton processes, adjustment of the pH to acidic levels limits the efficiency of the process. In addition, pH regulation to acidic levels entails the risk of releasing sulfide contained in the wastewater, in the form of H_2S gas. Electro-electrodialysis (EED) and bipolar membrane electrodialysis (BEMD) were studied by Wei et al. (Wei et al. 2012, 2013) on SCS. However, those systems were used solely for NaOH recovery, excluding information on the actual treatment of the SCS, e.g. the HS^- or Chemical Oxygen Demand (COD) removal.

Direct electrochemical desulfurization of alkaline streams has been studied extensively (Anani et al. 1990; Burke et al. 2002; Mao et al. 1991; Petrov and Srinivasan 1996), with synthetic SCS, which might obscure difficulties occurring during treatment of real SCS. In addition, these studies were suffering from certain limitations, such as a lack of providing an application perspective overview

(Pikaar et al. 2015). Previously, we proposed a novel electrochemical method for wastewater desulfurization (Dutta et al. 2008; Rabaey et al. 2006; Vaiopoulou et al. 2016), where in an electrolysis cell, simultaneous anodic HS^- oxidation to mainly elemental sulfur (S^0) and cathodic NaOH recovery were conducted (Vaiopoulou et al. 2016). In that setup, NaOH was recovered as a concentrate via cathodic OH^- production, which combines with Na^+ migrating from the anolyte to the catholyte. This allowed for additional S^0 and hydrogen gas (H_2) recovery, a potentially valuable resource. The operational costs in that case were mainly associated with the power input in the electrochemical cell, while the lower energy requirements of this method compared to advanced oxidation processes, are associated with lower CO_2eq emissions (Chatzisymeon et al. 2013).

We previously reported excellent performance on synthetic SCS treatment in an electrochemical flow cell (Vaiopoulou et al. 2016), where a 5.1 ± 0.9 wt.% NaOH stream was recovered and simultaneously HS^- was removed with 67 ± 5% removal efficiency at 50 A m^{-2}. Still, these results were achieved with a synthetic SCS solely containing HS^-. It is thus crucial to assess this treatment approach in a more complex matrix, loaded with complex organics additional to sulfide pollutants. This will allow for a realistic evaluation of the application potential of electrochemical industrial SCS treatment. In this work we investigated the direct electrochemical treatment of a real, industrial SCS. First, we studied the sulfide removal and the caustic recovery as a function of current density, using a synthetic SCS as electrolyte. The sulfide oxidation product distribution over time was also studied. As a second step we investigated the operational aspects of such treatment in a two compartment electrochemical cell configuration for the treatment of real SCS obtained from a chemical industry, under fixed current density. Finally, we assessed the feasibility of this treatment for real application with concomitant caustic regeneration on the industrial site, and proposed a preliminary economic assessment of this application.

4.2 Materials and methods

4.2.1 Cell configuration and electrochemical techniques

All electrochemical experiments were conducted with a 20 × 5 × 2 cm, CEM divided, two compartment electrochemical cell as described in paragraph 2.2.2 of this thesis (additional tests were conducted in a three compartment cell, described in A3.1.2 and Figure A3.1). An iridium mixed-metal oxide titanium-based (Ti) electrode (Ir MMO) (Magneto Special Anodes (an Evoqua brand), The Netherlands) was used as anode and a stainless steel thin mesh (Solana, Belgium) was used as a cathode. The two electrodes were planar with a projected surface area of 100 cm^2 (20 × 5 cm) and were positioned parallel to each other (distance between electrodes was ~8 mm). A saturated calomel electrode (SCE) (BAS Inc., Japan, +0.244 V vs. SHE at 25 °C) was used as reference electrode (RE) in the anodic compartment. All reported potentials refer to the standard hydrogen electrode (SHE). The

electrochemical cell was controlled galvanostatically with a DC power supply (Velleman LABPS3005 0 – 30 V, 0 – 5 A, Belgium) and electrochemical techniques were performed with a VSP potentiostat (Bio-Logic Science Instruments SAS, France). All current densities are reported with respect to the projected surface area of the anode (0.01 m^2). Prior to cell operation, the uncompensated resistance (Ru) between the anode and the reference electrode, and the cell resistance (R_{cell}) were measured with the current interrupt (CI) method (Allen J. Bard and Faulkner 2001) in 10 successive cycles (cycles of 50 ms at 100 mA followed by 50 ms open circuit with a recording period of 0.2 ms). The electrolyte used was synthetic SCS (1 M Na_2S and 1 M NaOH) and the resistances measured were lower than 1 Ω (Table A3.1). The anode potential (E_{WE}) and cell voltage (E_{cell}) were monitored with the potentiostat by chronopotentiometry (CP).

4.2.2 Analytical techniques

Samples for sulfide (HS^-), sulfite (SO_3^{2-}), thiosulfate ($S_2O_3^{2-}$) and sulfate (SO_4^{2-}) analysis were treated with sulfide antioxidant buffer (SAOB) and analyzed with a 930 Compact Ion Chromatograph Flex (Metrohm, Switzerland), as described in Chapter 2. The sum of S^0 and polysulfides was calculated as the difference between the initial sulfide added in the electrochemical reactor (in moles) and the rest of the soluble sulfur species (i.e. HS^-, SO_3^{2-}, $S_2O_3^{2-}$ and SO_4^{2-}), as described previously (Chapter 2). Organic solvents were analyzed with GC-2010 Plus AF IVD (Shimadzu, Japan), GC capillary column RTX-624, 0.18 mm internal diameter, 1 µm film thickness, 30 m length, temperature range 40 – 240 °C. The total COD was analysed with Nanocolor® kits (Test 0 – 29, 1 – 15 g/L) (CODE; Macherey-Nagel) (APHA et al. 1999). Conductivity was measured with a Consort C6010 conductivity meter (Consort, Belgium). The NaOH concentration was calculated by measuring the alkalinity, determined by titration with a Metrohm 719S titrino (Metrohm, Switzerland) using HCl 0.02 N (Chem-Lab Nv, Belgium).

4.2.3 Experiments and conditions

4.2.3.1 Batch mode operation with synthetic SCS feed

Batch galvanostatic experiments of 8 h were performed initially in the two compartment electrochemical cell to determine the efficiency of HS^- removal and the distribution of the HS^- oxidation products in a synthetic stream in function of time and supplied charge. A synthetic stream of 1 M Na_2S and 1 M NaOH was used as anolyte and 1 M NaOH as catholyte. The total volume of each electrolyte solution was 500 mL and the electrolyte recirculation flow rate was 6 L h^{-1}. Each compartment was connected to a 500 mL recirculation bottle. Galvanostatic experiments were run in duplicate at three different current densities of 100, 200 and 300 A m^{-2}.

4.2.3.2 Continuous operation with real SCS feed in a two compartment electrolysis cell

Continuous galvanostatic experiments with real SCS (Table 4.1) at 300 A m^{-2} were performed for a period of 20 days. The current density selection was based on previous results on synthetic SCS (Vaiopoulou et al. 2016) and on the batch tests conducted with synthetic SCS, as to maintain a high HS^- removal, without secondary pollution (production of sulfur oxyanions). The SCS was provided continuously at the anodic compartment of the cell while the catholyte, with a total volume of 500 mL was recirculated through a 500 mL Schott bottle. A 3 M NaOH solution was used initially (to limit ohmic drop) as catholyte. The anolyte flow and the catholyte recirculation rate were maintained at 1.67 L d^{-1}, resulting in a 205 ± 60 g S L^{-1} d^{-1} HS^- loading rate (for 0.4 L total electrochemical cell volume). The operational performance of the cell during the continuous experiments was monitored based on the same parameters as during the batch experiments, with an additional monitoring of organics in both the anodic and cathodic compartments and the energy input for SCS (wastewater) treatment (Eq. S6). A 10 L gas bag filled with nitrogen gas (N_2) was connected to the anolyte storage bottle to maintain anaerobic conditions during the experiment. Preliminary batch tests to assess the suitability of a three compartment electrochemical cell were conducted with real SCS and are described in A3.1.2.

*Table 4.1 – Characteristics of the industrial spent caustic stream (SCS) used as anolyte in the continuous experiment**

Parameter	Range
pH	>13
Electrical Conductivity	0.6 – 0.8 S cm^{-1}
NaOH	3.8 – 4.1 M (15.1 – 16.3 wt.%)
NaHS	1.4 – 1.9 M
COD**	158.2 – 179.2 g L^{-1}

* the range of parameters is the result of different batches of the industrial SCS

** ~35% is represented by low-molecular weight organic solvents

4.2.4 Calculations

The operational performance of the electrochemical cell was monitored based on the HS^- removal efficiency (RE_{HS-}) (Equation 4.1), coulombic efficiency (CE_{HS-}) (Equation 2.4), NaOH recovery efficiency

(R_{NaOH}) (Equation 4.2), the energy input for the removal of HS^- as pollutant (Equation 2.5), the energy input for recovery of NaOH (Equation 4.3) and the energy input for wastewater treatment (Equation 4.4).

$$RE_{HS^-}\ (\%) = \frac{(C_{HS}^{in} - C_{HS}^{an}) \times Q \times \Delta t}{C_{HS}^{in} \times Q \times \Delta t} \times 100 \quad (4.1)$$

where C_{HS}^{in} is the HS^- concentration in the inflow (mol L^{-1}), C_{HS}^{an} is the concentration in the anolyte (mol L^{-1}), Q is the flow rate of the influent SCS in the anolyte and Δt is the time period between two sampling times (d).

$$R_{NaOH}(\%) = \frac{n_{NaOH}^{t0} - n_{NaOH}^{\Delta t}}{n_{NaOH}^{t0}} \times 100 \quad (4.2)$$

where n_{NaOH}^{t0} and $n_{NaOH}^{\Delta t}$ are the number of OH^- moles in the catholyte at time t = 0 and Δt, respectively.

The energy input for the sulfur species removal (kWh kg^{-1} S removed), the NaOH recovery (kWh kg^{-1} NaOH recovered), and the SCS treatment (kWh m^{-3} SCS treated), were calculated based on equations 2.5, 4.3 and 4.4, respectively:

$$Energy\ input\ for\ NaOH\ recovery = \frac{E_{cell} \times I \times \Delta t \times \frac{\left(\frac{10^{-6}}{3.6}\right) kWh}{J}}{m_{NaOrecovered}} \quad (4.3)$$

where $m_{NaOH\_recovered}$ is the mass of NaOH recovered during the experiment in the catholyte i.e. the final mass of NaOH subtracted by the initial one (kg NaOH) (the catholyte was running in batch, both in the configuration with the synthetic and the industrial SCS).

$$Energy\ input\ for\ wastewater\ treatment = \frac{E_{cell} \times I \times \frac{\left(\frac{10^{-6}}{3.6}\right) kWh}{J}}{Q_{SCS}} \quad (4.4)$$

where Q_{SCS} is the inflow SCS flow rate (L d^{-1}).

4.2.5 Elemental sulfur characterization

To verify the purity and morphology of the S^0 particles, contact angle measurements and scanning electron microscopy with energy dispersive X-ray spectroscopy (SEM/EDX) were conducted. The determination of the affinity of the S^0 particles towards water was conducted with contact angle measurements. Prior to the measurement, the sample was completely dried for 12 h at 30 °C. A high

speed ball mill was used to powder the S^0 sample collected. A sample of 2.5 g was pressed for 30 min with a carver platen press under P > 165 MPa. Contact angle measurements were conducted using 10, 2 and 20 μL drops of deionized water, pure diodomethane and glycerol, respectively, as solvents, using the sessile drop method in a Tracker tensiometer (Teclis, France). The composition of the S^0 particles collected from the anodic chamber were measured with SEM/EDX, in a FEG SEM JSM-7600F (JEOL) at a magnification of 400 × using 20 keV.

4.3 Results and discussion

4.3.1 Sulfide is anodically removed and caustic is cathodically recovered, as a function of current density

4.3.1.1 Applied current density dictates anode potential and thus sulfur speciation

Batch experiments of 8 h were conducted on synthetic SCS in a two compartment electrochemical cell to study the effect of current density on the sulfide oxidation product distribution and the operational efficiency of the system. As expected, with an increase of current density, the RE_{HS^-} (Figure 4.1a) increased, from 27.2 ± 1.1% at 100 A m^{-2} to 54.9 ± 0.5 and 59.2 ± 0.0% at 200 and 300 A m^{-2}, respectively. With an increase of the applied current density, a more diverse product spectrum was observed over time (Figure 4.2).

In a galvanostatically controlled electrochemical cell performing anodic sulfide oxidation, the product distribution will be determined by the availability of the electron donor (sulfide bulk concentration and mass transport properties), the current density (itself defining the anode potential and therefore the possible oxidation reactions (Allen J. Bard and Faulkner 2001)) and the electrode material used (this thesis, Chapter 3). In a batch mode operation and under high current densities, sulfide is quickly depleted and the anode switches to more positive potentials, where more energy demanding sulfur oxyanions will start being produced, with concomitant oxygen evolution (this thesis, Chapter 3) (Table A3.2). Behm and Simonsson (Behm and Simonsson 1997) reported side reactions and production of more oxidized sulfur forms at increased anode potentials, which was signified by a decrease in their coulombic efficiency towards sulfur formation. In their study with domestic wastewater (< 0.5 mM HS^- L^{-1}), Pikaar et al (Pikaar et al. 2011b) also reported increased production of sulfur oxyanions, due to the limited availability of electron donor close to the electrode surface.

In our study, at 100 and 200 A m^{-2}, S^0 was the main oxidation product after 8 h, while at 300 A m^{-2} the S^0 to removed HS^- ratio decreased, due to increasing production of sulfur oxyanions. More specifically, this ratio, determined analytically, was 0.6 ± 0.0, 0.8 ± 0.0, 0.4 ± 0.1 at 100, 200 and 300 A m^{-2} respectively. This corresponded well with the calculated CE_{HS^-} of 69.3 ± 8.8%, 77.8 ± 10.2 % and 41.3 ± 2.8% (Figure 4.1b). The CE_{HS^-} obtained at 300 A m^{-2} was lower than at 200 A m^{-2},

indicating that oxygen evolution occurred after consumption of HS^- as the available electron donor and the increased production of more oxidized sulfur oxyanions, mainly thiosulfate ($S_2O_3^{2-}$) (Figure 4.2). The oxygen evolution reaction at the anode is further supported by the increased anode potential, which was -0.16 ± 0.09 to 0.00 ± 0.04 and 0.57 ± 0.54 V vs. SHE, obtained at 100, 200 and 300 A m^{-2}, respectively (Figure 4.1c). At 300 A m^{-2}, the anode potential was initially 0.10 ± 0.01 V vs SHE and after 4 h, oscillated between values of 0.2 and 1.4 V, with an average value (for experimental period 4 to 8 h) of 1.03 ± 0.4 V vs SHE (Figure A3.2) where both HS^- oxidation and oxygen evolution happened concomitantly, in a process previously described (A. Chen and Miller 2004; Fornés and Bisang 2017) (this thesis, Chapter 3). At pH 13 – 14 the expected theoretical potential for oxygen evolution is between 0.46 and 0.40 V (Allen J. Bard and Faulkner 2001) and the expected oxygen production was also visually confirmed. Therefore, after the first 4 h of this experiment concomitant sulfide oxidation and oxygen evolution occurred, which renders the concomitant direct and indirect oxidation a plausible scenario.

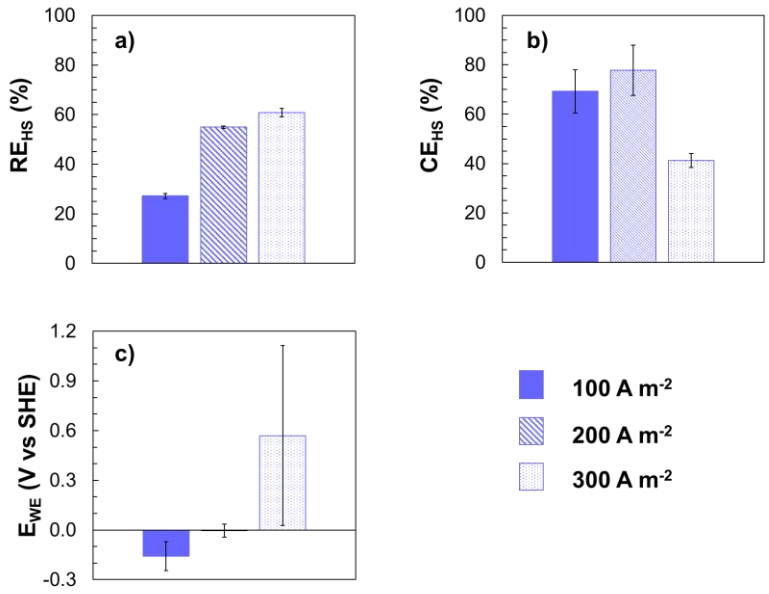

Figure 4.1 – Operational performance during the 8 h batch experiments given as a) sulfide removal efficiency (RE_{HS-}, %), b) coulombic efficiency (CE_{HS-}, %) and c) anode potential (E_{WE}, V) for 100, 200 and 300 A m^{-2}, n = 2 replicates

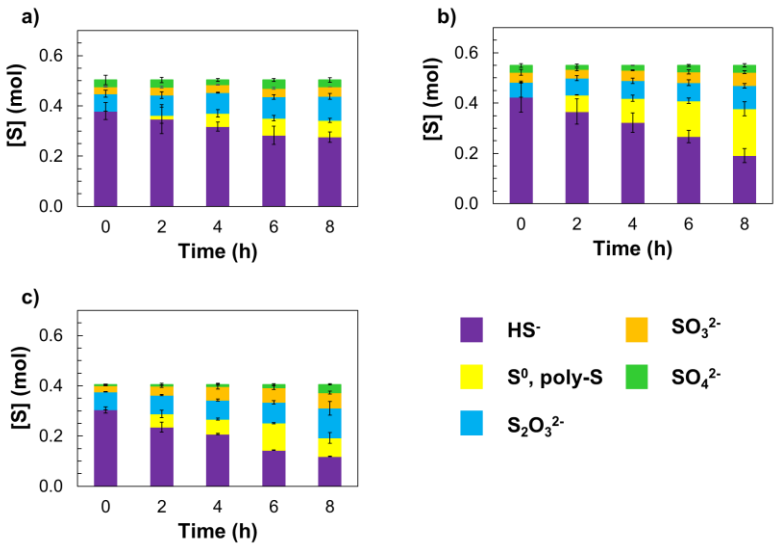

Figure 4.2 – Evolution of sulfur speciation during the batch experiments with synthetic SCS, operated at a) 100 A m^{-2}, b) 200 A m^{-2} and c) 300 A m^{-2}, n = 2 replicates

4.3.1.2 Effect of current density on NaOH recovery and energy input

The increase of current density resulted in a decrease of alkalinity and conductivity of the anolyte, as a result of the HS^- oxidation and Na^+ migration to the cathode, with a concomitant increase in the catholyte, as a result of the OH^- evolution and Na^+ accumulation. Through the experiments, the alkalinity and conductivity of the anolyte decreased from an initial 11.8 ± 0.0 wt.% and 0.6 ± 0.0 S cm^{-1}, respectively, to reach 5.9 ± 0.1 wt.% and 0.3 ± 0.0 S cm^{-1}, respectively, at 300 A m^{-2}. In contrast, the alkalinity and the conductivity of the catholyte increased from an initial 4.5 ± 0.5 wt.% and 0.2 ± 0.0 S cm^{-1}, respectively, to reach 9.0 ± 0.0 wt.% and 0.5 ± 0.0 S cm^{-1}, respectively, at 300 A m^{-2}. This catholyte alkalinity increase corresponded at 300 A m^{-2} to a R_{NaOH} of 80.4 ± 0.6 % (Figure 4.3a).

The electrical power input per electron is determined by the cell voltage. Since in electrochemical treatment the power input is the main contributor to operational costs, the cell voltage needs to be minimized, for a given current density. The average cell voltages measured here were 1.32 ± 0.09, 1.67 ± 0.04 and 2.44 ± 0.58 V for 100, 200 and 300 A m^{-2}, respectively (Fig 4.3b). The high standard deviation observed at 300 A m^{-2} was induced by the large potential oscillations.

Hence, an increase of applied current density was related to an increase in the RE_{HS^-} but also in the energy input, which increased from 3.2 ± 0.3 to 9.9 ± 1.7 kWh kg^{-1} S removed, for 100 to 300 A m^{-2}, respectively (Figure 4.3c). The increase of energy input can be attributed to an increase of the anode potential, which can be attributed partially to a decrease in the anolyte conductivity and partially to a combination of HS^- depletion and initial coverage of the active sites on the electrode surface with the deposition of S^0 particles (Figure 4.1c). The contribution of the 50% decrease in conductivity during

the 300 A m^{-2} can be narrowed down to 60 mV, considering the 0.02 Ω uncompensated resistance (Table A3.2) measured with the CI method prior to this experimental cycle.

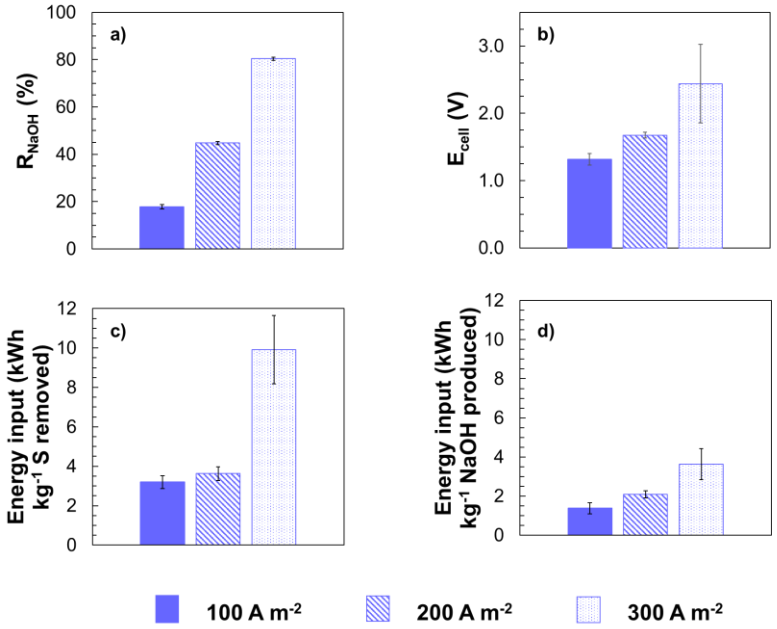

Figure 4.3 – Operational performance during the 8 h batch experiments given as a) cathodic NaOH recovery efficiency (R_{NaOH}, %) and b) average cell voltage (E_{cell}, V), c) energy input for sulfide removal (in kWh kg^{-1} S removed), d) energy input for cathodic recovery of NaOH (in kWh kg^{-1} NaOH produced) for 100, 200 and 300 A m^{-2}, n = 2 replicates

The S^0 particles produced on the electrode surface will either enter the electrolyte through chemical dissolution to form polysulfides (Mao et al. 1991), or in the colloidal form by a de-flaking process through oxygen bubble formation on the anode (Vaiopoulou et al. 2016), or they will get further oxidized to sulfur oxyanions (Behm and Simonsson 1997). Behm and Simonsson (Behm and Simonsson 1997) described a plausible scenario where the outer particles of the sulfur layer are released in the electrolyte, while the inner particles are oxidized to SO_4^{2-} and $S_2O_3^{2-}$. When high anodic potentials are reached during electrolysis, it is possible that the S^0 particles are removed by oxygen bubbles formed on the electrode surface. This is a plausible scenario for the batch experiment at 300 A m^{-2}, after the first 4 h (Figure A3.2), where the anode potential reached an average value of 1.03 ± 0.4 V vs SHE. Ultimately, when the electrolyte is saturated with sulfur, the S^0 particles start to precipitate (Mao et al. 1991) in the electrolyte chamber, or in the electrolyte recirculation bottles.

Similarly to the RE_{HS-}, the energy input for NaOH recovery increased with increasing current density from 1.4 ± 0.3 kWh kg^{-1} NaOH at 100 A m^{-2} to a maximum of 3.6 ± 0.8 kWh kg^{-1} NaOH produced in the cathodic side at 300 A m^{-2} (Figure 4.3d). This energy input is in the same range as conventional

membrane electrolysis in the chlor-alkali industry providing NaOH with an energy investment of ~2.5 kWh kg^{-1} NaOH (Brinkmann et al. 2014). Evidently, the process described here fulfils several functions simultaneously, which implies that the energy investment principally needs to be redistributed over the different products.

4.3.2 Continuous sulfide removal and caustic recovery with electrochemical treatment of industrial SCS

4.3.2.1 Sulfide is continuously and selectively removed at 1.75 V average E_{cell}

To assess the applicability of electrochemical SCS treatment, a two compartment electrochemical system was operated with industrial SCS (Table 4.1) for 20 successive days at 300 A m^{-2}. The main product of the HS^- oxidation was S^0, which was supported by the high CE_{HS-} and the low E_{WE} (0.09 ± 0.02 V vs SHE), maintained during the course of the experiment (Figure 4.4, Table 4.2). This low anode potential excludes the possibility of oxygen evolution during this experiment, therefore the main mechanism for S^0 removal from the electrode surface appears to be through chemical dissolution in the alkaline sulfidic electrolyte. A joint mechanism where the outer particles of the sulfur layer are released while the inner particles are further oxidized to sulfur oxyanions could also be considered here (Behm and Simonsson 1997; Vaiopoulou et al. 2016), hence a limited increase of sulfur oxyanions in the anolyte effluent was observed (Figure 4.4). This electrode self-cleaning process could be the main reason for the stable operation of the system during the 20 days of operation. The lower E_{WE} obtained with the industrial SCS at the same current density, compared to the synthetic, is attributed to the higher concentrations of sulfide and NaOH. The mass transport of sulfide to the electrode surface is key in an electrochemical oxidation process and thus higher concentration in the electrolyte will lead to higher concentration at the electrolyte – electrode interface, increasing the coulombic efficiency. However, this assumption requires model verification.

The average RE_{HS-} obtained with a 205 ± 60 g S L^{-1} d^{-1} HS^- loading rate was 38.0 ± 7.7%, combined with a stable E_{cell} (1.75 ± 0.12 V) (Table 4.2). The E_{cell} obtained with the industrial SCS is comparable with the one obtained with the synthetic SCS, which shows that the proposed system can work equally well when applied for the treatment of more complex matrices. A RE_{HS-} of 67% when operated at 200 A m^{-2} was reported by Vaiopoulou et al. with synthetic SCS and similar electrolysis system (loading rate 47 g S L^{-1} d^{-1}). The differences in the HS^- loading rates can explain the differences in RE_{HS-} (Vaiopoulou et al. 2016) and also be linked with less oxidized sulfur species produced (Figure 4.4).

Table 4.2 – Operational and performance parameters of the continuous industrial SCS treatment at 300 A m^{-2}

Parameter	Unit	Average ± SD
Anode potential (E_{WE})	V vs SHE	0.09 ± 0.02
Cell voltage	V	1.75 ± 0.12
HS^- removal efficiency (RE_{HS-})	%	38.0 ± 7.7
Anodic coulombic efficiency (CE_{HS-})	%	79.9 ± 31.0
NaOH recovery efficiency (R_{NaOH})	%	54.0
Cathodic coulombic efficiency (CE_{OH^-})	%	33.0*
Energy input for wastewater treatment	kWh m^{-3} SCS treated	75.3 ± 5.0
Energy input for pollutant removal	kWh kg^{-1} S removed	3.7 ± 0.6
Energy input for NaOH recovery	kWh kg^{-1} NaOH recovered	6.3 ± 0.4

* The average achieved during the continuous operation (99.3 % highest achieved)

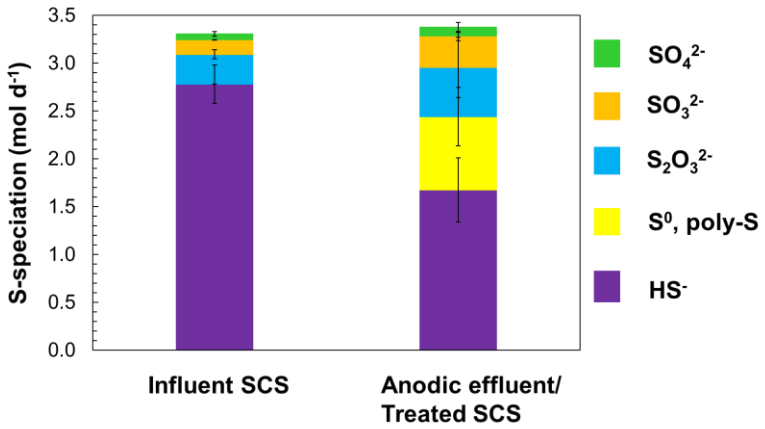

Figure 4.4 – Averaged sulfur speciation during the electrochemical oxidation of industrial SCS and the anolyte, under continuous operation for 20 days at 300 A m^{-2}

The particles of S^0 collected in the anodic chamber and on the anode surface were identified as hydrophobic (θ_{av}^{water} = 71.4°) (Figure A3.3) and orthorhombic sulfur (α-S_8) (Figure 4.5). The production of hydrophobic α-S_8 has been previously reported in chemical and electrochemical HS^- oxidation (Selvaraj et al. 2016; Steudel 1996). The S^0, provided it does not contain contaminations, could be

used as commercial sulfur for sulfuric acid production, in lithium–sulfur batteries or, as feedstock for production of polymeric materials (Chung et al. 2013).

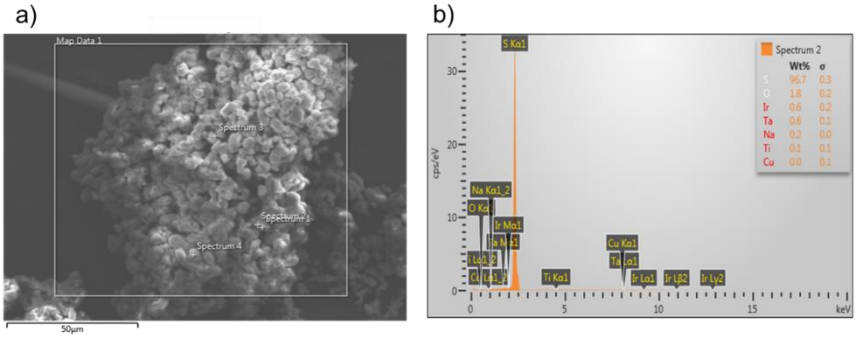

Figure 4.5 – a) SEM image and b) SEM-EDX spectrum of S^0 recovered from the anodic chamber of the electrochemical cell working with industrial SCS. Magnification 400 X using 20 keV. The black bar represents 50 µm.

Beside the high HS^- concentration and high alkalinity, the SCS contained a matrix of low molecular weight (cut-off < 200 g mol^{-1}) organic compounds, representing ~35% of the total COD, while the rest is represented by HS^-. There was no oxidation of organics observed in the anodic compartment and no organic compounds were transported to the cathodic compartment (Figure A3.4). Consequently, deterioration of the operational performance of the anode and the CEM due to the presence of organics is not expected during the 20 consecutive days of operation. This opens an avenue for selective removal of sulfide and reuse of these organic solvents on-site, if the sulfide load is further minimized.

4.3.2.2 Concentrated NaOH (12.3 wt.%) is recovered in the cathodic compartment

Both the alkalinity and the conductivity increased in the cathodic compartment following the recovery of NaOH during the 20 days of continuous operation. The final NaOH concentration achieved was 24.7 wt.%, with a concomitant conductivity increase from 0.9 to 1.2 S cm^{-1} (Figure 4.6). The result was a net increase of NaOH concentration by 12.3 wt.%, which provides a solution that can be reused for several industrial applications on site (Alnaizy 2008; Brinkmann et al. 2014). For example, 5 – 10 wt.% NaOH solutions are commonly applied in oil refineries for hydrocarbons desulfurization (Ben Hariz et al. 2013). It is important to note here that no sulfur components, nor organics, were detected in the catholyte, which highlights the cleanness of the recovered NaOH. In the treated SCS (anodic compartment), the alkalinity decreased from an initial NaOH concentration of 15.7 ± 0.6 wt.% to a final 12.5 ± 0.6 wt.% with a corresponding decrease of conductivity from 0.7 ± 0.1 S cm^{-1} to 0.6 ±

0.1 S cm^{-1}. A decrease in alkalinity, and thus conductivity, of the treated SCS is essential to enable further treatment of the stream in a wastewater treatment plant (WWTP) and it is the basis of the cost alleviation that electrochemistry is providing to SCS treatment.

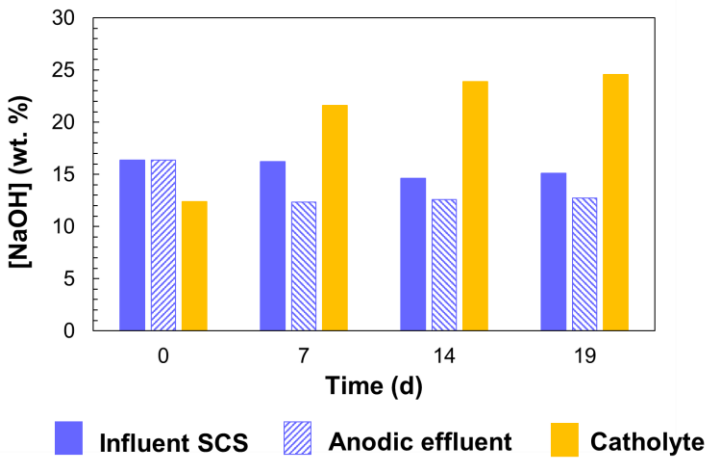

Figure 4.6 – Evolution of NaOH concentrations (wt.%) in the SCS influent, anodic effluent and cathodic batch, during the 20 days of continuous operation at 300 A m^{-2}

The CE_{OH^-} reported (Table 4.2) was the highest value achieved during the 20 days of continuous operation. The value was calculated for the first 2 days of the experiment due to a decrease over time of the CE_{OH^-} to reach 10% after the 20 days of operation. This was indicated as well by the stabilization in the NaOH concentration after 15 days of operation, which was attributed to the high strength of NaOH obtained in the catholyte and induced the termination of the continuous operation. The low CE_{OH^-} at the end of the experiment can be explained by 2 phenomena: 1) hydroxide ions (OH^-) back-diffusion from the cathodic to the anodic compartment and 2) water (H_2O) transport from the anodic to the cathodic compartment due to osmotic pressure. The OH^- back diffusion has been reported in many studies for electrolysis cells used for NaOH recovery (H.-W. Lin et al. 2016; Pikaar et al. 2013; Thiel et al. 2017) and it is more prominent when the catholyte is strongly alkaline (pH > 12 – 13) (Jörissen and Simmrock 1991). The mole balance between the OH^- theoretically consumed during HS^- oxidation and the alkalinity decrease measured in the anodic compartment suggest that the decrease of alkalinity over time was due to OH^- back diffusion (Figure A3.5). However, due to the complexity of the HS^- oxidation reactions, closing the H^+/OH^- balance to establish that effect remains difficult.

4.3.2.3 Sulfide is removed and NaOH is recovered from industrial SCS at 75 kWh m^{-3} SCS treated

The operation of the cell for 20 days resulted in an average energy investment of 75.3 ± 5.0 kWh m^{-3} SCS treated (Table 4.2). For the electrochemical treatment of sulfide-loaded tannery wastewater with a COD range from 0.25 to 2.5 g L^{-1}, Szpyrkowicz et al. (Szpyrkowicz et al. 2005) tested three different titanium based electrodes, in an undivided electrolysis cell, operated at 200 and 400 A m^{-2} current density. Depending on the electrode tested, the energy input was ranging from 50 to 250 kWh m^{-3} treated wastewater as a result of the high cell voltages, between 5 and 7 V. The COD in the current study, comprising the sulfide and the organics, was ~169 g L^{-1} and the cell voltage measured was 1.75 ± 0.12 V (Table 4.2). The low cell voltage is mainly the result of the very high conductivity of the SCS, in combination with the close spacing between the electrodes (~ 8 mm). The low cell voltage enables SCS electrochemical treatment with high energy efficiency.

Only few studies have reported the energy investment for sulfide removal. For example, Wang et al. (Y. Wang et al. 2012), reported an energy input of approximately 139 kWh kg^{-1} S for the electrochemical removal of sulfide from an oil field effluent, that was treated with coagulation and precipitation prior to the electrochemical treatment. In that study, similarly, Ir MMO anodes were used, but with lower sulfide concentration (50 mg S L^{-1}), compared to the present study. The energy input towards sulfide removal in the current study is lower when compared to previous work (Szpyrkowicz et al. 2005; Y. Wang et al. 2012; Wei et al. 2013). This can be explained by the low cell voltage, the high sulfide loading and the continuous mode, where the latter two, constantly supply electron donor in the system. Most of the studies for sulfide removal are reporting a general cost per kg sulfur removed, thus further comparison for the energy and cost efficiency is discussed in section 4.3.3.

The approach followed here resulted in a high energy efficiency, compared to what has been reported before for similar systems used to recover NaOH from SCS. In a comparative study Wei et al. compared EED and BMED for the treatment of SCS from the petrochemical industry and calculated the energy input as 8.06 and 8.20 kWh kg^{-1} NaOH recovered for the EED and BMED, respectively. In our study, the energy input for NaOH recovery was 6.3 ± 0.4 kWh kg^{-1} NaOH, which showed a positive advantage to other similar systems. However, conventional membrane electrolysis in the chlor-alkali industry is providing NaOH with an energy investment of ~2.5 kWh kg^{-1} NaOH (considering that per ton Cl_2 produced, 1.1 ton of NaOH is coproduced) (Brinkmann et al. 2014; Chaplin 2019). The highest power investment in our case though can be downsized with the scale-up of the system. Moreover, the extra energy input when compared to chlor-alkali industry, is compensated by using a waste stream instead of pure NaCl as feedstock. It is important to note that a key driver for the SCS treatment besides minimizing NaOH needs is a reduction in the salinity of the effluents, as their treatment and discharge is becoming more and more problematic.

4.3.3 Economic perspectives of a scaled-up system

A preliminary economic feasibility study was based on the laboratory scale system (total electrochemical cell volume of 0.4 L) operation during the treatment of industrial SCS in a continuous mode for 20 days (Table 4.3). The process cost estimation was based on a 40 m^3 daily (Table A3.3) SCS supply to the electrochemical cell, which results in 2.3 ton of S. Considering the operational efficiency of the studied system, after the process still 1.4 ton of HS^- – S will be directed to further treatment, assumed with H_2O_2-based oxidation. This means that the use of H_2O_2 as an oxidant for the treatment of SCS, can be avoided for 0.9 ton of HS^- – S. Consequently, the cost savings from the proposed technology were calculated based on the savings in H_2O_2 consumption from the partial removal of HS^- with electrochemical treatment and the recovery of NaOH. No discharge costs for either the H_2O_2 treatment or the electrochemical treatment were taken into account in the cost estimation calculations, as the outflow of both options will be directed for further treatment, COD and SO_4^{2-} removal, in a WWTP.

Table 4.3 - Process cost estimation, based on an assumed electrochemical unit treating 40 m^3 of SCS per day (additional information given in Table A3.3)

Operational conditions	
Required current input (A) [1]	38,240
Applied current density (A m^{-2})	300
Required anode surface area (m^2)	239.5
Power input (kW)	6967
Energy consumption (kWh d^{-1})	1,606
Operational costs	
Daily electrolysis energy costs (€ d^{-1})	177.8
Daily energy costs for SCS treatment (€ m^{-3} SCS)	4.44
Daily energy cost for HS^- removal (€ kg^{-1} S)	0.20
Daily energy costs for NaOH production (€ kg^{-1} NaOH)	0.24
Total investment costs (€) [2]	**1,437,126**
Total daily costs for SCS treatment (€ m^{-3} SCS)	231.12

Total daily costs for HS^- removal (€ kg^{-1} S)	4.69
Total daily costs for NaOH production (€ kg^{-1} NaOH) [3]	8.41
Cost savings	
Daily savings from NaOH recovery (€) [4]	333
Daily savings from decreased H_2O_2 consumption (€) [5]	1,949
Total daily savings (€)	2,282

[1] the theoretical current required to remove 877 kg HS^-, removed in the laboratory system with an average of 80% coulombic efficiency

[2] 6,000 € m^{-2} assumed as total investment costs, including electrodes (Ir MMO as anode and stainless sheet as cathode), membranes (considering the CEM from Fumasep, reported in paragraph 2.1) and engineering costs. The total investment costs were multiplied with the calculated required anode surface area

[3] calculated based on the total energy input divided by the total NaOH recovered in an up-scaled system, that would exhibit the NaOH recovery efficiency obtained in the lab tests and taking into account the investment costs

[4] calculated with an average 54% coulombic efficiency for NaOH recovery (obtained during the batch test conducted at 300 A m^{-2})

[5] calculated based on reaction stoichiometry, where 4 mol of H_2O_2 are required for 1 mol of H_2S

From the economic assessment it is clear that the main contributor to the total cost of the treatment is the investment cost which is mainly attributed to the electrodes and the membranes (Chaplin 2019; Pikaar et al. 2013; Thiel et al. 2017). Without taking into account the cost savings, the total cost for sulfide removal is in the lower price range reported for physicochemical and biological removal of sulfide (Pikaar et al. 2013). More specifically, in the lowest range are H_2O_2 oxidation and biological treatment with 1.9 – 4.2 and 1.5 – 8.9 € kg^{-1} S, respectively, while with a range between 3.7 – 7.2 € kg^{-1} S iron salts addition is a more costly approach (L. Zhang et al. 2008). It is worth mentioning though that these ranges are reported for sewer control, where the sulfide concentrations are 3 orders of magnitude lower than in the treated SCS of this study. The total daily savings can be translated to savings of 2.6 € kg^{-1} S removed, which is in the same range as what has been reported for cost savings in replacement of physicochemical methods for H_2S removal with biotrickling filters (Lebrero et al. 2011).

Regarding the NaOH recovery, Wei et al. (Wei et al. 2013) reported an energy cost of 0.62 € kg^{-1} NaOH produced when treating SCS with EED or BMED. This is more than 3 times higher than what

was achieved in the current study. Compared to the typical commercial NaOH solution (50% w/w), the current system resulted in an energy cost that is 2 times higher than the commercial 0.123 € kg^{-1} NaOH (Thiel et al. 2017), albeit in the commercial case 0.075 € kWh^{-1} are considered for the cost estimation.

There is clearly some uncertainty in this figure. However, from the total daily savings calculated it is obvious that galvanostatic electrolysis can be a profitable approach for industrial SCS treatment. In addition to that, the revenue from sulfur recovery, hydrogen production and even heat (Du et al. 2018) could further be calculated and added to the total treatment scheme. Moreover, the upscaling of the system can result in operational costs downscaling, by efficient electrochemical design to decrease internal losses and tackle osmotic pressure and back-diffusion phenomena, thus by allowing for a decrease in the total energy investment required for product recovery and pollutant removal.

4.3.4 Implications for practice and further application

The treatment of an industrial SCS and the resources recovery possibilities were demonstrated in this study and a preliminary economic analysis highlighted the scaling up perspectives. The results showed that a lab-scale electrochemical system could treat a highly loaded industrial SCS and decrease substantially the total load, while decreasing the content of sulfide and the alkalinity. However, before moving to further application and scale-up, a few limitations of the proposed technology should be addressed, without considering the high investment cost due to the use of expensive anode materials and ion-exchange membranes.

First is the optimization of the coulombic efficiency for the NaOH recovery, an implication suggested in several alkaline electrochemical systems (Jörissen and Simmrock 1991; Wei et al. 2013). An increase in coulombic efficiency could be achieved either with the fabrication of ion-exchange membranes that are more resistant to high alkalinity and high alkalinity differences between the electrochemical cell compartments, or by selecting an engineering approach that will downsize these differences. For example, dilution could be proposed in the catholyte, with deionized water (Vaiopoulou et al. 2016) or addition of a middle compartment between anodic and cathodic compartments which we also tested in that study (Figure A3.1 and A3.6). However, the latter will increase the cell resistance and thus the energy investment, as proven also previously by Wei et al. (Wei et al. 2013). Thus, one will have to make an educated decision based on the energetic gains and losses of this approach, compared to the one that we have followed here.

Second is the further decrease of the alkalinity and conductivity in the treated SCS, to enable final discharge to a wastewater treatment plant. The remaining alkalinity and conductivity can be treated with successive electrochemical cycles, or with further oxidation, a concept that was considered in the economic assessment. Successive electrochemical cycles can also be applied to minimize further the

remaining HS^-, in order to provide a clean stream of organics after the treatment, that could be potentially reused on-site. In that concept, the system will provide two clean, potentially reusable streams, an alkaline stream and an organic stream free of sulfide and with decreased alkalinity, leading to up-scaling possibilities for treatment of complex industrial waste streams.

4.4 Conclusion

The feasibility of electrochemical treatment as an alternative to H_2O_2 oxidation for HS^- removal from an industrial SCS was demonstrated in this chapter, and additionally, simultaneous electrochemical NaOH recovery was showcased. This treatment concept was tested in a divided electrolysis cell controlled galvanostatically at 300 A m^{-2} and operated for 20 consecutive days in a continuous mode. In particular, the success of the electrochemical treatment was reflected through the maintenance of a low (1.75 ± 0.12 V) cell voltage as well as a low (0.09 ± 0.02 V vs SHE) anode potential, that remained stable during continuous operation. In addition, the high maximum coulombic efficiency of 80% obtained, highlighted that the biggest part of the invested energy was directed towards HS^- oxidation for sulfur formation, instead of side, energetically more demanding, reactions. Additionally to the SCS treatment for HS^- removal, the on-site NaOH recovery in the proposed configuration holds great potential in decreasing the costs associated with purchasing and transport of this chemical to industrial sites. Low energy input towards pollutant removal (3.7 kWh kg^{-1} S removed) and moderate energy input for wastewater treatment and NaOH recovery (75.3 kWh m^{-3} SCS treated and 6.3 kWh kg^{-1} NaOH recovered) were achieved. Based on the aforementioned energy inputs, the NaOH recovery and a comparison with the current, H_2O_2 oxidation-based, treatment methods, a preliminary economic assessment conducted in this chapter suggests economic viability for the proposed treatment concept.

CHAPTER 5

Sulfide inhibition of H_2/CO_2 acetogenesis

Adapted from:

Eleftheria Ntagia, Ioanna Chatzigiannidou, Adam J. Williamson, Jan B. A. Arends, Korneel Rabaey (2020). Homoacetogenesis and microbial community composition are shaped by pH and total sulfide concentration. Microbial Biotechnology. 13(4). p.1026-1038, doi: 10.1111/1751-7915.13546

Abstract

Biological CO_2 sequestration through acetogenesis with H_2 as electron donor, is a promising technology to reduce greenhouse gas emissions. Today, a major issue is the presence of impurities such as hydrogen sulfide (H_2S) in CO_2 containing gases, as they are known to inhibit acetogenesis in CO_2 based fermentations. However, exact values of toxicity and inhibition are not well defined. To tackle this uncertainty, a series of toxicity experiments were conducted, with a mixed homoacetogenic culture, total dissolved sulfide concentrations ([TDS]) varied between 0 and 5 mM and pH between 5 and 7. The extent of inhibition was evaluated based on acetate production rates and microbial growth. Maximum acetate production rates of 0.12, 0.09 and 0.04 mM h^{-1} were achieved in the controls without sulfide at pH 7, 6 and 5. The half maximal inhibitory concentration (IC_{50}^{rAc}) was 0.86, 1.16 and 1.36 mM [TDS] for pH 7, 6 and 5. At [TDS] above 3.33 mM, acetate production and microbial growth were completely inhibited at all pHs. 16S rRNA gene amplicon sequencing revealed major community composition transitions that could be attributed to both pH and [TDS]. Based on the observed toxicity levels, treatment approaches for incoming industrial CO_2 streams can be determined.

5.1 Introduction

Carbon dioxide (CO_2) emitted from industrial activities can be utilized by reduction into commodity chemicals within a general Carbon Capture and Utilization (CCU) scheme. One such avenue of CO_2 utilization is through gas fermentations, where homoacetogenic bacteria are employed to convert CO_2 to acetate, using hydrogen (H_2) as electron donor, through the Wood-Lungdahl pathway, which allows for linear CO_2 fixation (Drake et al. 2008). This pathway allows acetogenic bacteria to grow on C1 substrates, which signifies the importance of these bacterial cultures for industrial biotechnology applications. Starting with the isolation of *Clostridium aceticum* (Wieringa 1939) more than 100 acetogenic species have been isolated to date. A detailed overview of the acetogenic communities, the mechanism of the Wood-Lungdahl pathway, as well as gas fermentation operational perspectives is given in several reviews (Drake et al. 2008; Liew et al. 2016).

Gas emissions from point sources by some of the largest CO_2 emitting industries, such as petroleum refineries (Perez 2013; Vostrikov et al. 2017), steel (Mochizuki and Tsubouchi 2017), pulp and paper (de Souza 1988) and power production industry (particularly geothermal) (Kristmannsdóttir et al. 2000) as well as biogas production, are often accompanied by various impurities (Osorio and Torres 2009; Vostrikov et al. 2017). A major concern when upgrading these gas streams in the context of CCU, is that H_2S, as one of the more common impurities, can already be toxic for microorganisms, both in pure culture or within microbial communities, at concentrations of a few ppm (Wu et al. 2015). Several strategies for H_2S removal exist (Mandal et al. 2004; Pikaar et al. 2015; Vaiopoulou et al. 2016), but these processes will only lower the concentration of H_2S and a fraction of it will inevitably end up in a gas fermentation reactor, where it can affect the microbial activity. The amount of H_2S in the fermentation reactor will be dependent on the prior H_2S removal steps (Kristmannsdóttir et al. 2000). These steps will increase the total process costs, which can be avoided if we achieve a better understanding of the inhibitory effect and extent of certain impurities (Liew et al. 2016). Complete removal is also not desirable as anaerobic microorganisms require sulfide as nutrient (Dhar et al. 2012).

Sulfide toxicity has been reported for both mammalian and bacterial cells and the mechanisms of toxicity may range from a general inhibition of respiratory activity (Bouillaud and Blachier 2011; Y. Chen et al. 2008), DNA damage and protein denaturation (Wu et al. 2015) to inhibition of specific activities, unique for specific organisms. Sulfide impairs a number of specific metabolic activities such as anammox and denitrification, as well as sulfate reduction, by decreasing the heme c content (Jin et al. 2013), by inhibiting the N_2O reductase activity (Pan et al. 2013) and the sulfur reductase activity of cytochrome c3 (Reis et al. 1992), respectively. In the case of homoacetogenic bacteria, the information provided include either studies on CO–utilizing acetogens, usually employed in synthesis gas conversion (Grethlein et al. 1992; Vega et al. 1990), or homoacetogens as part of a general anaerobic community active during anaerobic digestion (Colleran et al. 1998; Dar et al. 2008;

Vincent O'Flaherty et al. 1998). Importantly, the primary focus of studies to date has been on neutral to alkaline pH systems, thus have not yet considered lower pH systems (pH 5-6) typical of CO_2-fed fermentations that aim for steering the bioproduction to higher value products, such as ethanol (Liew et al. 2016). Furthermore, these studies rarely consider actual sulfide concentrations in solution during their activity tests, thus the inhibitory sulfide concentrations are often misestimated (Y. Chen et al. 2008; McCartney and Oleszkiewicz 1991). Homoacetogens are a highly versatile group of bacteria that thrive in both acidic and alkaline pH environments (Drake et al. 2008) with a growth optimum between pH 5.5 (Grimalt-Alemany et al. 2018) and neutral (Ayudthaya et al. 2018; Braun and Gottschalk 1982; Grimalt-Alemany et al. 2018).

The extent of sulfide inhibition is expected to be determined by the operational pH applied in a fermentation reactor, since this directly affects the sulfide speciation (Lewis 2010) as well as the microbial activity. It remains unclear whether hydrogen sulfide (H_2S), or the bisulfide ion (HS^-) is responsible for the toxicity effect (Y. Chen et al. 2008; Küster et al. 2005). However, there is a general consensus that the undissociated H_2S molecule can more easily penetrate the bacterial cell membrane, diffuse in the cell (Küster et al. 2005; Saad et al. 2017) and hinder the bacterial metabolic processes. Nevertheless, O'Flaherty et al. reported that the concentration of the undissociated H_2S molecule [H_2S] was related to inhibition at the lower tested pH (6.8 – 7.2) and total dissolved sulfide concentration [TDS] at a pH above 7.2 (Vincent O'Flaherty et al. 1998). Information on the operational pH is rarely reported, making it impossible to reach a valid conclusion on the effective inhibitory concentrations (Y. Chen et al. 2008). It is also not known whether there are large differences between bacterial acetogenic species in terms of sensitivity.

Given the above, it is of importance to assess the tolerance of gas fermenting microbial communities and pure cultures for their response to sulfide concentration and pH driven speciation. In this work, a series of toxicity experiments were conducted in serum flasks, inoculated with a mixed homoacetogenic microbial community and exposed to a range of sulfide concentrations, from 0 up to 5 mM [TDS]. The pH values selected for hydrogenotrophic homoacetogenic growth ranged between 5 and 7. Inhibition was evaluated based on acetate production by the microbial community and biomass growth. The pH, sulfide concentration in liquid and gas phase and the partial pressure in each serum flask were closely monitored. The half maximal inhibitory concentration (IC_{50}) of the mixed homoacetogenic community was subsequently calculated at three different pH levels (7, 6 and 5) thus providing a dataset of inhibitory TDS/ $H_2S_{(aq)}$/ HS^- concentrations that has been lacking till now. This dataset provides tolerable levels of TDS (= sum of $H_2S_{(aq)}$ and HS^-) and the individual influence of bisulfide (HS^-) and dissolved hydrogen sulfide ($H_2S_{(aq)}$) for future development of microbial CO_2 conversion schemes, starting from waste gasses.

5.2 Materials and Methods

5.2.1 Enrichment and batch experiments

A mixed microbial community was obtained from the cathode effluent of a working microbial electrosynthesis (MES) reactor, reducing CO_2 mostly via electrogenerated H_2 and producing acetate (Patil et al. 2015). To exclude pH interferences on sulfide toxicity, the reactor community was pre conditioned at pH 5, 6 or 7. Cultures were sequentially transferred (10%) four times when a stable acetate production rate was observed. For the sulfide toxicity experiments, the preconditioned pH 5, 6 and 7 cultures were augmented with increasing sulfide concentrations (0 – 5 mM [TDS]), by addition of a 100 mM $Na_2S \cdot 9H_2O$ stock solution. Initially the addition of Na_2S in each serum flask was calculated for a total mass addition of 400 µmol of Na_2S – S, equivalent to 10 mM concentration. This resulted in a [TDS] of 5 mM, due to the sulfide dissociation and furthermore to actual concentrations of 3.33 ± 0.34 mM ([TDS]) (average for the three different pH levels), due to reaction of the sulfide with traces of oxygen still remaining in the medium and some of the trace elements. Through the manuscript, the actual [TDS] are reported (detailed in Table A4.1), taking into account the standard deviation resulting from initial handling of the triplicates. The serum flasks were incubated at 28 °C in a horizontal position in order to increase the gas exchange surface. Sampling was conducted over a 240 h period every 48 h and volatile fatty acids (VFAs), sulfur components, pH, pressure and optical density were measured. Samples for DNA extraction were also taken at the beginning and end of the experiment (240 h). Flow cytometry for total cell counts was conducted in the beginning and at the end of the experiments (t=0 and 240 h).

For both the preconditioning steps and the subsequent batch experiments, 40 mL of media was added to each 250 mL serum flask. The medium was prepared according to (Patil et al. 2015), excluding cysteine (in order to have only one source of sulfur in the medium) and bicarbonate (leaving CO_2 as the primary carbon source for acetogenesis) (Table A4.2). Prior to inoculation, the flasks were sealed with viton rubber stoppers and the headspace flushed with a gas mixture of N_2:CO_2, 90:10% through a series of overpressure-vacuum cycles to create anaerobic conditions. The flasks were subsequently autoclaved (121 °C for 20 min). After autoclaving, the headspace was once again exchanged and pressurized to 1.54 ± 0.04 bar with a gas mixture of H_2 and CO_2 (H_2:CO_2, 70:30%). This two-step procedure was selected based on safety reasons, to avoid autoclaving a serum flask filled with 70% H_2 gas.

After the head-space exchange, appropriate pH buffer (1M Tris-HCl buffer for pH 7 and NaOH adjusted 1M MES for pH5 and 6) and sulfide (from a 100 mM $Na_2S \cdot 9H_2O$ stock solution) were added and the serum flasks were left in a horizontal position overnight to equilibrate. After 24h, 0.4% (v/v) of a vitamin solution (prepared according to Patil et al. (Patil et al. 2015) (Table A4.2) was added. After the equilibration and the addition of the vitamin solution, the actual [TDS] and [H_2S_{aq}] changed,

due to binding of initially provided sulfide to metals from the trace element solution (Table A4.3) or reaction with residual oxygen, therefore, the [TDS] and [H_2S_{aq}] were measured throughout the incubation period in each individual flask. The initial experimental conditions (t=0), e.g. acetate and cell concentrations, pH, [TDS] and [H_2S_{aq}], are provided in Table A4.1.

5.2.2 Sampling and analytical methods

Samples were taken from the headspace of the flasks and were analysed for H_2, O_2, CO_2, H_2S and CH_4. Samples for sulfur components (sulfide (TDS), sulfite (SO_3^{2-}) and thiosulfate ($S_2O_3^{2-}$) were immediately prepared for analysis to minimize the potential for oxidation. Samples were taken from experimental flasks with aseptic technique with N_2/CO_2 flushed syringes, then diluted with treated Milli-Q water (addition of 50 % v/v NaOH (1:1000) and 37% formaldehyde (1:1000) in Milli-Q and subsequently flushed with Argon). The samples for sulfur components analysis were prepared according to Chapter 2.

The gas phase composition was analyzed with a Compact GC (Global Analyser Solutions, Breda, The Netherlands), according to De Vrieze et al (Vrieze et al. 2016). The total pressure of the serum flasks headspace was measured by using UMS-Tensiometer (Infield 7) device. The [H_2Saq] concentrations were calculated by Henry's law (Equation A4.1.1.1), using measured pressure and CGC (Compact Gas Chromatograph) mol % H_2S. Based on the [H_2Saq] and the pH measured, the [HS^-] was determined with Visual MINTEQ model for acid-base equilibria (Equation , A4.1.1.2), for $pKa_{H2Saq/HS-}$ 7.05 (Perrin 1982) (detailed in Table A4.4). The sum of $H_2S_{(aq)}$ and HS^- was used for the calculation of [TDS], which was crosschecked with the [TDS] results analysed by IC. The pH was measured with a Metrohm 744 pH meter at room temperature (~ 24 °C) (Table A4.1 and A4.5) and the OD of the bacterial culture was measured with a UV/Vis spectrophotometer (Isis 9000, Dr Lange, Germany) at 600nm. The OD measurements were normalized to the OD_{600} at t0 (i.e. δOD_{600} = OD_{600} difference between t0 and t each sampling time, e.g. 48 h) at the beginning of the incubation (t=0) and the subsequent measurement (every 48 hours) is reported here as δOD_{600} (i.e. the difference between the measured OD_{600} at time t=0 and 240 h). VFA analysis was conducted as previously described, using a 930 Compact Ion Chromatography (IC) Flex (Metrohm, Switzerland) system with inline bicarbonate removal (MCS). Separation was done on a Metrosep organic acids (250/7.8) column at 35 °C behind a Metrosep organic acids (4.6) guard column. (Gildemyn et al. 2015). Liquid samples prepared for sulfur components were analysed with the same IC with Professional UV/VIS detector Vario and equipped with a Metrosep A Supp 15-150/4.0 column as described previously (Vaiopoulou et al. 2016).

The sulfide toxicity in the bacterial cells was determined based on overall volumetric acetate production rates (r_{Ac}), calculated as in Equation 5.1. The maximum volumetric acetate production rates (r_{Ac}^{max}),

determined between each sampling event was calculated based on Equation 5.2. Partial pressure for each of the gases in the headspace was calculated every sampling event, based on the total pressure of the headspace.

Acetate production rate:

$$r_{Ac} = \frac{[Ac^-]^{t=240\,h} - [Ac^-]^{t=0h}}{dt} \quad (5.1)$$

where r_{Ac} is the acetate production rate in mM h^{-1}, $[Ac^-]^{t=240h}$ and $[Ac^-]^{t=0h}$ are the acetate concentrations at the end and at the beginning of the experiment, respectively, in mM and dt is the experimental period, in this case 240 h.

Maximum acetate production rate:

$$r_{Ac}^{max} = \frac{[Ac^-]^{t'} - [Ac^-]^{t}}{(t'-t)} \quad (5.2)$$

where r_{Ac}^{max} is the maximum acetate production rate in mM h^{-1} calculated every 48 h of the experimental period, $[Ac^-]^{t'}$ and $[Ac^-]^{t}$ are the acetate concentrations at $t' = 48+t$ h and t, respectively, in mM. The IC_{50} values were generated with GraphPad Prism 6 (GraphPad Software, Inc., La Jolla, CA, U.S.A) following a standard log-dose inhibition curve as in (Carlson et al. 2015), with 95% confidence intervals (CI). All the values reported are the mean of 3 biological replicates.

5.2.3 Total cell counts with flow cytometry (FCM)

In the beginning of the experiment (t=0) and at experimental end points (t=240 h), samples were taken from each serum flask following the aforementioned sampling procedure for total cell counts with FCM. The biomass was suspended and no agglomeration of the cells was observed. The samples were appropriately diluted with PBS buffer and afterwards stained with SYBR Green I (SG), suitable for a total cell count. The SYBR Green I (10,000X concentrate in DMSO, Invitrogen) stain was diluted 100 times in 0.22 μm-filtered DMSO (IC Millex, Merck, USA). The samples were stained with 10 μL mL^{-1} staining solution according to Prest et al. (2013) (Prest et al. 2013) and incubated for 13 min at 37 °C.

All measurements were conducted with a FACSVerse cytometer (BD Biosciences, Belgium). The instrument was calibrated with the CS&T calibration beads (BD Biosciences, Belgium) daily. The blue laser (488nm) was used for the excitation of the stains. The optical filters used were 527 nm with a bandpass of 32 nm for the green fluorescence and 700 nm with a bandpass of 54 nm for the red fluorescence. A minimum of 10000 cells per sample were measured to allow accurate quantification. The data of each sample were denoised from (in)organic noise by a filtering approach using the flowCorepackage (v1.38.1) in R (v3.3.2). The bacterial cell population was extracted by a manual gate applied on the primary fluorescence emission channels.

5.2.4 16S rRNA Gene amplicon sequencing

Samples for DNA extraction were taken at t=0 and t=240 h from the triplicate serum flasks representing of sets 1, 6 and 8 (Table A4.1), representing averaged (for the pH 7, 6 and 5) total dissolved sulfide concentrations of 0.06 ± 0.01, 1.26 ± 0.23 and 3.33 ± 0.34 mM [TDS]. Throughout the manuscript these concentrations will be reported as 0.06, 1.26 and 3.33 mM [TDS]. The samples were pelleted by centrifugation for 10 min at 10000 g. Pellets were stored at -20 °C till further processing. DNA was extracted according to Vilchez-Vargas et al. (2013) (Vilchez-Vargas et al. 2013). DNA quality was evaluated on a 1% (w/v) agarose gel. 16S rRNA gene amplicon sequencing analysis was performed as described before (Domingos et al. 2017; Vrieze et al. 2016). Near full length 16S rRNA gene sequencing was performed using the Sanger method. Information on the DNA extraction methods, Gene amplicon sequencing analysis, clone library methods and data processing details can be found in in Appendix 4, paragraph A4.1.1.

All statistical sequence analysis was performed in R (v3.3.2). The reads received from 16S rRNA gene amplicon sequencing were imported in R. OTUs with no more than one read in every sample (singletons) were removed (McMurdie and Holmes 2014). The Estimated Absolute Abundances (EAA) of the different genera were calculated by projecting the relative abundances, obtained by sequencing, to the cell numbers obtained by FCM (Props et al. 2016). The graphs representing the 15 most relative or absolute abundant genera were generated using the phyloseq package 7 in R (v3.3.2). Non-metric multidimensional scaling (NMDS) plots of relative abundances were prepared based on the Jaccard distance to visualise the effect of pH and [TDS] on the β-diversity. The confidence ellipses were computed using the function 'stat-ellipse' in R (v 3.3.2) with confidence level 0.95.

Accession number(s). The flow cytometry data (.fcs format) have been submitted to the FlowRepository archive under repository ID FR-FCM-ZYX5. The sequences of the 16S rRNA gene have been submitted to the NCBI Sequence Read Archive (SRA) under accession number SRP157026.

5.3 Results

5.3.1 Sulfide concentration induces inhibition of microbial growth and homoacetogenic acetate production

To ensure sulfide was the primary source of inhibition on the communities, the microbial community was acclimated prior to the experiments at pH 7, 6 and 5 (Figure A4.1). The inoculation of every serum flask was done with an equal initial cell concentration, average of 6.54 ± 0.58 × 10^7 cells mL^{-1} (Figure A4.2). The preconditioning induced differences within the initial microbial community (Figure

5.1). The β-diversity NMDS plot revealed two distinct clusters for the samples grown in pH 5 and 7, while the pH 6 samples appeared between the two clusters. The inhibition results are discussed based solely on [TDS] (defined as the sum of the HS^- and H_2S_{aq}), as these sulfide species will be present in the liquid phase, and as a function of pH (sulfide speciation).

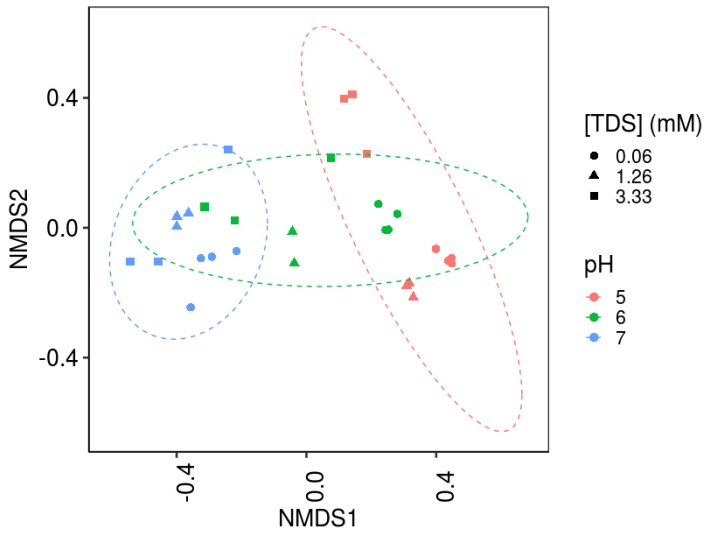

Figure 5.1 – Non-metric multidimensional scaling (NMDS) presenting the β-diversity between different samples, calculated for n=3 biological replicates, showing community dissimilarities with the pH shifts. A 95% confidence ellipse is drawn.

Sulfide inhibition was initially assessed through microbial growth. Prior to inoculation (t0), sulfide augmentation resulted in turbidity in the media, particularly at higher sulfide concentrations. This could represent some sulfide oxidation with residual oxygen and/or colloidal sulfide-metal complexes with the trace elements present in the medium (Table A4.3). Sulfide concentrations remained stable after addition, confirming no oxidation had occurred over time. Direct cell counts were thus assessed using flow cytometry (FCM), rather than optical density measurements. The biomass production in all pHs tested was significantly (P value <0.05) impaired by increasing [TDS] (Figure 5.2a and A4.3). For pH 7, the difference in total cell counts between low and high sulfide additions was 7.37 ± 0.45 $\times 10^8$ cells mL^{-1} (Figure 5.2, Table A4.5) and the IC_{50}^{growth} was 0.90 mM [TDS], 0.55 mM [H_2S_{aq}] and 0.34 mM [HS^-] (Table 5.1). At pH 6 the total cell counts differed by 5.08 ± 0.94 $\times 10^8$ cells mL^{-1} (Figure 5.2a, Table A4.5) and the IC_{50}^{growth} was 1.33, 1.15 and 0.17 mM [TDS], [H_2S_{aq}] and [HS^-], respectively (Table 5.1). At pH 5 the greatest difference (8.71 ± 2.91 $\times 10^8$ cells mL^{-1}) in total cell counts between low and high sulfide additions was observed (Figure 5.2, Table A4.5) and the IC_{50}^{growth} was 1.29 mM [TDS], 1.05 mM [H_2S_{aq}] and 0.07 mM [HS^-] (Table 5.1).

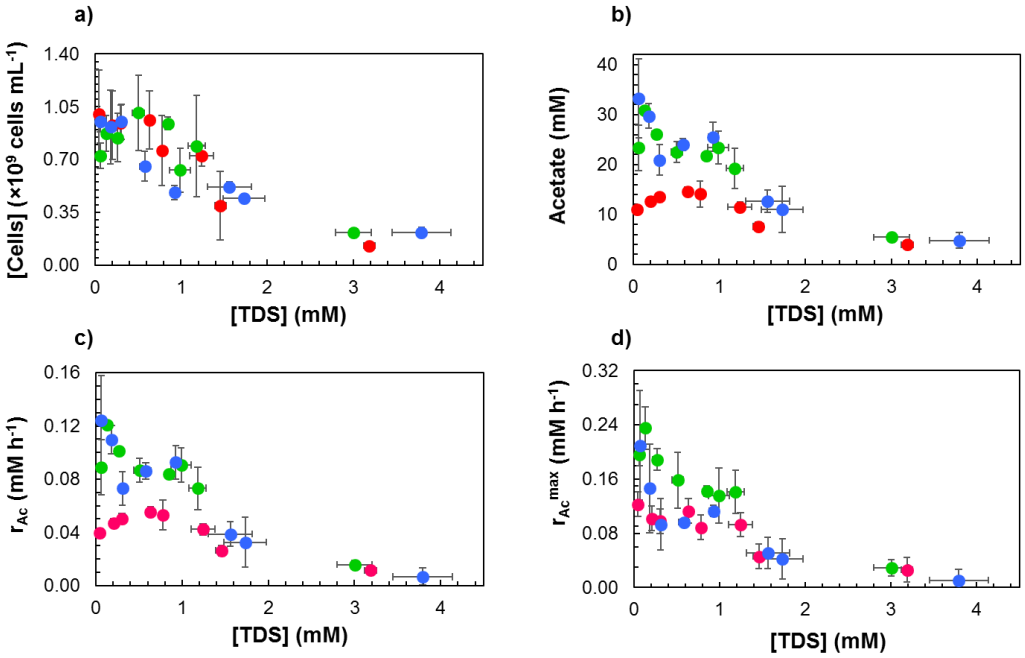

Figure 5.2 – Plotted against initial total dissolved sulfide concentration ([TDS]) (mM) are a): Total cell concentration ([Cells], $\times 10^9$ cells mL^{-1}), b): Final acetate concentration (mM), c): Overall acetate production rate (r_{Ac}, mM h^{-1}) and d): Maximum acetate production rate (r_{Ac}^{max}, mM h^{-1}), calculated on a 48 h basis, at pH 7 (●), 6 (●) and 5 (●), respectively. Data are averages of 3 incubations, error bars represent standard deviations of biological triplicates. Complementary data are given in Figures A4.2, A4.4 and A4.5.

The overall acetate production rate (r_{Ac}) was selected as the primary indicator of microbial activity (Figure 5.2). Complete inhibition of microbial activity (<0.02 mM h^{-1} r_{Ac} and lowest final acetate concentration achieved) was observed at all pH values at the highest tested [TDS] (averaged [TDS] over all pH conditions = 3.33 ± 0.34 mM) (Table 5.1, Figure 5.2b, 5.2c and A4.3). At all pH conditions, the optimum overall acetate production rates were observed in the lowest sulfide amended systems. At pH 7, the highest overall acetate production rate (Equation 5.1) (r_{Ac}) (0.12 ± 0.03 mM h^{-1}) was achieved. The IC_{50}^{rAc} at pH 7 was calculated as 0.86 mM [TDS], 0.51 mM [H_2S_{aq}] and 0.34 mM [HS^-] (Table 5.1). At pH 6, a lower (0.09 ± 0.02 mM h^{-1}) r_{Ac} was achieved at the lowest sulfide addition (Figure 5.2c, Table A4.5) and the IC_{50}^{rAc} values were 1.16 mM [TDS], 1.01 mM [H_2S_{aq}] and 0.14 mM [HS^-] (Table 5.1). At pH 5, the lowest rates were reached, with 0.04 ± 0.01 for highest r_{Ac}, with a corresponding IC_{50}^{rAc} of 1.36 mM [TDS], 1.11 mM [H_2S_{aq}] and 0.08 mM [HS^-] (Table 5.1).

Table 5.1 – Summary of the inhibition values (total inhibition and IC_{50} for overall and maximum acetate production rates (IC_{50}^{rAc} and $IC_{50}^{rAc\_max}$) and biomass growth based on FCM analysis (IC_{50}^{growth}). All IC_{50} values are reported in mM and are given as mean values and below, in brackets, the range of IC_{50}

values, as calculated by GraphPad Prism 6 with a 95% Confidence Interval (CI). All values are results of biological triplicates. Significant difference between inhibitors at different pH levels is noted on the table with "" and "**", calculated based on two-sample t test with equal variances (samples with P value < 0.05 were considered significantly different).*

	Inhibitor (mM)	Total inhibition	IC_{50}^{rAc}	$IC_{50}^{rAc\_max}$	IC_{50}^{growth}
pH 7	TDS	3.79 (3.45 to 4.13)	0.86 (0.58 to 1.24)	0.44 (0.24 to 0.76)	0.90 (0.67 to 1.20)
	H_2S	1.96 (1.87 to 2.05)	0.51* (0.34 to 0.73)	0.27*,** (0.15 to 0.46)	0.55* (0.43 to 0.69)
	HS^-	1.82 (0.96 to 2.68)	0.34* (0.22 to 0.49)	0.17 (0.09 to 0.29)	0.34* (0.24 to 0.51)
pH 6	TDS	3.00 (2.80 to 3.21)	1.16 (0.84 to 1.63)	0.92 (0.66 to 1.27)	1.33 (1.01 to 2.16)
	H_2S	2.37 (2.16 to 2.58)	1.01 (0.74 to 1.40)	0.81* (0.59 to 1.10)	1.15 (0.90 to 1.76)
	HS^-	0.64 (0.62 to 0.66)	0.14 (0.09 to 0.23)	0.10 (0.07 to 0.16)	0.17 (0.11 to 0.39)
pH 5	TDS	3.19 (3.12 to 3.25)	1.36 (1.23 to 1.57)	1.16 (0.80 to 1.61)	1.29 (1.00 to 1.71)
	H_2S	2.81 (2.75 to 2.87)	1.11* (1.00 to 1.27)	0.98** (0.77 to 1.21)	1.05* (0.88 to 1.29)
	HS^-	0.37 (0.34 to 0.10)	0.08* (0.06 to 0.10)	0.06 (0.03 to 0.10)	0.07* (0.05 to 0.12)

The difference between overall and maximum acetate production rates are critical for scale up operations of CO_2 capture by homoacetogenic communities, since it will affect the fermentation reactor sizing and operation. In contrast to the overall acetate production rate as discussed above, the maximum acetate production rate (r_{Ac}^{max}) was calculated every 48 h of the experimental period. Similarly to r^{Ac}, the r_{Ac}^{max} decreased with decreasing pH at the lowest sulfide addition and at the highest sulfide addition the metabolic response was limited (<0.02 mM h^{-1} r_{Ac}^{max} at [TDS] = 3.33). The IC_{50} of r_{Ac}^{max} increased with decreasing pH trend but with lower absolute values compared to IC_{50}^{rAc} (Table 5.1). At pH 7, the r_{Ac}^{max} difference achieved by the bacteria between the lowest and the highest sulfide addition was ~0.21 mM h^{-1} (Figure 5.2d Table A4.5). The $IC_{50}^{rAc\_max}$ was 0.44 mM [TDS], 0.27 mM [H_2S_{aq}] and 0.17 mM [HS^-], almost half of the IC_{50}^{rAc} (Table 5.1). At pH 6 the difference between the highest and lowest r_{Ac}^{max} was ~0.18 mM h^{-1} (Figure 5.2d, Table A4.5) and the $IC_{50}^{rAc\_max}$ was calculated as 0.92, 0.81 and 0.10 mM [TDS], [H_2S_{aq}] and [HS^-], respectively (Table 5.1). Finally, at pH 5 the

aforementioned difference was calculated as ~0.09 mM h^{-1} and the $IC_{50}^{rAc\_max}$ was 1.16, 0.98 and 0.06 mM [TDS], [H_2S_{aq}] and [HS^-], respectively (Table 5.1).

5.3.2 Microbial community shifts in response to pH and sulfide concentration

To understand if an increase in biomass production was due selective genera or a full community response, FCM was coupled to Illumina sequencing to estimate the absolute abundance (EAA) of individual community members (Figure 5.3, A4.2, A4.6). Overall, the EAA of the top 15 genera present in the microbial community and presented here, decreased with increased sulfide concentrations (Figure 5.3 and A4.6). At pH 7, *Wolinella* was the most abundant genus recovered in the sequencing data. The EAA of this genus decreased significantly (P value $=0.008 < 0.05$) by 3.0 $\pm$ 0.3 $\times 10^8$ cells mL^{-1}, between 0.06 and 3.33 mM [TDS] (Figure 5.3). At pH 6 the most abundant genus was *Sphingobium*, with a significant (P value $=0.011 < 0.05$) EAA decrease of 2.2 $\pm$ 0.8 $\times 10^8$ cells mL^{-1} between highest and lowest [TDS] (Figure 5.3). At pH 5 *Sphingobium* was also the most abundant genus and again the EAA decreased significantly (P value $=0.008 < 0.05$) by 5.5 $\pm$ 1.5 $\times 10^8$ cells mL^{-1} when the [TDS] was increased to 3.33 mM.

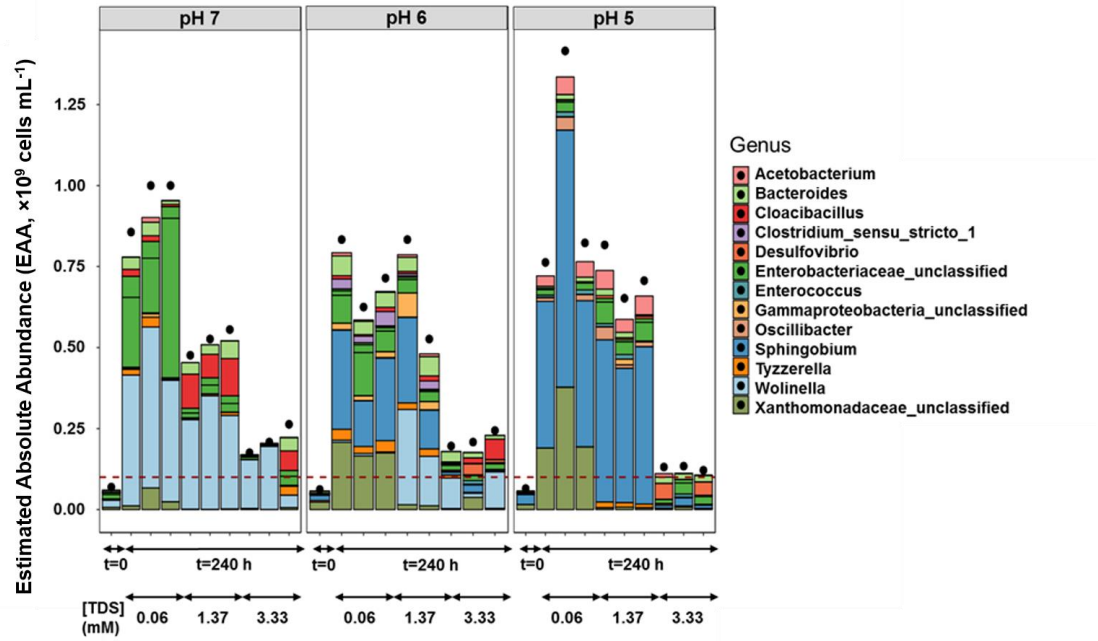

Figure 5.3 – Estimated Absolute Abundances (EAA) (cells mL^{-1}) of the 15 most abundant OTUs, calculated as relative abundances normalised for the flow cytometric counts, in 3 biological replicates (and in 2 biological replicates at pH 6 and 1.26 mM [TDS]). Black dots indicate the sum of EAA of all the OTUs identified with 16S rRNA gene amplicon sequencing analysis. The red dashed line represents the limit of 10^8 cells mL^{-1}. Non-normalized relative abundances are shown in Figure A4.6.

The most abundant genus that is known for homoacetogenesis recovered in this study, was *Acetobacterium* (Balch et al. 1977). The EAA of the *Acetobacterium* at time 0 was similar for pH 7 and 6, with 8.23 $\times$ 10^5 and 6.61 $\times 10^5$ cells mL^{-1}, respectively, but higher (3.94 $\times 10^6$ cells mL^{-1}) for pH 5, although the overall acetate production in this case was the lowest among all pH levels. At the lowest addition of sulfide, the EAA of *Acetobacterium* increased with decreasing pH, however, this genus accounted for less than 10% of the total relative abundances under all pH conditions and sulfide additions (Figure 5.3).

In the pH 7 incubation, the *Acetobacterium* EAA decreased gradually with increasing sulfide concentrations from an average of 5.8 $\pm$ 6.2 $\times 10^6$ cells mL^{-1} at 0.06 mM [TDS] to 4.7 $\pm$ 3.4 $\times 10^5$ cells mL^{-1} at 3.33 mM [TDS] (Figure 5.3 and A4.7). At pH 6 the same trend was observed, with a decrease of EAA from an average of 5.8 $\pm$ 3.0 $\times 10^6$ cells mL^{-1} at 0.06 mM [TDS] to 5.7 $\pm$ 2.3 $\times 10^5$ cells mL^{-1} at 3.33 mM. At pH 5, the *Acetobacterium* EAA dropped significantly (P value $=0.005 < 0.5$) from 4.5 $\pm$ 0.9 $\times 10^7$ to 4.8 $\pm$ 4.0 $\times 10^6$ cells mL^{-1} at 0.06 and 3.33 [TDS], respectively. In the pH 6 and 5 incubations at 1.26 mM [TDS], the abundance was higher than the one at 0.06 mM [TDS],suggesting that there is an optimal concentration of [TDS] for *Acetobacterium* species. This needs to be further explored in pure culture studies. The functional role of *Acetobacterium* in acetate production can be deduced from the correlation of EAA with final acetate concentrations (Figure 5.4a) indicated by the production of acetate as the sole metabolic product. An analogous correlation can be found for the genera *Sphingobium* and *Oscillibacter* (Figure 5.4c and 5.4d), but not for *Wolinella* (Figure 5.4b), although it should be mentioned here that any correlation in the case of genera that are not known for homoacetogenic bioproduction does not indicate a direct involvement of those genera in homoacetogenesis.

It is important to note that methane production was only observed at pH 7. This could be an indication of pH effect at first, considering that the majority of methanogens thrive in neutral up to slightly alkaline environments (Liu and Whitman 2008). Nevertheless, at pH 7, a clear sulfide toxicity effect on methanogens was observed, with only minor methane production detected at 192 h (final [CH_4] detected was 0.03 mM CH_4 at 240 h) and only for the lowest [TDS] (0.06 $\pm$ 0.01 mM).

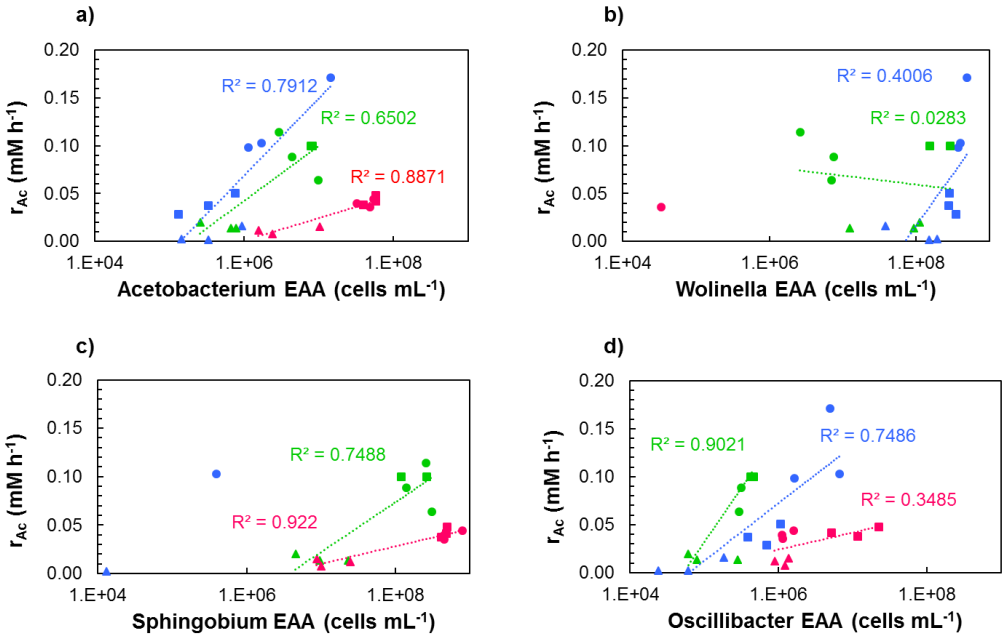

Figure 5.4 – Overall acetate production rate (r_{Ac} in mM h^{-1}) correlated with the Estimated Absolute Abundances (EAA) (cells mL^{-1}) of the genera a): Acetobacterium, b): Wolinella, c): Sphingobium and d): Oscillibacter at pH 7 (●), 6 (●) and 5 (●), respectively and at 0.06 (●), 1.26 (▲) and 3.33 (■) mM [TDS]

5.4 Discussion

5.4.1 Acetate production rates show higher sulfide sensitivity compared to biomass growth

In this study the extent of sulfide toxicity on the growth and metabolic activity of a mixed homoacetogenic microbial community was examined at pH 5, 6 and 7. This allowed for quantification of the maximum [TDS], [H_2S_{aq}] and [HS^-] conducive to growth, as well as the IC_{50}, inhibitory levels for homoacetogenic activity under both neutral and acidic conditions, data missing so far from literature. Overall, sulfide toxicity had a more profound effect on the rate of acetogenesis compared to total biomass growth, since the IC_{50}^{growth} was higher than both the IC_{50}^{rAc} and $IC_{50}^{rAc\_max}$, in all pH levels tested (Table 5.1). In general, the TDS IC_{50} of all responses (growth, r_{Ac} and r_{Ac}^{max}) increased with decreasing pH, suggesting a higher tolerance in low pH homoacetogenic communities. The observation that the perceived weaker performing homoacetogenic community (lowest r_{Ac} at pH 5) displayed a higher resistance to sulfide is an interesting one. Typically, weaker systems are more susceptible to environmental stresses such as sulfide. The opposite was observed here, hence the [TDS] as inhibitor could be less impactful under these already limited conditions.

The impact on the r_{Ac}^{max} was more profound with increasing pH; at pH 7 the $IC_{50}^{rAc\_max}$ was half of the IC_{50}^{rAc} and IC_{50}^{growth} (0.44 vs 0.86 and 0.90, respectively, when defined with [TDS]), whereas at pH 5

they are similar (1.16 vs 1.36 and 1.29, respectively, when defined with [TDS]). This was also supported by a longer lag phase in pH 5, compared to 7, observed in the incubations. The mechanisms of the different sulfide species that inhibited the cell growth and activity in this study are currently unknown, and may represent a combination of parameters governed by the equilibrium of HS^-/H_2S_{aq} inside and outside of the bacterial cell (Howsley and Pearson 1979) together with the obvious direct impact of pH. This difference in inhibition at different pH levels might indicate differentiation in environmental adaptation (Lloyd et al. 2005). The lower IC_{50} (defined with [TDS]) at pH 7 could be associated with increased susceptibility to the H_2S (Koster et al. 1986), or conversely the higher IC_{50} at pH 5 could be associated with a decreased exposure to HS^-.

Growth inhibition and reduced activity of different anaerobic microbial populations under sulfide stress, including sulfate reducing, methanogenic and some syntrophic and fermentative bacteria, has been reported in operational results of anaerobic systems (Colleran et al. 1998; Dar et al. 2008; V O'Flaherty et al. 1998). More specifically, the inhibition of methanogenesis by sulfide is already well described in literature (Y. Chen et al. 2008; Koster et al. 1986; McCartney and Oleszkiewicz 1991), and it has been reported that methanogens are more susceptible to sulfide toxicity than acetogens (Grimalt-Alemany et al. 2018). The results of the present study are in accordance with the results of McCartney and Oleszkiewicz (McCartney and Oleszkiewicz 1991) where by testing anaerobic digestion of lactate and acetate under sulfide stress they observed that higher pH values and longer incubation times favoured methane production, while at lower pH values, methane production was decreasing with increasing total sulfide (TS) concentrations.

Despite the toxicity effect, sulfide is a molecule essential for the survival of the bacterial cells, preventing them from oxidative stress (Wu et al. 2015) or metal toxicity (Lloyd et al. 2005) while also an essential macronutrient for the survival of most anaerobic organisms (Dhar et al. 2012). In any case, it appears that the mere H_2S concentration cannot be used as sole discriminant towards inhibition.

5.4.2 The microbial community shifts with sulfide concentration and speciation

Whilst pH was the primary driver of initial community composition (Figure 5.1), the subsequent addition of sulfide had a clear impact on the community structure and EAA (Figure 5.3). A decrease in the total cell numbers was observed in all pH incubations at high [TDS], accompanied with an increase in the community diversity (Fig 5.2a and 5.3). Prior to sulfide addition, *Wolinella* was the most abundant genus at pH 7, whereas at pH 6 and pH 5 the genus *Sphingobium* was dominant (Figure 5.3). Nevertheless, *Wolinella* and *Sphingobium*, are not classified in the class of Clostridia, to which most of the known homoacetogens belong (Drake et al. 2008).

The presence of *Acetobacterium*, a known homoacetogen is not surprising and has been observed in many studies involving pure homoacetogenic as well as mixed culture studies for CO_2 reduction

(Arends et al. 2017; Kantzow et al. 2015; Liew et al. 2016). The relatively low relative abundances measured (~10%) in this study indicate that other species might be additionally responsible for homoacetogenic bioproduction. Interestingly, *Acetobacterium* was the only genus that showed a similar EAA at 0.06 and 1.26 mM [TDS] (Figure 5.3) at pH 6 and 5, which suggests a higher tolerance to sulfide. Further linking of this genus to the IC_{50} values is not possible, as inhibition could be due to individual toxicity or synergistic community effects. Low concentrations of sulfide (~0.5 mM) have been reported to facilitate the growth of *Acetobacterium* on heterotrophic substrates (Heijthuijsen and Hansen 1989), however the influence of this higher sulfide concentration on this genus growing on H_2/CO_2 clearly warrants further investigation.

In order to be able to compare with literature data regarding the specific activity of *Acetobacterium*, an assumption was made for the cell dry weight of the community as previously described (Demler and Weuster-Botz 2011; Kantzow et al. 2015). The highest specific activity calculated for *Acetobacterium* was approximately 33 $g_{acetate}/ g_{CDW}$ d, obtained at pH 7 and at 1.26 mM [TDS] in this study. This value is higher than the highest reported metabolic activity (20 $g_{acetate}/ g_{CDW}$ d) of the *Acetobacterium* genus (Kantzow et al. 2015; Straub et al. 2014) which reinforces that it is likely that *Acetobacterium* was not the only active acetogen in the mixed culture studied here. The hypothesis of heterotrophic acetate production can be abandoned based on a number of observations proving homoacetogenic activity. More specifically; (i) H_2 and CO_2 were consumed from the headspace, indicating autotrophic CO_2 fixation, (ii) Acetate was the sole product of acetogenesis, (iii) The biomass concentration increased during the incubation, which serves as a counter argument for necrotrophic growth.

Wolinella was highly abundant in the homoacetogenic cultures at pH 6 and 7, however little is known about its metabolic capacities and in the incubations studied here, no correlation of the *Wolinella* EAA with acetate production was possible (Figure 5.4b). Based on existing literature, its presence could be explained by their ability (i) to gain energy through polysulfide respiration with H_2 as electron donor (Dietrich and Klimmek 2002; Hedderich et al. 1999) or (ii) through elemental sulfur respiration (Ringel et al. 1996). Whilst no chemical analysis of elemental sulfur or polysulfides was conducted in our study, the sulfide concentration remained stable over the 240 h incubations. Furthermore, Fe^{2+} has been demonstrated to be crucial in this process, however Fe^{2+} was 4 orders of magnitude lower in our system than in Ringel et al. (Ringel et al. 1996) thus such processes appear unlikely (Table A4.3). The role of *Wolinella* as a H_2 scavenger in co-cultures with fermentative anaerobic bacteria has been described before (Cord-Ruwisch et al. 1988; Parameswaran et al. 2010), thus in the current study, syntrophic growth of *Wolinella* on H_2 could be also the most probable association. Total growth inhibition of *Wolinella* by sulfide has been previously reported in co-culture with *Geobacter* at ~1mM added sulfide (Kaden et al. 2002), whilst in this study, a higher tolerance to sulfide was observed (~28

% decrease in cells at 1.33 mM), with growth inhibition occurring only at the highest sulfide concentration (~3 mM) [TDS] (Figure 5.3).

The genus of *Sphingobium* has been reported to contain mostly aerobic and facultative anaerobic soil bacteria (Berney et al. 2014; Chaudhary et al. 2017; Esposti and Romero 2017; Singh and Lal 2009; Ushiba et al. 2003). It has also been reported to perform sulfur respiration (Y. Xia et al. 2017) i.e. capable of producing H_2S through reduction of organosulfur compounds and oxidizing this self-produced H_2S, under aerobic conditions. Since the current study was performed in anaerobic conditions, a clone library was made from the sample with the most abundant community of *Sphingobium* to confirm the sequencing results (A4.1.3). From the clone library, 25% of sequences were identified as *Sphingobium* with 96 - 97% identity (A4.1.3). This limited sequence similarity most likely indicates a novel genus in this case. Although there are no metabolic data available yet that can explain the presence of this genus in an anaerobic system performing homoacetogenic production, in our incubation a correlation of its EAA with the acetate concentration, especially at pH 5 (Figure 5.4c) was observed. It should be mentioned again that any correlation in this case indicates a plausible mechanism but not causation. Another possible explanation for its presence could be that it functions in organosulfur compound metabolism (Aylward et al. 2013). The metabolic capabilities of the *Wolinella* and *Sphingobium* species recovered in this study and under these conditions should be further explored using pure culture or isolates.

5.4.3 Technological implications and future perspectives

In this study we determined the impact of sulfide on anaerobic homoacetogenic microbial consortia incubated at pH 5, 6 and 7. A typical biogas stream produced by anaerobic digestion of wastewater treatment plant sludge may contain up to 2000 ppmv H_2S (Osorio and Torres 2009) whereas other feedstocks for anaerobic digestion can lead to 30000 ppmv H_2S in the biogas (Barrera et al. 2013). In our study, maximum acetate production rates (r_{Ac}^{max}) were observed for all pH levels tested in the lowest H_2S addition, corresponding to 450 ppmv. Acetate production and microbial growth subsequently decreased with increasing [TDS]. Overall, we observed that the IC_{50} for homoacetogenic bioproduction (IC_{50}^{rAc}) in our study lies between 0.86 and 1.36 mM [TDS], 0.34 and 1.27 mM [H_2S_{aq}] and 0.06 and 0.22 mM [HS^-] for a pH range of 5 – 7 for a mixed microbial community. The average IC_{50}^{rAc} [TDS] value corresponds to a [H_2S_g] of approximately 6500 ppmv in the gas phase, showing a potentially high resistance of the studied microbial community to sulfide loaded waste gases. The difference in the IC_{50} values between the overall and the maximum acetate production rates implies that a continuous CO_2 reducing/acetate producing reactor could operate under a sulfide induced ''inhibited steady state''(Fotidis et al. 2014). Whilst future applications of a reactor operated at pH 5 with the studied microbial community could lead to lower acetate production rates, it would alleviate

the need for extensive addition of chemicals via intensive gas pre-treatment steps and pH adjustments. In addition, it needs to be highlighted that the microbial community performing homoacetogenic fermentation could potentially adapt to higher sulfide concentrations over time, which warrants further investigation.

The genera obtained by the 16S rRNA gene amplicon sequencing revealed that this resulted in the formation of a complex microbial system where, instead of solely homoacetogenesis, other metabolic interactions could have taken place, such as sulfur respiration with polysulfides or sulfur as potential electron acceptors. Nevertheless, the main metabolic outcome was still homoacetogenic acetate production. The only known homoacetogen detected in this study, *Acetobacterium*, showed resistance and even enhanced growth in the presence of moderate sulfide concentration (1.26 ± 0.23 mM TDS), compared to the other dominant community members, *Sphingobium* and *Wolinella*. Whilst correlations could be made on sulfide impact on these key community members, definitive statements on key homoacetogens in these communities could not be made. Metatranscriptomic and proteomic studies could allow for identification of the metabolic pathways expressed under sulfide stress and therefore understand if acetatogenesis is conducted under the same pathway. Furthermore, these techniques could shed light upon the differential expression of certain stress factors or mechanisms developed by bacteria to tolerate sulfide stress and help understanding differences in toleration levels, developed among different taxa.

5.5 Conclusion

In this chapter the effect of hydrogen sulfide (H_2S) in a mixed homoacetogenic community was studied at a pH window of 5 – 7. The IC_{50}^{rAC} values for acetogenesis inhibition by sulfide were quantified between 0.86 and 1.36 mM [TDS]. A [TDS] above 3.33 mM was found to completely inhibit acetate production and microbial growth. Higher tolerance levels were exhibited at pH 5, possibly due to higher community robustness developed already at cultivation of lower than physiological pH. 16S rRNA gene Amplicon sequencing in combination with flow cytometry have been used as a tool to reveal major community composition transitions that could be attributed to both pH and [TDS]. Further research on the study of individual homoacetogenic species at different pH and sulfide levels could give important insights on the effects of sulfide on specific homoacetogenic genera, however excluding any syntrophic or synergistic interactions that are common in mixed community reactor systems. Future operation of homoacetogenic fermenters will have to consider both the pH and sulfide concentration, as both of them will play, either individually or as combined stresses, a role in the stimulation or inhibition of the bioproduction. Long-term homoacetogenic fermentation should be investigated to establish to what extent adaptation to higher [TDS] is possible at the various pH levels. The results of

this study can be used as a tool to indicate the absolutely essential gas pre-treatment level while allowing for efficient acetogenic bioproduction in a waste gas fermenter.

CHAPTER 6

Sulfide inhibition of 10-L scale H_2/CO_2 fermentation

Adapted from:

Eleftheria Ntagia, Ioanna Chatzigiannidou, José M. Carvajal Arroyo, Jan B. A. Arends, Korneel Rabaey. Continuous H_2/CO_2 fermentation for acetic acid production under transient and continuous sulfide inhibition. (Manuscript in preparation).

Abstract

Waste gas fermentation is achieving full-scale (86 kton a^{-1}) application for products such as ethanol. However biological production inhibition induced by pollutants, for instance sulfide, inherent to waste gases might emerge, requiring additional gas treatment. In this work, acetogenesis and methanogenesis inhibition by sulfide was studied in a 10-L mixed-culture fermenter supplied with CO_2 and connected with a water electrolysis unit for electricity-powered H_2 supply. Three cycles of inhibition (1.3 mM total dissolved sulfide (TDS) and recovery were applied, then the fermenter was operated at 0.5 mM TDS for 35 days. Upon sulfide addition methanogenesis and acetogenesis were instantly inhibited, whilst upon removal of the inhibitor, methanogenesis presented a 5 days lag-phase of recovery, compared to acetogenesis. During final operation at 0.5 mM TDS, the acetate production rate reached 7.1 ± 1.5 $mmolC_{acetate}$ L^{-1} d^{-1}, whereas methanogenesis appeared continuously suppressed. A 44 ± 16 % of the electrons provided as H_2 in the system were distributed to acetate and an 8 ± 4 % to butyrate, the second most abundant fermentation product. The microbial community was dominated by an unclassified member of the *Eggerthellaceae* family and the genera *Eubacterium* and *Proteiniphilum*. The taxonomic diversity of the community decreased and conversely the phenotypic diversity increased, during operation.

6.1 Introduction

Waste gas fermentations powered by renewable electricity can provide a competitive and sustainable route for bioproduction. Aiming towards a significant decrease in anthropogenic carbon emissions into the atmosphere, biotechnological approaches for carbon utilization hold a crucial and leading role, as they are potentially more sustainable compared to intensive chemical routes. Nevertheless, they still need to prove financially competitive. The importance of waste gas fermentations for the scientific and industrial community is reflected through the rising number of reviews and opinion letters on this topic over the last decade (Agler et al. 2011; Liew et al. 2016; Molitor et al. 2016; Prévoteau et al. 2020; Takors et al. 2018), as well as by an increasing uptake in governmental support and subsidies for demonstration units (Schievano et al. 2019). Many studies are now moving from the fundamental understanding of gas fermentations towards tackling the two main limitations, 1) methanogenesis and 2) product separation/ downstream processing, which highlight the readiness of this process for full-scale applications.

Bioproduction by gas fermentation follows the Wood-Lunghdahl pathway (WLP), utilized by acetogenic bacteria. Through reductive acetogenesis, H_2 and CO_2 are converted to acetic acid and other products including butyric acid, ethanol, and caproic acid (Ragsdale and Pierce 2008). Starting from batch operated reactor studies (Demler and Weuster-Botz 2011) for fundamentally understanding acetogenesis and the metabolic pathways involved, the focus has turned towards continuous operation as this is the desired deliverable when commercialization of the process is considered (Heffernan et al. 2020). Most commonly pure cultures of *Clostridium*, *Acetobacterium or Moorella* species (Demler and Weuster-Botz 2011; Kantzow et al. 2015; Riegler et al. 2019; Steger et al. 2017) have been studied so far, as they allow for a more defined product spectrum. Mixed culture fermentations are applicable to a wider range of substrates, owing to microbial diversity. Additional advantages within the industrial biotechnology scope include robustness towards operational upsets and the avoidance of intensive process control (Heijstra et al. 2017; Kleerebezem and van Loosdrecht 2007), both of which ultimately result in lower operational and maintenance costs.

H_2S is a common contaminant of CO_2 containing waste gases and 3 Mt H_2S are emitted annually from industrial point sources (Ausma and De Kok 2019). Mainly natural gas plants, petrochemical refineries, geothermal power production and pulp and paper industries are responsible for anthropogenic H_2S emissions and secondarily sewage treatment plants and biogas installations (Habeeb et al. 2018; Pikaar et al. 2015; Rubright et al. 2017). The H_2S content of the waste gases poses a concern in the context of biotechnological CO_2 reduction, as H_2S can be toxic for microorganisms and in addition can corrode the combustion equipment. A vast toxicity window has been reported so far in literature, with inhibitory concentrations ranging from 60 µM (Joye and Hollibaugh 1995) to 25 mM (Y. Chen et al. 2008). The sulfide inhibition extent is, additionally to the concentration, directed by operational conditions such as pH (see Chapter 5) or the applied loading

rate (Choi and Rim 1991). H_2S reportedly impairs the metabolic activity of microbial cells through protein denaturation and in general, through interference with the electron transport mechanism within the cell (Y. Chen et al. 2008; Mirzoyan and Schreier 2014). Understanding the effect of gas impurities on gas fermentations is rudimentary for achieving high productivity rates and for designing a well monitored and economically attractive bioproduction process.

Therefore, we studied homoacetogenesis inhibition by sulfide and potential microbial adaptation using a 10-L CO_2 fermenter with H_2 as electron donor provided by an alkaline electrolysis unit. The resultant H_2/CO_2 gas mixture was continuously sparged over the liquid phase of the bioreactor. Based on previous bottle tests on homoacetogenesis under sulfide inhibition (see Chapter 5) the total dissolved sulfide (TDS) concentration was initially set at 1.3 mM TDS and three consecutive runs of "applied stress" and "removed stress" were applied after an initial period (33 days) of uninhibited, continuous gas fermentation. Finally, the reactor was operated under a minimal 0.5 mM TDS concentration for a period of 35 days. The specific objectives of this study were to: 1) assess the effect of sulfide in the productivity of a H_2/CO_2 gas fermenter operated continuously, 2) investigate the potential of sulfide as selective inhibitor towards methanogenesis and 3) to identify the prominent members of the microbial community under stress and hence indicate the expected communities in large-scale waste gas fermentation, after limited gas clean-up.

6.2 Materials and Methods

6.2.1 Experimental setup

The experimental setup consisted of a bioreactor (fermentation column), connected with a membrane unit for cell retention and an electrochemical cell for continuous production of hydrogen gas (H_2). The setup is depicted in Figure 6.1 and the description of the individual compartments is given based on the numbering on the figure. The operation of the setup, as well as monitoring and data acquisition was conducted with an in–house designed program, set with the LabVIEW 2018 software (National Instruments Belgium NV/SA, Zaventem, Belgium).

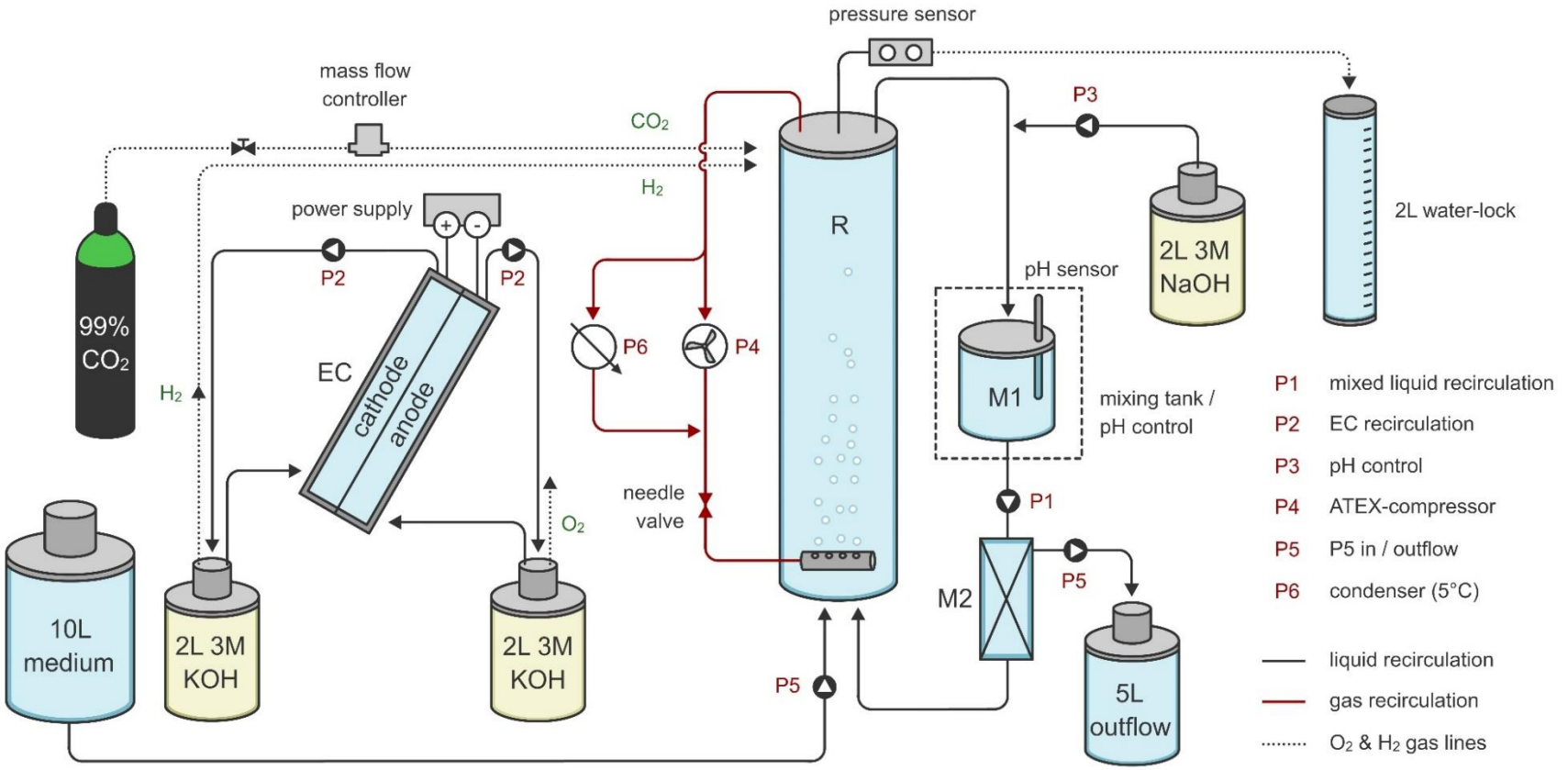

Figure 6.1 – Fermenter set-up scheme. A 10-L bubble column gas fermenter is connected to a water electrolysis cell for continuous power source controlled H_2 gas production. H_2 is mixed with bottle stored CO_2 in the headspace of the reactor and is sparged over the water column at the bottom of the fermenter. Cell retention is achieved with a hollow-fiber membrane (M2) connected in line with the fermenter.

6.2.1.1 Reactor setup

The fermenter (R in Figure 6.1) was constructed in-house as a transparent PMMA column (H=2 m, D=110mm; s=5mm), with top and bottom PVC-U glue flanges. The bottom and top flanges were sealed with EVA O-rings and screwed with stainless steel bolts to ensure gas tightness. Additionally, a PMMA vessel (H=13 cm, D=110mm; s=5mm) was connected to the main column (M1 in Figure 6.1), to allow for better mixing of the reactor mixed liquid and for pH control. The total working volume of the liquid in the reactor, including piping, was 10.5 L. The mixed liquid was continuously recirculated at 15 L min^{-1} with a Masterflex I/P® Brushless Process Drive, 33 to 650 rpm; 115/230 VAC (Metrohm Belgium nv, Antwerpen, Belgium) (P1 in Figure 6.1). The reactor was operated continuously and the effluent was withdrawn with a hollow fiber membrane (MINIKROS SAMPLER 41.5CM 0.2UM PES 1MM 3/4TC X 3/4TC,Repligen Europe B.V., Breda, The Netherlands) (M2 in Figure 6.1) that enabled complete biomass retention in the reactor. The membrane was operated at an elevated pressure between 16 and 20 psi and it was connected after the recirculation pump. The retentate was recirculated at the bottom of the reactor and the filtrate was directed with a Watson-Marlow 530UN/REM pump (Watson-Marlow NV, Zwijnaarde, Belgium) (P6 in Figure 6.1) to a 5-L outflow bottle. A Consort R3610 pH controller (Consort bvba, Turnhout, Belgium) connected with a dosing pump (P3 in Figure 6.1) dosing 3 M NaOH was used to continuously monitor and control the pH in the reactor.

6.2.1.2 Electrolysis cell

The electrolysis cell used for H_2 gas production (EC in Figure 6.1) was an Electro Syn Cell (ElectroCell Europe A/S, Skjern, Denmark) with 0.04 m^2 projected electrode area and frames made of polypropylene. An Ir MMO mesh electrode was used as anode and a stainless steel mesh as cathode, with 5 mm electrode gap. The anolyte and catholyte compartments were separated with a CMI-7000 cation exchange membrane (CEM) (Membranes International Inc, Ringwood, USA). A 3 M KOH solution was used as anolyte and catholyte to ensure reduced ohmic drop and minimize the need for frequent electrolyte replacement. The KOH solution was recirculated through two 2 L Schott bottles, respectively, at 215 rpm (approximately 1.2 L min^{-1}) with a Masterflex L/S® Digital Drive, 600 rpm; 115/230 VAC (Metrohm Belgium nv, Antwerpen, Belgium). The electrolysis cell was controlled with a DC RND 320-KA3305P power supply (Reichelt elektronik GmbH & Co. KG, Sande, Germany). The headspace of the anolyte storing bottle was open to air and the headspace of the catholyte was connected to the headspace of the fermenter, to provide H_2 gas for the fermentation.

6.2.1.3 Gas distribution

The headspace of the fermenter was connected to a KNF-N922FTE 8L Atex pump (KNF-VERDER NV, Aartselaar, Belgium) (P4 in Figure 6.1) for gas recirculation over the liquid column and an exit, ending up in a water lock of around 2 L (1900 mL) (see Figure 6.1) that enabled control at the maximum overpressure in the reactor, at 40 mbar. A pressure sensor was connected to the headspace of the reactor (see Figure 6.1) to allow for pressure monitoring via LabVIEW. CO_2 gas was provided to the reactor by a Bronkhorst EL-FLOW F-201 CV-050-AGD mass flow controller (Gefran Benelux NV/SA, Olen, Belgium) (see Figure 6.1). The headspace gas mixture (H_2/CO_2) was recirculated continuously through a condensation line, consisting of a glass gas trap immersed in a 5 °C water bath (P6 in Figure 6.1) to avoid liquid condensation in the gas pump. The gas mixture (H_2/CO_2) was continuously recirculated over the liquid phase with an in-house stainless steel tube accommodating three sintered polyethylene spargers (PE, gesinterd, M5, Mattech, Lelystad, Netherlands), connected at the bottom inner side of the reactor (see Figure 6.1).

6.2.2 Experimental procedures

The gas flows and pressure in the reactor were controlled and regulated with the LabVIEW software. Through the specific program, the pressure drop in the reactor, signified the biological consumption of the H_2/CO_2 gas mixture. The maximum pressure allowed in the reactor was set at 40 mbar overpressure and the minimum at 25 mbar. A measurement below 25 mbar in the reactor triggered the starting of the power supply and thus the start of electrolysis and hydrogen production. At the same time the CO_2 gas mass flow was regulated with a 1:2 molar ratio based on the current provided for hydrogen production. The electrolysis was controlled between 0.001, to avoid chemical transformation of the electrodes, as the anode and cathode used here cannot be considered inert electrodes (Allen J. Bard and Faulkner 2001), and 4 A and accordingly the CO_2 mass flow between 0 and 12 mL min^{-1}, running for as long as it needed to increase the pressure, measured in the headspace of the reactor, from 25 to 40 mbar.

The reactor was initially inoculated with a mixed acetogenic culture coming from previous flask tests for acetogenesis, in a 5% of its volume, while the rest of the volume was filled with a salt medium, devoid of yeast extract and tryptone and aided with a vitamin solution (Table A4.2). After two initial batch tests at pH 7 and pH 6.5, respectively (Figure A5.1), aiming to achieve the highest possible acetate concentration ($\sim$ 12g L^{-1} was achieved) continuous operation was initiated. During continuous operation the pH was controlled at pH 6.5, by dosing a 3 M NaOH solution. The HRT was set to 7 days (D=0.14 d^{-1}), which was calculated based on the growth rate of the mixed microbial community obtained at the first batch experiment (Figure A5.1A). New medium was fed to the reactor from a 10-L storage bottle, connected to a 5-L gas bag filled with N_2/CO_2:90/10 gas mixture, to maintain

anaerobic conditions in the medium storage bottle. The new medium was inserted at the bottom of the reactor (see Figure 6.1).

After initial continuous operation in the absence of sulfide, 3 consecutive runs of sulfide stress (1.3 mM TDS) alternated with sulfide-free-medium periods were conducted. The end of every run was defined when the concentration of acetic acid decreased below 0.4 g acetate L^{-1}. At that point the sulfide-amended medium was replaced with one devoid of sulfide till the acetic acid concentration was recovered to concentrations of approximately 2 g acetate L^{-1}. After this triplicate run of sulfide addition, the reactor was operated under a mimimal stress concentration of 0.5 mM total dissolved sulfide (TDS) till the end of the experiment.

6.2.2.1 Medium preparation

Medium was prepared weekly and resazurin (0.1% final concentration) was added as indicator of anaerobic conditions and Na_2S stock solution (0.5 mM final concentration) as a reducing agent. Consequently, the medium was sparged with a 90:10/N_2:CO_2 gas mixture for approximately 1 hour, till the solution would become completely transparent. Before use, the trace elements, vitamins and tungstate selenium (Table A4.2) were added, under continuous sparging. Finally, the desired according to the requirements of the individual experimental steps Na_2S volume was added from the stock solution,. The bottle was covered with aluminium foil to minimize light exposure and a 5 L gas bag filled with a 90:10/N_2:CO_2 gas mixture was connected to the headspace to ensure anaerobic conditions.

6.2.3 Sampling and analytical methods

Liquid samples were taken daily from the reactor mixed liquid and the outflow and were analysed for organic acids, sulfide and biomass content. The organic acids and sulfide samples preparation and analysis were conducted as described previously(see Chapter 5), as well as the biomass concentration analysis with spectrophotometry. In addition, biomass was quantified with Volatile Suspended Solids (VSS) analysis according to standard methods (Greenberg et al. 1992), as well as spectrophotometrically, measuring the optical density (OD) at 600 nm wavelength. For the specific acetate production rates, as well as the carbon and electron balances, calculations, the results of the OD measurement were selected, as a OD demonstrated the highest correlation with live (intact) cells in the samples analysed with flow cytometry (Figure A5.2). A 0.6 conversion factor between OD and cell dry weight (CDW in g L^{-1}) (Myers et al. 2013) was then selected to determine the biomass concentration.

Gas samples were taken daily from the headspace of the reactor and were analysed for H_2, O_2, CO_2, H_2S and CH_4 with a Compact GC, as described previously (see Chapter 5). The soluble fraction of CH_4 was also taken into account in the construction of the carbon and electron balances, using 1.4×10^{-5} mol m^{-3} Pa^{-1} as Henry's constant for 25 °C. The electron and carbon balances were constructed based on the flow of H_2 and CO_2 provided to the system and monitored by the LabVIEW software.

In a weekly, or biweekly basis the total cell count of the reactor as well as the ratio of intact to damaged cells was determined with flow cytometric analysis (FCM). The samples were diluted in sterile PBS, stained with the nucleic acid stain SYBR® Green I and Propidium Iodide for permeabilized cells and analysed with a Accuri C6 Plus cytometer (BD Biosciences, Erembodegem, Belgium), as described previously (Chatzigiannidou et al. 2020). The FCM data were imported in R (v 4.0.2) (R Core Team 2012) using the flowCore package (v2.0.1) (Hahne et al. 2009). A quality control of the data set was performed through the flowAI package (v1.18.5) (Monaco et al. 2016). The data were transformed using the arcsine hyperbolic function, and the background was removed by manually drawing gates on the primary fluorescent channels for the intact and damaged cell population (for an example see Figure A5.3). The Phenoflow package (v1.1.2) (Props et al. 2016) was used to assess the phenotypic community structure of the intact bacterial populations based on the FL1-H, FL3-H, FSC-H and SSC-H channels as described in Heyse et al. (Heyse et al. 2019) subsampled to 3000 cells. Alpha diversity was calculated with the Hill Diversity (Heyse et al. 2019) number D2 using the Diversity function of the Phenoflow package, which corresponds to Inverse Simpson index.

6.2.4 16S rRNA Gene amplicon sequencing

Samples for DNA extraction were taken weekly (HRT=7d) and pelleted by centrifugation for 5 min at 14000 g and the DNA samples processing was conducted as described in paragraph 5.2.4 of this thesis. The graphs representing the 12 most relative or absolute abundant genera were generated using the phyloseq package (v1.32.0) in R (McMurdie and Holmes 2013).

Accession number(s). Raw FCM data are available on FlowRepository under accession ID FR-FCM-Z3FWF. Raw 16S rRNA gene sequences for bacteria and archaea were deposited on the NCBI SRA under BioProject ID PRJNA698443.

6.3 Results and Discussion

6.3.1 A concentration of 1.3 mM TDS impairs acetogenic activity, but the effect is reversible

Continuous inhibition of the acetogenic activity under even a minimal 0.5 mM TDS concentration in the fermenter was demonstrated, as the volumetric acetate production rate averaged at 30% of the rate achieved during uninhibited operation. The gas fermenter was continuously operated for 168 days without intermediate re-inoculation. Three consecutive runs of sulfide stress addition and removal took place during reactor operation and eventually, the reactor run continuously under ~0.5 mM TDS for 35 days (day 133 – 168) (Figure 6.2 and A5.4 for TDS measurements). This concentration was selected after the third round of sulfide addition, as it was the concentration of sulfide remaining in the reactor, at which the acetogenic, but not the methanogenic, activity resumed.

During the uninhibited, initial continuous operation of the reactor (days 0 – 43) the average volumetric acetate production rate was 22.5 ± 7.0 mmol $C_{acetate}$ L^{-1} d^{-1} (0.7 ± 0.2 g acetate L^{-1} d^{-1}). By the first medium amendment with sulfide, resulting in 1.3 mM TDS in the reactor (day 43), the production rate dropped from 28.0 ± 1.4 mmol $C_{acetate}$ L^{-1} d^{-1} (0.8 ± 0.0 g acetate L^{-1} d^{-1}) to 2.0 ± 0.1 mmol $C_{acetate}$ L^{-1} d^{-1} (0.1 ± 0.0 g acetate L^{-1} d^{-1}) (day 63). Next, medium amendment was stopped and the reactor was allowed to recover till the next sulfide addition (day 77). During this period the acetogenic activity resumed, but only at around half of the one previously achieved, as the maximum rate was 11.3 ± 0.5 mmol $C_{acetate}$ L^{-1} d^{-1} (0.3 ± 0.0 g acetate L^{-1} d^{-1}). Upon the second sulfide addition the production dropped again to 2.2 ± 0.1 mmol $C_{acetate}$ L^{-1} d^{-1} (0.1 ± 0.0 g acetate L^{-1} d^{-1}) within 14 days (2×HRT) (day 91) and resumed back to 11.6 ± 0.9 mmol $C_{acetate}$ L^{-1} d^{-1} (0.3 ± 0.0 g acetate L^{-1} d^{-1}) within another 15 days of operation with non-amended medium (day 106). Next, the third cycle of sulfide inhibition started and within the next 2 weeks of operation the acetate volumetric production rate dropped to as low as 0.6 ± 0.0 mmol $C_{acetate}$ L^{-1} d^{-1} (0.0 ± 0.0 g acetate L^{-1} d^{-1}) (day 121). Subsequently, the final resumption of the acetogenic activity started, up to when the TDS concentration in the reactor had dropped to 0.5 mM (day 133), when the rate achieved was 7.5 ± 0.5 mmol $C_{acetate}$ L^{-1} d^{-1} (0.2 ± 0.0 g acetate L^{-1} d^{-1}).

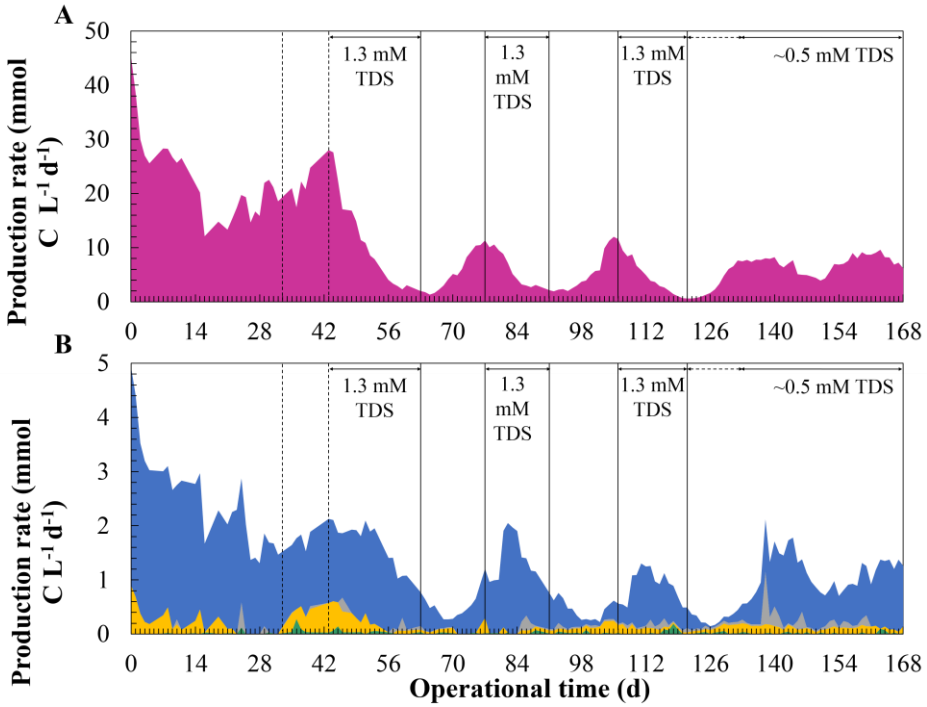

Figure 6.2 – Panel A: Volumetric acetate production rate (in mmol C L^{-1} d^{-1}) (pink). Panel B: Volumetric production rate of the carboxylic acids, exempting acetate, (in mmol C L^{-1} d^{-1}) obtained in the reactor, during the total 168 days of continuous operation: formic acid (green), propionic acid (yellow), lactic acid (grey) butyric acid (blue), during the total 168 days of continuous operation. The pH was maintained at 6.5. The two dotted vertical lines represent a batch operation after a failure of the continuously operated reactor and the parts in between TDS addition, the reactor recovery periods.

Starting from day 133, the TDS concentration in the reactor was maintained at 0.5 mM and the average production rate during this final 35 days period (days 133 – 168) was 7.1 ± 1.5 mmolC L^{-1} d^{-1} (0.2 ± 0.0 g acetate L^{-1} d^{-1}) (Figure 6.2A). Concurrently, 1.0 ± 0.3 mmol$C_{butyrate}$ L^{-1} d^{-1} and 0.6 ± 0.1 mmol$C_{formate}$ L^{-1} d^{-1} were produced (Figure 6.2B and A5.5). Comparing the rates achieved here with previously reported ones is an intricate process, as not only an inhibitor was affecting the overall performance of the reactor studied here, but in addition, different operational conditions and reactor configurations have been studied throughout the gas fermentation research. For example, Zhang et al. (F. Zhang et al. 2013) with a similar HRT (9 days) in a continuous H_2 fed reactor with cell retention via a hollow fiber membrane achieved 13 mmol C (as acetate) L^{-1} d^{-1} under uninhibited conditions, which was an order of magnitude lower than the one achieved by Wang and colleagues (256 mmol C L^{-1} d^{-1}) (Y. Q. Wang et al. 2017) with a 2.5 days HRT. Therefore, the selection of an optimal HRT is crucial for obtaining high acetate production rates, however, in case of inhibited conditions production

optimisation should be focused on microbial community acclimation to the inhibitor.

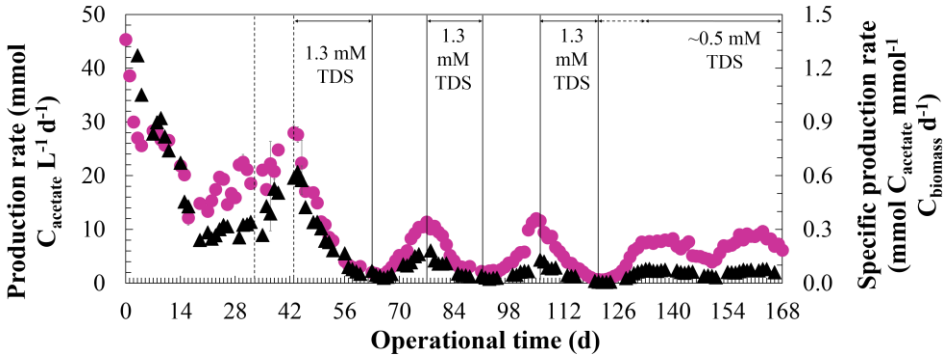

Figure 6.3 – Volumetric acetate production rate (in mmol $C_{acetate}$ L^{-1} d^{-1}) (pink circles) and the specific acetate production rate (mmol $C_{acetate}$ mmol $C_{biomass}^{-1}$ d^{-1}) (black triangles) during the total 168 days of continuous operation (n = 2 technical replicates). The two dotted vertical lines represent a batch operation after a failure of the continuously operated reactor and the parts in between TDS addition, the reactor recovery periods.

During uninhibited operation (day 0 – 43) the specific acetate production rate averaged at 0.5 ± 0.3 mmol $C_{acetate}$ mmol $C_{biomass}^{-1}$ d^{-1} (0.7 ± 0.4 g acetate g CDW^{-1} d^{-1}) (Figure 6.3) with an average 1.0 ± 0.3 g CDW L^{-1} (OD_{600} = 1.7 ± 0.5) (Figure A5.6). For the rest of the periods the specific acetate production rate was maintained at a minimum 0.1 mmol $C_{acetate}$ mmol $C_{biomass}^{-1}$ d^{-1}, which is expected as the biomass concentration experiences small changes during the inhibition, maintained at an average 1.4 ± 0.5 g CDW L^{-1} during sulfide stress application and removal. In the last 35 days the biomass concentration measured averaged at 2.5 ± 0.1 g CDW L^{-1}, which can most probably attributed to an increase in dead biomass in the reactor that was picked up by the analytical tools for biomass analysis (additional biomass concerns are further raised in paragraphs 6.3.3 and 6.3.4).

The highest acetate concentration achieved here (4.5 ± 1.0 g L^{-1}) during uninhibited operation is almost 4 times lower than the highest reported for continuously operated gas fermenters in literature (~17 g acetate L^{-1}) (Kantzow et al. 2015; Steger et al. 2017), whilst the one achieved under inhibition is more than ten times lower (1.5 ± 0.3 g L^{-1}) (Figure A5.5). This difference in production can be attributed to sulfide as an inhibitor at first, but also to a rather high HRT (7 days) applied and the mixed nature of the microbial community employed. Toxicity concentrations higher than 1.3 mM TDS have been reported in literature for anaerobic microorganisms, such as sulfate reducers and concentrations up to 3.4 mM are detected in a healthy human digestion system. However, it has been reported that when sulfide is exogenously supplied, and not produced intracellularly, concentrations as low as 50 µM can be detrimental to cell viability and thus, metabolic activity (Cao et al. 2010).

The microbial community here showed a resilient response towards sulfide inhibition, as after removal of sulfide the acetogenic activity resumed, after 48h (Figure 6.2A). However, an acclimation of the microbial community in sulfide cannot be claimed, as the average acetate production rate achieved under ~0.5 mM TDS was only 30% of the one obtained under uninhibited operation. The continuous and stable production of acetate under a minimal sulfide concentration during the last 35 days of operation (Figure 6.2A) shows an opportunity for future community acclimation and stable organic acids production with less stringent requirements for gas pre-treatment. Adaptation to elevated concentrations of sulfide has been demonstrated for photosynthetic cyanobacteria (Cohen et al. 1986), microbial communities colonizing bio-trickling filters for waste gas desulfurization (Sercu et al. 2005) and for nitrifiers (Sekine et al. 2020). In these studies, microbial adaptation has been assumed through maintenance of activity or reactor efficiency, or by acquiring a stable, in terms of diversity, microbial community. However, differentiation in gene expression triggered by sulfide stress (Kelley et al. 2016) was not demonstrated. For a sound comment on potential long-term adaptation of the community, molecular studies on gene expression under sulfide as a physicochemical stressor should be considered.

6.3.2 Methanogenesis is suppressed under 0.5 mM TDS

After addition of 1.3 mM TDS, both acetogenesis and methanogenesis were inhibited. Acetogenic activity resumed within 48 h of operation with non-amended medium, however, methanogenic activity only resumed after 7 days (1×HRT) and only after the sulfide concentration in the reactor had dropped to lower than 0.5 mM TDS. This was consistently observed across the three cycles of adding and removing sulfide. Therefore, methanogenic activity required a lag-phase after stress recovery compared to acetogenic activity. In addition, methanogenic activity was suppressed after cyclic sulfide inhibition and this suppression was maintained, during the last 35 days of continuous operation under 0.5 mM TDS (Figure 6.4 and A5.7). A similar response was not observed for acetogenesis, as the production rates resumed during the 0.5 mM TDS period back to values obtained during previous recovery periods. The distribution of electrons and carbon towards CH_4 was decreased compared to all previous periods, as a result of the cyclic addition of sulfide. In particular, between days 133 and 168, 0.6 ± 1.3% of the carbon and 0.9 ± 2.1% of the electrons distributed to the reactor were directed to CH_4, as opposed to 2.5 ± 2.3% and 4.0 ± 3.6%, respectively, during periods of recovery from sulfide inhibition (Figure 6.4).

As such, the inhibition of methanogenesis appears to be irreversible as opposed to acetogenesis that could be considered reversible. Irreversibility in whole or in part of the methanogenic community has been reported in literature for a wide array of inhibitors including sulfide, formaldehyde, oxygen and selenium oxyanions (Gonzalez-Gil et al. 2000; P. N.L. Lens et al. 2003; Lenz et al. 2008; Pedizzi et

al. 2016). The absence, or decrease in previously non-inhibiting levels after inhibitor removal, of methanogenic activity, as well as in some cases the decrease in the absolute archaeal cell numbers have been used as indicators of the irreversibility. However, in our study, only the microbial community composition was studied, therefore it is not possible to conclude whether the suppressed methanogenic activity was a result of irreversible toxicity (cell disruption) of part of the archaeal community or of a decreased activity due to sulfide tolerance development from the total community (Windels et al. 2020).

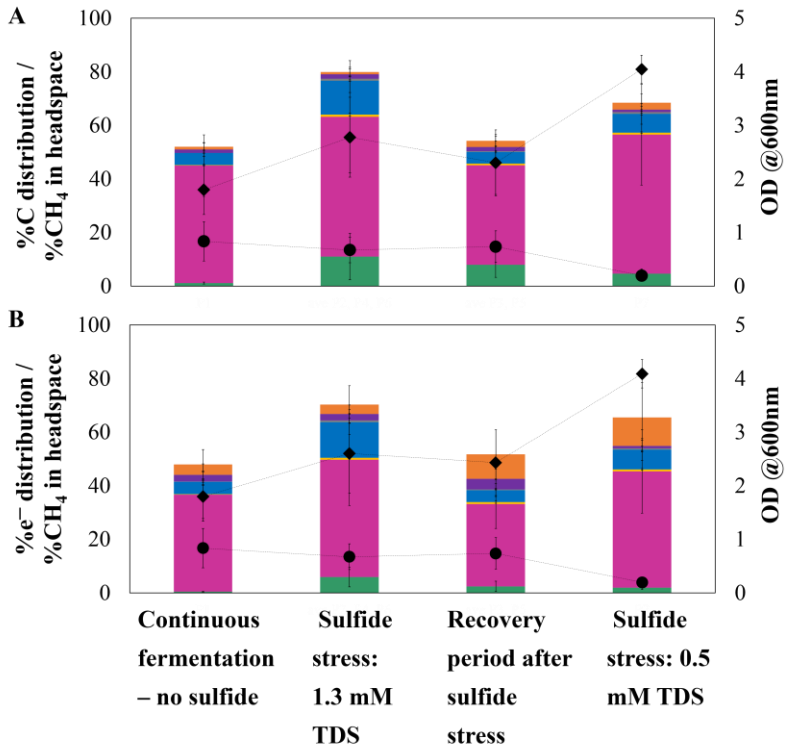

Figure 6.4 – Panel A: Carbon balance. Panel B: Electron balance for the four distinct periods of operation: formic acid (green), acetic acid (pink), propionic acid (yellow), butyric acid (blue), lactic acid (grey), methane (purple), biomass (orange), CH4% in headspace (black circle), biomass concentration measured with OD at 600 nm (black diamond). The standard deviation arises from the distribution of every balance during the four periods: 1) Continuous fermentation – no sulfide: days 0 – 43, 2) Sulfide stress: 1.3 mM TDS: days 46 – 63, 79 – 91, 108 – 121, 3) Recovery period after sulfide stress: days 65 – 77 and 93 – 106 and 4) Sulfide stress 0.5 mM TDS: days 135 – 168.

Methanogenesis is one of the two crucial bottlenecks to overcome for successful application of mixed culture gas fermentations, the other one being product separation. The importance of strict inhibition of both aceticlastic and hydrogenotrophic methanogenesis is highlighted in Agler et al 2011 (Agler et al. 2011), where three inhibition options are proposed :1) heat-shock of the inoculum, which limits

applicability to batch systems, 2) lower pH levels and 3) adding a selective inhibitor, such as BES (bromoethanosulfonate). Additionally, selective enrichment of acetogens over methanogens by sequential community transfers after limited inoculation time has been proposed in literature (Patil et al. 2015). The approach followed here relates to the third option, although sulfide cannot be considered a selective inhibitor, as upon addition both acetogenic and methanogenic activity is suspended. However, the lag-phase in the methanogenic activity underlines a selective recovery after initial inhibition, hence sulfide could be a potential selective methanogenic activity suppressor in mixed community waste gas fermentations. A differentiation in inhibition by sulfide between propionate degrading bacteria and archaea has been reported in literature (H.-Z. Wang et al. 2019), as well as among members of the nitrogen cycle (Sekine et al. 2020; Seuntjens et al. 2018).

Addition of BES is usually cost prohibitive for large scale operation, thus alternatives ought to be sought to favour acetogenesis over methanogenesis (Agler et al. 2011). Thus, the results shown above highlight an opportunity for sulfide, an inhibitor inherent in the waste gases used for fermentation, to prove a fit for use alternative. Sulfide could be occasionally used, in a similar way as the heat-shocks, as it was shown from the repetitive, occasional sulfide-shock, in the present study. Additional advantage would be that sulfide can be applied during a continuous operation and represents a low energy investment. In case sulfide containing gases are used as feedstock for the bioreactors, the pre-treatment could be occasionally shut down, and therefore contribute to lower pre-treatment operational costs and at the same time inhibit methanogenesis.

6.3.3 Carbon and electrons are distributed towards acetate and butyrate under sulfide stress

The main metabolic product detected in the reactor was acetate, regardless of the presence or absence of sulfide. During the initial uninhibited operation and the two recovery periods, 44 ± 12 % and 39 ± 11 % of the carbon provided to the system was directed to acetate, whilst during the 1.3 mM and 0.5 mM TDS periods, the distribution of carbon averaged at 50 ± 21 % and 52 ± 19 % (Figure 6.5A). This coincides well with the observation that during sulfide inhibition methanogenesis is intensively inhibited, which allows for a higher availability of carbon and electrons for acetogenesis. Additionally, during the periods of inhibited operation, more carbon was distributed to the rest of the fermentation products. The distribution of carbon to formate averaged at 14 ± 9 % during the cycles of 1.3 mM sulfide and at 5 ± 2 % at 0.5 mM TDS. Similarly, for the same periods carbon was distributed to butyrate by 15 ± 5 % and 7 ± 4 %, respectively. The high standard deviations obtained for the production rates indicate the transient conditions of the system, at least in the first three periods of operation.

A similar trend was followed in the distribution of electrons within the fermentation products. During the initial uninhibited operation and the two recovery periods, 36 ± 9 % and 33 ± 9 % of the electrons provided to the system was directed to acetate, whilst during the 1.3 mM and 0.5 mM TDS periods, the distribution of electrons averaged at 42 ± 17 % and 44 ± 16 % (Figure 6.5B). Electrons were distributed by 6 ± 4 % during the cycles of 1.3 mM sulfide and at 2 ± 1 % at 0.5 mM TDS to formate and by 15 ± 5 % and 8 ± 4 % to butyrate. The bigger challenge in closing the electron balance (Figure 6.5B), compared to the carbon balance, could be attributed to the lower solubility of H_2 and most likely gas losses taking place in the tubing connections between the electrochemical cell and the main reactor part (Figure 6.1). Loss of H_2 from the cathodic to the anodic compartment of the electrolysis cell was excluded as no H_2 gas could be detected at the headspace of the anolyte recirculation bottle.

An interesting observation was the transient increase in butyrate and formate production, after sulfide addition, in contrast to an immediate decrease in acetate production (Figure A5.8). This is also depicted in the higher distribution of carbon and electrons to those two products under strict inhibition, compared to the numbers at the 0.5 mM TDS inhibition period. It has been reported previously in literature that a molybdate and sulfide complex inhibited the formation of active hydrogenase during glucose fermentation, ultimately resulting in electron uptake for CO_2 reduction to formate (Wolin and Miller 1980). It is therefore possible that a similar mechanism might take place in the case of sulfide inhibition, where the available electrons, otherwise used in acetate formation, are used in butyrate production, possibly again from more resistant to inhibition butyrate producing bacteria. Another plausible scenario could be that upon methanogenesis inhibition, the spared H_2 is incorporated into butyrate and formate. A shift from acetate to propionate, for example, has been described when methanogenesis was inhibited in the rumen (Ungerfeld 2015), however here, an increase of propionate production under stress periods was not as prominent as the shifts towards formate and bytyrate.

Under increased inhibition, a 0.9 ± 2.0 % of the carbon and 3.6 ± 7.0 % of the electrons were directed to new biomass formation, as opposed to 1.0 ± 1.4 % C and 3.9 ± 6.0 % e^- during initial uninhibited operation and 2.3 ± 2.3 % C and 9.1 ± 9.2 % e^- during recovery periods. The average percentages for, at least, electrons, thus hydrogen, distribution to biomass is on par with the commonly reported 10% for hydrogen consuming anaerobes (Parameswaran et al. 2010). Nevertheless, in the last period of operation, under 0.5 mM both the carbon and electrons distribution to biomass seemed to increase, to levels similar to the uninhibited periods. During the final 35 days of operation the carbon distribution to biomass averaged at 2.7 ± 3.2 % and the distribution of electrons at 10.7 ± 12.9 %. This higher percentage could be attributed to the higher cell debris accumulated in the reactor over the operation under inhibition. During this period the average biomass concentration in the reactor was 2.5 ± 0.1 CDW g L^{-1} (OD_{600} = 4.1 ± 0.2) (Figure A5.6), the highest compared to the all

the periods tested which is also depicted in the increased content of dead cells in the reactor (Figures 6.4A and A5.9).

6.3.4 Sulfide treatment increases the phenotypic diversity and decreases the taxonomic diversity of the microbial community

The total cell count in the reactor fluctuated marginally, during the 168 days of operation, ranging from a minimum of 1.3×10^{9} to a maximum of 4.8×10^{9} intact cells mL^{-1} (Figure A5.9) and from a minimum of 9.2×10^{8} to a maximum of 5.3×10^{9} damaged cells mL^{-1}. The highest number of damaged and the lowest of intact cells were observed in the beginning of the continuous operation, depicted by the lowest intact to damaged cell ratio (Figure 6.5A), as a result of the previous batch operation of the reactor. Further on, this ratio increased as intact cells retention was aided by the hollow fiber membrane connected to the reactor (Figure 6.1) and lysed cells were discarded with the continuous effluent. Eventually, after consecutive sulfide inhibition steps, cell decay was faster than the growth rate in the reactor, depicted in the decrease of the intact over damaged cells ratio that from a maximum of 2.4 dropped to 1.2 at the end of the operation (Figure 6.5A). The higher than 1.2 value obtained for day 168, is a result of a decrease in dead cells measured in FCM (Figure A5.9), that does not coincide with an operational failure, therefore cannot be explained otherwise currently.

The phenotypic diversity among the samples clearly increased (Figure 6.5B) during the continuous operation and thus, during consecutive application of sulfide stress. When pure cultures are considered, this is an expected observation as it is well documented that phenotypic heterogeneity can be triggered by exogenous environmental stress factors, such as antibiotics, (García-Timermans et al. 2020) or in the case of this study, sulfide. Phenotypic heterogeneity is not necessarily an unwanted treat, as it promotes adaptation to dynamic and often extreme environments, nonetheless at the cost of decreased metabolic efficiency and thus, bioproduction (Badyaev 2005; J. Kim et al. 2020).

A negative effect of sulfide on the taxonomic diversity was demonstrated by the calculation of the D2 number (see Figure A5.10 and Table A5.1). The D2 calculated for the initial bacterial sample (Batch 1) was 8.2 and already decreased to 4.9 in the start of the continuous operation (day 0) and dropped to 3.5 by the end of the operational period (day 168) (Table A5.1). Decreased taxonomic diversity has been reported in fermentation related studies, where the microbial community was inhibited by ammonia evolution (Lv et al. 2019) and chloroform-cyclodextrin addition (Martinez-Fernandez et al. 2016). Although in previous studies, the phenotypic diversity was found to correlate with the taxonomic diversity (Props et al. 2016), here we observed the opposite trend, phenotypic diversity increased whereas taxonomic diversity was decreasing (Figures 6.5A and 6.5B). A possible explanation is that although only a few taxa dominate the community their phenotypic fingerprint might change due to the sulfide imposed, or a shift in metabolic activity.

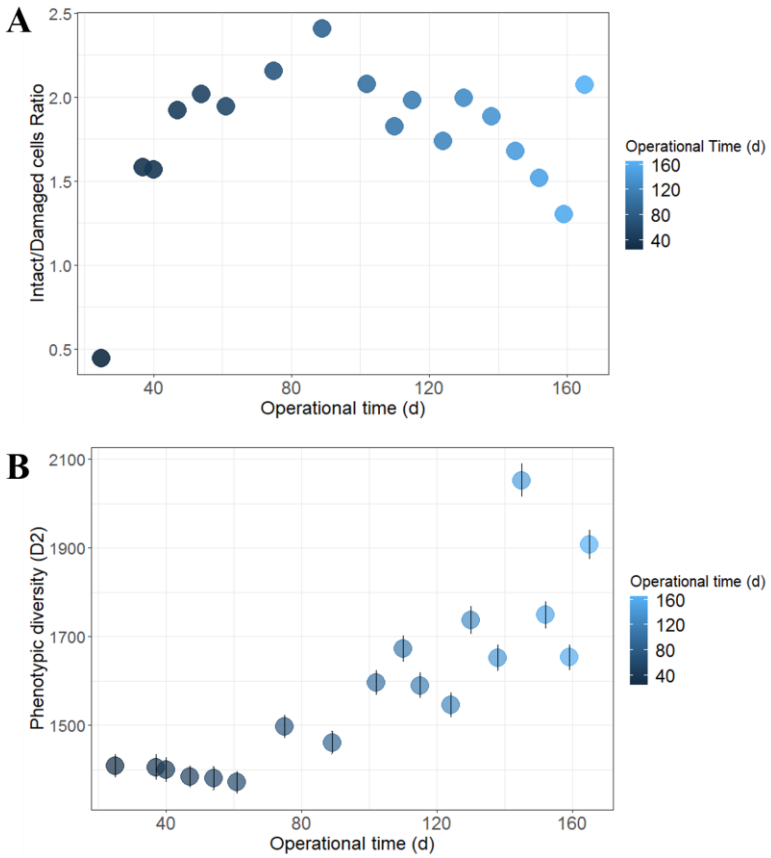

Figure 6.5 – Panel A: Intact to damaged cells ratio Panel B: Phenotypic diversity evolution. The graph was produced based on the cell count of intact cells, during the 168 days of operation. The vertical lines represent the standard deviation of the diversity indices averages.

The decrease in taxonomic diversity is also depicted in the changes in the relative abundances of the most abundant phyla and genera. The sum of the relative abundances of the three most dominant phyla *Firmicutes*, *Bacteroidetes* and *Actinobacteria* increased from an initial 77% to a final 96% (Figure 6.6A). During during the 0.5 mM TDS period, only three genera, *Proteiniphilum*, *Eubacterium* and an unclassified *Eggerthellaceae* made up to 80% of the total relative abundance, highlighting a community of decreased diversity. A low diversity could be assumed also for the archaeal community dominated by only two genera with a shift from monodominance of the one strain to monodominance of the other, observed during reactor operation. Initially, the archaeal community was dominated by the genus of *Methanobacterium*, with 100% abundance, which eventually shifted to 100% of the genus *Methanobrevibacter* (Figure A5.12). This shift however cannot be attributed solely to sensitivity towards sulfide inhibition, as it started well before the first sulfide addition.

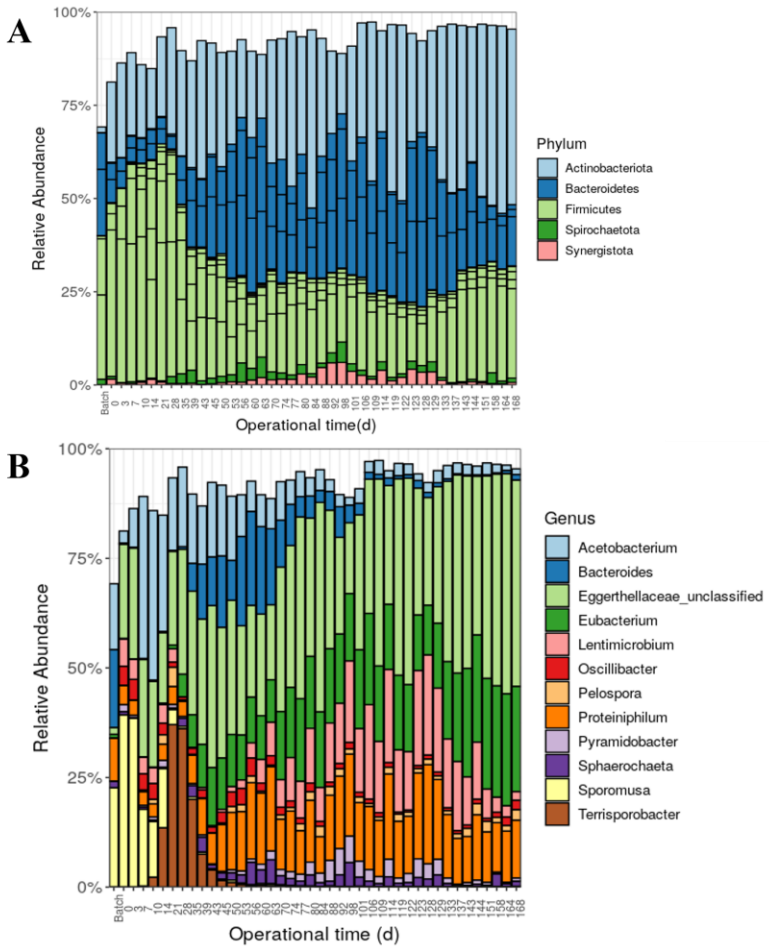

Figure 6.6 – Panel A: Relative abundance of the most abundant phyla, detected in the reactor biomass samples, during continuous operation and consecutive sulfide stress addition. Panel B: Relative abundance of the 12 most abundant bacterial genera (see Figure A5.11 for the 20 most abundant genera)

6.3.5 Sulfide treatment selects for unclassified *Eggerthellaceae*, *Eubacterium* and *Proteiniphilum* as the dominating genera

At the genus level, a clear shift in the predominance of specific genera from the phylum of *Firmicutes* was observed. The initial bacterial community (Batch 1, Figure 6.6B) was dominated by the genera *Acetobacterium* and *Sporomusa*. *Acetobacterium* was negatively affected by the addition of sulfide, depicted in a relative abundance decrease after day 43 that sulfide was initially added, but differently, *Sporomusa* decreased before inhibition, already by switching from batch to continuous operation. *Eubacterium*, the third abundant genus of *Firmicutes* in the seed community, followed the opposite trend. Initially present with a 0.8% relative abundance, eventually it became the dominant genus in the *Firmicutes* phylum, with a final ~25% relative abundance in the last 35 days of operation (Figures 6.6B and A5.13). Thus this genus demonstrated increased resistance towards sulfide, reflected

through the *Firmicutes* community shift from an *Acetobacterium* and *Sporomusa* dominated to a *Eubacterium* dominated one.

A switch from a prevalence of acetate production and presence of *Acetobacterium* to butyrate production with a switch from batch to continuous operation of a microbial electrolysis cell (MES) has been observed by Arends et al (Arends et al. 2017), although in their case they pointed at *Rummeliibacillus* as the genus most probably responsible for butyrate production. *Eubacteria* are commonly associated with CO fermentation (Diender et al. 2015; Park et al. 2017) and although no information could be traced on a specific *Eubacterium* resistance to sulfide, this genus has been identified in microbial samples from environments with increased presence of sulfide, such as oil-fields (Voordouw et al. 1996) and the human gut (Mukherjee et al. 2020). Strains of *Eubacterium* are known butyrate producers (Genthner et al. 1981; Rode et al. 1981), therefore, the establishment of a stable butyrate concentration in the reactor could be a result of an establishment of a stable *Eubacterium* presence in the mixed microbial community.

The increase in the abundance of the *Actinobacteriota* phylum from only 3% in the seed community (Batch1, Figure 6.6A) to a 47% relative abundance at the end of the operation (day 168, Figure 6.6A) was mainly a result of the increase in the abundance of *Eggerthellaceae* (Figures 6.6B and A5.14). Thus, a positive time effect on the selection of this genus in the reactor community could be observed, and a resistance, towards sulfide. For these unclassified bacteria, information is not available, therefore, an attempt to explain their dominant presence in the reactor will be done based on the genus that shares the same name with the family, *Eggerthella*. Originally isolated by Eggerth from human faeces and assigned to the genus Bacteroidetes (Eggerth 1935), they are commonly associated with human pathogenicity, such as infections of the gastrointestinal tract (GIT) (Gardiner et al. 2015).

The third most abundant phylum positively correlated with sulfide stress (Figure 6.6A) was *Bacteroidetes,* commonly found in anaerobic environments such as the human gut (Faith et al. 2013), anaerobic digesters (S. Chen and Dong 2005; L. Sun et al. 2016) and microbial electrosynthesis cells that conduct reductive acetogenesis (Arends et al. 2017; Croese et al. 2013; Y. Jiang et al. 2020). The three genera that dominated the *Bacteroidetes* phylum were *Bacteroides*, *Proteiniphilum* and *Lentimicrobium* (Figure 6.6B). Resistance towards sulfide stress was demonstrated by the genus *Proteiniphilum*, that was established in the final community landscape with a ~12% relative abundance (Figures 6.6B and A5.15). Members of the genus *Proteiniphilum* are not known for homoacetogenesis, thus it is not clear what might have caused the increased presence of this genus. However, *Proteiniphilum* is a known fermentative acetogen able to grow on organic substrates (Duan et al. 2016) and can even use specific amino acids as a carbon source (S. Chen and Dong 2005; Marshall et al. 2017). Therefore, it is possible that the increase of its abundance at the end of the cycle was a result of a dead biomass increase in the reactor (Figure 6.5A).

6.3.6 Technological implications and further research

Industrial waste gases fermentation has the potential to compete conventional acetic acid production both in sustainability and financial terms. When using waste CO_2 for acetic acid production, the industrial route for the production of methanol and iodomethane is avoided and even the chemicals for pH control of the fermentative route can be produced via electrolysis. A deep understanding of the effect of pollutants, inherent in waste gases, on the gas fermentation productivity and products distribution will allow for optimal design of future fermentation units, by limiting the gas pre-treatment to the absolutely essential.

A key challenge we addressed here was the competition between acetogenesis and methanogenesis. In parallel, the selective inhibition effect of sulfide on methanogenesis was demonstrated. Here we achieved methanogenesis suppression, first in a cyclic trend, by adding and removing the sulfide stress and by taking advantage of the slower recovery of methanogens opposed to acetogens. Next to that continuous methanogenesis suppression was achieved, by working under a limited, but constant, sulfide stress. Furthermore, we elucidated the steering of the gas fermentation from acetate to butyrate, upon addition of sulfide. Butyrate was the second most abundant product of acetogenesis under sulfide stress, giving an indication of a possible steering of the fermentation products, using an inhibitor, rather than a vitamin or a trace element, to ultimately push the production towards a desirable product. However, it is not yet clear whether this could be considered as a permanent effect on the production characteristics and the possibility of steering the fermentation towards specific products by addition of sulfide requires further warrant.

A further screening of the microbial community could reveal the specific function of the most abundant genera identified by illumina sequencing here and comment on whether they were actively involved in the production of acetate. Acetogens are a very versatile physiologically and phylogenetically bacterial group, and the genera *Acetobacterium* and *Clostridium* harbor the most acetogenic species isolated to date. Therefore, the next step would be to conduct a gene targeted PCR and next, illumina sequencing to identify genes specific to the metabolic functions essential for acetogenesis. One of the function specific genes within the acetyl-CoA pathway, common in all acetogens, is the gene sequence formyltetrahydrofolate synthetase (FTHFS) which is rather conservative (Lovell and Leaphart 2005), consequently it has been widely used as a molecular marker for the identification of reductive acetogenesis (Hylemon et al. 2018; Ottesen and Leadbetter 2010). For example, there have been a number of recent studies that identified the fhs gene in the genome of different *Eggerthella* strains (Hädrich et al. 2012; Harris et al. 2018; Hylemon et al. 2018; Ottesen and Leadbetter 2010). Thus, new acetogenic species will have to show similarities with the genes harboured by *Clostridia* and *Acetobacteria*, to prove their acetogenic activity.

At last, the recovery of the fermentation products, being either a single or a mix of VFA will have to be considered, in order to provide a product of commercial significance. Physicochemical approaches including membrane extraction, distillation, electrodialysis and adsorption (Ramos-Suarez et al. 2021) have been primarily explored so far for the recovery of VFA from the fermentation broth. However, mixes of VFA as well as low titers, such as the ones obtained here (2 g L^{-1} acetate and 0.2 g L^{-1} butyrate), will require a combination of recovery techniques and will result in increased energy consumption. Thus, another approach could be suggested for the produced here fermentation effluent, which contains acetate and butyrate, as well as traces of formate, and is already devoid of bacterial cells, after filtration via the hollow fiber membrane. This mix of VFA could be directly used as the carbon source for the production of either polyhydroxyalkanoates (PHA) or microbial protein, in subsequent biological steps. In a similar concept Al-Rowaihi and colleagues combined H_2/CO_2 fermentation with acetate-fed polyhydroxybutyrate (PHB) production (Al Rowaihi et al. 2018). Individual, as well as mixes of, VFA have been tested for the production of fungal (Wainaina et al. 2020) and bacterial (Alloul et al. 2019; Sakarika et al. 2020) protein. The presence of butyrate and formate, rather than solely acetate, in the fermentation broth, is expected to boost microbial protein and PHB production, but it will also affect the nutritional value of the first and the mechanical properties of the second one (Alloul et al. 2019; Chakraborty et al. 2009).

6.4 Conclusion

The long-term operation of a 10-liter scale mixed community acetogenic system and the recovery after sulfide stress addition of the tested system show the potential for scaled-up application of acetate bioproduction from waste gases and electrolytically produced hydrogen. During the 0.5 mM TDS run, the acetate production rate averaged at 7.1 ± 1.5 mmolC L^{-1} d^{-1} with a 44 ± 16 % provided as H_2 and 52 ± 19 % of the carbon provided as CO_2 were distributed to acetate and 8 ± 4 % of the electrons and 7 ± 4 % of the carbon to butyrate, as the second most abundant fermentation product. Less than 1% of the electrons was directed to CH_4 production, showing a strong inhibition of methanogenesis even at low TDS concentrations, after consecutive sulfide inhibition. In addition, the results highlight the microbial community changes that occur in a reactor system that under operational changes preserved a stable cell count. A less diverse microbial community was developed, with the genera, *Eubacterium*, *Proteiniphilum* and the unclassified *Eggerthellaceae* showcasing robustness to sulfide stress and a potential future application in waste gas fermentation reactors.

CHAPTER 7

Discussion and outlook

7.1 Summary of key-findings

This thesis is centered around electrochemical processes as the link between waste gas treatment and bioproduction. Several aspects, key for electrochemical treatment for sulfide removal from waste gases, were studied, as well as the limitations that sulfide as a pollutant poses for waste gases fermentation, hence bioproduction. The key-findings of this thesis are summarized below, in a chapter-by-chapter demonstration.

In **Chapter 2** a large-scale gas absorption column to treat 0.4 kg of gas per second was simulated using the Aspen Plus software. Next, the resulting liquid stream was effectively downsized to examine electrochemical treatment in a lab-scale system. **The electrochemical cell configuration selected here demonstrated no need for additional electrolytes, i.e. chemicals, as the produced scrubber effluent was serving as both anolyte and catholyte, which is rarely the case in electrochemical wastewater treatment.** The operational time was limited to 10 h due to heavy S^0 precipitation in the reactor and the connection tubing, clogging the flow. Therefore, **future electrochemical set-ups treating high flows of sulfide** (59 g S L^{-1} d^{-1}) **need to address clogging issues, by efficient S^0 separation, preferably inside the electrochemical reactor.** HS^- was efficiently removed with this system operated at 300 A m^{-2} with 90% efficiency and with 4.96 ± 0.11 kWh kg S^{-1} energy investment. Concurrently a continuous flow of 46 g d^{-1} NaOH was obtained at the electrochemical cell effluent, ready for reuse. **Future applications can rely on a direct connection of a scrubber with an electrochemical cell for immediate HS^- removal, without the need for long-term storage of scrubbing liquids. The gas absorption operation of a H_2S loaded gas stream can partially rely on the electrochemical system for regeneration of the scrubbing solution.** As demonstrated here, 60% of the initial scrubbing liquid, NaOH solution, could be continuously recovered.

In **Chapter 3** we investigated the impact of the anode catalyst choice on the catalytic activity towards sulfide oxidation and the robustness against passivation from deposited elemental sulfur (S^0) under highly alkaline conditions. Six commercially available electrode materials (Ir Mixed Metal Oxide (MMO), Ru MMO, Pt/IrOx, Pt, PbOx and TiO_2/$IrTaO_2$ coated titanium-based electrodes) were tested to evaluate the sulfide removal and final sulfide oxidation product, as well as to determine the stability of the electrocatalyst. The results of the study highlighted that **the catalyst type impacts the anode potential and the sulfide oxidation reaction products while a high differentiation in stability performance among the catalysts is to be expected. Ir MMO should be considered as the most stable electrode for sulfide oxidation** as no catalyst loss was observed and only a small increase in potential (< 0.5 V) during the stability tests. **Ru MMO is an active material towards sulfide oxidation** with a CE_{HS-} of 63.2 ± 0.5% and an average anode potential of 0.92 V ± 0.17 V vs SHE for a constant current density of 50 A m^{-2}, **however the of activity this catalyst was counteracted by a lower stability than Ir MMO. The TiO_2/$IrTaO_2$ electrode cannot yet be considered as a suitable material towards sulfide oxidation, as it was unable to operate at the low anode potential that is desired for direct**

sulfide oxidation. The experimental conditions applied in this study highlighted the instability of Pt/IrOx for sulfide oxidation. **High alkaline, sulfidic and oxidative conditions deteriorated the electrocatalyst loading and a good trade-off will need to be established between activity, stability and cost for a future educated selection of the suitable electrocatalyst to treat sulfur containing wastewater.**

Chapter 4 covered the study of electrochemical treatment applied for removal of sulfide and NaOH recovery from an industrial, sulfidic, spent caustic stream (SCS). The feasibility of the treatment was demonstrated for **20 days of continuous operation at 300 A m^{-2} by a maximum CE_{HS^-} of 80% achieved and the low cell voltage (1.75 ± 0.12 V) maintained throughout the experimental period**. The operation demonstrated a low energy input towards pollutant removal, with **3.7 kWh kg^{-1} S removed** and moderate energy input for wastewater treatment with **75.3 kWh m^{-3} SCS treated**. An industrially relevant **~12 wt.% NaOH solution can be recovered from industrial sulfidic SCS,** at **6.3 ± 0.4 kWh kg^{-1} NaOH** recovered, an energy input not far from the one invested in conventional brine electrolysis widely applied in the chlor-alkali industry. The on-site NaOH recovery in the proposed configuration illustrates a great future potential in decreasing the costs associated with the purchase and the transport of this chemical to industrial sites at the present time. The maximum concentration of NaOH achieved was limited by alkalinity differences between the two electrode compartments and more robust membranes in that aspect should be the focus of further investigation. **A preliminary economic assessment that compared the proposed solution with the common treatment method currently applied for SCS treatment, oxidation via H_2O_2, implies cost-efficiency, mostly due to NaOH recovery and replacement of H_2O_2 as the oxidative agent.**

In **Chapter 5** the effect of hydrogen sulfide (H_2S) in the microbial communities employed in CO_2 containing gas fermentation was studied, as a means to estimate the required gas pretreatment needed. Indeed, the effect of gas pollutants that may be toxic to fermentation communities as well as the extend of inhibition is of utmost importance for the design of successful and cost-effective waste gas fermentation for bioproduction, linked directly to operational and capital costs. A series of toxicity experiments were conducted, with a mixed homoacetogenic culture, total dissolved sulfide concentrations ([TDS]) varied between 0 and 5 mM and pH between 5 and 7. The extent of inhibition was evaluated based on acetate production rates and microbial growth. **Key finding of this study is the identification of the inhibitory concentrations window for sulfide, with IC_{50}^{rAc} values between 0.86 and 1.36 mM [TDS]. A [TDS] above 3.33 mM, completely inhibits acetate production and microbial growth at a pH window of 5 – 7. Sulfide and pH combinations will determine the microbiological landscape in a gas fermenter performing acetogenesis, as different tolerance levels are exhibited by the bacterial genera constituting a mixed microbial community.** Higher tolerance levels were exhibited at pH 5, possibly due to higher community robustness developed already at cultivation of lower than physiological pH. **16S rRNA gene Amplicon sequencing in combination with flow cytometry can be used as a tool to identify changes in the community and highlight strains that exhibit higher robustness**

towards an inhibitor. This would help for future applications of pure cultures obtained, that show higher tolerance to inhibitions and therefore would allow operation at lesser clean waste gases. Whilst correlations could be made of sulfide impact on these key community members, definitive statements on key homoacetogens in these communities could not be made.

In **Chapter 6 a** continuous, sulfide inhibited, 10-L scale fermentation of a CO_2 gas stream using reducing power obtained by electrolysis was examined. Main objectives were to demonstrate, large scale potential of waste gas fermentation, the possibility for powering the fermentation with renewable energy and the limitations arising from pollutants inherent to waste gases. The fermentation activity, projected in the acetate production rate was transiently decreased, after sulfide inhibition at 1.3 mM TDS and recovered with removal of the inhibition. In this study it was demonstrated that **methanogenesis presents a lag-phase in sulfide post-inhibition recovery compared to acetogenesis. In addition, cyclic sulfide inhibition treatment can be applied to selectively suppress methanogens in a mixed microbial community operated in a gas fermenter.** A volumetric acetate production rate of 7.1 ± 1.5 mmolC L^{-1} d^{-1} can be achieved and maintained under minimal inhibition at 0.5 mM TDS and after microbial community inhibition treatment at higher inhibitory concentrations of 1.3 mM TDS. In addition, the results highlight the microbial community changes that occur in a reactor system that under operational changes preserved a stable cell count. A less diverse microbial community was developed, with the genera*, Eubacterium*, *Proteiniphilum* and the unclassified *Eggerthellaceae* showcasing robustness to sulfide stress and a potential future application in waste gas fermentation reactors. **It was thus clearly demonstrated that sulfide as an inhibitor induces taxonomic diversity decrease. Under sulfide stress the product spectrum is shifted towards higher butyrate and formate production**. Known acetogenic genera such as *Acetobacterium* and *Moorella* are strongly inhibited by sulfide and future studies should focus on the effect of sulfide on individual bacterial strains to confirm the observations here.

7.2 Linking electrochemical technology with gas fermentation: Impact and significance

There are numerous industrial activities that emit waste, polluting gases and as life expectancy and standards are increased within the human society, the industry will intensify its activities to meet the increasing demands for commodities. Electrochemical treatment as a technology places itself in the junction were intensification of industrial activities and increase of renewable energy availability in the near future meet. It can aid the increasing demands of modern society in parallel with aiding its decarbonisation by recovering highly consumed chemical commodities, while relying on renewable energy. Additionally, it can decrease substantially the water and salts consumption, a concurrently environmental and financial burden for the waste and wastewater treatment.

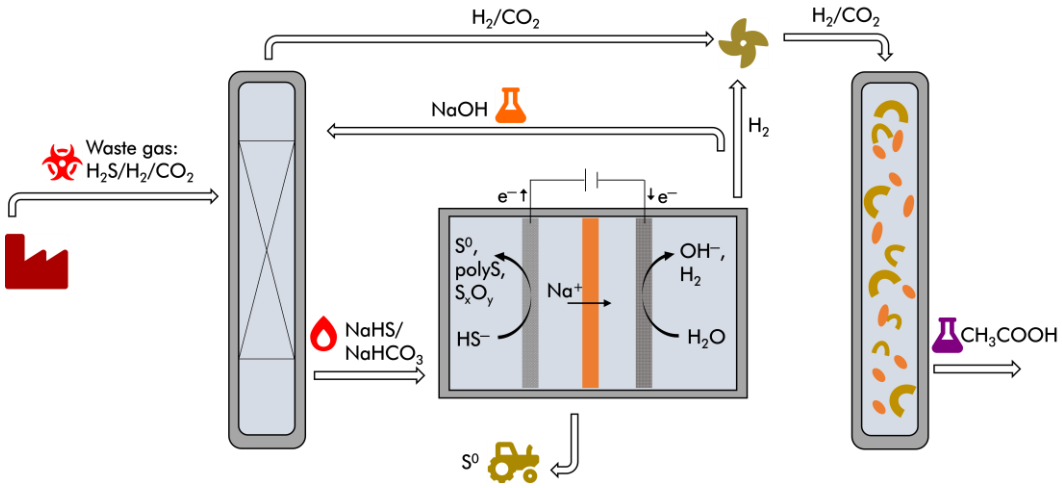

Figure 7.1 – Proposed process scheme of waste gases treatment that will enable bioproduction, by linking waste gas clean-up through absorption, electrochemical treatment for the absorbed pollutant removal and chemical commodities recovery and further valorisation of the gas stream via gas fermentation

The separate studies conducted in this thesis are ultimately concerned with making a proposal for a waste gases treatment process scheme that will enable bioproduction, by linking waste gas clean-up through absorption, electrochemical treatment for the absorbed pollutant removal and chemical commodities recovery and further valorisation of the gas stream via gas fermentation (Figure 7.1). The proposed scheme is expected to have primarily a significant impact on the current operational mode of H_2S emitting industrial activities and plants that are utilizing caustic scrubbers to treat the produced waste gases. The proposed electrochemical step will reduce consumption of hazardous chemicals and potentially provide additional revenue and enable downstream bioproduction of commodity chemicals. Next to the possible revenue, electrochemistry aided on-site chemicals recovery can render the treatment facilities independent from the highly variable commodity chemicals market.

Currently, caustic consumption for gas absorption constitutes the primary contributor to the operational costs of caustic scrubbers. In addition, the resulting scrubbing liquid poses a hazard for the industry due to long-term storage, or otherwise adds to the total costs, as further treatment at elevated temperature and pressure is required to ultimately remove H_2S in the form of S^0. The advantage of electrochemical over the currently applied processes for H_2S treatment is that it relies on the excellent redox properties of H_2S, making the process thermodynamically and financially favourable. Among the gas treatment approaches so far it is the only one that can provide recoverable caustic for scrubbing without the extreme conditions applied currently in industries. In addition, cathodic H_2 recovery serves as energy source for the bioproduction of chemicals, such as acetic acid. As the shift towards biorefinery and waste gases valorisation becomes more prominent, the identification of inhibitors in waste gases and the thorough study of their effects on the bioproduction

efficiency is of utmost importance. In short, the highlight of the process is that removes H_2S which is a toxicant, through an elegant process, avoiding the use of additional chemicals and limiting the energy input. And the latter is only additional to alleviating the environmental and health impacts that arise from the daily, gas emitting, industrial activities.

7.3 Bottlenecks encountered and strategies to unlock them

When one considers the individual studies presented in the chapters of this thesis, one becomes aware of certain limitations that have been encountered during the tests. To unlock the full potential of electrochemical treatment for sulfide removal, NaOH recovery and enable unhindered waste gas fermentation, these limitations need to be taken into consideration and, wherever possible, addressed. Through this paragraph the most important and reoccurring bottlenecks will be summarized and possible strategies to overcome them will be unfolded.

7.3.1 Electrochemical treatment

7.3.1.1 Formation and accumulation of sulfur in the electrochemical cell

First and foremost comes the accumulation of formed S^0 in the electrochemical reactor and the obstruction of liquid flows. Sustained S^0 production without further oxidation rate decrease, as successfully demonstrated in Chapter 2 and reflected through maintaining a stable anode potential, is a ratification of potential long-term stable and successful operation. However, the clogging issues encountered during operation, point towards the opposite direction. It is rather clear that before large-scale application this limitation should be addressed by selecting for a different electrochemical cell design. In the studies presented in Chapters 2 and 5, a parallel plate channel-flow cell was applied, a configuration largely applied in the chlor-alkali industry and in many cases in electrolytic wastewater treatment. Main advantage is the increased mass-transfer and therefore the fast reactant conversion (Arenas et al. 2020). Nevertheless, electrolytic engineering solutions rarely involve solids formation, except for some recent exceptions such as the electrochemical recovery of calcium phosphate (Lei et al. 2019) and generally, electro-coagulation approaches (Moussa et al. 2017).

Consequently, we propose here as a solution the vertical plates in a stirred-tank (generally referred to as "plate-in-tank" cells) configuration, similar to the one used in the electroplating industry (Arenas et al. 2020). The tank should be additionally equipped with an embedded, conical precipitation part for easy separation and recovery of the S^0. This was the idea behind designing a larger lab-scale reactor for the treatment of petrochemical wastewater and NaOH recovery in our lab (Figure 7.2). Agitation in this case is not recommended, especially not in the precipitation area, as it can interfere with the precipitation process. Ultimately in this scenario, some of the reactant conversion efficiency will have

to be compensated with efficient solids removal and the avoidance of clogging that adds to the maintenance costs.

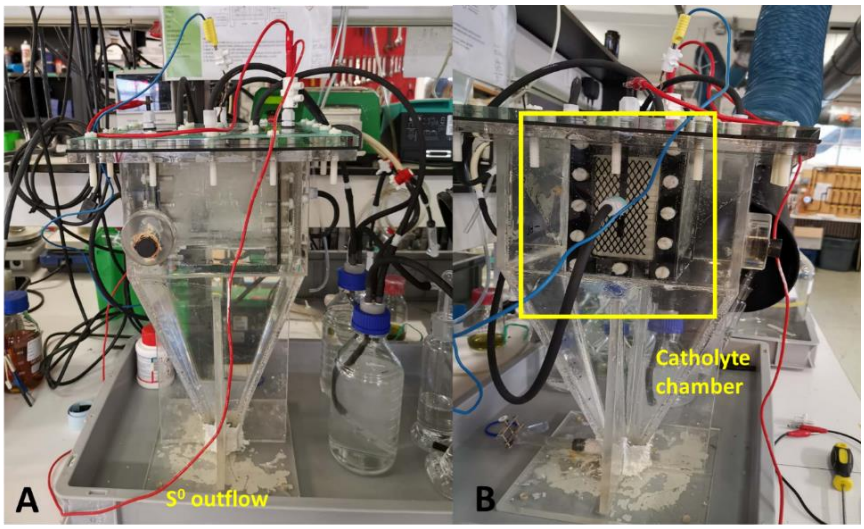

Figure 7.2 – Lab-scale electrochemical reactor for efficient S^0 removal with embedded precipitation tank. Panel A: side view showcasing the precipitation tank. Panel B: side view showcasing the catholyte chamber and one of the anodes

Additional steps that could be proposed to minimize operation hindrance from S^0 deposition and clogging are intermittent mechanical removal of the S^0 film formed on the electrode surface aided by soft, moving brushes incorporated in the cell reactor, or intermittent cleaning steps. In the latter, the reactor, and thus the anodes, can be immersed in an alkaline sulfidic solution and S^0 can be removed chemically as polysulfides. This solution can be reused up to a point of saturation, having some very limited impact in the operational costs. The intermittent cleaning steps suggest a batch, rather than continuous, operation. Indeed, during batch operation the S^0 produced can efficiently precipitate and be collected at the bottom of the reactor by the end of the operation. After separation of the particles, the electrode surface can be washed again with the alkaline sulfidic solution under current relaxation. This is presumably the least invasive approach for the electrode surface cleaning, as it does not involve application of high anode potentials that could destruct the catalytic surface. In addition, NaOH can be recovered in batches in lower strength, however in higher current efficiency, by avoiding osmotic pressure phenomena (see further paragraph 7.3.1.3).

7.3.1.2 Limited electrode lifetime

The high capital cost of electrochemical cells is a principal concern when electrochemistry, as opposed to conventional chemistry, is proposed for wastewater treatment. Although it is commonly accepted

that the anode catalyst, usually consisted of noble-metals such as Pt, Ir, Ru, holds the lion's share of the capital costs, it has been estimated that it only contributes to around 6% of it (Spöri et al. 2017). However, the noble character of these metals and market changes in the availability and demand of the catalysts have raised the interest for production of electrodes that can exhibit a longer lifetime. In Chapter 3, the electrode lifetime of different commercial electrodes was tested for 305 h, under operating conditions relevant to alkaline sulfidic streams. This experimental time was determined by the first failing electrode, Pt/IrOx. During this limited, considering the relatively low applied current density (Spöri et al. 2017), experimental time, all electrodes, but Ir MMO, experienced a certain catalyst loss, different for every electrode. This observation signifies that proving the financial competence of long-term electrochemical sulfide application at conditions relevant for electrochemical treatment of SCS will be a challenge.

The actual lifetime of the Ir MMO catalyst under the conditions applied here is a key point that is yet to be addressed. Although, in comparison, its behaviour seems promising, the absolute lifetime of this electrode under the specific tested conditions is yet to be quantified. Longer-term (field) studies of the electrode performance operated with real SCS are needed to quantify it. A number of researchers have investigated different approaches to enhance the activity, or stability, as well as to reduce the catalyst loading, and thus the cost, of MMO electrodes used in oxygen evolution reactions (OER). These include different methods of electrode preparation, combination of the Ru and Ir noble metals with less noble catalysts such as Sn or Ta or routes to effectively reduce the Ir catalyst loading, without sacrificing the activity or stability of the electrode (Santos et al. 2019; Spöri et al. 2017). An example of reducing the catalyst loading but maintaining a longer robust performance is the $TiO_2/IrTaO_2$ tested here (Y. Yang and Hoffmann 2016). However, it exhibited an oxidation performance not desired for the application and the stability was not evaluated here. Further research and additional lab-scale experimental data with the aforementioned electrodes at alkaline and sulfidic solutions could give us an indication of their suitability for electrochemical sulfide oxidation applications, thus possibly a future opportunity to strike a good balance between, activity and stability, hence removal efficiency and cost of the electrodes.

7.3.1.3 Concentrated NaOH solutions recovery

Next in the limitations encountered in the electrochemical cell operation is the decrease in the alkalinity recovery rate over time, demonstrated in Chapter 4. The maximum NaOH that can be recovered, in a system that is concentrating NaOH by batch operation of the cathodic compartment, will be dictated also by the concentration gradient, thus by the NaOH concentration differences between the anodic and cathodic compartment (Allen J. Bard and Faulkner 2001; Budiarto et al. 2017). The permselectivity of the membrane will also play a role, as a decrease of it can result in OH^- back

diffusion and thus loss of cathodic current efficiency (Mendoza et al. 2017). In addition, osmotic pressure differences can lead to water cross-over from the anodic to the cathodic compartment, ultimately diluting the already produced NaOH. This is a limitation commonly addressed in alkaline electrochemical systems for NaOH recovery (Jörissen and Simmrock 1991; Wei et al. 2013) and it is often attributed to the inability of the ion-exchange membrane to resist pH/alkalinity differences between the electrode compartments. An increase in coulombic efficiency could be achieved either with the fabrication of ion-exchange membranes that are more resistant to high alkalinity and high alkalinity differences between the electrochemical cell compartments. Alternatively, several batches of recovered NaOH of lower concentration can be produced and in a next step up-concentrated to the concentration desired by the party interested in the NaOH, with residual heat. Residual heat is the by-product of many industrial processes, but also is produced in the electrochemical cell as a result of the ohmic losses and the operational temperature and pressure. For example, Saxe and Alvfors have calculated that an alkaline electrolysis cell for H_2 production, operated at 80 °C and 10 bar, with incoming electrolyte temperature at 20 °C can produce up to 1.42 kWh Nm^{-3} H_2 waste heat (Saxe and Alvfors 2007).

7.3.2 Bioproduction

7.3.2.1 Acetogenic community evolution

An implication applying to both Chapters 5 and 6 is that the microbial community evolution in the system is limited to the specific system studied. This is reflected through the differences in the genera comprising the microbial communities of the flask (Chapter 5) and the continuous larger-scale fermentation experiments (Chapter 6). The reason behind that could be that when an inhibitor is applied to a mixed community the general response will not only be a function of the concentration of the inhibitor but it will always be a function of the operational parameters applied in the system, as this will as well select for a certain microbial landscape. Differences between the two systems, except for the liquid and headspace volume, were the experimental time, the hydrogen concentration and the gas mixing conditions. All of the aforementioned can select first for specific acetogens to thrive. Consequently, the inhibition will be relevant only for the species that initially prevailed. Sulfide is reportedly inhibiting microbial growth and thus bioproduction, by interfering with certain cytochromes in the respiratory chain, while different detoxification mechanisms have been reported so far, including among others mitochondrial sulfide oxidation (Jingjing Jiang et al. 2016; Rubright et al. 2017). In order for sulfide to interfere with the respiratory chain, the first step is to cross the cellular membrane and as the latter is cell type specific (N. J. Yang and Hinner 2015), a different sulfide inhibition extent could be expected by different bacterial strains. Hence, the actual sulfide concentrations causing inhibition, could also be strain specific.

Furthermore, a toxicant applied in a mixed microbial community will trigger different responses at different groups of bacteria, thus the inhibition effect to specific genera will not be a clear response to the inhibitor. Hence the conclusions cannot be generalised, but they apply specifically to the specific system tested. In order to make a more universal and scientific just argument for the sulfide toxicity in homoacetogenesis, experiments with pure homoacetogenic strains, generally encountered in acetogenic reactors need to be conducted. A good start would be the study of sulfide inhibition to pure cultures of *Eubacterium* strains, a known acetogenic genus that has demonstrated increased robustness towards sulfide inhibition, as highlighted in Chapter 6.

7.4 Adding value through product recovery

Waste treatment is of utmost important to secure human health and a safe living environment. However, in the context of circular economy waste removal is not of added-value. To ensure application attractiveness and make a sound economic argument for novel waste treatment technologies, economically attractive products recovery needs to be demonstrated. Within the context of gas clean-up and gas fermentation that are highlighted in this thesis, value-added product recovery can be demonstrated too. A list of potentially recoverable chemicals through the process train proposed here is given below in increasing price order. One should keep in mind however, that a substantial burden on the actual price of these chemicals is the transport to the utilization site. Except for adding value, the risks of handling and storage of chemicals on-site are minimized, as well as financial and carbon emissions burdens, associated with their transport.

7.4.1 Elemental sulfur (S^0)

Upon sulfide (H_2S/HS^-) oxidation at the anode surface, elemental sulfur (S^0) is produced, which can be easily separated from the electrolyte solution through common precipitation or filtration (Figure 7.3). The produced elemental sulfur (S^0), via electrolysis is in the pure, orthorhombic chemical form usually purchased industrially and can be used on-site as is, or after thermal treatment, such as simple evaporation, to remove any remaining liquid electrolyte.

Sulfur is commercially produced from H_2S contained in the exhaust gases of the oil refinery through the Claus process and is majorly used for sulfuric acid (H_2SO_4) production. The latter is a chemical building block primarily used in the production of phosphate-based and other fertilizers (Rubright et al. 2017). Additionally, it can be used in autotrophic wastewater treatment processes, such as in sulfur based drinking or underground water denitrification reactors, as an electron donor and a compensator for decreased alkalinity (Ucar et al. 2020). A breakthrough application for S^0 is as building additive or in sulfur batteries, but these are applications still under research and they do not

constitute actual markets currently. Sulfur is a low value commodity, especially as it is produced in excess in oil refineries. The price of sulfur produced by the EU oil refinery in 2016 was 22$/t, reported in CONCAWE 2020 (Valdenaire and Mennecier 2020) and an average, between 2014 and 2019, price for clean sulfur could be considered as 70 € t^{-1} (Statista 2019). The low value of S^0 blocks financial arguments for transport from the place of recovery to an industry that would use it, so a simple solution for use would be on-site use as a fertilizer on the green areas surrounding the industry.

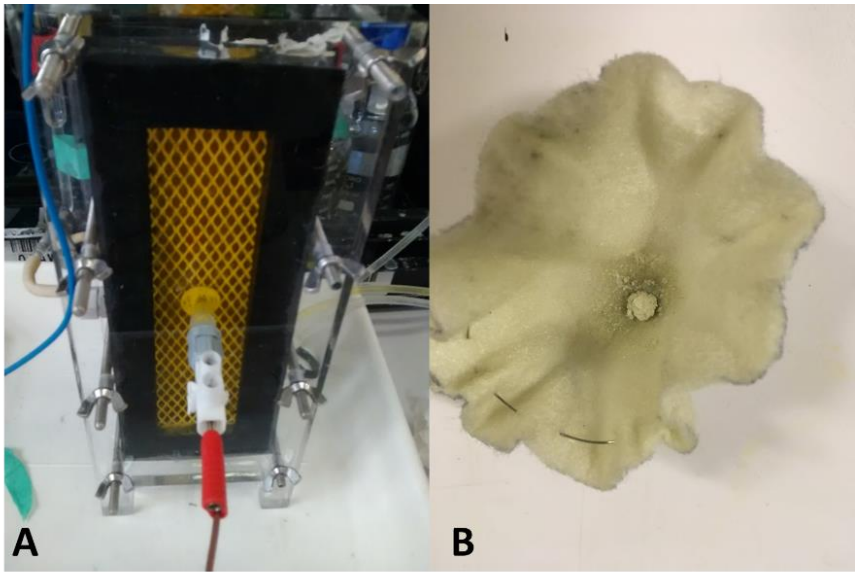

Figure 7.3 – Panel A: Sulfur precipitation on the electrode surface and Panel B: Sulfur particles recovery on the cloth filter used for S^0 particles separation in Chapter 2

7.4.2 Caustic soda (NaOH)

The main recoverable product of the electrochemical treatment proposed in this thesis is sodium hydroxide (NaOH) or commonly known as caustic soda, obtained through cathodic reduction of water to hydroxyl ions (OH^-) and hydrogen gas (H_2). It is a commodity chemical majorly used in the pulp and paper and the alumina industry, as well as in the chemical manufacturing industry, the petrochemical refinery and in wastewater treatment (Euro Chlor 2010). As the common name suggests, it is highly corrosive and irritating to human skin, therefore considered a hazard for storage and handling. Caustic soda production is inherently linked to chlorine production due to the brine electrolysis process that co-produces these two commodities. However linked in production, the two products are of interest for different industries, therefore their supply and demand, and hence their price, is often conflicting. As an example, during the COVID-19 pandemic the availability of the European caustic soda drastically decreased, as a cascading effect of the reduced automobiles demand and thus, the chlorine demand from the automobile industry. The total chlor-alkali demand

decreased by 74% (ICIS 2020). Therefore, price volatility for caustic soda is rather expected, with the prices ranging from 250 to 1000 € and a general stable average of 400 € m^{-1} dry ton (Bowen 2019; C.Baker 2020).

Several advantages arise only from producing NaOH on-site, aside from the sustainability argument of producing it from waste streams. First of all avoiding the need for transport, which contributes substantially to the commodities price and in addition to the carbon footprint of the chemical. Therefore production on-site makes for a sound economical, but also environmental argument. Secondly, storing of hazardous chemicals on-site raises health and safety concerns that can be avoided with on-site and on-demand production. Thirdly, independence from price and production fluctuations and therefore stable operation. Additionally, the modular nature of electrochemical treatment allows for applications of on-site, small scale testing equipment, where the wastewater to treat can be easily electrochemically treated and the produced NaOH can be fast checked in terms of purity to conclude on its fit for specific purposes. At last, the production of NaOH by the membrane process mainly applied in Europe, requires 3 kWh kg^{-1} NaOH produced (Euro Chlor 2010), therefore, electrochemical treatment of highly conductive SCS that decrease the power input per kg NaOH recovered can be not only environmentally advantageous, but also financially competitive.

7.4.3 Acetic acid (CH_3COOH)

The main product of gas fermentation in this thesis was acetic acid (CH_3COOH), with a minimum in parallel production of butyric acid. As acetic acid was produced in excess, an evaluation of the recovery benefits of acetic acid for the industry will be explained further. Acetic acid is a moderate value commodity chemical, with a similar price range to caustic soda and similar price volatility due to its production dependence on petrochemical industry. However the moderate price, it is an industrially significant commodity chemical, with global size market expected to reach almost 12 million tonnes by 2026 (Expert Market Research 2020). It is used largely in the production of polymers fit for the paint industry, but also important for the food industry and as a precursor for the production of butyric acid and ethanol. It is categorized as hazardous and is irritating for the human skin, therefore its production on-site entails a health risk, however the smaller the volumes stored on-site, the lower the occupational risk.

Acetic acid is largely produced industrially through methanol carbonylation, with iodomethane used as a reaction intermediate (Pulidindi and Pandey 2019), or via microbial ethanol oxidation to acetate (Agler et al. 2011; Li et al. 2015). By substituting the general industrial acetic acid production route with a biological fermentative process, the advantages are both financial and environmental. They arise from the bypass of chemicals with increased carbon footprint and the use of waste CO_2. In the first case, the bypass of methanol, the process can be sustained by avoidance of a chemical that has

a fluctuating cost, but also avoidance of the use of iodomethane, which is not only an additional cost in the process, but also possesses toxic properties. In the case of using waste CO_2, the industrial route for the production of methanol and iodomethane is avoided and even the chemicals for pH control of the fermentative route can be produced via electrolysis and thus potentially renewable power.

After fermentation downstream processing will be necessary to reach desired purity of the product, as acetic acid is rarely produced as the sole product of gas fermentations. Additionally thermal treatment is to be expected for up-concentration, as well as a membrane process for the removal of bacterial cells. In the scheme proposed in this thesis, the last step can be avoided as the cell retention and thus separation, is already taking place as part of the reactor set-up, through the incorporation of a hollow-fiber membrane at the recirculation of the fermentation liquid.

7.4.4 Hydrogen gas (H_2)

Hydrogen gas (H_2) is produced via water reduction at the cathodic compartment of the electrolysis cell treating SCS. The resulting H_2 is a clean gas, devoid of other pollutants, due to membrane separation between the anodic and cell compartments, therefore fit-for-use at the site of production. In particular, electrolysis of highly-loaded industrial wastewater, like SCS, is conducted at high current densities, 10 – 40 mA cm^{-2} (Szpyrkowicz et al. 2005; Vaiopoulou et al. 2016), therefore allowing for increased daily flows of pure H_2 on-site. H_2 is an energy carrier extensively discussed within the context of circular economy as it has the potential, along with electrification, to drive the transition towards a carbon-free economy.

The shift towards electrification and clean H_2 production couldn't be better reflected than through the North-CCU-Hub project. The project was launched in 2018, aiming to serve with methanol the North Sea Industry, by capturing its CO_2 emissions and turning them into green methanol with the help of H_2 production powered by wind energy (North-CCU-Hub 2021). Ultimate aim is to scale up to a 600 MW electrolyzer by 2030 and extend its chemical platform to ammonia and formic acid production. The scale and the vision of this project demonstrate that Environmental, Societal and Governmental (EGS) will most likely be the drivers for industrial development in the coming decades (Hydrogen Council 2020). The current global demand for hydrogen is 70 Mt/a with 96% of it being produced by CO_2 emitting processes such as natural gas reforming, coal gasification and partial oil oxidation and only 4% by electrolysis (S&P Global Platts 2020; Valente et al. 2020). With the decarbonisation and desulfurization of the industrial and transport sectors directives globally introduced (European Commission 2019; IMO 2020), the hydrogen demand is expected to reach 41 Mt/a, only as demand for oil refineries, that constitute 33% of the total global H_2 consumption (IEA 2019).

Main processes that consume H_2 in the oil refinery are hydrotreating and hydrocracking for sulfur compounds removal (De Crisci et al. 2019). Secondly, H_2 constitutes an industrial feedstock for

ammonia fertilizers and methanol production (IEA 2019; S&P Global Platts 2020). The market price of conventional H_2 in 2020 hit a global average of 2 €/kg H_2 with lowest margin less than 1 €/kg H_2 in the Middle East. Green hydrogen, produced via PEM electrolysis is currently produced at 4.5 €/kg H_2, which needs to drop to at least the conventional price, to become financially attractive (Hydrogen Council 2020; IEA 2019; S&P Global Platts 2020). The advantage of electrochemical treatment of sulfur containing waste gas streams at the production site of for example petrochemical refineries is that the produced H_2 can be reused for hydrotreating, therefore completing elegantly a cyclic process. In another, newer concept, H_2 can be used as an energy booster of CO/CO_2 fermentations for low-grade acids or alcohols generation (Liew et al. 2016). In industrial applications were hydrogen is not of use for specific applications, it can serve as a boiler fuel for heating purposes.

7.5 Taking the process to full-scale

The overview scheme of treatment of waste gases to enable bioproduction proposed in this thesis considers a treatment train of three processes: selective H_2S absorption in a simple caustic (NaOH) scrubber – electrochemical treatment of the produced scrubber liquid for H_2S removal and recovery of primarily NaOH and secondarily S^0 and H_2 – gas fermentation of CO_2/H_2 escaping the caustic absorption and electrochemically produced H_2 for acetic acid production.

7.5.1 Up-scaling and evaluating gas absorption

The first unit that is considered is a caustic scrubber that is applied to treat a H_2S loaded gas stream, product of geothermal power production activities. The characteristics of the gas stream considered have been presented in Chapter 2 and the treatment process can be applied to any relevant stream with H_2S content similar or lower, as this simple approach of scrubbers is usually reported for a daily sulfur removal of maximum 10 ton (Mcintush et al. 2013). In principle, a simple caustic scrubbing process set-up would include the gas absorption column, a heat exchanger and a basic pumping system. Therefore the daily operational costs will arise from the use of concentrated NaOH streams and the electricity use of the heat exchanger and the recirculation pumps. A preliminary cost evaluation was conducted based on the gas and NaOH flows calculated in Chapter 2.

The scenario examined was a caustic scrubber, to treat daily 34.56 ton gas with absorption in 15.55 ton NaOH per day, resulting in a liquid stream of 7.04 ton S d^{-1} to be directed to electrochemical treatment. In the simulation of Chapter 2 a packed column 2 m of height and 0.5 m of diameter was considered, however here the CAPEX costs were based on an installed gas absorption unit for biogas desulfurization, of similar gas volumetric flow rate as in our study (1000 m^3 h^{-1} vs 1243.86 m^3 h^{-1} in our case) (Lemmens et al. 2007). In the daily cost distribution, a CAPEX contribution per day was

considered, as well as average recent prices for the electricity and NaOH (Table 7.1).

Table 7.1 - Cost distribution in gas absorption calculated based on the unit simulated with ASPEN Plus in Chapter 2, to treat 30 × 10^3 m^3 waste gas daily

Component	Daily consumption	Daily cost (EUR d^{-1})	Contribution to daily costs (%)	Baseline information
Caustic soda (NaOH)	15.55 (ton d^{-1})	-9,720.00	-99.52	[1.1]
Electricity consumption	17.91 (kWh d^{-1})	-1.79	-0.02	[1.2]
Daily personnel costs	—	-13.70	-0.14	[1.3]
CAPEX daily distribution	—	-41.10	-0.32	[1.4]
Total daily costs (EUR d^{-1})	—	-9,767.00	—	

[1.1] Based on 250 – 1000 € ton^{-1} dry NaOH (Bowen 2019; C.Baker 2020)

[1.2] Based on lower and higher energy use for gas absorption (0.2 – 1 kWh/ 1000m3 h^{-1}) (VITO/Infomil 2009) and electricity price for industries in Belgium in 2019 (0.08 – 0.12 € kWh^{-1}) (statista 2020)

[1.3] Based on assumed 5000 € invested yearly for personnel costs, with an average of 4 h per week occupation (VITO/Infomil 2009)

[1.4] Based on 80000 – 150000/ 1000 m3 h^{-1} CAPEX cost (Lemmens et al. 2007) and an assumed CAPEX depreciation time of 10 years

With a 99.52% contribution, the NaOH holds the lion's share in the daily costs, while electricity, salaries and the construction costs represent less than 1%. By recovering 60% of the NaOH with the electrochemical system, as demonstrated in Chapter 2, we can assume a 60% recovery of the daily operational costs for the gas absorption column. However, the electrochemical treatment of the scrubbing liquid serves additionally for H_2S removal, as well as possible H_2 and S^0 recovery. The first one serves for decreasing the environmental burden of the process and aids abidance of the industrial activity with environmental regulations, and the two last ones are a source of possible revenue for the

industrial site. In the following section the cost analysis and possibility for scale-up of an electrolysis cell applied for the treatment of the produced scrubbing liquid will be developed.

7.5.2 Up-scaling and evaluating the electrolysis of scrubbing liquid

The scrubbing liquid, product of the ASPEN Plus simulation was downsized to enable electrochemical treatment in a lab-scale system, which has been discussed in Chapter 2. For this discussion chapter, the electrochemical cell cost analysis was up-scaled by 2×10^5 times to meet the treatment needs of a large sized gas absorption system, as presented in the previous paragraph. Up-scaling of electrochemical systems is conducted via increasing the total electroactive surface area where the reactions of interest are conducted. The latter can be achieved by increasing the electrode size and by adding and connecting together several electrochemical subunits (Arenas et al. 2020). The design of an up-scaled electrochemical cell as proposed here should consider a total anode surface area of 2000 m^2 for an applied 300 A m^{-2} current density (Chapter 2), to treat daily 576 m^3 of produced scrubbing liquid. The lab-scale electrochemical treatment performance results, selected here as calculation inputs, were 6.5 V operating cell voltage, 6.4 tonnes of sulfur removed (and also assumed recovered as S^0) and 9.2 tonnes NaOH recovered, daily. A daily cost CAPEX contribution with a 10 years depreciation time was considered as well as average, recent prices for the electricity and all the chemicals (Table 7.2). Baseline information for the NaOH and energy pricing and the personnel costs can already be found in Table 7.1.

A total cost recovery of 31.15% is possible within the current scheme and performance, with the NaOH recovery being the highest contributor to the cost recovery. Additional daily revenue from the H_2 production and S^0 recovery can be obtained, although their contribution to the cost recovery is one order of magnitude smaller than the one of NaOH. As expected, the construction costs are the primary contributor to the total costs of electrochemical treatment, which is confirmed by the 60% contribution of CAPEX to the daily costs (Table 7.2). The CAPEX costs for water electrolysis cells are at the moment at around 30 thousand euros per square meter of electrode projected surface area (Spurgeon and Kumar 2018) which renders electrochemical waste treatment a technology difficult to prove financially interesting. However, to prove the former argument wrong, one could increase the current density and therefore decrease the electrode surface needed, hence the capital cost. Attention should be paid here, to ensure ideal mixing conditions and optimal contact of the electrolyte with the active sites of the electrode.

Based on the aforementioned argument, a second case was built assuming a higher applied current density to estimate how the decrease in electrochemical cell assembly area, hence CAPEX, would affect the cost efficiency of the process. The Danish company "Electrocell" designs electrochemical cell modules for lab- to full-scale applications. The biggest module provided is the "Electro Prod Cell", with

16 m^2 maximum projected electrode surface area and maximum allowed applied current density 4 kA m^{-2} (ElectroCell 2017). Based on this maximum current density the second case was built with a calculated 150 m^2 projected anode surface area required. A comparison of the daily costs between the two cases, highlights that in the first case, 300 A m^{-2}, the CAPEX dominates the daily expenses while in the second case, 4 kA m^{-2}, it is the electricity consumption that is dominating, with a 90% contribution to daily costs. In the second case it would also possible to recover 70% of the total daily costs, as the initial investment costs are lowered by 14 times, due to the decreased surface area of the electrochemical cell selected.

Table 7.2 – Cost distribution in the electrochemical cell, up-scaled at 2000 and 150 m^2 projected electrode surface area, for the treatment of scrubbing liquid

Component	Daily consumption/production	Daily costs (EUR d^{-1})	Contribution to daily costs (%)	Baseline information
Electricity consumption	93.60 (MWh d^{-1})	-9,360.00	-40.09	
Daily personnel costs	—	-13.70	-0.06	
CAPEX daily distribution	—	-13,972.60	-59.85	[2.1]
Total daily costs (EUR d^{-1})	—	-23,346.30	—	
Caustic soda (NaOH)	9.20 (ton d^{-1})	+5,750.00	+24.63	
Hydrogen gas (H_2)	0.54 (ton d^{-1})	+1074.57	+4.60	[2.2]
Sulfur powder (S^0)	6.40 (ton d^{-1})	+448.00	+1.92	[2.3]
Alternative operation at 4 kA m^{-2} current density				
Electricity consumption	93.60 (MWh d^{-1})	-9,360.00	-89.81	
Daily personnel costs	—	-13.70	-0.13	

CAPEX daily distribution	—	-1,047.95	-10.06	[2.1]
Total daily costs (EUR d^{-1})	—	-10,421.64	—	
Caustic soda (NaOH)	9.20 (ton d^{-1})	+5,750.00	+55.17	
Hydrogen gas (H_2)	0.54 (ton d^{-1})	+1,074.57	+10.31	[2.2]
Sulfur powder (S^0)	6.4 (ton d^{-1})	+448	+4.30	[2.3]

[2.1] Based on 25,500 € m^{-2} as base case CAPEX for water electrolysis (15464 – 46391 $ m^{-2}) (Spurgeon and Kumar 2018)

[2.2] 2000 € ton^{-1} H_2, current average price of conventionally produced H_2 (Hydrogen Council 2020; IEA 2019; S&P Global Platts 2020)

[2.3] Average value between 2014 and 2019 and calculated with current $ to € ratio, 70 € ton^{-1} S^0 (Statista 2019)

A common practice industrially applied to treat produced on-site spent caustic streams (SCS) is oxidation with hydrogen peroxide (H_2O_2). The latter is a powerful chemical that oxidizes the sulfide in SCS to SO_4^{2-} under a 4:1 molar ratio. However, in addition to the problematic secondary pollution creation (SO_4^{2-} streams need to be further treated), H_2O_2 has a high price, between 500 – 1000 € ton^{-1} H_2O_2 (Ciriminna et al. 2016), which is also on the rise in the future, as announced by one of the biggest worldwide producers, the Belgian company "Solvay" (Solvay S.A. 2018). Therefore, the advantages of the electrochemical approach in terms of avoiding the purchase and use of H_2O_2 for sulfide oxidation are highlighted here as well.

First, the electrochemical cell as an autonomous unit was studied (Table 7.2) and as a second step, the electrochemical cell in connection with the gas absorption unit were considered to comment on the cost efficiency of the synched units (Table 7.3). Three different scenarios were considered: 1) whether the recovery of chemicals can cover the daily costs of construction and operation of the electrochemical cell solely, 2) whether electrochemical treatment can offer a revenue in SCS treatment facilities, by replacing the current practice, sulfide oxidation by H_2O_2 and 3) whether the chemicals recovery and avoiding H_2O_2 can cover the combined daily costs of gas absorption and electrochemical cell treatment (Table 7.3). As it can be seen, the electrochemical recovery of NaOH, H_2 and S^0 already provides a financial benefit to treatment facilities, that otherwise would only constitute a cost for the

industry. Based on the operation achieved in the lab-scale electrochemical test, a 31.15% of the daily costs of the electrochemical cell can already be recovered. In the second scenario, where a company wold select to switch between current treatment with H_2O_2 and future electrochemical treatment of SCS, profit can be achieved, up to 6500 € d^{-1}. In the third scenario, where a company would decide to treat the waste gases produced on-site, as well as the scrubber effluent, a 22% recovery of the daily costs can be achieved.

Table 7.3 – Comparison of the 3 scenarios examined for the cost effectiveness of the waste gas treatment through gas absorption and electrochemical sulfide treatment

	Scenario 1	Scenario 2	Scenario 3
Daily costs (EUR d^{-1})	23,346.30	23,346.30	33,113.30
Daily CAPEX cost contribution (EUR d^{-1})	13,972.60	13,972.60	14,004.11
Percentage of cost recovery (%)	31.15	884.74	21.96

7.5.3 Up-scaling and evaluating waste gas (H_2/CO_2) fermentation

The H_2S is quite selectively removed in the scrubber as proved in Chapter 2, with the CO_2 only partially co-absorbed (17%) and with H_2 completely escaping the scrubber. The resulting gas mixture escaping the scrubber, H_2/CO_2, can be directed to the gas fermenter as microbial feed to allow for acetic acid bioproduction. However, as reported in Chapters 4 and 5, the ideal theoretical molar ratio of H_2:CO_2 for acetic acid production is 2. The daily molar flow rates of the two gases escaping the scrubber (reported in Chapter 2) are 273.63 kmol H_2 d^{-1} and 453.51 kmol CO_2 d^{-1} and an additional flow of 270.00 kmol H_2 d^{-1} can be produced by the up-scaled electrochemical cell considered previously. Still, the molar ratio of the two gases is at 1.2, lower than 2, hence in the case of this specific gas stream, an additional 0.73 ton of H_2 needs to be purchased daily, to at least, meet the stoichiometric demand. A complete stroichiometric production of acetic acid was assumed, resulting in 13.62 ton acetic acid d^{-1}, based on the incoming CO_2 flow escaping the gas scrubber. For the reactor sizing, the best scenario in continuous acetogenesis was selected, which is the highest acetic acid production rate reported so far, 147 g acetate L^{-1} d^{-1}. The theoretically expected up-scaled acetate daily production in combination with the aforementioned production rate, result in an estimated 92.63 m^3 reactor volume.

The cost analysis in the fermenter is built around the additional H_2 that needs to be purchased (Table 7.4) and acetic acid as the product to provide revenue. In addition, the consumption of NaOH for pH regulation is taken into account. The process of chemicals and CAPEX depreciation years are similar with the above cost analyses, but the man-hours were increased to 12 hours per week, as the fermenter requires a more intensive monitoring and maintenance compared to the other two systems.

Table 7.4 – Cost distribution in the waste gas fermentation unit, receiving19.96 ton CO_2 d^{-1} to produce acetic acid

Component	Daily consumption/production	Daily costs (EUR d^{-1})	Contribution to daily costs (%)	Baseline information
Hydrogen gas (H_2)	0.73 (ton d^{-1})	-1,816.99	-11.23	
Caustic soda (NaOH)	9.07 (ton d^{-1})	-5,668.92	-35.04	
Electricity consumption	24.51 (MWh d^{-1})	-2,451.10	-15.15	
Daily personnel costs	—	-41.10	-0.25	[4.1]
CAPEX daily distribution	—	-4,383.56	-27.09	[4.2]
Total daily costs (EUR d^{-1})	—	-23,346.30	—	
Acetic acid (CH_3COOH)	13.62 (ton d^{-1})	+6127.74	37.88	[4.3]

[4.1] Based on assumed 15000 € invested yearly for personnel costs, with an average of 12 h per week occupation

[4.2] Based on a 16 M€ capital investment, calculated based on the average capital investments of two syngas fermentation installations by INEOS, with 24 kt ethanol y^{-1} production capacity, downsized 5 times to meet the production capacity assumed for this unit (Aresta et al. 2012)

[4.3] Based on 300 – 600 € t-1 acetic acid price range (Echemi 2019a)

Although it is a common perception that the high CAPEX is what hinders biorefinery from wider

application, as usually chemicals consumption for pH control are taken out of the calculation, it can be seen here that NaOH costs are the ones that are dominating. NaOH contributes to 35% of costs, a cost that could be completely recovered if gas fermentation was coupled to the electrochemical cell instead of the gas absorption (Table 7.2). In addition, a total of 60% of the H_2 and 100% of the CO_2 needed as inputs for the acetic acid production are already provided by a waste gas/electrolysis system, which not only highlights the cost efficiency of the process in terms of raw inputs, but also how environmental benign can be considered. In short, in both of the technologies, gas absorption and gas fermentation NaOH dominates the total costs, while in the electrochemical cell NaOH dominates the revenue, therefore it makes absolute sense to link these two technologies with the electrochemical cell in the center.

7.6 Outlook – Electrochemical gas treatment for sulfide removal in the oil refinery

In principle the 3-unit-treatment scheme proposed here could be applicable to any of the heavy gas producing industries, such as geothermal power stations, natural gas plants or oil refineries, which are also reportedly the point sources of industrially generated H_2S emissions (Habeeb et al. 2018). The cost effectiveness of the scheme will be also determined by the industry applied, as different $CO_2/H_2S/H_2$ ratios in the gas mixtures will not only affect the H_2S removal efficiency, but also the availability of residual gases H_2/CO_2 for gas fermentation. Moreover, the need for consumption of specific chemicals on-site, will also provide a more sound economic argument for the proposed technology. In addition, the availability of renewable energy in the vicinity of the application will affect the circularity of the process. In this section a niche application of the proposed system, as a whole treatment train or solely the gas absorption together with the electrochemical cell treatment will be proposed.

Petrochemical refineries are among the primary emitters of H_2S, which results from the processes of hydrotreating/hydrocracking, applied for desulfurization of crude oil. This applies mainly to the treatment of heavy, marine oil and jet fuel, that come with a higher sulfur content. In this context pure H_2 is used to remove sulfur compounds from the oil, in order to meet SO_2, released upon fuel combustion, emissions regulations. In particular, the IMO Global Sulphur Cap came into force in the 1st of January 2020 as an effort to ensure SO_2 reduction emissions by shipping and thereby improve air quality and ultimately human health. The directive requires limiting the sulfur content in marine fuels to as low as 0.5% m/m (500 ppm) from the previously allowed 3.5% m/m (3500 ppm) by either using low sulfur fuels or by applying gas exhaust treatment strategies on board (IMO 2020). As the regulations for sulfur emissions become more and more stringent, the petrochemical refinery in Europe is targeting investments on hydrotreating units, such as Distillate Hydrocrackers (DHC), Residue Hydrocrackers (RHC), Diesel Hydrodesulphurisation (HDS) and Coking (COK) units, in an attempt to

produce distillation products that would compete in sustainability the bio-based fuels (CONCAWE Refinery Technology Support Group 2013).

Between 6 and 7 Mt sulfur per annum need to be removed from the total sum of the crude oil that is produced in Europe. This requires an additional 1.6 Mt of H_2 for the total hydrodesulfurization processes (CONCAWE Refinery Technology Support Group 2013) and thus, additional capital investment from the oil refineries, which is also their main concern. The total european refinery energy investment in 2030 is expected to be around 40 Mtoe y^{-1} and the specific energy investment 66 toe kt^{-1} feed. The two are expected to follow an inverse trend, with the first one decreasing as a result of general fuel energy efficiency increase and the second increasing due to the anticipated intensification of desulfurization processes (CONCAWE Refinery Technology Support Group 2013).

However, capital investment is not the only challenge encountered, but also the sustainability of the process is questioned, as currently, close to 100% of all the H_2 available comes from steam reforming processes. The total CO_2 emissions from the European refinery are expected to reach 154 Mt in 2030. There are currently 76 refineries in Europe and if it were to assume that the total sulfur to be removed can be divided equally to each of them, the flow of sulfur that they would be called to treat daily can be calculated at an average 235 tonnes. Considering our previously studied case, this would call for a 35 times up-scaling of our system, resulting in a total electrochemical surface area of 70000 m^2. The operation of such an electrochemical cell at 300 A m^{-2} would result in a daily production of 322 tonnes of NaOH, as well as 19 tonnes of H_2. This daily production of H_2 could cover 1/3 of the total additional H_2 needed for hydrocracking (1.6 Mt to be divided over 76 refineries). At the same time the system could recover 60% of the NaOH needed to absorb the H_2S, by-product of hydrocracking, while removing all of the sulfur that would otherwise result in SO_2 and in addition recover daily more than 200 tonnes of S^0. Therefore, the application of our technology in oil refineries would not only allow for efficient H_2S treatment, but also for NaOH and H_2 recovery for reuse on-site, thereby reducing substantially the operational costs and the environmental burden. As the electrolytically produced H_2 will be redirected to the hydrocracking process, depending on the CO_2 point emissions produced in the oil refinery, a case for turning these emissions into acetic acid, or other commodity chemicals could be made, with application of additional electrolysis units.

Bringing the specific technology however at large scale for on-site treatment for such high flows will require optimization of the system. More cost-effective materials with longer lifetime should be employed to allow for cost minimization, in parallel with higher applied current densities. So far, the hydrodynamic behaviour of electrochemical cells as reactors for wastewater treatment has not been studied as extensively as for bioreactors. Modelling and simulation tools will be crucial in the effort of up-scaling, by allowing deep understanding of the hydrodynamic behaviour of the system, by making a uniform proposal on the effect of current density on the removal efficiency of different pollutants and by optimizing the mass and charge transfer (Arenas et al. 2020; Garcia-Rodriguez et al. 2020).

Increased mass transfer, by ensuring well mixed-conditions, with rotating cylinder electrodes or reactors along with solids efficient removal with embedded in the electrochemical reactor precipitation tanks, should be promoted for an increase in operational efficiency. Ultimately, ensuring higher quality product or, in good communication with the company, ensuring the product quality of interest will allow for product use on-site, which will eliminate transport costs and thus increase the total cost efficiency of the process.

7.7 Opportunities for further research

Integrated systems are of utmost importance in industrial waste treatment, urged by the complexity of the streams and the need for circularity. A single technology is not sufficient anymore neither to meet the governmental regulations for certain pollutants, nor to take full advantage of the recovery possibilities of every stream. In this thesis, two technologies aimed for integration were tested in a laboratory scale and one was simulated, however not linked to each other. An integrated system connecting a gas absorption column, an electrochemical cell and a gas fermenter should be the next step investigated. Connecting and balancing the flows and recoverable products of these three modules is expected to be challenging and the design and operation of it could be a task for an applied study, close to process engineering. The results of the proposed study will also demonstrate whether continuous connection of these three systems is realistic, or whether they will need to be operated separately, with intermediate storage of products and flows where and when needed.

To aid further optimization of the electrochemical treatment, the reaction mechanisms at the electrode/electrolyte interface and in the bulk electrolyte need to be studied. These may differ depending on the nature of the electrode material and the electrolyte and on operational conditions, such as the concentration of HS^-, the HS^- loading rate and the pH. Based on operational data obtained in this thesis, it is hypothesized that the HS^- oxidation reaction rate shifts, after initial deposition of S^0 particles on the electrode surface in the first operational stages. Yet, the exact mechanism of the S^0 deposition on the electrode surface and the interactions of the S^0 deposited film with the HS^- containing bulk electrolyte have not yet been studied. Understanding these interactions is of great importance as they will determine the final product of HS^- oxidation in a continuously operated electrochemical reactor, or the activity of the electrode over time (inactivation by S^0 deposition).

Regarding the fermentation part, known acetogenic genera such as *Acetobacterium* and *Moorella* have demonstrated here strong inhibition by sulfide. Future studies should focus on sulfide effects on individual bacterial strains to confirm the observations in this thesis, however in the expense of excluding any syntrophic or synergistic interactions that are common in mixed community reactor systems. This should be studied in particular when pure culture fermentation is of interest and gas pre-

treatment is desired to be minimized to reduce costs. In addition, *Eubacterium* as the known acetogen that demonstrated increased robustness to sulfide can be studied as a strain capable of cultivation as a pure culture that can tolerate higher sulfide levels. Metatranscriptomic and proteomic approaches can be employed to gain insight into the molecular mechanisms responsible for higher tolerance to H_2S. Furthermore, these techniques could shed light upon the differential expression of certain stress factors or mechanisms developed by bacteria to tolerate sulfide stress and help understanding differences in toleration levels, developed among different taxa.

Finally, the decreased acetate production rate and whether this would increase with ultimate adaptation of the community to higher levels of sulfide warrants further research. Special focus on operational parameters, such as HRT and pH to optimize acetate production under sulfide inhibition could also satisfy the need for higher production rates. As highlighted in Chapter 6, under sulfide stress the product spectrum was shifted towards higher butyrate and formate production. Further research could reveal whether this product shift is permanent and sulfide can be a driver for steering production towards more reduced products. what is the exact function in acetic and butyric acid and how could sulfide affect individually the highlighted members of the gas fermentation column.

APPENDIX 1

A1.1 Supplementary material for Chapter 2

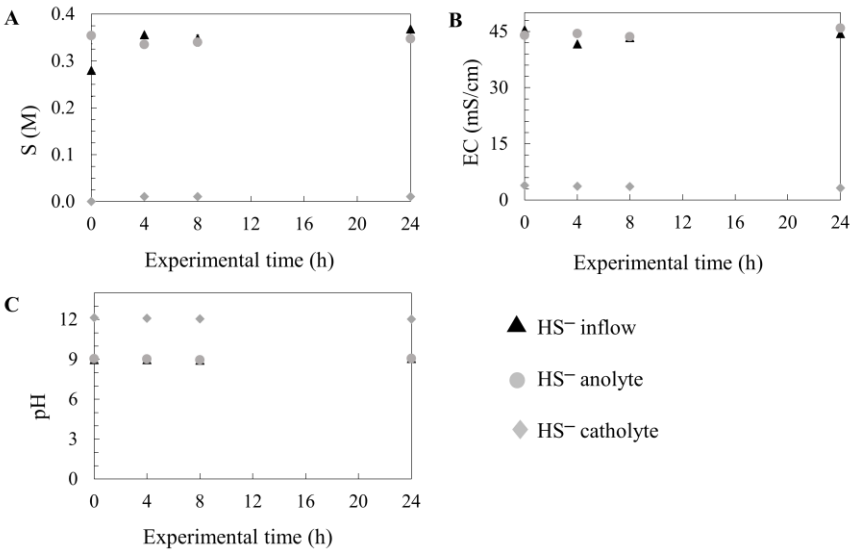

Figure A1.1 – Results of the open circuit potential (OCP) test performed prior to the experiments to test changes in: A) sulfur concentration, B) conductivity and C) pH. The OCP test was conducted for 24 h with no experimental replicates

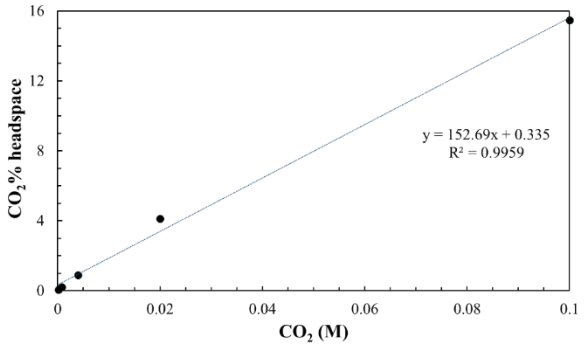

Figure A1.2 – Calibration curve for CO_2/HCO_3^- headspace analysis constructed with 0.16×10^{-3}, 0.8×10^{-3}, 4×10^{-3}, 20×10^{-3} and 100×10^{-3} M $NaHCO_3$ and NaHS standard solutions (n = 4 replicates)

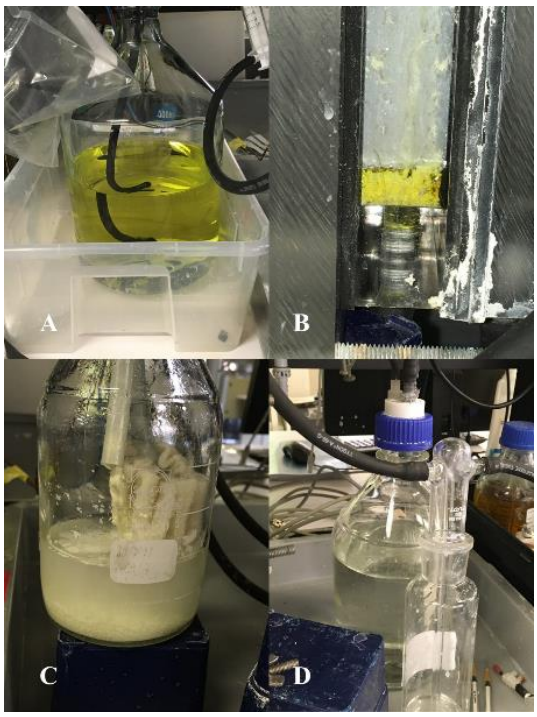

Figure A1.3 – Synthetic solution progression during the electrochemical treatment starting from: A) a 0.5 M H_2S + 0.16 M CO_2 yellow coloured solution, B) Elemental sulfur (S^0) production and precipitation in the bottom of the anodic compartment, C) precipitation in the cloth filter, and in the precipitation bottle between the anodic and cathodic compartments in and D) clear NaOH recovered solution, containing ~0.04 M H_2S + 0.03 M CO_2

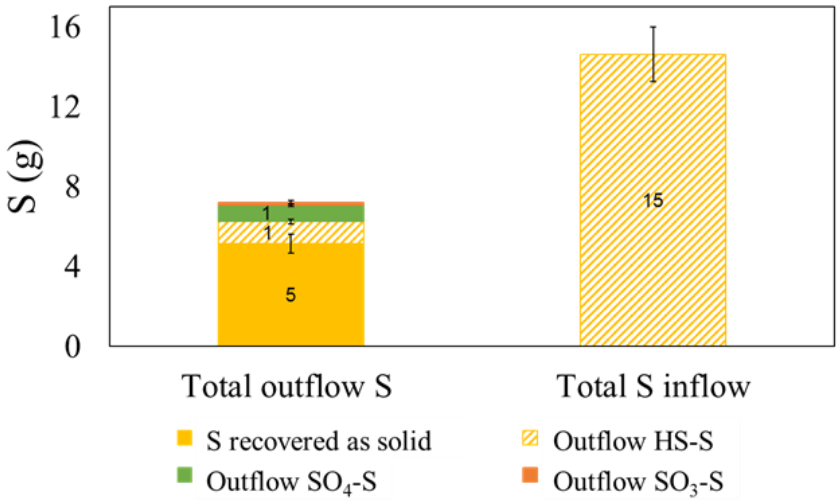

Figure A1.4 – Sulfur balance across the electrochemical cell over the 10 h of the experimental period (n = 3 experimental replicates). The outflowing HS-S, SO_4-S and SO_3-S concentrations were measured at sampling point 3 (catholyte outflow) and the solid S (S^0 particles) was recovered from the precipitation bottle as well as partially from the anodic compartment.

Table A1.1 – Uncompensated resistance between anode and reference electrode (Ru) and cell resistance (Rcell) obtained with the current interrupt (CI) method performed in synthetic SCS (0.5 M NaHS + 0.16 M $NaHCO_3$) (n = 3 experimental replicates)

Cell configuration	Ru (Ω)	Rcell (Ω)
Two compartment	0.33 ± 0.016	0.472 ± 0.056

APPENDIX 2

A2.1 Supplementary material for Chapter 3

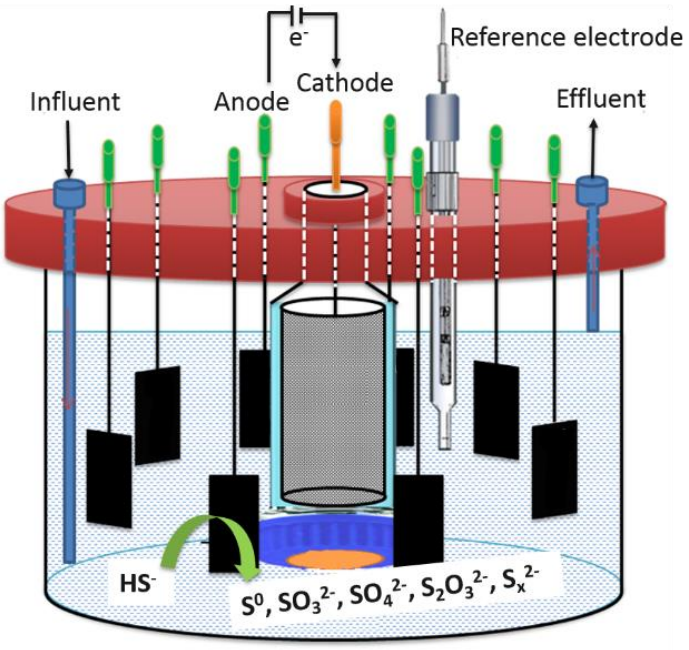

Figure A2.1 – Two compartment reactor setup for activity and stability tests. The reactor allows to simultaneously test multiple anodes in identical conditions with a common counter electrode and a common reference electrode. Sufficient mixing with a magnetic stirrer insures good homogeneity (Adapted from (K. Guo et al. 2014)).

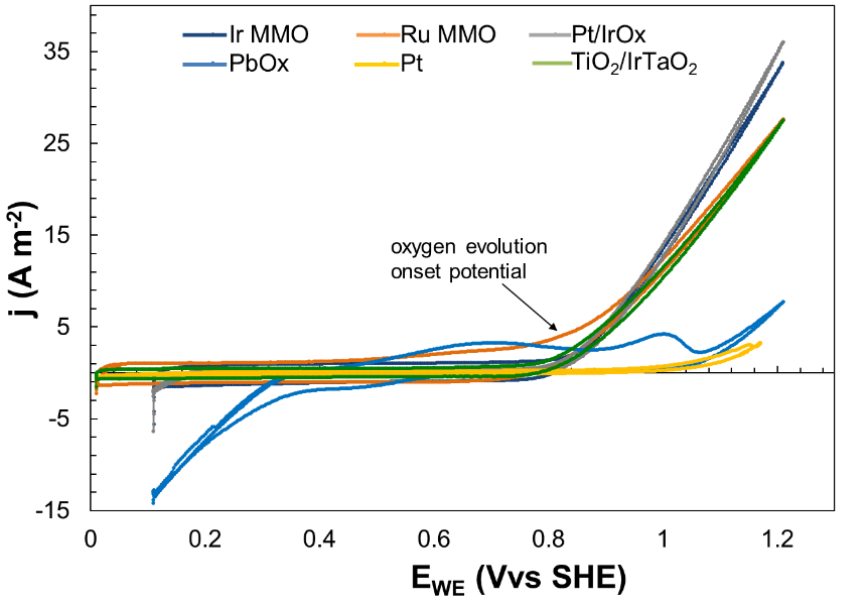

Figure A2.2 – Cyclic voltammograms of the different electrode materials in 50 mM NaOH, recorded at 5 mV s^{-1} between 0 and 1.2 V vs SHE. The C_{app} results are presented in Table A2.1.

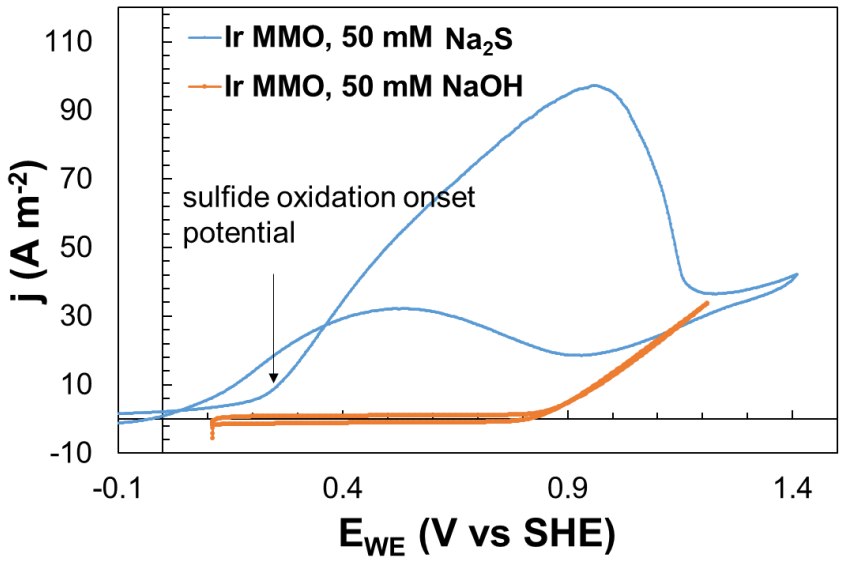

Figure A2.3 – Cyclic voltammograms of Ir MMO electrode with and without sulfide as electron donor recorded at 5 mV s^{-1} between 0.1 and 1.2 V vs SHE and between -0.1 and 1.4 V vs SHE, for 50 mM NaOH and 50 mM Na_2S electrolytes, respectively. On the figure the onset potential of sulfide oxidation is noted at 0.3 V vs SHE.

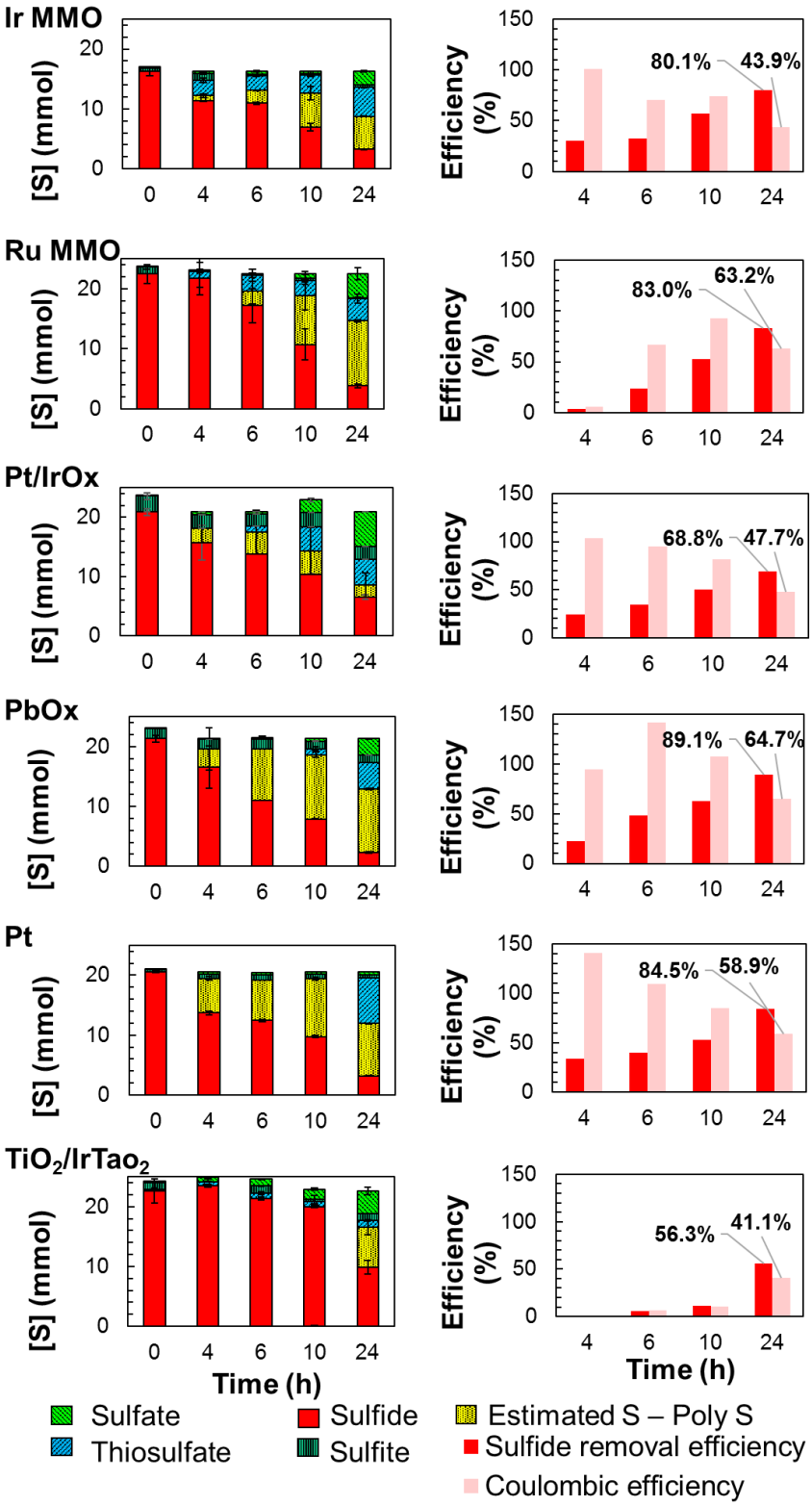

Figure A2.4 – Activity tests of 24 h for all electrode materials. Evolution over time of the: 1) Sulfur species speciation, 2) Sulfide removal efficiency (%) and coulombic efficiency (%). The electrode materials tested are stated by their name accordingly. Coulombic efficiencies higher than 100 % observed in some of the materials are here attributed to the formation of polysulfides (regarding the pH > 12 preserved in this study), occurring via chemical dissolution of S^0 in the sulfide containing alkaline solution (Behm and Simonsson 1997; Mao et al. 1991; Vaiopoulou et al. 2016).

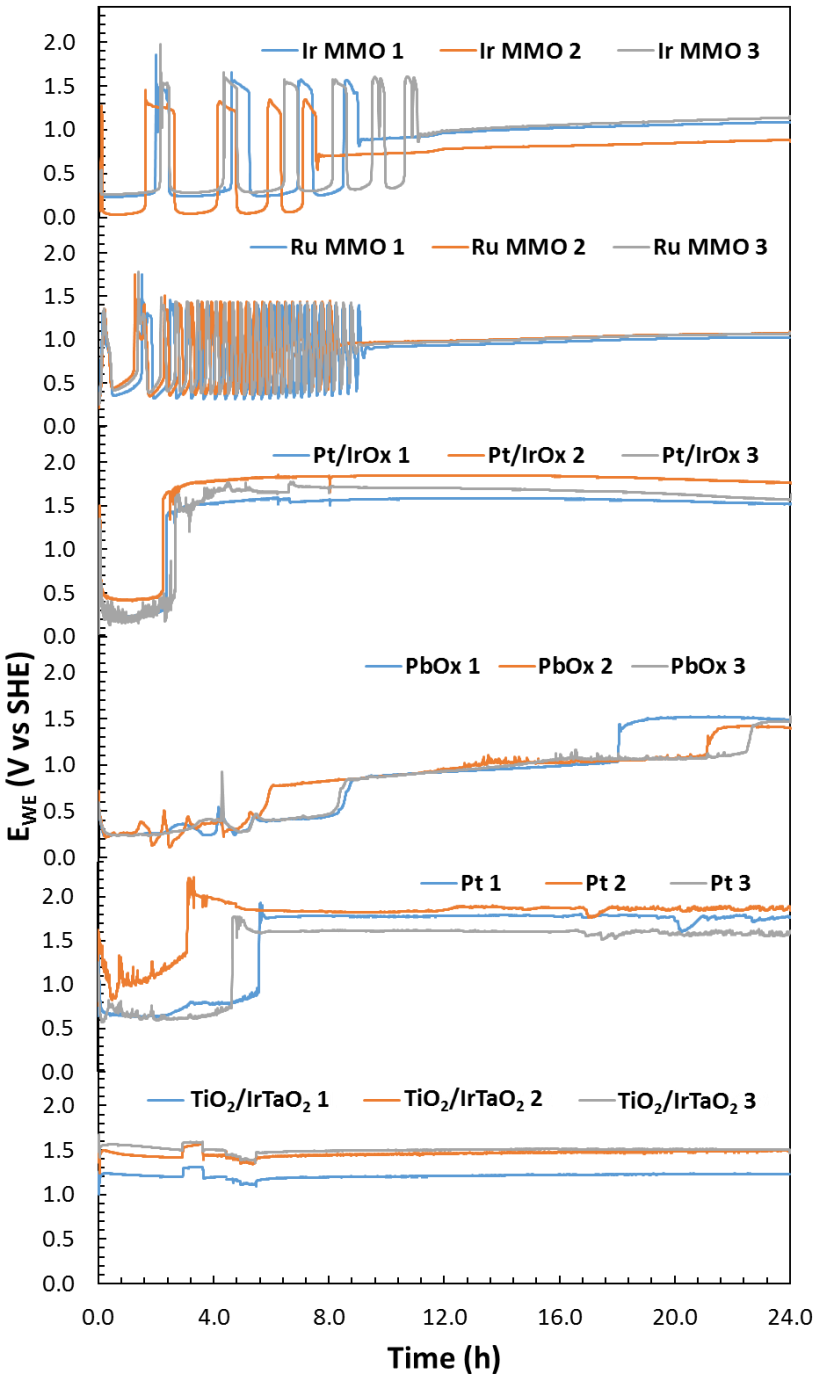

Figure A2.5 – Evolution of the anode potential in the electrode materials during the activity tests at a constant current density of j = 50 A m^{-2}. Triplicates of the chronopotentiograms of the activity tests for all the electrodes tested. The potentials are reported with uncompensated resistance correction.

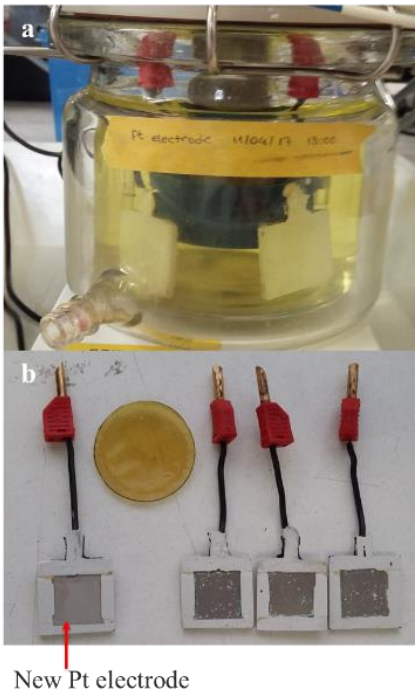

Figure A2.6 – Elemental sulfur (S^0) produced during the 24 h activity tests with Pt electrode contributed to the yellowish colour of the anolyte obtained during the experiment: a) Anolyte yellowish colour after production of S^0, b) Triplicates of used Pt electrodes in comparison with an unused Pt electrode. Particles of S^0 can be seen deposited on the electrode surface

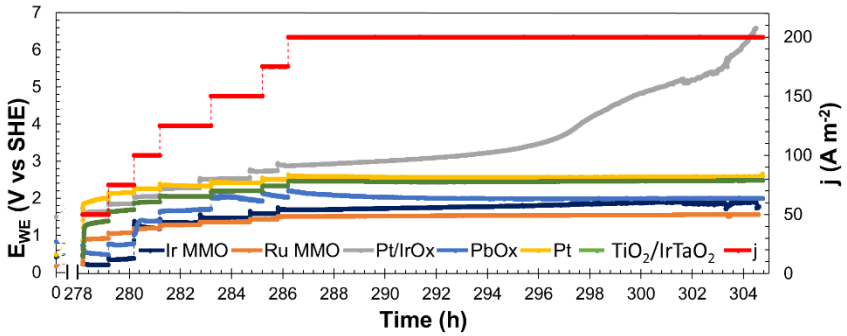

Figure A2.7 – Evolution of anode potential during incremental increase of current density, recorded at the end of the stability tests during the last 27 hours for the different electrode materials (Anolyte: 50 mM Na_2S, 50 mM NaOH)

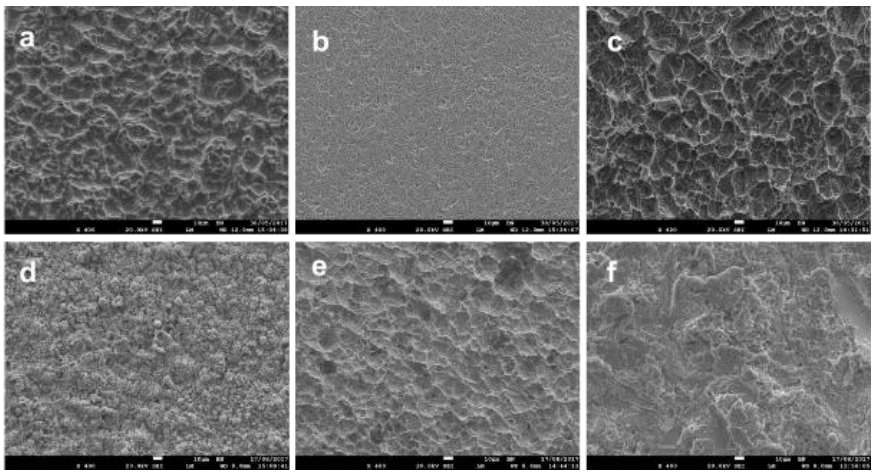

Figure A2.8 – SEM images after the stability tests of a) Ir MMO, b) Ru MMO, c) Pt/IrOx, d) PbOx, e) Pt and f) $TiO_2/IrTaO_2$. Magnification 400 X using 20 keV, before electrochemical sulfide oxidation. The white bars represent 10 µm.

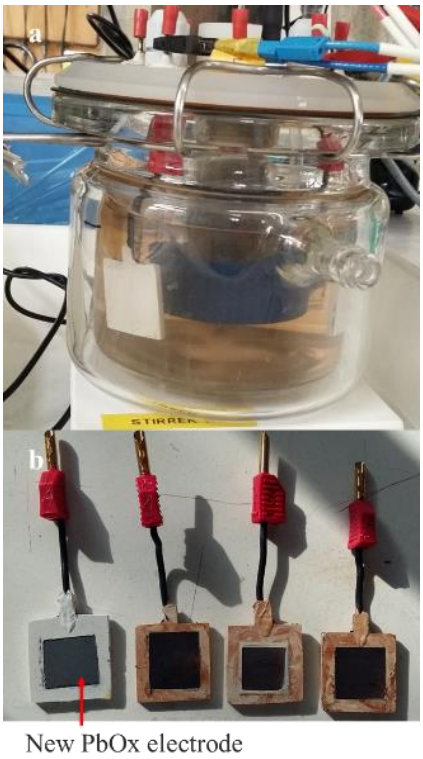

Figure A2.9 – Lead dissolution in the alkaline anolyte during the 24 h activity tests with PbOx as anode material: a) Anolyte obtained a brown - reddish colour after apparent dissolution of PbO_2, b) Triplicates of PbOx electrodes used, in comparison with an unused PbOx electrode. Reddish deposition on the epoxy glue is associated with PbO_2 dissolution.

Table A2.1 – Uncompensated resistance (R_u) measured for the three replicates electrodes during the activity tests

Electrode material	R_u 1 (Ohm)	R_u 2 (Ohm)	R_u 3 (Ohm)	Average +/− SD
Ir MMO	7.3	8.2	4.8	6.8 ± 1.4
Ru MMO	8.3	6.8	9.0	8.0 ± 0.9
Pt/IrOx	12.7	7.4	21.7	13.9 ± 5.9
PbOx	10.8	20.3	11.4	14.2 ± 4.3
Pt	9.6	12.3	16.1	12.7 ± 2.7
$TiO_2/IrTaO_2$	9.1	7.8	9.7	8.9 ± 0.8

Table A2.2 – Uncompensated resistance (R_u) measured before and after the stability tests

Electrode material	Initial R_u (Ohm)	Final R_u (Ohm)
Ir MMO	6.5	8.6
Ru MMO	6.4	6.0
Pt/IrOx	8.9	10.5
PbOx	9.4	8.8
Pt	9.1	7.8
$TiO_2/IrTaO_2$	9.0	7.8

Table A2.3 – Intrinsic properties comparison among electrodes. Apparent capacitance (C_{app}) calculated based on the equation A2.1.1.2 measured, from the cyclic voltammograms in Figure A2.3, oxygen evolution onset potential (OEP) and sulfide oxidation potential (SOP) for Ir MMO, Ru MMO, Pt/IrOx, Pt and $TiO_2/IrTaO_2$ electrodes. The C_{app} and OEP were determined at 50 mM NaOH electrolyte and the SOP at 50 mM Na_2S + 50 mM NaOH solution.

Electrode material	C_{app} (mF cm^{-2})	OEP (V vs SHE)	SOP (V vs. SHE)

Ir MMO	19.44	0.80	-0.01
Ru MMO	27.19	0.75	0.04
Pt/IrOx	7.63	0.77	-0.35
PbOx	N/A	1.06	0.51
Pt	3.06	1.01	0.58
$TiO_2/IrTaO_2$	7.63	0.75	-0.05

Table A2.4 – Activity performance of the electrode materials: the sulfide removal efficiency (RE_{HS^-} %); the coulombic efficiency (CE_{HS^-} %); the initial potential (E_i), final potential (E_f) and averaged potential recorded all along the experiment (E_{av}) of the anodes (V vs SHE). Values reported for the total experimental period of the activity tests. The potentials are reported without uncompensated resistance correction. All experiments were conducted in triplicate.

Electrode material	R_{HS^-} (mmol/h)	CE_{HS^-} (%)	E_i (V)	E_f (V)	E_{av} (V)
Ir MMO	0.5 ± 0.0	43.9 ± 0.2	0.38 ± 0.02	1.24 ± 0.01	1.01 ± 0.30
Ru MMO	0.8 ± 0.0	63.2 ± 0.5	0.57 ± 0.03	1.23 ± 0.03	1.08 ± 0.17
Pt/IrOx	0.6 ± 0.0	47.7 ± 1.3	0.62 ± 0.09	1.95 ± 0.10	1.54 ± 0.60
PbOx	0.8 ± 0.0	64.7 ± 0.3	0.53 ± 0.10	1.75 ± 0.05	1.14 ± 0.37
Pt	0.7 ± 0.0	58.9 ± 0.1	1.00 ± 0.11	2.00 ± 0.07	1.84 ± 0.32
$TiO_2/IrTaO_2$	0.5 ± 0.0	41.1 ± 4.2	1.68 ± 0.06	1.67 ± 0.02	1.66 ± 0.03

Table A2.5 – Anode potential values of the different electrode materials during the last step of stability tests (200 A m^{-2} applied for 14 hrs), initial (E_{WE}, i), final (E_{WE}, f) and average WE potential (E_{WE}, av) (V vs SHE)

Electrode material	E_{WE}, i	E_{WE}, f	E_{WE}, av
Ir MMO	1.73	1.80	1.82 ± 0.07
Ru MMO	1.54	1.59	1.56 ± 0.02

Pt/IrOx	2.93	6.60	3.89 ± 1.01
PbOx	2.22	2.03	2.04 ± 0.04
Pt	2.59	2.60	2.60 ± 0.01
$TiO_2/IrTaO_2$	2.49	2.51	2.48 ± 0.01

Table A2.6 – Compositional variations based on SEM-EDX surface analysis, before (initial) and after (final) the stability tests

Electrode material	Initial Catalyst Content (wt%)	Initial base metal content (wt%)	Final Catalyst Content (wt%)	Final base metal content (%)
Ir MMO	37.3 ± 0.7	1.4 ± 0.0	57.2 ± 0.1	2.9 ± 0.1
Ru MMO	23.7 ± 0.1	37.1 ± 0.2	19.7 ± 0.1	36.0 ± 0.7
Pt/IrOx	Pt: 29.8 ± 0.4, Ir: 9.5 ± 0.4	43.3 ± 0.8	Pt: 0.4 ± 0.1, Ir: 0.5 ± 0.1	77.4 ± 0.2
PbOx	79.1 ± 5.4	-	79.8 ± 0.8	-
Pt	73.3 ± 1.9	12.4 ± 0.2	67.1 ± 0.7	11.1 ± 0.4
$TiO_2/IrTaO_2$	Ti: 65.5 ± 0.3	-	Ti: 46.1 ± 1.4, Ir: 3.4 ± 0.3, Ta: 1.4 ± 0.3	-

A2.1.1 Calculations

- Resistance measurements

The uncompensated resistance between each WE and the reference was assessed by the current interrupt method. An electrical current *i* of 5 mA was imposed across the cell then switched off (i.e. open circuit) with a period of 10 ms 5 times successively. The evolution of the WE potential was recorded every 0.2 ms. The instantaneous change in potential (during the first interval of 0.2 ms after switching on or off the current) can be assumed to be the ohmic drop $i \times R$ since the other processes involved in the voltage amplitude (faradaic and diffusional) present much slower relaxation times. The uncompensated resistance is then obtained by the Ohm's law:

$$R = \frac{\Delta E}{i} \quad \text{(A2.1.1.1)},$$

where R is the uncompensated resistance between the WE and the reference electrode (Ω), ΔE is the instantaneous ohmic drop (V) and i the current drop (A).

- Capacitance measurements

$$j(t) = C_{app}\frac{dV}{dt} \quad \text{(A2.1.1.2)},$$

where j is the (pseudo)capacitive current density (A m^{-2}), C_{app} is the apparent, geometric capacitance of the material with respect to the projected surface area (F m^{-2}), dV/dt is the scan rate of the cyclic voltammetry (V s^{-1}). The capacitance is here called "apparent" since: (i) the value strongly depends on the specific surface area of the electrode and (ii) pseudocapacitive phenomena can also arise in the catalyst layer, i.e. an oxidation/reduction cycle of some catalyst element (faradaic process).

- Reported electrode potential

$$E_{WE} = E_{app} - \Delta E \quad \text{(A2.1.1.3)},$$

where E_{WE} (V) is the reported electrode potential, E_{app} (V) is the apparent electrode potential measured by the potentiostat and ΔE is the instantaneous ohmic drop (V).

APPENDIX 3

A3.1 Supplementary material for Chapter 4

A3.1.1 Materials and Methods

Table A3.1 – Uncompensated resistance between anode and reference electrode (Ru) and cell resistance (Rcell) obtained with the current interrupt (CI) method performed in synthetic SCS

Cell configuration	Ru (Ω)	Rcell (Ω)
Two compartment	0.02	0.25

Table A3.2 – Sulfide oxidation reactions putatively taking place in a galvanostatically controlled cell depending on the obtained anode potential, based on Bouroushian (Bouroushian 2010)

Electrochemical reactions	E^0 (V vs SHE)
$HS^- \leftrightarrow S^0 + H^+ + 2e^-$	-0.065
$nHS^- \leftrightarrow S_n^{2-} + nH^+ + 2e^-$	-0.053 to +0.298
$2HS^- + 3H_2O \rightarrow S_2O_3^{2-} + 8H^+ + 8e^-$	+0.200
$HS^- + 4H_2O \rightarrow SO_4^{2-} + 9H^+ + 8e^-$	+0.252

A3.1.2 Introduction to the three compartment cell

The three compartment cell was constructed as described in Chapter 2 by creating a middle compartment between the anodic and the cathodic compartment (Fig. A3.1b). An anion exchange membrane (AEM) (fumasep® FAB PK-130, Fumatech GmbH, Germany) separates the anodic and middle compartment and a cation exchange membrane (CEM) (Fumasep© FKL-PK-130, Fumatech GmbH, Germany) separates the cathodic from the middle compartment, allowing internal volume of 200 mL for each compartment. An iridium mixed metal oxide (Ir MMO) titanium-based (Ti) electrode (Magneto special anodes B.V., The Netherlands) was used as anode. As cathode, a stainless steel thin

mesh (Solana, Belgium) was used. All electrodes had a projected surface area of 20 x 5 cm. The three compartment cell was operated with real SCS in batch for 8 h, in increasing current densities of 100, 200 and 300 A m^{-2}. The influent was inserted in the middle compartment with 1.67 L d^{-1} flow rate, the same as in the anodic flow rate of the two-compartment cell. As anolyte and catholyte initially a 4 wt.% NaOH solution was used to ensure sufficient initial conductivity and avoided putative non-electrically driven diffusion of sodium across the CEM (Vaiopoulou et al. 2016).

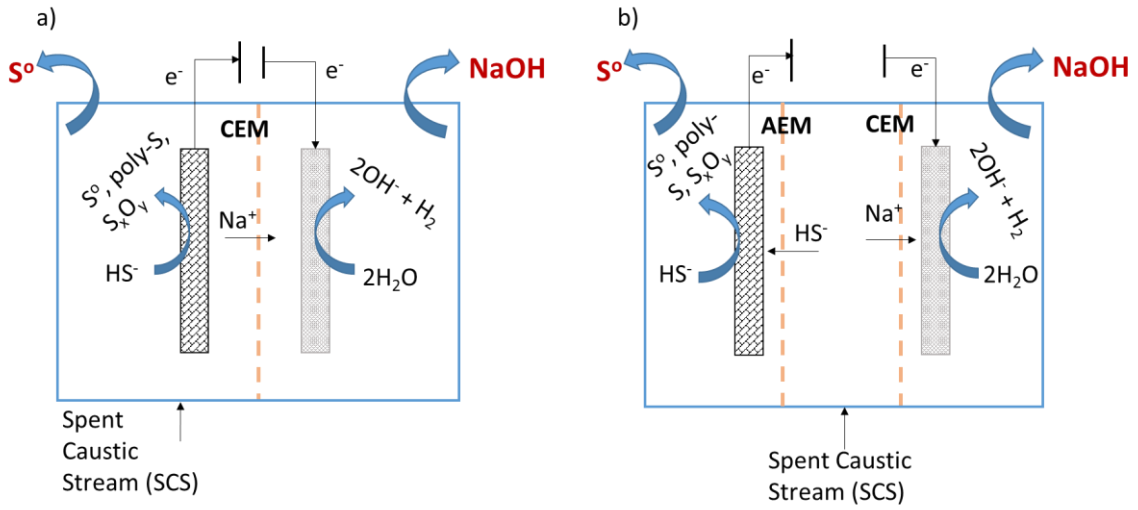

Figure A3.1 – Schematic representation of a) the two compartment electrolysis cell separated by a cation exchange membrane (CEM) and b) the three compartment cell, where an anion exchange membrane (AEM) separates the anodic and middle compartment and a CEM separates the cathodic from the middle compartment

A3.1.3 Results and Discussion

Table A3.3 - Process cost estimation, based on an electrochemical unit treating 40 m^3 of SCS per day

Operational conditions		References
Average cell voltage (V)	1.75	
SCS flow rate (m^3 d^{-1})	40	0.5 – 15 gallon per minute (gpm) are the typical NaOH flow rates in refineries (European Comission 2000; Barthe et al. 2015).

Hydraulic residence time (h)	2.87	Selected based on experimental setup, taking into account the flow rate (1.67 L d^{-1}) and the volume of each electrode compartment (0.2 L).
H_2O_2 market price (€ ton^{-1})	500	The market price of H_2O_2 was selected for 90% (Ciriminna et al. 2016).
NaOH market price (€ ton^{-1})	450	The market price of NaOH was selected based on the average market prices between January 2016 and 2019 (Echemi 2019b; Jonathan Chou 2018).
Electricity cost (€ kWh^{-1})	0.11	Industrial electricity charge input cost for small industries (500 – 2,000 MWh annual electricity consumption) in Belgium (2017) (statista 2020).

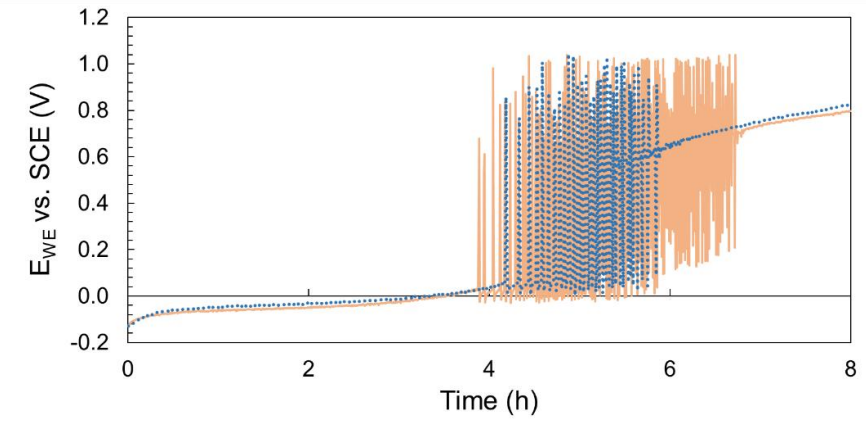

Figure A3.2 – Anode potential oscillations of Ir MMO anode, during the batch tests with synthetic SCS at 300 A m^{-2} (n=2) The different colours represent the two replicates.

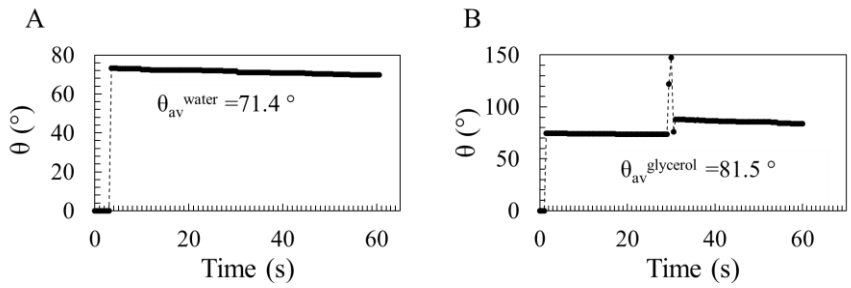

Figure A3.3 – Contact angle (ϑ in °) measurement results for the S^0 produced particles with A) water and B) glycerol

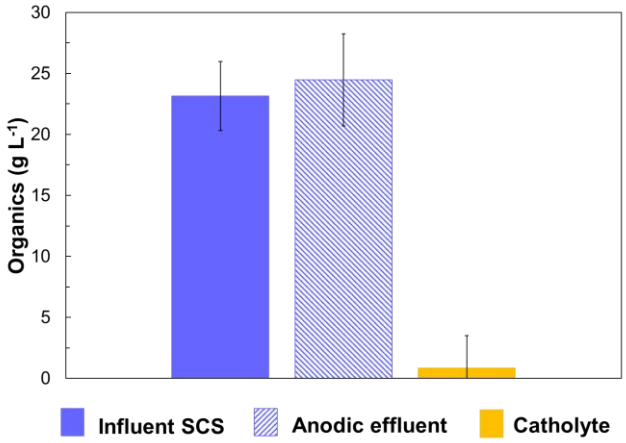

Figure A3.4 – Organics (ethanol) concentrations (g L^{-1}) in the SCS influent, anodic effluent and cathodic batch, during the 20 days of continuous operation at 300 A m^{-2} applied current density

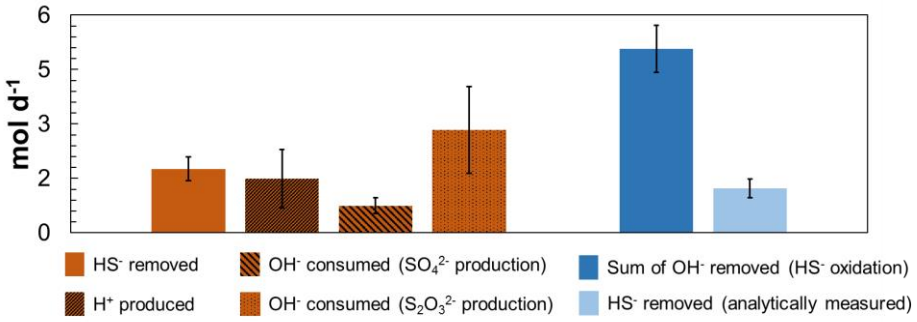

Figure A3.5 – Averaged mole balance of OH^- and H^+ formed during the continuous tests with industrial SCS in the anodic chamber with Ir MMO electrode, based on the reactions given in Bouroushian (Bouroushian 2010) *given in Table A3.2*

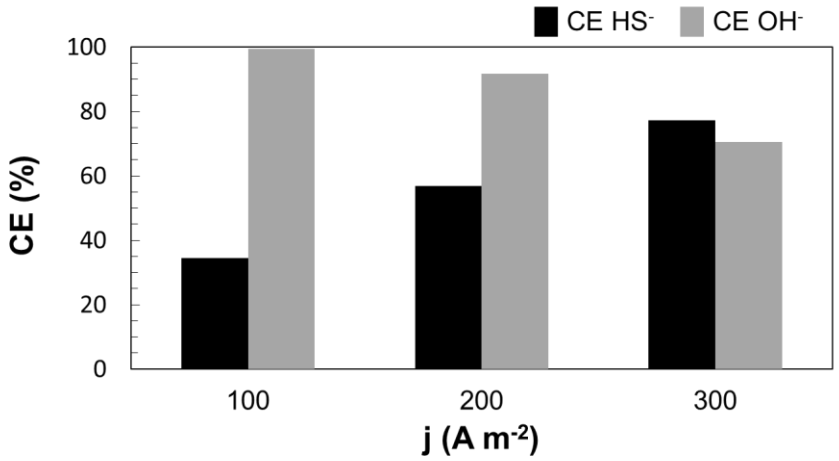

Figure A3.6 – Coulombic efficiency (CE, %) versus the current density (j, A m^{-2}), obtained from preliminary batch tests with a 3-compartment cell and an Ir MMO electrode (Fig. A3.1b), with synthetic SCS. The CE_{HS^-}% was calculated based on the removal of HS^- from the middle compartment and the CE_{OH}% based on the NaOH recovery in the cathodic compartment.

APPENDIX 4

A4.1 Supplementary material for Chapter 5

A4.1.1 Materials and methods

16S rRNA Gene amplicon sequencing. In brief, DNA extraction was performed by means of bead beating with a PowerLyzer instrument (Qiagen, Venlo, Netherlands) and phenol/chloroform extraction. The 16S rRNA gene V3-V4 hypervariable regions were amplified by PCR using primers 341F (5'-CCT ACG GGN GGC WGC AG -3') and 785Rmod (5'-GAC TAC HVG GGT ATC TAA KCC-3'). The reverse primer was adapted from Klindworth et al. (Klindworth et al. 2013), to increase coverage. PCR was performed using Taq DNA Polymerase with the Fermentas PCR Kit according to the manufacturers' specifications (ThermoFisher Scientific, Waltham, MA, USA). The obtained PCR product was ran on a 2% agarose gel for 30 minutes at 100V. 10μl of the original genomic DNA extract was send out to LGC Genomics GmbH (Berlin, Germany) for library preparation and sequencing on an Illumina Miseq platform with v3 chemistry with the primers mentioned above. Read assembly and cleanup was largely derived from the MiSeq SOP described by the Schloss lab (Kozich et al. 2013; Schloss et al. 2011). In brief, mothur (v.1.39.5) was used to assemble reads into contigs, perform alignment-based quality filtering (alignment to the mothur-reconstructed SILVA SEED alignment, v. 123), remove chimeras, assign taxonomy using a naïve Bayesian classifier (Q. Wang et al. 2007) and and SILVA NR v128 and cluster contigs into OTUs at 97% sequence similarity. All sequences that were classified as Eukaryota, Archaea, Chloroplasts and Mitochondria were removed. Also, if sequences could not be classified at all (even at (super)Kingdom level) they were removed. For each OTU representative sequences were picked as the most abundant sequence within that OTU.

Clone library. PCR was performed using a recombinant Taq DNA Polymerase kit, Fermentas (Thermo Fischer Scientific, Waltham, MA, USA), in 25μl reactions containing: 2.5 μl 10x Taq buffer (+KCl – $MgCl_2$), 0.5 μl of 10mM dNTP, 2 μl of 25 mM $MgCl_2$, 2.5 μl of 10μM Primer 27f AGAGTTTGATCMTGGCTCAG, 2.5 μl of 10μM Primer 1492r TACGGYTACCTTGTTACGACTT, 0.125 μl of 5 U/μL Taq polymerase, 0.065 μl of 20mg/mL BSA (Roche Holding AG, Basel, Switzerland), 14.81 μl PCR-water and 1 μl Sample. Amplification was ran including initial denaturation for 7 min at 95°C, followed by 32 cycles of 1 min denaturation at 95°C, 1 min anneal at 55°C and 2 min extension at 72°C. A final elongation step was included at 72°C for 10 min. The product was ran for 30 min at 100V on a 2% agarose gel and was visualized using a UV transilluminator. The fragment was purified using the innuPREP PCRpure Kit (Analytik Jena, Jena, Germany) and the concentration was measured with a DS-11 Microvolume Spectrophotometer (DeNovix, Wilmington, DE, USA). The purified fragment was cloned into a pCR™2.1-TOPO® vector and subsequently introduced into One

Shot® DH5α™-TOP10 cells using the TOPO® TA Cloning® kit (Thermo Fisher Scientific, Waltham, MA, USA). Following blue-white screening, 16 white colonies were picked and used in colony-PCR using the above mentioned protocol and primers M13F GTAAAACGACGGCCAG and M13R CAGGAAACAGCTATGAC. The PCR was checked on a 2% agarose gel, the 16 positive products were purified with the innuPREP PCRpure Kit and their concentrations measured with a DS-11 Microvolume Spectrophotometer (DeNovix, Wilmington, DE, USA). Subsequently, 4 μl from a 5 μM stock of one of the M13 primers was added to 10 μl of 40 ng/μl of PCR product, for both forward and reverse sequencing reactions. The reactions were send out to LGC Genomics (LGC Genomics GmbH, Berlin, Germany). The resulting sequences were blasted using NCBI's BLAST (https://blast.ncbi.nlm.nih.gov/Blast.cgi).

Calculations

The [H_2Saq] concentrations were calculated using measured pressure and CGC (Compact Gas Chromatograph) mol % H_2S, according to the following equation:

$$[H_2S_{aq}] = K_{H2S} * P_{H2S} = K_{H2S} * P_{tot} * mol\%H_2S \quad \text{(A4.1.1.1)}$$

, where $K_{H2S} = 10^{-3}$ mol m^{-3} Pa^{-1} (Sander 2015)

$$pKa_{H2S/\,HS-} = log\frac{[H_2S_{aq}]}{[HS^-]\times[H^+]} \quad \text{(A4.1.1.2)}$$

Table A4.1 – Initial conditions in flask experiments. Three pH values (7, 6 and 5) were tested with 8 initial sulfide concentrations in triplicate. Initial (t=0) total dissolved sulfide concentration ([TDS], mM), measured pH values, H_2S_{aq} concentration ([H_2S_{aq}], mM), acetate concentration ([Ac^-], mM) and cell density ([Cells], Cells mL^{-1}) after inoculation are presented.

Run	Set	[TDS] (mM)	pH	[H_2S_{aq}] (mM)	[Ac^-] (mM)	[Cells] (10^7 Cells) mL^{-1})
	Average	n.a.	6.81 ± 0.12	n.a.	3.32 ± 0.23	7.36 ± 0.89
pH 7	1	0.06 ±	6.80 ± 0.09	0.04 ± 0.01	3.48 ± 0.11	7.63 ± 0.56
	2	0.18 ±	6.74 ± 0.05	0.12 ± 0.02	3.41 ± 0.29	7.35 ± 0.95
	3	0.31 ±	6.73 ± 0.04	0.20 ± 0.03	3.39 ± 0.09	7.05 ± 1.04
	4	0.58 ±	6.78 ± 0.07	0.37 ± 0.04	3.27 ± 0.36	7.53 ± 0.96
	5	0.93 ±	6.67 ± 0.08	0.63 ± 0.01	3.30 ± 0.23	6.94 ± 1.32

	6	1.56 ±	6.89 ± 0.06	0.79 ± 0.06	3.35 ± 0.09	8.05 ± 0.05
	7	1.73 ±	6.86 ± 0.09	0.96 ± 0.05	3.15 ± 0.15	7.27 ± 0.65
	8	3.79 ±	6.99 ± 0.06	1.96 ± 0.09	3.21 ± 0.17	7.05 ± 0.25
	Average	n.a.	6.06 ± 0.16	n.a.	1.77 ± 0.25	6.13 ± 0.79
pH 6	1	0.06 ± 0.01	5.91 ± 0.04	0.06 ± 0.01	2.04 ± 0.42	6.07 ± 0.77
	2	0.13 ± 0.03	5.94 ± 0.01	0.12 ± 0.03	1.85 ± 0.13	5.72 ± 0.68
	3	0.27 ± 0.05	5.95 ± 0.00	0.24 ± 0.05	1.90 ± 0.01	6.46 ± 0.71
	4	0.51 ± 0.07	6.02 ± 0.04	0.46 ± 0.06	1.73 ± 0.12	5.60 ± 0.90
	5	0.85 ± 0.04	6.05 ± 0.04	0.76 ± 0.04	1.70 ± 0.18	6.20 ± 0.52
	6	0.99 ± 0.12	6.09 ± 0.02	0.88 ± 0.11	1.63 ± 0.27	5.81 ± 0.45
	7	1.18 ± 0.10	6.15 ± 0.04	1.04 ± 0.10	1.69 ± 0.18	6.38 ± 0.76
	8	3.00 ± 0.21	6.41 ± 0.04	2.37 ± 0.21	1.64 ± 0.16	6.83 ± 0.58
	Average	n.a.	5.58 ± 0.28	n.a.	1.35 ± 0.10	6.13 ± 0.49
pH 5	1	0.04 ± 0.00	5.23 ± 0.03	0.04 ± 0.00	1.43 ± 0.07	6.22 ± 0.32
	2	0.20 ± 0.02	5.29 ± 0.02	0.20 ± 0.02	1.46 ± 0.04	6.48 ± 0.19
	3	0.30 ± 0.02	5.39 ± 0.01	0.29 ± 0.02	1.43 ± 0.03	6.64 ± 0.37
	4	0.63 ± 0.03	5.52 ± 0.03	0.61 ± 0.03	1.37 ± 0.05	5.97 ± 0.17
	5	0.78 ± 0.02	5.58 ± 0.02	0.75 ± 0.02	1.37 ± 0.05	6.10 ± 0.37
	6	1.24 ± 0.14	5.72 ± 0.03	1.18 ± 0.13	1.35 ± 0.05	5.77 ± 0.41
	7	1.45 ± 0.06	5.80 ± 0.03	1.37 ± 0.06	1.26 ± 0.05	6.23 ± 0.32
	8	3.19 ± 0.07	6.13 ± 0.05	2.81 ± 0.06	1.17 ± 0.06	5.60 ± 0.63

Table A4.2 – Composition of modified homoacetogenic medium adapted from Patil et al. (2015) (Patil et al. 2015)

K_2HPO_4	0.2 g L^{-1}
NH_4Cl	0.25 g L^{-1}
KCl	0.5 g L^{-1}
$CaCl_2.2H_2O$	0.15 g L^{-1}
$MgCl_2.6H_2O$	0.6 g L^{-1}
NaCl	1.2 g L^{-1}
Tryptone	0.2 g L^{-1}

Yeast extract	0.5 g L^{-1}

Addition in 1 L of medium

Trace metal solution*	1 mL
Vitamin solution**	2.5 mL
Tungstate-selenium solution***	0.1 mL

***Composition of trace metal solution (g L^{-1})**

Nitrilotriacetic acid (dissolve with KOH; pH 6.5)	1.5
$Mg_2Cl_2.6H_2O$	3.0
$MnCl_2.2H_2O$	0.5
NaCl	1
$FeCl_2$	0.1
$CoCl_2$	0.1
$CaCl_2.2H_2O$	0.1
$ZnCl_2$	0.1
$CuCl_2$	0.01
$AlCl_3.6H_2O$	0.01
H_3BO_3	0.01
$Na_2MoO_4.2H_2O$	0.01

****Composition of vitamin solution (mg L^{-1})**

Sodium ascorbate	10
Biotin	4
Folic acid	4
Pyridoxine hydrochoride	20

Thiamine hydrocloride	10
Riboflavin	10
Nicotinic acid	10
DL-calcium pantothenate	10
Vitamin B12	0.2
p-aminobenzoic acid	10
Lipoic(thioctic) acid	10
Myo-inositol	10
Choline chloride	10
Niacinamide	10
Pyridoxal hydrochloride	10

***Composition of tunstate- selenium solution

0.1mM Na_2WO_4 + 0.1mM Na_2SeO_3 in 20mM NaOH

Table A4.3 – Metal availability with increasing sulfide concentrations at the end of the experimental cycle (t = 240 h) conducted at pH 7, analysed with ICP-MS, as previously described (Folens et al. 2018)

samples	[TDS] (mM)	Fe ($\mu g\ L^{-1}$)	Mn ($\mu g\ L^{-1}$)	Mg ($mg\ L^{-1}$)
inoculated	0.06	634	168	74.7
inoculated	1.26	254	159	69.6
inoculated	3.33	241	157	64.8
control	0.06	854	209	80.3
control	1.26	424	208	78.1
control	3.33	384	187	72.3

Table A4.4 – Sulfide fractionation based on acid-base equilibria for a pH = 4.5 – 7.5, derived by Visual MINTEQ

pH	HS^- %	H_2S (aq) %
4.5	0.335	99.665
4.6	0.422	99.578
4.7	0.532	99.468
4.8	0.670	99.330
4.9	0.844	99.156
5.0	1.064	98.936
5.1	1.341	98.659
5.2	1.690	98.310
5.3	2.128	97.872
5.4	2.364	97.636
5.5	2.960	97.040
5.6	3.703	96.297
5.7	4.623	95.377
5.8	5.758	94.242
5.9	7.153	92.847
6.0	8.856	91.144
6.1	10.917	89.083
6.2	13.389	86.611
6.3	16.320	83.680
6.4	19.748	80.252
6.5	23.695	76.305
6.6	28.155	71.845
6.7	33.092	66.908

6.8	38.430	61.570
6.9	44.062	55.938
7.0	49.848	50.152
7.1	55.634	44.366
7.2	61.268	38.732
7.3	66.611	33.389
7.4	71.555	28.445
7.5	76.027	23.973

A4.1.2 Results

Table A4.5 – Maximum values obtained during the batch experiments, for the 3 different runs (pH 7, 6 and 5). Total acetate production rate (r_{Ac}, mM h^{-1}), maximum acetate production rate (r_{Ac}^{max}, mM h^{-1}), maximum delta optical density measured at 600 nm (δOD_{600}^{max}) and cell density ([Cells], Cells mL^{-1}), measured at the end of each batch experiment (t=240h) are presented.

Run	Set	r_{Ac} (mM h^{-1})	r_{Ac}^{max} (mM h^{-1})	δOD_{600}^{max} (-)	[Cells] (10^7 Cells mL^{-1})	pH
	Average	n.a.	n.a.	n.a.	n.a.	6.56 ± 0.34
pH 7	1	0.12 ± 0.03	0.21 ± 0.08	0.71 ± 0.14	95.2 ± 6.77	6.03 ± 0.45
	2	0.11 ± 0.01	0.15 ± 0.07	0.57 ± 0.02	91.7 ± 24.5	6.31 ± 0.17
	3	0.07 ± 0.01	0.09 ± 0.04	0.57 ± 0.11	95.1 ± 11.7	6.56 ± 0.05
	4	0.09 ± 0.01	0.10 ± 0.00	0.42 ± 0.05	65.4 ± 9.96	6.49 ± 0.03
	5	0.09 ± 0.01	0.11 ± 0.01	0.33 ± 0.04	48.1 ± 4.67	6.47 ± 0.10
	6	0.04 ± 0.01	0.05 ± 0.02	0.24 ± 0.02	51.9 ± 3.28	6.80 ± 0.10
	7	0.03 ± 0.02	0.04 ± 0.03	0.20 ± 0.07	44.2 ± 1.79	6.83 ± 0.05
	8	0.01 ± 0.01	0.01 ± 0.02	0.15 ± 0.08	21.6 ± 3.62	6.99 ± 0.03
	Average	n.a.	n.a.	n.a.	n.a.	5.47 ± 0.38
pH 6	1	0.09 ± 0.02	0.20 ± 0.02	0.74 ± 0.12	72. ± 8.53	5.09 ± 0.11
	2	0.12 ± 0.00	0.24 ± 0.03	0.89 ± 0.06	87.4 ± 11.9	4.99 ± 0.03
	3	0.10 ± 0.00	0.19 ± 0.02	0.78 ± 0.10	84.5 ± 16.0	5.21 ± 0.03

	4	0.09 ± 0.01	0.16 ± 0.04	0.67 ± 0.09	88.9 ± 22.2	5.44 ± 0.07
	5	0.08 ± 0.00	0.14 ± 0.01	0.51 ± 0.05	90.9 ± 0.00	5.55 ± 0.03
	6	0.09 ± 0.01	0.16 ± 0.07	0.49 ± 0.12	62.9 ± 14.5	5.53 ± 0.10
	7	0.07 ± 0.02	0.14 ± 0.03	0.54 ± 0.15	56.1 ± 10.6	5.71 ± 0.10
	8	0.02 ± 0.00	0.02 ± 0.01	0.08 ± 0.01	21.6 ± 2.03	6.27 ± 0.01
	Average	n.a.	n.a.	n.a.	n.a.	5.21 ± 0.45
pH 5	1	0.04 ± 0.00	0.12 ± 0.02	0.71 ± 0.10	100 ± 29.5	4.80 ± 0.07
	2	0.05 ± 0.00	0.10 ± 0.02	0.71 ± 0.12	92.6 ± 22.8	4.79 ± 0.04
	3	0.05 ± 0.00	0.10 ± 0.01	0.75 ± 0.10	94.5 ± 11.5	4.84 ± 0.04
	4	0.06 ± 0.00	0.11 ± 0.01	0.66 ± 0.04	96.1 ± 19.2	4.96 ± 0.01
	5	0.05 ± 0.01	0.09 ± 0.03	0.48 ± 0.04	76.0 ± 23.0	5.13 ± 0.15
	6	0.04 ± 0.00	0.09 ± 0.01	0.33 ± 0.04	72.5 ± 6.85	5.44 ± 0.03
	7	0.03 ± 0.00	0.05 ± 0.01	0.22 ± 0.08	39.4 ± 22.6	5.67 ± 0.04
	8	0.01 ± 0.00	0.03 ± 0.02	0.09 ± 0.02	12.9 ± 0.54	6.09 ± 0.01

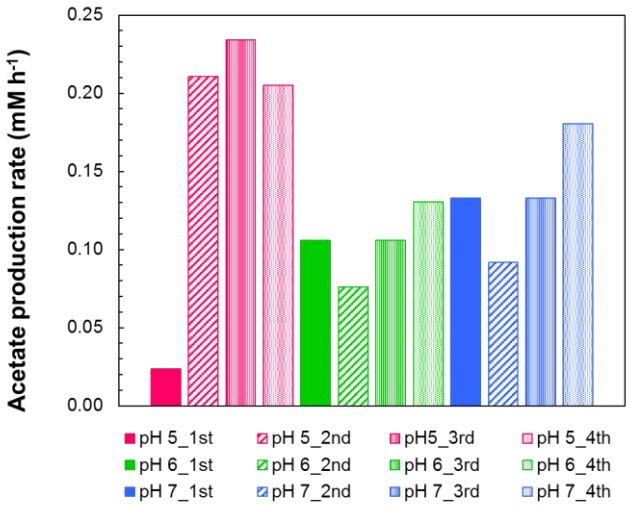

Figure A4.1 – Initial inoculation at different pH values. Every inoculation lasted for ~7 days and on the figure, 4 consecutive transfers are displayed.

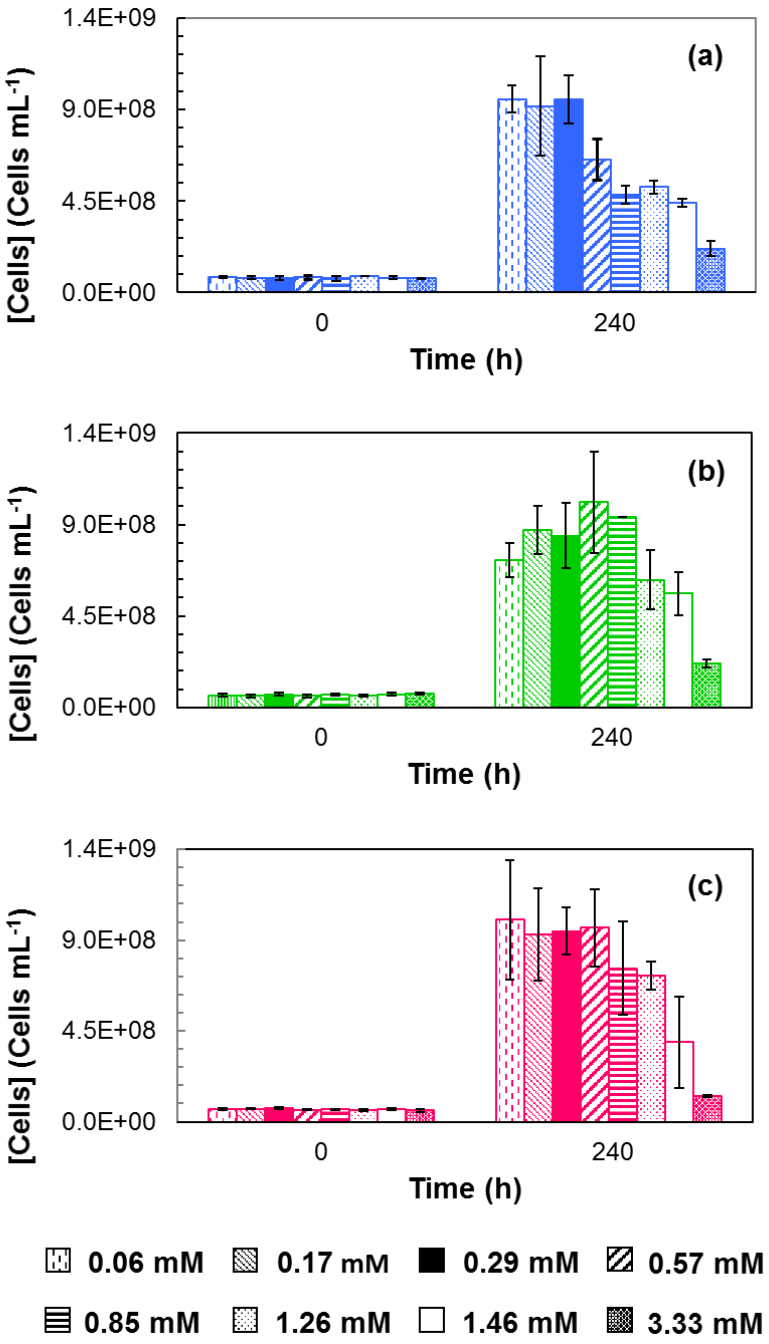

Figure A4.2 – Total cell counts for the different incubation experiments obtained with flow cytometry (FCM) at t=0 h and t=240 h. In the plot the average TDS concentrations of the different incubations are presented, at pH 7 (●), 6 (●) and 5 (●), respectively. Data are averages of 3 incubations, error bars represent standard deviations of biological triplicates.

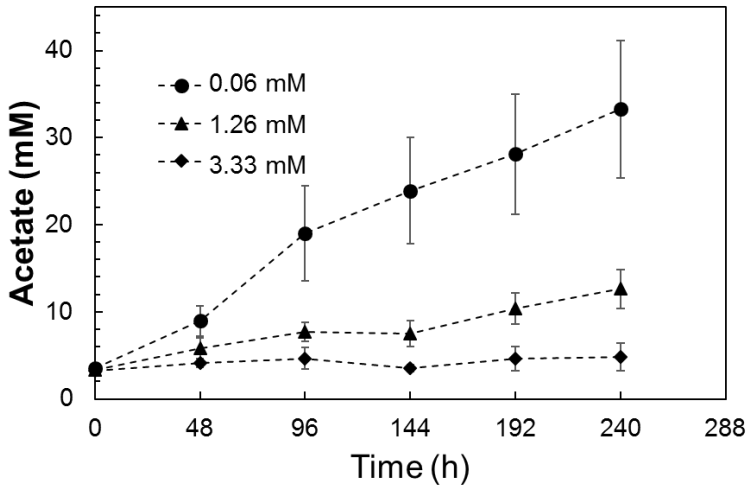

Figure A4.3 – Time course graph for acetate production (mM) at pH 5 and 0.06, 1.26 and 3.33 mM TDS. Example representative of all incubations at different pH levels and TDS concentrations. Data are averages of 3 incubations, error bars represent standard deviations of biological triplicates.

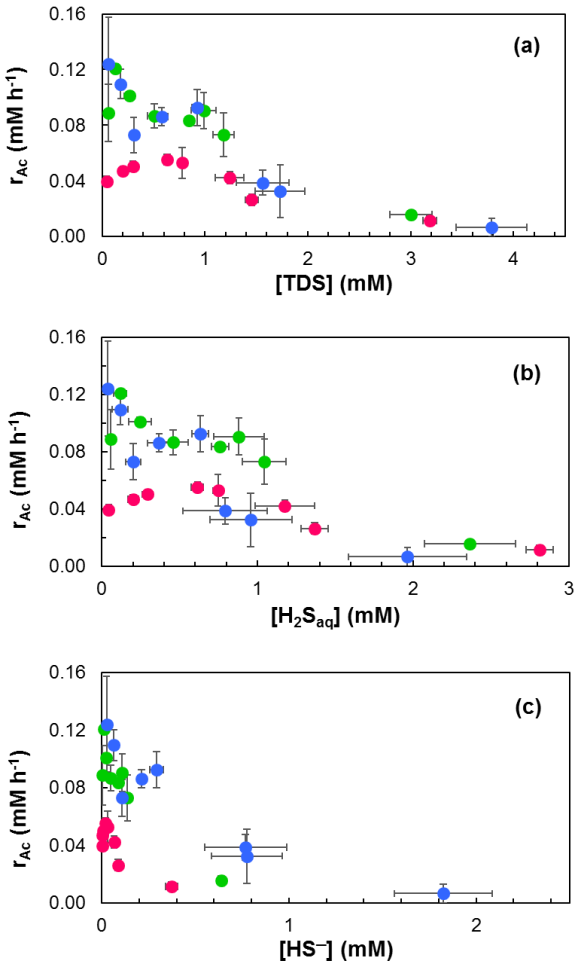

Figure A4.4 – Total acetate production rate (r_{Ac}) (mM h^{-1}) as a function of: (a) initial total dissolved sulfide concentration ([TDS]) (mM), (b) initial hydrogen sulfide dissolved ([H_2S_{aq}]) (mM) and (c) initial

bisulfide concentration ([HS⁻]) (mM) at pH 7 (●), 6 (●) and 5 (●). Data are averages of 3 incubations, error bars represent standard deviations of biological triplicates.

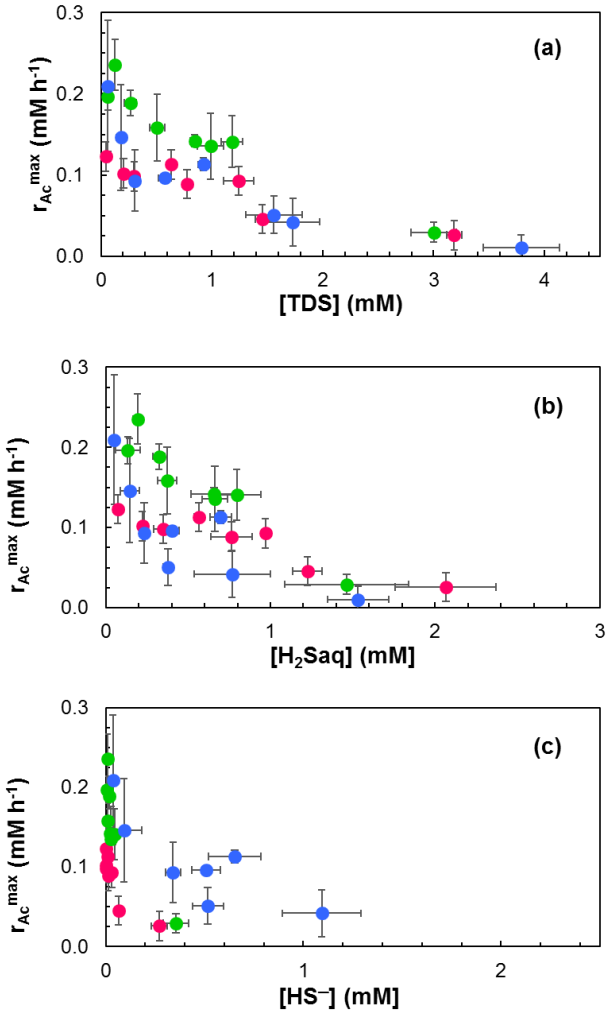

Figure A4.5 – Maximum acetate production rate (mM h^{-1}), calculated in a 48 h basis, plotted against: (a) initial total dissolved sulfide concentration ([TDS]) (mM), (b) initial dissolved hydrogen sulfide concentration ([H_2S_{aq}]) (mM) and (c) initial bisulfide concentration ([HS^-]) (mM) at pH 7 (●), 6 (●) and 5 (●). Data are averages of 3 incubations, error bars represent standard deviations of biological triplicates.

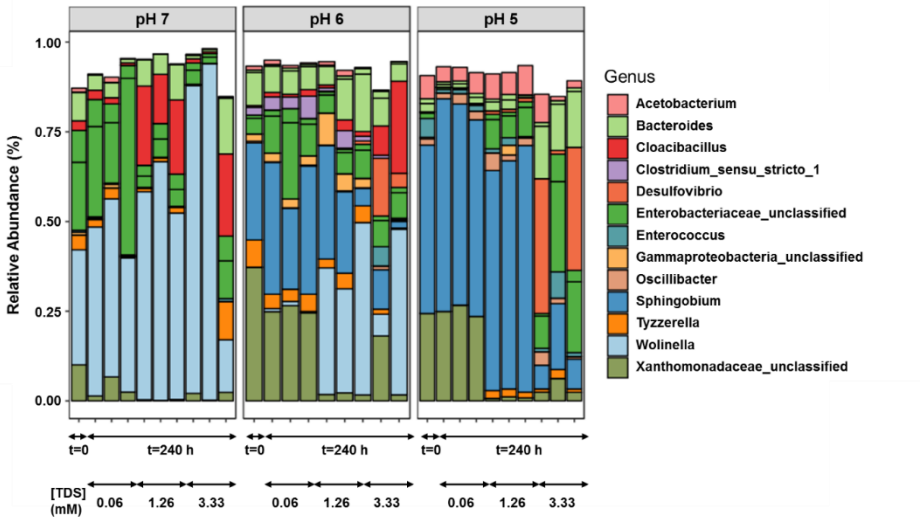

Figure A4.6 – Relative Abundances (%) of the 15 most abundant OTUs, in 3 biological replicates (2 biological replicates at pH 6 and 1.26 mM [TDS]) at t=240h

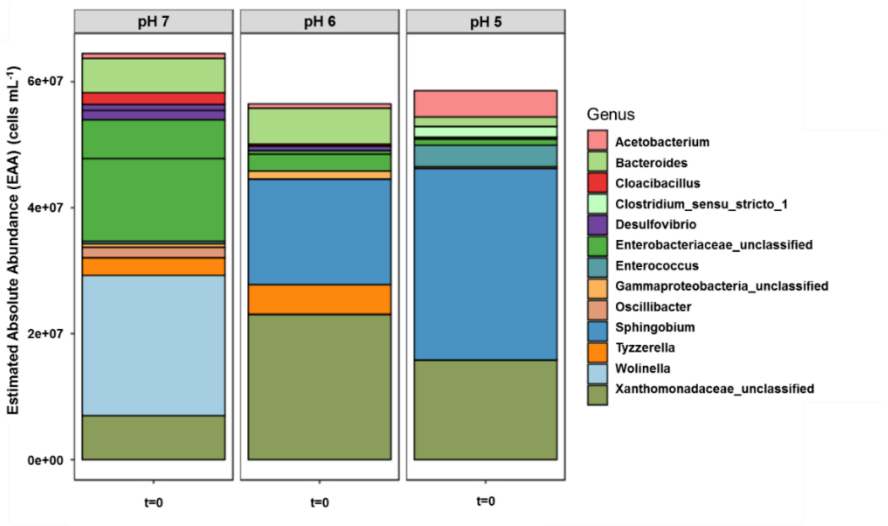

Figure A4.7 – Estimated Absolute Abundances (EEA) in (cells mL^{-1}) of the 15 most abundant OTUs, calculated as relative abundances normalised for the flow cytometric counts at t0, after culture preconditioning (4 transfers over 28 days) at pH 7, 6 and 5, respectively

A4.1.3 Clone library results

Forward sequencies where the genus *Sphingobium* was identified.

>ElefF08.F

AGAGTTTGATCCTGGCTCAGAACGAACGCTGGCGGCATGCCTAATACATGCAAGTCGAACGAAC
TCTTCGGAGTTAGTGGCGCACGGGTGCGTAACGCGTGGGAATCTACCCAGAGGTTCGGAATAA
CGGTTGGAAACGACTGCTAATACCGGACGATGTCGAGAGACCAAAGATTTATCGCCTTTGGATGA
GCCCGCGTAAGATTAGCTAGTTGGTGAGGTAAAGGCTCACCAAGGCTACGATCTTTAGCTGGTCT
GAGAGGATGATCAGCCACACTGGGACTGAGACACGGCCCAGACTCCTACGGGAGGCAGCAGT
AGGGAATATTGGACAATGGGGGCAACCCTGATCCAGCAATGCCGCGTGAGTGATGAAGGCCTT
AGGGTTGTAAAGCTCTTTTACCCGGGATGATAATGACAGTACCGGGAGAATAAGCTCCGGCTAAC
TCCGTGCCAGCAGCCGCGGTAATACGGAGGGAGCTAGCGTTGTTCGGAATTACTGGGCGTAAA
GCGCACGTAGGCGGGCTATTTAAGTCAGAGGTGAAAGCCCGGGGCTCAACCCCGGAACTGCC
TTTGAGACTGGATAGCTTGAATCCTGGAGAGGTGAGTGGAATTCCGAGTGTAGGAGGTG

>ElefF10.F

TACGGCTACCTTGTTACGACTTCACCCCAGTCGCTGATCCCACCGTGGTCGCCTGCCTCTCTTGC
GAGTTAGCGCAGCGCCTTCGGGTGAAACCAACTCCCATGGTGTGACGGGCGGTGTGTACAAGG
CCTGGGAACGTATTCACCGCGGCATGCTGATCCGCGATTACTAGCGATTCCGCCTTCATGCTCTC
GAGTTGCAGAGAACAATCCGAACTGAGACGACTTTTGGAGATTAGCTACCCCTCGCAGGGTTGCT
GCCCACTGTAGTCGCCATTGTAGCACGTGTGTAGCCCAACGCGTAAGGGCCATGAGGACTTGA
CGTCATCCCCACCTTCCTCCGGCTTATCACCGGCGGTTACCTTAGAGTGCCCAACTAAATGATGG
CAACTAAGGTCGAGGGTTGCGCTCGTTGCGGGACTTAACCCAACATCTCACGACACGAGCTGAC
GACAGCCATGCAGCACCTGTCACTTATCCAGCCGAACTGAAGAAAAGCATCTCTGCTAATCACGA
TAAGGATGTCAAACGTTGGTAAGGTTCTGCGCGTTGCTTCGAATTAAACCACATGCTCCACCGCTT
GTGCAGGCCCCCGTCAATTCCTTTGAGTTTTAATCTTGCGACCGTACTCCCCAGGCGGATAACTTA
ATGCGTTAGCTGCGCCACCCAAGTTCCATGAACCCGGACAGCTAGTTATCATCGTTTACGGCGTG
GACTACCAGGGTATCTAATCCTGTTTGCTCCCCACGCTTTCGCACCTCAGCGTCAATACCTGTCCA
GTGAGCCGCCTTCGCCACTGGTGTTCTTCCGAATATCTACGAATTTCACCTCTACACTCGGAATTC
CACTCACCTCTCCAGGATTCAAGCTATCCAGTCTCAAAGGCAGTTCCGGGGTTGAACCCCGGGC
TTTCACCTCTGACTTAAATAGCCGCCTACTGGCGCTTTACTCCCAGGAATTCCGAACAACGCT

>ElefF11.F

AGAGTTTGATCCTGGCTCAGAACGAACGCTGGCGGCATGCCTAATACATGCAAGTCGAACGAAC
TCTTCGGAGTTAGTGGCGCACGGGTGCGTAACGCGTGGGAATCTACCCAGAGGTTCGGAATAA
CGGTTGGAAACGACTGCTAATACCGGACGATGTCGAGAGACCAAAGATTTATCGCCTTTGGATGA
GCCCGCGTAAGATTAGCTAGTTGGTGAGGTAAAGGCTCACCAAGGCTACGATCTTTAGCTGGTCT
GAGAGGATGATCAGCCACACTGGGACTGAGACACGGCCCAGACTCCTACGGGAGGCAGCAGT
AGGGAATATTGGACAATGGGGGCAACCCTGATCCAGCAATGCCGCGTGAGTGATGAAGGCCTT
AGGGTTGTAAAGCTCTTTTACCCGGGATGATAATGACAGTACCGGGAGAATAAGCTCCGGCTAAC
TCCGTGCCAGCAGCCGCGGTAATACGGAGGGAGCTAGCGTTGTTCGGAATTACTGGGCGTAAA

GCGCACGTAGGCGGCTATTTAAGTCAGAGGTGAAAGCCCGGGGCTCAACCCCGGAACTGCCTT
TGAGACTGGATAGCTTGAATCCTGGAGAGGTGAGTGGAATTCCGAGTGTAGAGGTGAAATTCGTA
GATATTCGGAAGAACACCAGTGGCGAAGGCGGCTCACTGGACAGGTATTGACGCTGAGGTGCG
AAAGCGTGGGGAGCAAACAGGATTAGATACCCTGGTAGTCCACGCCGTAAACGATGATAACTAG
CTGTCCGGGTTCATGGAACTTGGGTGGCGCAGCTAACGCATTAAGGTTATCCGACCTGGGG

>ElefF16.F

TACGGTTACCTTGTTACGACTTCACCCCAGTCGCTGATCCCACCGTGGTCGCCTGCCTCTCTTGC
GAGTTAGCGCAGCGCCTTCGGGTGAAACCAACTCCCATGGTGTGACGGGCGGTGTGTACAAGG
CCTGGGAACGTATTCACCGCGGCATGCTGATCCGCGATTACTAGCGATTCCGCCTTCATGCTCTC
GAGTTGCAGAGAACAATCCGAACTGAGACGACTTTTGGAGATTAGCTACCCCTCGCAGGGTTGCT
GCCCACTGTAGTCGCCATTGTAGCACGTGTGTAGCCCAACGCGTAAGGGCCATGAGGACTTGA
CGTCATCCCCACCTTCCTCCGGCTTATCACCGGCGGTTACCTTAGAGTGCCCAACTAAATGATGG
CAACTAAGGTCGAGGGTTGCGCTCGTTGCGGGACTTAACCCAACATCTCACGACACGAGCTGAC
GACAGCCATGCAGCACCTGTCACTTATCCAGCCGAACTGAAGAAAAGCATCTCTGCTAATCACGA
TAAGGATGTCAAACGTTGGTAAGGTTCTGCGCGTTGCTTCGAATTAAACCACATGCTCCACCGCTT
GTGCAGGCCCCCGTCAATTCCTTTGAGTTTTAATCTTGCGACCGTACTCCCCAGGCGGATAACTTA
ATGCGTTAGCTGCGCCACCCAAGTTCCATGAACCCGGACAGCTAGTTATCATCGTTTACGGCGTG
GACTACCAGGGTATCTAATCCTGTTTGCTCCCCACGCTTTCGCACCTCAGCGTCAATACCTGTCCA
GTGAGCCGCCTTCGCCACTGGTGTTCTTCCGAATATCTACGAATTTCACCTCTACACTCGGAATTC
CACTCACCTCTCCAGGATTCAAGCTATCCAGTCTCAAAGGCAGTTCCGGGGTTGAGCCCCGGGC
TTTCGCCTCTGACTTAAATAAGCCGCCTACGTGCGCTTTACGCCCAGTAATTCCGAACAACGCTAG
CTCCCTCCGTATTACCGCGGCTGCTG

APPENDIX 5

A5.1 Supplementary material for Chapter 6

A5.1.1 Materials and Methods

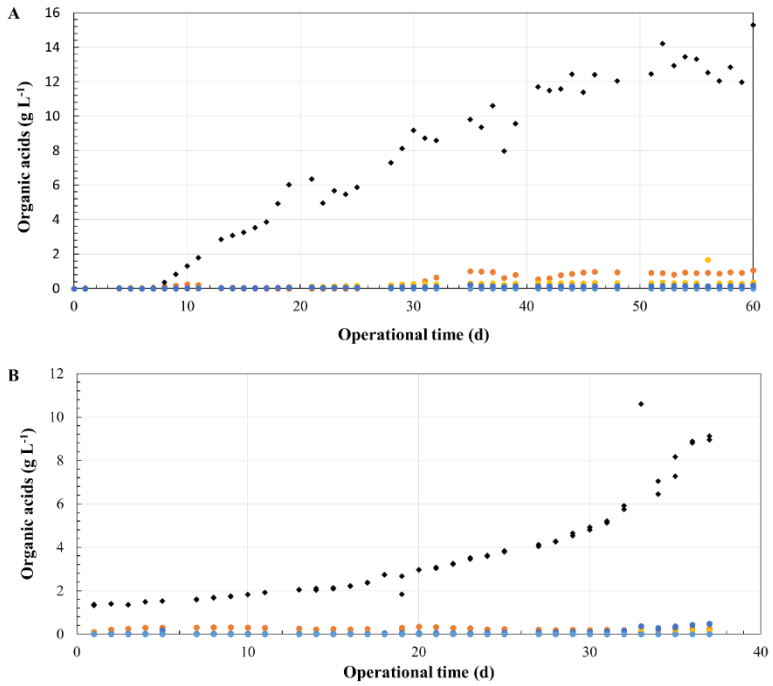

Figure A5.1 – Organic acids concentration during: Panel A: First batch operation at pH 7, lasted 60 days, Panel B: Second batch operation at pH 6.5, lasted 37 days, after which, continuous operation started: formic acid (orange), acetic acid (black), propionic acid (yellow), butyric acid (dark blue), lactic acid (light blue)

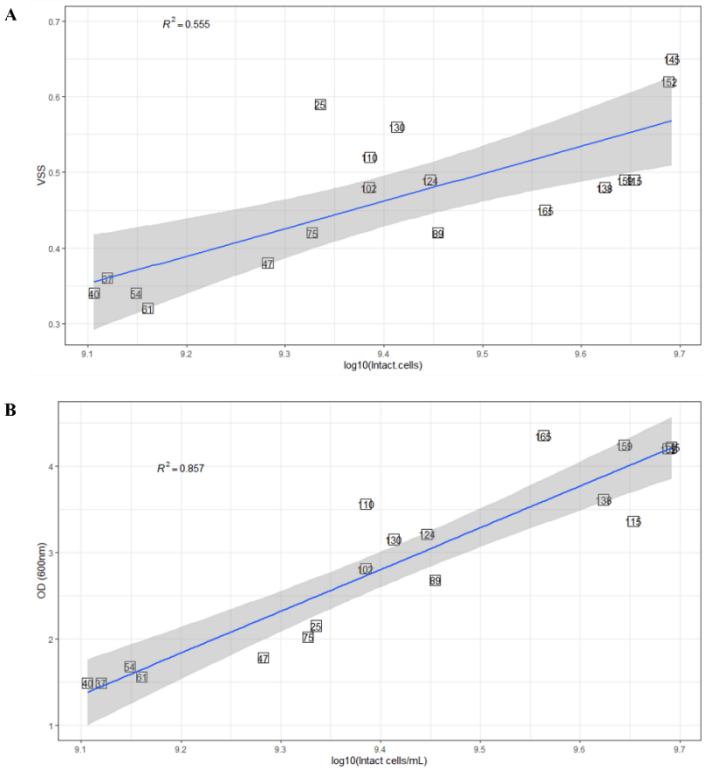

Figure A5.2 – Correlation of two methods for biomass analysis with the intact cells concentration measured by flow cytometry (FCM). Panel A: Volatile suspended solids (VSS) vs Intact cells. Panel B: Optical density (OD) vs Intact cells

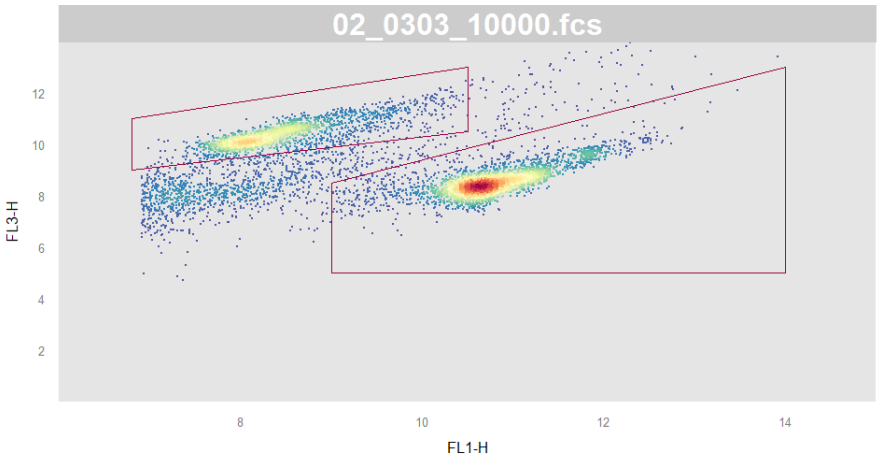

Figure A5.3 – The analysis of the flow cytometry (FCM) data was conducted by splitting the detected cells in an intact and a damaged population by creating two gates on the primary fluorescent channels.

A5.1.2 Results

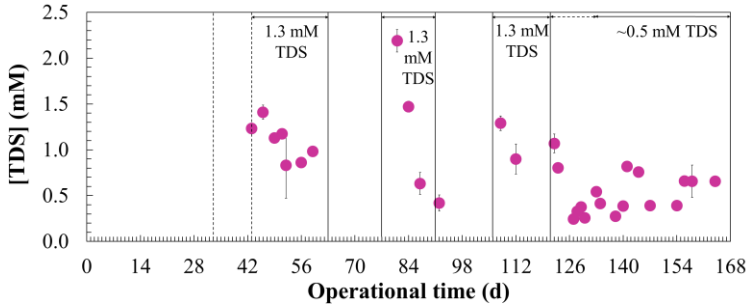

Figure A5.4 – Time course measurement of the total dissolved sulfide (TDS) concentration in the fermenter

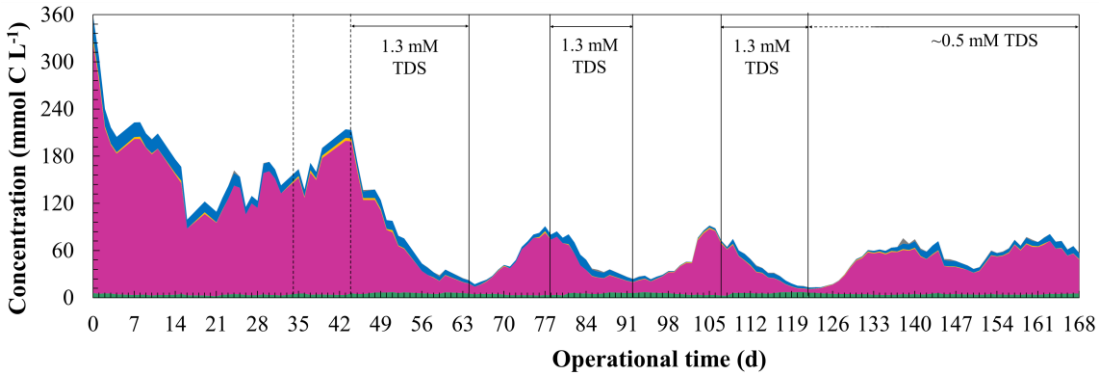

Figure A5.5 – Profile of carboxylic acids (in mmol C L^{-1}) distribution in the reactor, during the total 168 days of continuous operation: formic acid (green), acetic acid (pink), propionic acid (yellow), butyric acid (blue), lactic acid (grey). during the total 168 days of continuous operation (n = 2 technical replicates). The two dotted vertical lines represent a batch operation after a failure of the continuously operated reactor and the parts in between TDS addition, the reactor recovery periods.

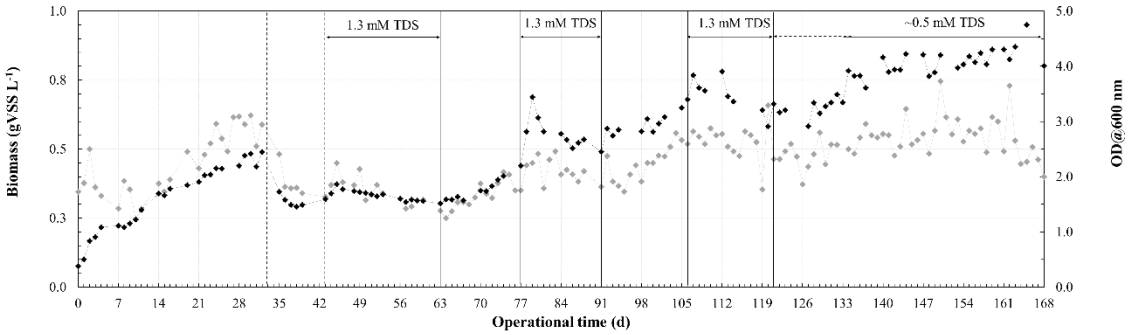

Figure A5.6 – Biomass concentration (gVSS L^{-1}) (black diamond) and OD_{600} measurement (grey diamond) during the 168 days of continuous operation

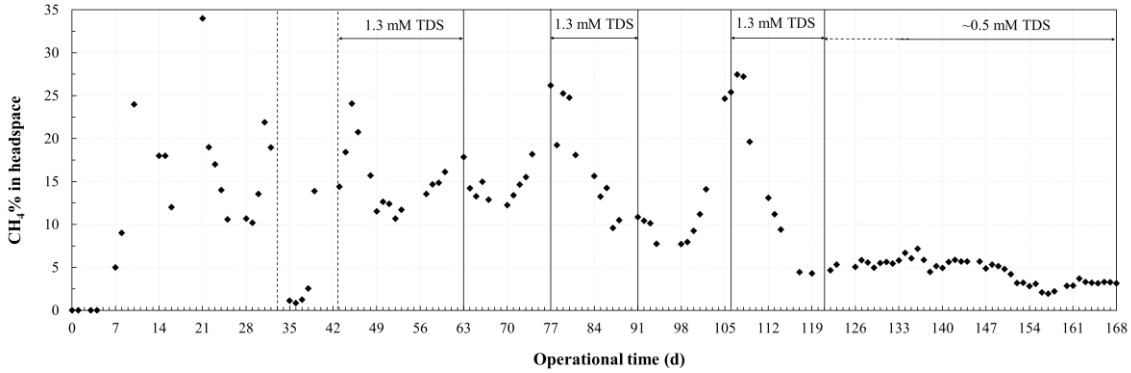

Figure A5.7 – Percentage concentration of methane gas (CH_4%) in the headspace of the reactor during the 168 days of continuous operation

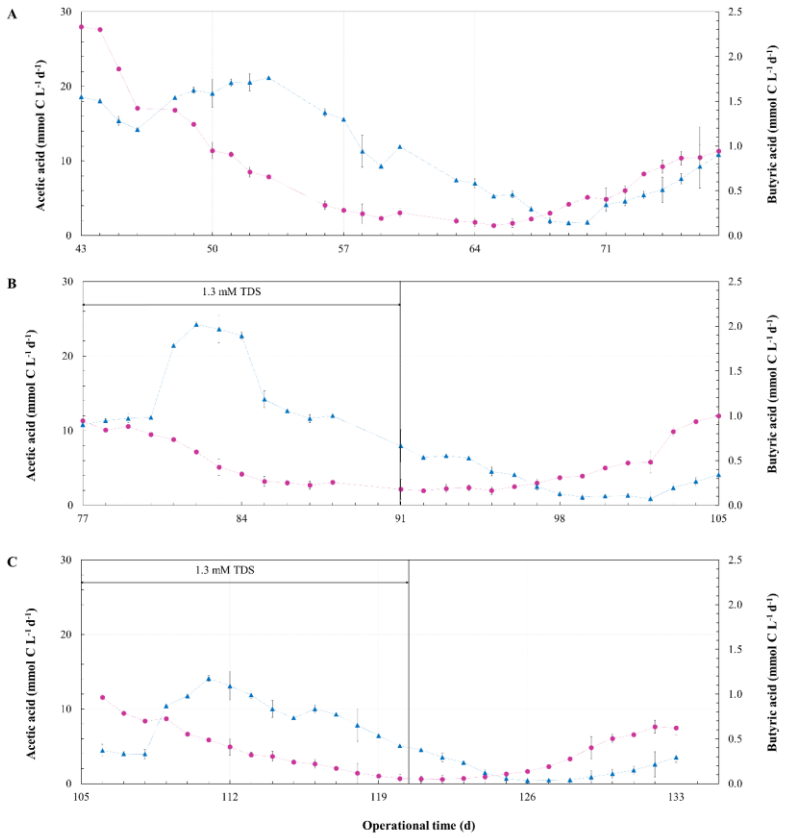

Figure A5.8 – Acetic acid and butyric acid production rates in the three distinct periods of addition and removal of sulfide stress. Panel A: days 43 – 77, Panel B: days 77 - 106, Panel C: days 106 – 133: acetic acid (pink circles), butyric acid (blue triangles) (n = 2 technical replicates)

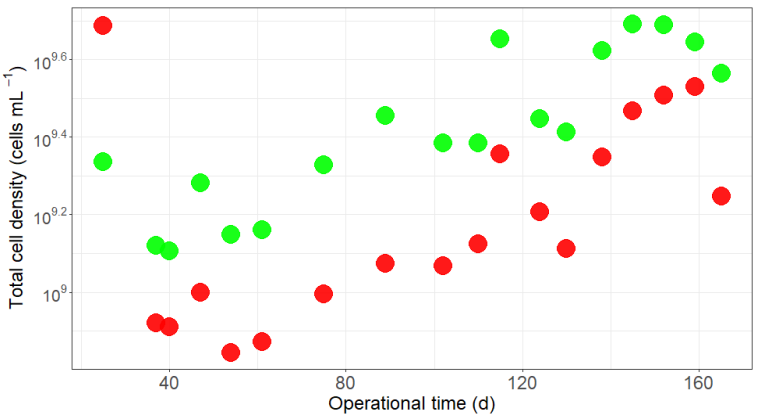

Figure A5.9 – Cell density (cells mL^{-1}) of intact (green circle) and damaged (red circle) cells during the continuous reactor operation

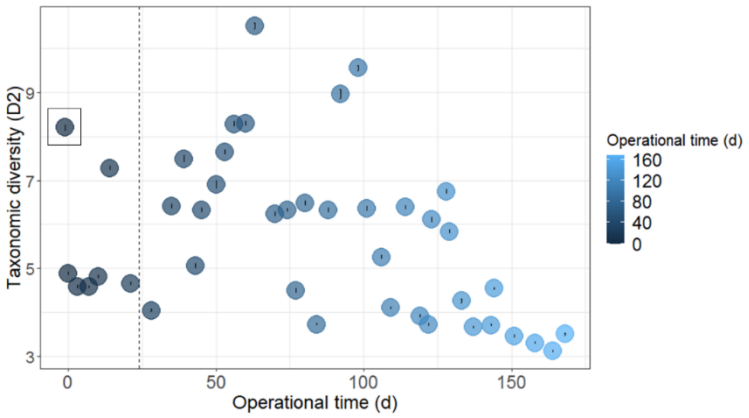

Figure A5.10 – Alpha diversity was calculated with the Hill Diversity number D2, which corresponds to Inverse Simpson index. The sample in the rectangular shape corresponds to the sample collected from the reactor inoculum during the first batch operation (Batch1), while the rest are samples taken during the continuous operation of the reactor. The dotted line represents the date that samples started being analysed with FCM.

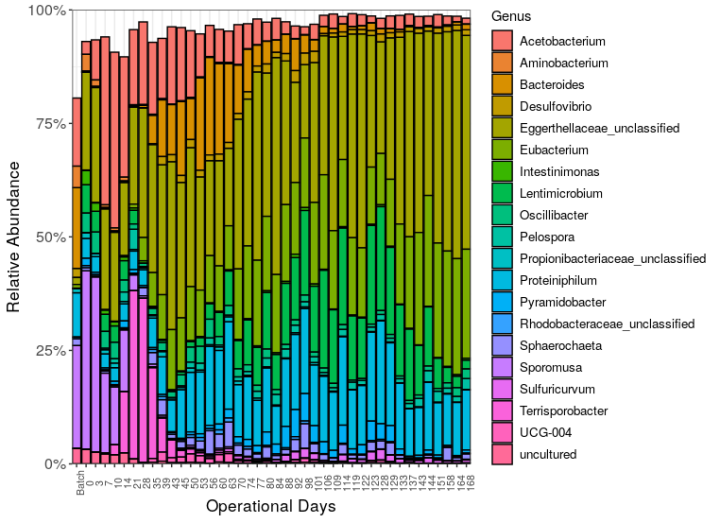

Figure A5.11 – Relative abundance of the 20 most abundant genera detected in the reactor biomass samples, during continuous operation and consecutive sulfide stress addition

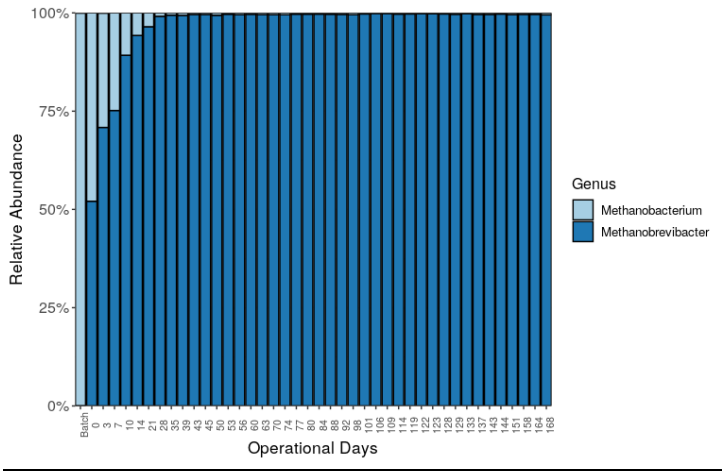

Figure A5.12 – Relative abundance of the two archaeal genera detected in the reactor biomass samples, during continuous operation and consecutive sulfide stress addition

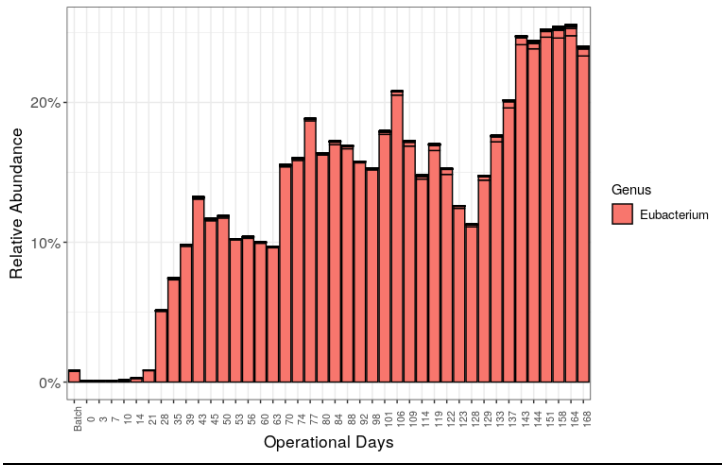

Figure A5.13 – Relative abundance of the genus Eubacterium detected in the reactor biomass samples, during continuous operation and consecutive sulfide stress addition

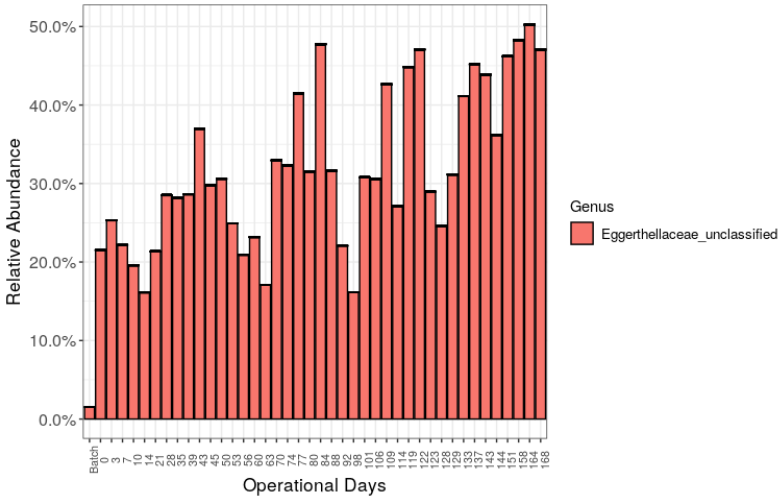

Figure A5.14 – Relative abundance of the genus Eggerthellaceae_unclassified detected in the reactor biomass samples, during continuous operation and consecutive sulfide stress addition

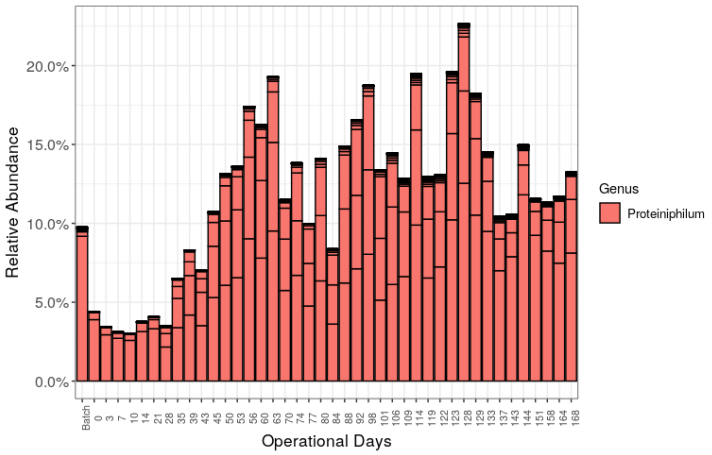

Figure A5.15 – Relative abundance of the genus Proteiniphilum detected in the reactor biomass samples, during continuous operation and consecutive sulfide stress addition

Table A5.1 – Taxonomic diversity indexes for the mixed microbial culture samples collecting during the 168 days of continuous operation and the initial microbial community sample, collected from the reactor inoculum during the first batch operation (Batch1)

		Taxonomic diversity index			
Sample name	Operational Day	Shannon	Simpson	InvSimpson	D2
A_EN_BAC_01	Batch 1	2.6	0.9	8.2	8.2
A_EN_BAC_12	0	2.3	0.8	4.9	4.9
A_EN_BAC_13	2	2.2	0.8	4.6	4.6
A_EN_BAC_14	7	2.1	0.8	4.7	4.6

A_EN_BAC_15	10	2.3	0.8	4.8	4.8
A_EN_BAC_16	15	2.5	0.9	7.3	7.3
A_EN_BAC_17	21	2.1	0.8	4.7	4.7
A_EN_BAC_18	28	1.9	0.8	4.0	4.0
A_EN_BAC_19	35	2.5	0.8	6.4	6.4
A_EN_BAC_20	39	2.7	0.9	7.5	7.5
A_EN_BAC_21	43	2.2	0.8	5.1	5.1
A_EN_BAC_22	45	2.4	0.8	6.3	6.3
A_EN_BAC_23	50	2.6	0.9	6.9	6.9
A_EN_BAC_24	53	2.6	0.9	7.6	7.6
A_EN_BAC_25	56	2.6	0.9	8.3	8.3
A_EN_BAC_26	60	2.7	0.9	8.3	8.3
A_EN_BAC_27	63	2.8	0.9	10.5	10.5
A_EN_BAC_28	70	2.5	0.8	6.2	6.2
A_EN_BAC_29	74	2.5	0.8	6.3	6.3
A_EN_BAC_30	77	2.2	0.8	4.5	4.5
A_EN_BAC_31	80	2.5	0.8	6.5	6.5
A_EN_BAC_32	84	2.0	0.7	3.7	3.7
A_EN_BAC_33	88	2.4	0.8	6.3	6.3
A_EN_BAC_34	92	2.7	0.9	9.0	9.0
A_EN_BAC_35	98	2.7	0.9	9.6	9.6
A_EN_BAC_36	101	2.5	0.8	6.4	6.4
B_EN_BAC_01	106	2.1	0.8	5.3	5.3
B_EN_BAC_02	109	2.0	0.8	4.1	4.1
B_EN_BAC_03	114	2.3	0.8	6.4	6.4
B_EN_BAC_04	119	1.9	0.7	3.9	3.9
B_EN_BAC_05	122	1.9	0.7	3.7	3.7
B_EN_BAC_06	123	2.3	0.8	6.1	6.1
B_EN_BAC_07	128	2.4	0.9	6.7	6.7
B_EN_BAC_08	129	2.3	0.8	5.8	5.8
B_EN_BAC_09	133	2.0	0.8	4.3	4.3
B_EN_BAC_10	137	1.8	0.7	3.7	3.7
B_EN_BAC_11	143	1.8	0.7	3.7	3.7
B_EN_BAC_12	144	2.0	0.8	4.5	4.5
B_EN_BAC_13	151	1.8	0.7	3.5	3.5
B_EN_BAC_14	158	1.8	0.7	3.3	3.3
B_EN_BAC_15	164	1.7	0.7	3.1	3.1
B_EN_BAC_16	168	1.9	0.7	3.5	3.5

BIBLIOGRAPHY

BIBLIOGRAPHY

Åberg, J., & Wallin, M. B. (2014). Evaluating a fast headspace method for measuring DIC and subsequent calculation of pCO_2 in freshwater systems. *Inland Waters*, *4*(2), 157–166. https://doi.org/10.5268/IW-4.2.694

Agler, M. T., Wrenn, B. A., Zinder, S. H., & Angenent, L. T. (2011). Waste to bioproduct conversion with undefined mixed cultures: The carboxylate platform. *Trends in Biotechnology*, *29*(2), 70–78. https://doi.org/10.1016/j.tibtech.2010.11.006

Al-Kharafi, F. M., Saad, A. Y., Ateya, B. G., & Ghayad, I. M. (2010). Electrochemical oxidation of sulfide ions on platinum electrodes. *Modern Applied Science*, *4*(3), 2–11.

Al Rowaihi, I. S., Kick, B., Grötzinger, S. W., Burger, C., Karan, R., Weuster-Botz, D., et al. (2018). A two-stage biological gas to liquid transfer process to convert carbon dioxide into bioplastic. *Bioresource Technology Reports*, *1*, 61–68. https://doi.org/10.1016/j.biteb.2018.02.007

Alcántara, S., Velasco, A., Muñoz, A., Cid, J., Revah, S., & Razo-Flores, E. (2004). Hydrogen sulfide oxidation by a microbial consortium in a recirculation reactor system: Sulfur formation under oxygen limitation and removal of phenols. *Environmental Science & Technology*, *38*(3), 918–923.

Alloul, A., Wuyts, S., Lebeer, S., & Vlaeminck, S. E. (2019). Volatile fatty acids impacting phototrophic growth kinetics of purple bacteria: Paving the way for protein production on fermented wastewater. *Water Research*, *152*(2019), 138–147. https://doi.org/10.1016/j.watres.2018.12.025

Alnaizy, R. (2008). Economic analysis for wet oxidation processes for the treatment of mixed refinery spent caustic. *Environmental Progress*, *27*(3), 295–301. https://doi.org/10.1002/ep

Amatore, C., Berthou, M., & Hébert, S. (1998). Fundamental principles of electrochemical ohmic heating of solutions. *Journal of electroanalytical chemistry*, *457*, 191–203.

Anani, A. A., Mao, Z., White, R. E. E., Srinivasan, S., Appleby, A. J., M, Z., et al. (1990). Electrochemical production of hydrogen and sulfur by low-temperature decomposition of hydrogen sulfide in an aqueous alkaline solution. *Journal of The Electrochemical Society*, *137*(9), 2703–2709. https://doi.org/10.1149/1.2087021

Anderson, A., & Rezaie, B. (2019). Geothermal technology: Trends and potential role in a sustainable future. *Applied Energy*, *248*(March), 18–34. https://doi.org/10.1016/j.apenergy.2019.04.102

APHA, AWWA, & WPCF. (1999). *Standard methods for the examination of water and wastewater*. (L. S. Clesceri, A. E. Greenberg, & A. D. Eaton, Eds.) (20th ed.). American Public Health

Association, American Water Works Association, Water Environment Federation. https://doi.org/10.1016/0043-1354(82)90249-4

Aradóttir, E. S. P., Gunnarsson, I., Sigfússon, B., Gunnarsson, G., Júliusson, B. M., Gunnlaugsson, E., et al. (2015). Toward cleaner geothermal energy utilization: Capturing and sequestering CO_2 and H_2S emissions from geothermal power plants. *Transport in Porous Media*, *108*, 61–84. https://doi.org/10.1007/s11242-014-0316-5

Arenas, L. F., Ponce de León, C., & Walsh, F. C. (2020). Critical review—The versatile plane parallel electrode geometry: An illustrated review. *Journal of The Electrochemical Society*, *167*(2), 023504. https://doi.org/10.1149/1945-7111/ab64ba

Arends, J. B. A., Patil, S. A., Roume, H., & Rabaey, K. (2017). Continuous long-term electricity-driven bioproduction of carboxylates and isopropanol from CO_2 with a mixed microbial community. *Journal of CO_2 Utilization*, *20*, 141–149. https://doi.org/10.1016/j.jcou.2017.04.014

Aresta, M., Dibenedetto, A., & Dumeignil, F. (2012). *Biorefinery: From biomass to chemicals and fuels*. De Gruyter.

Aromaa, J., & Forsén, O. (2006). Evaluation of the electrochemical activity of a Ti–RuO_2–TiO_2 permanent anode. *Electrochimica Acta*, *51*, 6104–6110.

Asdrubali, F., Baldinelli, G., D'Alessandro, F., & Scrucca, F. (2015). Life cycle assessment of electricity production from renewable energies: Review and results harmonization. *Renewable and Sustainable Energy Reviews*, *42*, 1113–1122. https://doi.org/10.1016/j.rser.2014.10.082

Ateya, B. G., & Al-Kharafi, F. M. (2002). Anodic oxidation of sulfide ions from chloride brines. *Electrochemistry*, *4*, 231–238.

Ateya, B. G., Al-Kharafi, F. M., Abdallah, R. M., & Al-Azab, A. S. (2005). Electrochemical removal of hydrogen sulfide from polluted brines using porous flow through electrodes. *Journal of Applied Electrochemistry*, *35*, 297–303.

Ateya, B. G., Alkharafi, F. M., & Al-Azab, A. S. (2003). Electrodeposition of sulfur from sulfide contaminated brines. *Electrochemical and Solid-State Letters*, *9*(6), 137–140.

Ausma, T., & De Kok, L. J. (2019). Atmospheric H_2S: Impact on plant functioning. *Frontiers in Plant Science*, *10*(June), 743. https://doi.org/10.3389/fpls.2019.00743

Aylward, F. O., Mcdonald, B. R., Adams, S. M., Valenzuela, A., Schmidt, R. A., Goodwin, L. A., et al. (2013). Comparison of 26 *Sphingomonad* genomes reveals diverse environmental adaptations and biodegradative capabilities. *Applied and Environmental Microbiology*, *79*(12), 3724–3733. https://doi.org/10.1128/AEM.00518-13

Ayudthaya, P. S. N., van de Weijer, A. H. P., van Gelder, A. H., Stams, A. J. M., de Vos, W. M., &

Plugge, C. M. (2018). Organic acid production from potato starch waste fermentation by rumen microbial communities from Dutch and Thai dairy cows. *Biotechnology for Biofuels*, 11:13. https://doi.org/10.1186/s13068-018-1012-4

Badyaev, A. V. (2005). Stress-induced variation in evolution: From behavioural plasticity to genetic assimilation. *Proceedings of the Royal Society B: Biological Sciences*, *272*(1566), 877–886. https://doi.org/10.1098/rspb.2004.3045

Balch, W. E., Schoberth, S., Tanner, R. S., & Wolfe, R. S. (1977). *Acetobacterium*, a new genus of hydrogen-oxidizing, carbon dioxide-reducing, anaerobic bacteria. *International Journal of Systematic Bacteriology*, *27*(4), 355–361.

Bard, Allen J., & Faulkner, L. R. (2001). *Electrochemical methods: Fundamentals and Applications*. (I. John Wiley & Sons, Ed.) (2nd ed.). New York: Wiley. http://elib.tu-darmstadt.de/tocs/95069577.pdf

Barrera, E. L., Spanjers, H., Dewulf, J., Romero, O., & Rosa, E. (2013). The sulfur chain in biogas production from sulfate-rich liquid substrates: a review on dynamic modeling with vinasse as model substrate. *Society of Chemical Industry*, *88*, 1405–1420.

Barthe, P., Chaugny, M., & Roudier, S. (2015). *Best Available Techniques (BAT) Reference Document for the Refining of Mineral Oil and Gas Prevention and Control)*. https://doi.org/10.2791/010758

Basosi, R., Bonciani, R., Frosali, D., Manfrida, G., Parisi, M. L., & Sansone, F. (2020). Life cycle analysis of a geothermal power plant: Comparison of the environmental performance with other renewable energy systems. *Sustainability (Switzerland)*, *12*(7), 1–29. https://doi.org/10.3390/su12072786

Behm, M., & Simonsson, D. (1997). Electrochemical production of polysulfides and sodium hydroxide from white liquor Part I: Experiments with rotating disc and ring-disc electrodes. *Journal of Applied Electrochemistry*, *27*, 507–518. https://doi.org/10.1023/A:1018486309601

Behm, M., & Simonsson, D. (1999). Nickel as anode material for the electrochemical production of polysulfides in white liquor. *Journal of New Materials for Electrochemical Systems*, *2*, 11–18.

Ben Hariz, I., Halleb, A., Adhoum, N., & Monser, L. (2013). Treatment of petroleum refinery sulfidic spent caustic wastes by electrocoagulation. *Separation and Purification Technology*, *107*, 150–157. https://doi.org/10.1016/j.seppur.2013.01.051

Bendall, E., Aiken, R. C., & Mandas, F. (1983). Selective absorption of H_2S from larger quantities of CO_2 by absorption and reaction in fine sprays. *AIChE Journal*, *29*(1), 66–72. https://doi.org/10.1002/aic.690290109

Berney, M., Greening, C., Conrad, R., Jacobs, W. R., & Cook, G. M. (2014). An obligately aerobic soil bacterium activates fermentative hydrogen production to survive reductive stress during hypoxia. *PNAS*, *111*(31), 11479–11484. https://doi.org/10.1073/pnas.1407034111

Bockris, J. O. (1972). *Electrochemistry of cleaner environments*. Plenum Press, New York.

Bontozoglou, V., & Karabelas, A. J. (1993). Simultaneous absorption of H_2S and CO_2 in NaOH solutions: Experimental and numerical study of the performance of a short-time contactor. *Industrial and Engineering Chemistry Research*, *32*, 165–172.

Bouillaud, F., & Blachier, F. (2011). Mitochondria and sulfide: A very old story of poisoning, feeding and signaling? *Antioxidants and redox signaling*, *15*(2), 379–391.

Bouroushian, M. (2010). Electrochemistry of the Chalcogens. In *Electrochemistry of Metal Chalcogenides* (1st ed., pp. 57–76). Springer-Verlag Berlin Heidelberg. https://doi.org/10.1007/978-3-642-03967-6

Bowen, B. (2019). Chemical profile: Caustic soda. *ICIS*. https://www.icis.com/explore/resources/news/2019/02/21/10322764/chemical-profile-caustic-soda/. Accessed 6 January 2021

Braun, M., & Gottschalk, G. (1982). *Acetobacterium wieringae* sp . nov ., a new species producing acetic acid from molecular hydrogen and carbon dioxide. *Zbl Bakt Hyg, I Abt Orig C*, *3*(3), 368–376. http://dx.doi.org/10.1016/S0721-9571(82)80017-3

Bravi, M., & Basosi, R. (2014). Environmental impact of electricity from selected geothermal power plants in Italy. *Journal of Cleaner Production*, *66*, 301–308. https://doi.org/10.1016/j.jclepro.2013.11.015

Brinkmann, T., Santonja, G. G., Schorcht, F., Roudier, S., & Delgado Sancho, L. (2014). *Best Available Techniques (BAT) reference document for the production of Chlor-alkali*. https://doi.org/10.2791/13138

Buckel, W., & Thauer, R. K. (2018). Flavin-based electron bifurcation, a new mechanism of biological energy coupling. *Chemical Reviews*, *118*(7), 3862–3886. https://doi.org/10.1021/acs.chemrev.7b00707

Budiarto, T., Esche, E., Repke, J. U., & Leksono, E. (2017). Dynamic model of chloralkali membrane process. *Procedia Engineering*, *170*, 473–481. https://doi.org/10.1016/j.proeng.2017.03.076

Buisman, C. J. N., Vellinga, S. H. J., Janssen, G. H. R., & Dijkman, H. (1999). Biological sulfide production for metal recovery. *Proceedings of the Symposium on Fundamentals of Lead and Zinc Extraction and Recycling, held at the 1999 TMS Annual Meeting*.

Buisman, C., Post, R., Ijspeert, P., Geraats, G., & Lettinga, G. (1989). Biotechnological process for

sulphide removal with sulphur reclamation. *Acta Biotechnologica*, *9*, 255–267.

Burke, A., Winnick, J., Xia, C., & Liu, M. (2002). Removal of hydrogen sulfide from a fuel gas stream by electrochemical membrane separation. *J. Electrochem. Soc.*, *149*(11), 160–166. https://doi.org/10.1149/1.1511190

Burstyn, I., Senthilselvan, A., Kim, H. M., Cherry, N. M., Pietroniro, E., & Waldner, C. (2007). Industrial sources influence air concentrations of hydrogen sulfide and sulfur dioxide in rural areas of Western Canada. *Journal of the Air and Waste Management Association*, *57*(10), 1241–1250. https://doi.org/10.3155/1047-3289.57.10.1241

C.Baker. (2020). Europe caustic soda Q1 price falls 10% as market readjusts. *ICIS*. https://www.icis.com/explore/resources/news/2020/01/28/10461663/europe-caustic-soda-q1-price-falls-10-as-market-readjusts. Accessed 6 January 2020

Cao, Q., Zhang, L., Yang, G., Xu, C., & Wang, R. (2010). Butyrate-stimulated H_2S production in colon cancer cells. *Antioxidants and Redox Signaling*, *12*(9), 1101–1109. https://doi.org/10.1089/ars.2009.2915

Carlos, T. M. S., & Clayton B. Maugans. (2000). Wet air oxidation of refinery spent caustic: A refinery case study. In *NPRA Conference, September 12* (pp. 1–12).

Carlson, H. K., Stoeva, M. K., Justice, N. B., Sczesnak, A., Mullan, M. R., Mosqueda, L. A., et al. (2015). Monofluorophosphate is a selective inhibitor of respiratory sulfate-reducing microorganisms. *Environmental Science & Technology*, *49*, 3727–3736.

Chakraborty, P., Gibbons, W., & Muthukumarappan, K. (2009). Conversion of volatile fatty acids into polyhydroxyalkanoate by *Ralstonia eutropha*. *Journal of Applied Microbiology*, *106*(6), 1996–2005. https://doi.org/10.1111/j.1365-2672.2009.04158.x

Chaplin, B. P. (2019). The prospect of electrochemical technologies advancing worldwide water treatment. *Accounts of Chemical Research*, *3*(52), 592–604. https://doi.org/10.1021/acs.accounts.8b00611

Chatzigiannidou, I., Teughels, W., Van de Wiele, T., & Boon, N. (2020). Oral biofilms exposure to chlorhexidine results in altered microbial composition and metabolic profile. *npj Biofilms and Microbiomes*, *6*(1), 1–8. https://doi.org/10.1038/s41522-020-0124-3

Chatzisymeon, E., Foteinis, S., Mantzavinos, D., & Tsoutsos, T. (2013). Life cycle assessment of advanced oxidation processes for olive mill wastewater treatment. *Journal of Cleaner Production*, *54*, 229–234. https://doi.org/10.1016/j.jclepro.2013.05.013

Chaudhary, D. K., Jeong, S., & Kim, J. (2017). *Sphingobium naphthae* sp. nov., with the ability to degrade aliphatic hydrocarbons, isolated from oil-contaminated soil. *International Journal of*

Systematic and Evolutionary Microbiology, *67*, 2986–2993. https://doi.org/10.1099/ijsem.0.002064

Chen, A., & Miller, B. (2004). Potential oscillations during the electrocatalytic oxidation of sulfide on a microstructured Ti/Ta_2O_5-IrO_2 electrode. *The Journal of Physical Chemistry B*, *108*(7), 2245–2251. https://doi.org/10.1021/jp036639h

Chen, S., & Dong, X. (2005). Proteiniphilum acetatigenes gen. nov., sp. nov., from a UASB reactor treating brewery wastewater. *International Journal of Systematic and Evolutionary Microbiology*, *55*(6), 2257–2261. https://doi.org/10.1099/ijs.0.63807-0

Chen, Y., Cheng, J. J., & Creamer, K. S. (2008). Inhibition of anaerobic digestion process: A review. *Bioresource Technology*, *99*(10), 4044–4064. https://doi.org/10.1016/j.biortech.2007.01.057

Cherevko, S., Geiger, S., Kasian, O., Kulyk, N., Grote, J., Savan, A., et al. (2016). Oxygen and hydrogen evolution reactions on Ru, RuO_2, Ir, and IrO_2 thin film electrodes in acidic and alkaline electrolytes: A comparative study on activity and stability. *Catalysis today*, *262*, 170–180.

Cherif, H., Coquelet, C., Stringari, P., Clodic, D., Pellegrini, L., Moioli, S., & Langé, S. (2016). Experimental and simulation results for the removal of H_2S from biogas by means of sodium hydroxide in structured packed columns. In *ICBST* (Vol. 18th Inter, p. PARIS, France). https://hal-mines-paristech.archives-ouvertes.fr/hal-01260220

Choi, E., & Rim, J. M. (1991). Competition and inhibition of sulfate reducers and methane producers in anaerobic treatment. *Water Science and Technology*, *23*(7–9), 1259–1264. https://doi.org/10.2166/wst.1991.0577

Choudhury, A., & Lansing, S. (2020). Biochar addition with Fe impregnation to reduce H_2S production from anaerobic digestion. *Bioresource Technology*, *306*(March), 123121. https://doi.org/10.1016/j.biortech.2020.123121

Chung, W. J., Griebel, J. J., Kim, E. T., Yoon, H., Simmonds, A. G., Ji, H. J., et al. (2013). The use of elemental sulfur as an alternative feedstock for polymeric materials. *Nature Chemistry*, *5*(June), 518–524. https://doi.org/10.1038/NCHEM.1624

Ciobanu, M., Wilburn, J. P., Krim, M. L., & Cliffel, D. E. (2007). Fundamentals. In C. G. Zoski (Ed.), *Handbook of Electrochemistry* (pp. 3–29). Elsevier.

Ciriminna, R., Albanese, L., Meneguzzo, F., & Pagliaro, M. (2016). Hydrogen peroxide: A key chemical for today's sustainable development. *ChemSusChem*, *9*(24), 3374–3381. https://doi.org/10.1002/cssc.201600895

Cohen, Y., Jorgensen, B. B., Revsbech, N. P., & Poplawski, R. (1986). Adaptation to hydrogen

sulfide of oxygenic and anoxygenic photosynthesis among cyanobacteria. *Applied and Environmental Microbiology*, *51*(2), 398–407. https://doi.org/10.1128/aem.51.2.398-407.1986

Colleran, E., Pender, S., Philpott, U., Flaherty, V. O., & Leahy, B. (1998). Full-scale and laboratory-scale anaerobic treatment of citric acid production wastewater. *Biodegradation*, *9*, 233–245.

Comninellis, Ch, & Vercesi, G. P. (1991). Characterization of DSA-type oxygen evolving electrodes: choice of a coating. *Journal of Applied Electrochemistry*, *21*, 335–345.

Comninellis, Christos, & Chen, G. (2010). *Electrochemistry for the Environment* (1st ed.). Springer.

CONCAWE Refinery Technology Support Group. (2013). *Oil refining in the EU in 2020, with perspectives to 2030*.

Cord-Ruwisch, R., Seitz, H.-J., & Conrad, R. (1988). The capacity of hydrogenotrophic anaerobic bacteria to compete for traces of hydrogen depends on the redox potential of the terminal electron acceptor. *Archives of Microbiology*, *149*, 350–357.

Croese, E., Keesman, K. J., Widjaja-Greefkes, (Aura) H.C.A., Geelhoed, J. S., Plugge, C. M., Sleutels, T. H. J. A., et al. (2013). Relating MEC population dynamics to anode performance from DGGE and electrical data. *Systematic and Applied Microbiology*, *36*(6), 408–416. https://doi.org/10.1016/j.syapm.2013.05.004

Dahl, C. (2020). A biochemical view on the biological sulfur cycle. In Piet N.L. Lens (Ed.), *Environmental Technologies to Treat Sulfur Pollution: Principles and Engineering* (2nd ed., pp. 55–96). IWA Publishing.

Dar, S. A., Kleerebezem, R., Stams, A. J. M., Kuenen, J. G., & Muyzer, G. (2008). Competition and coexistence of sulfate-reducing bacteria , acetogens and methanogens in a lab-scale anaerobic bioreactor as affected by changing substrate to sulfate ratio. *Environmental Biotechnology*, *78*, 1045–1055. https://doi.org/10.1007/s00253-008-1391-8

De Crisci, A. G., Moniri, A., & Xu, Y. (2019). Hydrogen from hydrogen sulfide: towards a more sustainable hydrogen economy. *International Journal of Hydrogen Energy*, *44*(3), 1299–1327. https://doi.org/10.1016/j.ijhydene.2018.10.035

de Souza, T. L. C. (1988). Sulphur gas analysis in the pulp and paper industry. *JAPCA*, *38*, 792–795. https://doi.org/10.1080/08940630.1988.10466419

Demler, M., & Weuster-Botz, D. (2011). Reaction engineering analysis of hydrogenotrophic production of acetic acid by *Acetobacterium woodii*. *Biotechnology and Bioengineering*, *108*(2), 470–474. https://doi.org/10.1002/bit.22935

Dhar, B. R., Elbeshbishy, E., & Nakhla, G. (2012). Influence of iron on sulfide inhibition in dark

biohydrogen fermentation. *Bioresource Technology*, *126*, 123–130. https://doi.org/10.1016/j.biortech.2012.09.043

Diender, M., Stams, A. J. M., & Sousa, D. Z. (2015). Pathways and bioenergetics of anaerobic carbon monoxide fermentation. *Frontiers in Microbiology*, *6*(NOV), 1–18. https://doi.org/10.3389/fmicb.2015.01275

Dietrich, W., & Klimmek, O. (2002). The function of methyl-menaquinone-6 and polysululfide reductase membrane anchor (PsrC) in polysulfide respiration of *Wolinella succinogenes*. *European Journal of Biochemistry*, *269*, 1086–1095.

Domingos, J. M. B., Martinez, G. A., Scoma, A., Fraraccio, S., Kerckhof, F.-M., Boon, N., et al. (2017). Effect of operational parameters in the continuous anaerobic fermentation of cheese whey on titers, yields, productivities, and microbial community structures. *ACS Sustainable Chem. Eng.*, *5*, 1400–1407. https://doi.org/10.1021/acssuschemeng.6b01901

Drake, H. L., Gössner, A. S., & Daniel, S. L. (2008). Old acetogens, new light. *Annals of the New York Academy of Sciences*, *1125*, 100–128. https://doi.org/10.1196/annals.1419.016

Drake, H. L., Küsel, K., & Matthies, C. (2013). Acetogenic Prokaryotes. In E. Rosenberg, E. F. DeLong, S. Lory, E. Stackebrandt, & F. Thompson (Eds.), *The Prokaryotes - Prokaryotic Biology and Symbiotic* (4th ed., pp. 3–60). Springer-Verlag Berlin Heidelberg. http://www.springer.com/us/book/9783642301933

Du, F., Warsinger, D. M., Urmi, T. I., Thiel, G. P., Kumar, A., & V, J. H. L. (2018). Sodium hydroxide production from seawater desalination brine: process design and energy efficiency. *Environmental Science & Technology*, *52*, 5949–5958. https://doi.org/10.1021/acs.est.8b01195

Duan, X., Wang, X., Xie, J., Feng, L., Yan, Y., & Zhou, Q. (2016). Effect of nonylphenol on volatile fatty acids accumulation during anaerobic fermentation of waste activated sludge. *Water Research*, *105*, 209–217. https://doi.org/10.1016/j.watres.2016.08.062

Dutta, P. K., Keller, J., Yuan, Z., Rozendal, R. A., & Rabaey, K. (2010). Conversion of sulfur species in bioelectrochemical systems. In K. Rabaey, L. Angenent, U. Schröder, & J. Keller (Eds.), *Bioelectrochemical systems: From extracellular electron transfer to biotechnological application* (pp. 243–262). IWA Publishing.

Dutta, P. K., Rabaey, K., Yuan, Z., & Keller, J. (2008). Spontaneous electrochemical removal of aqueous sulfide. *Water Research*, *42*(20), 4965–4975. https://doi.org/10.1016/j.watres.2008.09.007

Dutta, P. K., Rozendal, R. A., Yuan, Z., Rabaey, K., & Keller, J. (2009). Electrochemical regeneration of sulfur loaded electrodes. *Electrochemistry Communications*, *11*(7), 1437–1440.

https://doi.org/10.1016/j.elecom.2009.05.024

Echemi. (2019a). Glacial acetic acid price analysis. *Echemi Market Analysis*. https://www.echemi.com/productsInformation/pd20160820171503533-glacial-acetic-acid.html#:~:text=Reference price of Glacial Acetic,on 2021-01-08.&text=Reference price of Glacial Acetic Acid is 629.042USD%2FMT,on 2021-01-07. Accessed 15 January 2021

Echemi. (2019b). Caustic soda price analysis. https://www.echemi.com/productsInformation/pd20150901041-caustic-soda-pearls.html. Accessed 25 March 2019

Edwards, T. J., Maurer, G., Newman, J., & Prausnitz, J. M. (1978). Vapor- liquid equilibria in multicomponent aqueous solutions of volatile weak electrolytes. *AIChE Journal*, *24*(6), 966–976. https://doi.org/10.1002/aic.690240605

EEA. (2020). Indicator Assessment: Total greenhouse gas emission trends and projections in Europe. *European Environment Agency*. https://www.eea.europa.eu/data-and-maps/indicators/greenhouse-gas-emission-trends-6/assessment-3. Accessed 22 September 2020

Eggerth, A. H. (1935). The Gram-positive non-spore-bearing anaerobic bacilli of human feces. *Journal of Bacteriology*, *30*(3), 277–299. https://doi.org/10.1128/jb.30.3.277-299.1935

El-Sherif, S., Bejan, D., & Bunce, N. J. (2010). Electrochemical oxidation of sulfide ion in synthetic sour brines using periodic polarity reversal at Ebonex® electrodes. *Canadian Journal of Chemistry*, *88*, 928–936.

ElectroCell. (2017). Electrochemical Flow Cells, Technical Data. www.electrocell.com

Eow, J. S. (2002). Recovery of sulfur from sour acid gas: A review of the technology. *Environmental Progress*, *21*(3), 143–162. https://doi.org/10.1002/ep.670210312

Esposti, M. D., & Romero, E. M. (2017). The functional microbiome of arthropods. *PLoS ONE*, *12*(5), e0176573. https://doi.org/10.1371/journal.pone.0176573

Euro Chlor. (2010). *The European Chlor-Alkali industry: an electricity intensive sector exposed to carbon leakage*.

European Comission. (2000). ENI LIFE EVENT. Refinery absorption and recovery of sulphur. http://ec.europa.eu/environment/life/project/Projects/files/laymanReport/LIFE00_ENV_IT_000012_LAYMAN.pdf. Accessed 13 August 2019

European Commission. (2019). *The European Green Deal*. https://doi.org/10.2307/j.ctvd1c6zh.7

Expert Market Research. (2020). Global Acetic Acid Market to Reach 11.85 Million Tons by 2026. https://www.expertmarketresearch.com/pressrelease/global-acetic-acid-

market#:~:text=According to a new report,significant growth during 2016-2020. Accessed 27 December 2020

Fabbri, E., Habereder, A., Waltar, K., Kötz, R., & Schmidt, T. J. (2014). Developments and perspectives of oxide-based catalysts for the oxygen evolution reaction. *Catalysis Science & Technology*, *4*, 3800–3821.

Faith, J. J., Guruge, J. L., Charbonneau, M., Subramanian, S., Seedorf, H., Goodman, A. L., et al. (2013). The long-term stability of the human gut microbiota. *Science*, *341(6141):*, 1237439. https://doi.org/10.1126/science.1237439

Feng, Y., Yang, L., Liu, J., & Logan, B. E. (2016). Electrochemical technologies for wastewater treatment and resource reclamation. *Environmental Science: Water Research and Technology*, (2), 800–831.

Folens, K., Van Acker, T., Bolea-Fernandez, E., Cornelis, G., Vanhaecke, F., Du Laing, G., & Rauch, S. (2018). Identification of platinum nanoparticles in road dust leachate by single particle inductively coupled plasma-mass spectrometry. *Science of the Total Environment*, *615*, 849–856. https://doi.org/10.1016/j.scitotenv.2017.09.285

Fornés, J. P., & Bisang, J. M. (2017). Electrochemical production of colloidal sulphur by oxidation of sulphide ion at lead coated-2- and -3-dimensional rotating cylinder anode surfaces. *Electrochimica Acta*, *243*, 90–97. https://doi.org/10.1016/j.electacta.2018.10.164

Fotidis, I. A., Wang, H., Fiedel, N. R., Luo, G., Karakashev, D. B., & Angelidaki, I. (2014). Bioaugmentation as a solution to increase methane production from an ammonia-rich substrate. *Environmental Science & Technology*, *48*, 7669–7676.

Garcia-Rodriguez, O., Mousset, E., Olvera-Vargas, H., & Lefebvre, O. (2020). Electrochemical treatment of highly concentrated wastewater: A review of experimental and modeling approaches from lab- to full-scale. *Critical Reviews in Environmental Science and Technology*. https://doi.org/10.1080/10643389.2020.1820428

García-Timermans, C., Rubbens, P., Heyse, J., Kerckhof, F. M., Props, R., Skirtach, A. G., et al. (2020). Discriminating bacterial phenotypes at the population and single-cell level: A comparison of flow cytometry and Raman spectroscopy fingerprinting. *Cytometry Part A*, *97*(7), 713–726. https://doi.org/10.1002/cyto.a.23952

Gardiner, B. J., Tai, A. Y., Kotsanas, D., Francis, M. J., Roberts, S. A., Ballard, S. A., et al. (2015). Clinical and microbiological characteristics of *Eggerthella lenta* bacteremia. *Journal of Clinical Microbiology*, *53*(2), 626–635. https://doi.org/10.1128/JCM.02926-14

Genthner, B. R., Davis, C. L., & Bryant, M. P. (1981). Features of rumen and sewage sludge strains of *Eubacterium limosum*, a methanol- and H_2-CO_2-utilizing species. *Applied and Environmental*

Microbiology, *42*(1), 12–19. https://doi.org/10.1128/aem.42.1.12-19.1981

Georgiadis, A. G., Charisiou, N. D., & Goula, M. A. (2020). Removal of hydrogen sulfide from various industrial gases: A review of the most promising adsorbing materials. *Catalysts*, *10*(5). https://doi.org/10.3390/catal10050521

Gildemyn, S., Verbeeck, K., Slabbinck, R., Andersen, S. J., Prévoteau, Antonin, & Rabaey, K. (2015). Integrated production, extraction, and concentration of acetic acid from CO_2 through microbial electrosynthesis. *Environmental Science and Technology Letters*, *2*, 325–328.

Gonzalez-Gil, G., Kleerebezem, R., & Lettinga, G. (2000). Formaldehyde toxicity in anaerobic systems. *Water Science and Technology*, *42*(5–6), 223–229. https://doi.org/10.2166/wst.2000.0517

Greenberg, A. E., Clesceri, L. S., & Eaton, A. D. (1992). *Standard methods for the examination of water and wastewater*. (E. A. Greenberg AE, Clesceri LS, Ed.)*American Public Health Association Publications*. Washington. https://doi.org/10.1109/TMAG.1984.1063378

Grethlein, A. J., Soni, B. K., Worden, R. M., & Jain, M. K. (1992). Influence of hydrogen sulfide on the growth and metabolism of *Butyribacterium methylotrophicum* and *Clostridium acetobutylicum*. *Applied Biochemistry and Biotechnology*, *34–35*(1), 233–246. https://doi.org/10.1007/BF02920548

Grimalt-Alemany, A., Skiadas, I. V, & Gavala, H. N. (2018). Syngas biomethanation: state-of-the-art review and perspectives. *Biofuels, Bioproducts & Biorefining*, *12*, 139–158. https://doi.org/10.1002/bbb.1826

Guidotti, T. L. (2010). Hydrogen sulfide: Advances in understanding human toxicity. *International Journal of Toxicology*, *29*(6), 569–581. https://doi.org/10.1177/1091581810384882

Guo, K., Donose, B. C., Soeriyadi, A. H., Prévoteau, A., Patil, S. A., Freguia, S., et al. (2014). Flame oxidation of stainless steel felt enhances anodic biofilm formation and current output in bioelectrochemical systems. *Environ. Sci. Technol.*, *48*, 7151–7156.

Guo, Q., Qi, G., & Liu, Y. (2018). Study on the selective absorption of hydrogen sulfide from coal gas with high gravity technology. *Chemical Engineering Transactions*, *69*, 187–192. https://doi.org/10.3303/CET1869032

Habeeb, O. A., Kanthasamy, R., Ali, G. A. M., Sethupathi, S., & Yunus, R. B. M. (2018). Hydrogen sulfide emission sources, regulations, and removal techniques: A review. *Reviews in Chemical Engineering*, *34*(6), 837–854. https://doi.org/10.1515/revce-2017-0004

Hädrich, A., Heuer, V. B., Herrmann, M., Hinrichs, K. U., & Küsel, K. (2012). Origin and fate of acetate in an acidic fen. *FEMS Microbiology Ecology*, *81*(2), 339–354.

https://doi.org/10.1111/j.1574-6941.2012.01352.x

Hahne, F., LeMeur, N., Brinkman, R. R., Ellis, B., Haaland, P., Sarkar, D., et al. (2009). flowCore: A Bioconductor package for high throughput flow cytometry. *BMC Bioinformatics*, *10*, 106. https://doi.org/10.1186/1471-2105-10-106

Hamilton, I. C., & Woods, R. (1983). An investigation of the deposition and reactions of sulphur on gold electrodes. *Journal of Applied Electrochemistry*, *13*, 783–794.

Handler, R. M., Shonnard, D. R., Griffing, E. M., Lai, A., & Palou-Rivera, I. (2016). Life cycle assessments of ethanol production via gas fermentation: Anticipated greenhouse gas emissions for cellulosic and waste gas feedstocks. *Industrial and Engineering Chemistry Research*, *55*(12), 3253–3261. https://doi.org/10.1021/acs.iecr.5b03215

Harris, S. C., Devendran, S., Méndez- García, C., Mythen, S. M., Wright, C. L., Fields, C. J., et al. (2018). Bile acid oxidation by *Eggerthella lenta* strains C592 and DSM 2243 T. *Gut Microbes*, *9*(6), 523–539. https://doi.org/10.1080/19490976.2018.1458180

Hartle, M. D., & Pluth, M. D. (2016). A practical guide to working with H_2S at the interface of chemistry and biology. *Chemical Society Reviews*, *45*(22), 6108–6117. https://doi.org/10.1117/12.2549369.Hyperspectral

Hawari, A., Ramadan, H., Abu-Reesh, I., & Ouederni, M. (2015). A comparative study of the treatment of ethylene plant spent caustic by neutralization and classical and advanced oxidation. *Journal of Environmental Management*, *151*, 105–112. https://doi.org/10.1016/j.jenvman.2014.12.038

Hedderich, R., Klimmek, O., Kröger, A., Dirmeier, R., Keller, M., & Stetter, K. O. (1999). Anaerobic respiration with elemental sulfur and with disulfides. *FEMS Microbiology Reviews*, *22*, 353–381.

Heffernan, J. K., Valgepea, K., Lemgruber, R. de S. P., Casini, I., Plan, M., Tappel, R., et al. (2020). Enhancing CO_2-valorization using *Clostridium autoethanogenum* for sustainable fuel and chemicals production. *Frontiers in Bioengineering and Biotechnology*, *8*(March), 204. https://doi.org/10.3389/fbioe.2020.00204

Heijstra, B. D., Leang, C., & Juminaga, A. (2017). Gas fermentation: Cellular engineering possibilities and scale up. *Microbial Cell Factories*, *16*(1), 1–11. https://doi.org/10.1186/s12934-017-0676-y

Heijthuijsen, J. H. F. G., & Hansen, T. A. (1989). Selection of sulphur sources for the growth of *Butyribacterium methylotrophicum* and *Acetobacterium woodii*. *Applied Microbiology and Biotechnology*, *32*, 186–192.

Heyse, J., Buysschaert, B., Props, R., Rubbens, P., Skirtach, A. G., Waegeman, W., & Boon, N.

(2019). Coculturing bacteria leads to reduced phenotypic heterogeneities. *Applied and Environmental Microbiology*, *85*(8), 1–13. https://doi.org/10.1128/AEM.02814-18

Howsley, R., & Pearson, H. W. (1979). pH dependent sulphide toxicity to oxygenic photosynthesis in cyanobacteria. *FEMS Microbiology Letters*, *6*, 287–292.

Huertas, J. K., Quipuzco, L., Hassanein, A., & Lansing, S. (2020). Comparing hydrogen sulfide removal efficiency in a field-scale digester using microaeration and iron filters. *Energies*, *13*(18). https://doi.org/10.3390/en13184793

Hydrogen Council. (2020). *Path to hydrogen competitiveness: a cost perspective*. www.hydrogencouncil.com.

Hylemon, P. B., Harris, S. C., & Ridlon, J. M. (2018). Metabolism of hydrogen gases and bile acids in the gut microbiome. *FEBS Letters*, *592*(12), 2070–2082. https://doi.org/10.1002/1873-3468.13064

ICIS. (2020). Caustic soda prices, markets & analysis - Market overview updated to Q3 2020. https://www.icis.com/explore/commodities/chemicals/caustic-soda/. Accessed 6 January 2021

IEA. (2019). *The future of hydrogen*. https://doi.org/10.1016/S1464-2859(12)70027-5

IEA. (2020). *Renewables 2020, Analysis and forecast to 2025*.

IMO. (2020). Sulphur 2020 - cutting sulphur oxide emissions. http://www.imo.org/en/mediacentre/hottopics/pages/sulphur-2020.aspx. Accessed 5 January 2021

Ingimundarson, A., Arnarson, M. Þ., Sighvatsson, H., & Gunnarsson, T. (2015). Design of a H_2S absorption column at the Hellisheiði powerplant. In *Proceedings World Geothermal Congress* (pp. 1–5).

Isa, Z., Grusenmeyer, S., & Willy Verstraete. (1986). Sulfate reduction relative to methane production in high-rate anaerobic digestion: Microbiological aspects. *Applied and Environmental Microbiology*, *51*(3), 580–587. https://doi.org/10.1128/aem.51.3.572-579.1986

James F. McGehee. (n.d.). MERICON™: A Practical Low Cost Solution to Spent Caustics Treating. http://www.merichem.com/MERICON-Low-Cost-Spent-Caustic-Treating-Solution. Accessed 25 March 2019

Janssen, A. J. H., Lens, P. N. L., Stams, A. J. M., Plugge, C. M., Sorokin, D. Y., Muyzer, G., et al. (2009). Application of bacteria involved in the biological sulfur cycle for paper mill effluent purification. *Science of the Total Environment, The*, *407*(4), 1333–1343.

Jiang, Jingjing, Chan, A., Ali, S., Saha, A., Haushalter, K. J., Lam, W. L. M. R., et al. (2016).

Hydrogen sulfide-mechanisms of toxicity and development of an antidote. *Scientific Reports*, *6*(October 2015), 1–10. https://doi.org/10.1038/srep20831

Jiang, Juyuan, Hu, J., Cui, M., & Tian, H. (2012). Integration of hydrogen production and waste heat recovery in electrochemical wastewater treatment. *Renewable Energy*, *43*, 179–182.

Jiang, Y., Chu, N., Qian, D. K., & Jianxiong Zeng, R. (2020). Microbial electrochemical stimulation of caproate production from ethanol and carbon dioxide. *Bioresource Technology*, *295*(September 2019), 122266. https://doi.org/10.1016/j.biortech.2019.122266

Jin, R.-C., Yang, G.-F., Zhang, Q.-Q., Ma, C., Yu, J.-J., & Xing, B.-S. (2013). The effect of sulfide inhibition on the ANAMMOX process. *Water Research*, *47*, 1459–1469. https://doi.org/10.1016/j.watres.2012.12.018

Jonathan Chou. (2018). NE Asia caustic soda hits 28-month low on strong selling pressure. *ICIS*. https://www.icis.com/explore/resources/news/2018/12/05/10290679/ne-asia-caustic-soda-hits-28-month-low-on-strong-selling-pressure/. Accessed 25 March 2017

Jörissen, J., & Simmrock, K. H. (1991). The behaviour of ion exchange membranes in electrolysis and electrodialysis of sodium sulphate. *Journal of applied electrochemistry*, *21*, 869–876. https://doi.org/10.1007/BF01042453

Joye, S. B., & Hollibaugh, J. T. (1995). Influence of sulfide inhibition of nitrification on nitrogen regeneration in sediments. *Science*, *270*(5236), 623–625. https://doi.org/10.1126/science.270.5236.623

Jüttner, K. (2007). *Technical scale of electrochemistry, Encyclopedia of electrochemistry*. (A.J. Bard & M. Stratmann, Eds.)*Encyclopedia of Electrochemistry*. Weinheim: Wiley-VCH Verlag GmBH & Co. KGaA. https://doi.org/10.1002/9783527610426.bard050001

Kaden, J., Galushko, A. S., & Schink, B. (2002). Cysteine-mediated electron transfer in syntrophic acetate oxidation by cocultures of *Geobacter sulfurreducens* and *Wolinella succinogenes*. *Archives of Microbiology*, *178*, 53–58. https://doi.org/10.1007/s00203-002-0425-3

Kantzow, C., Mayer, A., & Weuster-Botz, D. (2015). Continuous gas fermentation by *Acetobacterium woodii* in a submerged membrane reactor with full cell retention. *Journal of Biotechnology*, *212*, 11–18. https://doi.org/10.1016/j.jbiotec.2015.07.020

Karlsdottir, M. R., Heinonen, J., Palsson, H., & Palsson, O. P. (2020). Life cycle assessment of a geothermal combined heat and power plant based on high temperature utilization. *Geothermics*, *84*(January 2019), 101727. https://doi.org/10.1016/j.geothermics.2019.101727

Katsounaros, I., Cherevko, S., Zeradjanin, A. R., & Mayrhofer, K. J. J. (2014). Oxygen

electrochemistry as a cornerstone for sustainable energy conversion. *Angewandte Chemie International Edition*, *53*, 102–121.

Keller-Lehmann, B., Corrie, S., Ravn, R., Yuan, Z., & Keller, J. (2006). Preservation and simultaneous analysis of relevant soluble sulfur species in sewage samples. *Proceedings of the Second International IWA Conference on Sewer Operation and Maintenance*, 26–28.

Kelley, J. L., Arias-Rodriguez, L., Patacsil Martin, D., Yee, M. C., Bustamante, C. D., & Tobler, M. (2016). Mechanisms underlying adaptation to life in hydrogen sulfide-rich environments. *Molecular Biology and Evolution*, *33*(6), 1419–1434. https://doi.org/10.1093/molbev/msw020

Khanongnuch, R., Di Capua, F., Lakaniemi, A. M., Rene, E. R., & Lens, P. N. L. (2019). Transient–state operation of an anoxic biotrickling filter for H_2S removal. *Journal of Hazardous Materials*, *377*(3), 42–51. https://doi.org/10.1016/j.jhazmat.2019.05.043

Kharafi, F. M. Al, Saad, A. Y., Ateya, B. G., & Ghayad, I. M. (2010). Electrochemical oxidation of sulfide ions on platinum electrodes. *Modern Applied Science*, *4*(3), 2–11.

Kim, J., Darlington, A., Salvador, M., Utrilla, J., & Jiménez, J. I. (2020). Trade-offs between gene expression, growth and phenotypic diversity in microbial populations. *Current Opinion in Biotechnology*, *62*, 29–37. https://doi.org/10.1016/j.copbio.2019.08.004

Kim, K., & Han, J. I. (2014). Performance of direct alkaline sulfide fuel cell without sulfur deposition on anode. *International Journal of Hydrogen Energy*, *39*(13), 7142–7146. https://doi.org/10.1016/j.ijhydene.2014.02.085

Klans Jüttner. (2007). Technical Scale of Electrochemistry. In P. S. AJ Bard, M Stratmann, D McDonald (Ed.), *Encyclopedia of Electrochemistry, vol.5, Electrochemical Engineering* (Vol. 5).

Kleerebezem, R., & van Loosdrecht, M. C. (2007). Mixed culture biotechnology for bioenergy production. *Current Opinion in Biotechnology*, *18*(3), 207–212. https://doi.org/10.1016/j.copbio.2007.05.001

Klindworth, A., Pruesse, E., Schweer, T., Peplies, J., Quast, C., Horn, M., & Glöckner, F. O. (2013). Evaluation of general 16S ribosomal RNA gene PCR primers for classical and next-generation sequencing-based diversity studies. *Nucleic Acids Research*, *41*(1), 1–11. https://doi.org/10.1093/nar/gks808

Kohl, A. L., & Nielsen, R. B. (1997). Sulfur Recovery Processes. In *Gas Purification* (pp. 670–730). https://doi.org/10.1016/b978-088415220-0/50008-2

Koster, I. W., Rinzema, A., Vegt, A. L. De, & Lettinga, G. (1986). Sulfide inhibition of the methanogenic activity of granular sludge at various pH-levels. *Water Research*, *20*(12), 1561–1567.

Kozich, J. J., Westcott, S. L., Baxter, N. T., Highlander, S. K., & Schloss, P. D. (2013). Development of a dual-index sequencing strategy and curation pipeline for analyzing amplicon sequence data on the MiSeq Illumina sequencing platform. *Applied and Environmental Microbiology*, *79*(17), 5112–5120. https://doi.org/10.1128/AEM.01043-13

Kristmannsdóttir, H., Sigurgeirsson, M., Ármannsson, H., Hjartarson, H., & Ólafsson, M. (2000). Sulfur gas emissions from geothermal power plants in Iceland. *Geothermics*, *29*, 525–538.

Küster, E., Dorusch, F., & Altenburger, R. (2005). Effects of hydrogen sulfide to *Vibrio fischeri*, *Scenedesmus vacuolatus*, and *Daphnia magna*. *Environmental Toxicology and Chemistry*, *24*(10), 2621–2629.

Lawrence, N. S., Thompson, M., Prado, C., Jiang, L., Jones, T. G. J., & Compton, R. G. (2002). Amperometric detection of sulfide at a boron doped diamond electrode: The electrocatalytic reaction of sulfide with ferricyanide in aqueous solution . *Electroanalysis*, *14*, 499–504.

Lebrero, R., Bouchy, L., Stuetz, R., & Muñoz, R. (2011). Odor assessment and management in wastewater treatment plants: A review. *Critical Reviews in Environmental Science and Technology*, *41*, 915–950. https://doi.org/10.1080/10643380903300000

Lei, Y., Remmers, J. C., Saakes, M., Van Der Weijden, R. D., & Buisman, C. J. N. (2019). Influence of cell configuration and long-term operation on electrochemical phosphorus recovery from domestic wastewater. *ACS Sustainable Chemistry and Engineering*, *7*(7), 7362–7368. https://doi.org/10.1021/acssuschemeng.9b00563

Lemmens, B., Ceulemans, J., Elsland, H., Vanassche, S., Brauns, E., & Vrancken, K. (2007). Beste Beschikbare Technieken (BBT) voor mestverwerking. *Academia Press*, 335.

Lens, P. N.L., Gastesi, R., & Lettinga, G. (2003). Use of sulfate reducing cell suspension bioreactors for the treatment of SO_2 rich flue gases. *Biodegradation*, *14*(3), 229–240. https://doi.org/10.1023/A:1024222020924

Lens, P N L, Visser, A., Janssen, A. J. H., Pol, L. W. H., & Lettinga, G. (1998). Biotechnological treatment of sulfate-rich wastewaters. *Critical Reviews in Environmental Science and Technology*, *28*(1), 41–88.

Lenz, M., Janzen, N., & Lens, P. N. L. (2008). Selenium oxyanion inhibition of hydrogenotrophic and acetoclastic methanogenesis. *Chemosphere*, *73*(3), 383–388. https://doi.org/10.1016/j.chemosphere.2008.05.059

Levillain, E., Demortier, A., & Lelieur, J. P. (2006). Sulfur. In W. E. Geiger & C. Pickett (Eds.), *Encyclopedia of Electrochemistry, Inorganic Electrochemistry, colume 7* (pp. 253–271). Wiley.

Lewis, A. E. (2010). Review of metal sulphide precipitation. *Hydrometallurgy*, *104*(September 2010),

222–234. https://doi.org/10.1016/j.hydromet.2010.06.010

Li, Y., He, D., Niu, D., & Zhao, Y. (2015). Acetic acid production from food wastes using yeast and acetic acid bacteria micro-aerobic fermentation. *Bioprocess and Biosystems Engineering*, *38*(5), 863–869. https://doi.org/10.1007/s00449-014-1329-8

Lide, D. R. (2004). *CRC Handbook of Chemistry and Physics*. *CRC Press* (84th ed.). https://doi.org/10.1016/0022-2860(92)85083-s

Liew, F., Martin, M. E., Tappel, R. C., Heijstra, B. D., Mihalcea, C., & Köpke, M. (2016). Gas fermentation — A flexible platform for commercial scale production of low-carbon-fuels and chemicals from waste and renewable feedstocks. *Frontiers in Microbiology*, *7*(May), 694. https://doi.org/10.3389/fmicb.2016.00694

Lin, H.-W., Cejudo-Marín, R., Jeremiasse, A. W., Rabaey, K., Yuan, Z., & Pikaar, I. (2016). Direct anodic hydrochloric acid and cathodic caustic production during water electrolysis. *Scientific Reports*, *6:20494*(February), 1–4. https://doi.org/10.1038/srep20494

Lin, H., Williams, N., King, A., & Hu, B. (2016). Electrochemical sulfide removal by low-cost electrode materials in anaerobic digestion, *297*, 180–192. https://doi.org/10.1016/j.cej.2016.03.086

Lin, S. H., & Peng, C. F. (1994). Treatment of textile wastewater by electrochemical method. *Water Research*, *28*(2), 277–282. https://doi.org/10.1016/0043-1354(94)90264-X

Liu, Y., & Whitman, W. B. (2008). Metabolic, phylogenetic, and ecological diversity of the methanogenic archaea. *Annals of the New York Academy of Sciences*, *1125*, 171–189. https://doi.org/10.1196/annals.1419.019

Lloyd, K. G., Edgcomb, V. P., Molyneaux, S. J., Bo, S., Wirsen, C. O., Atkins, M. S., & Teske, A. (2005). Effects of dissolved sulfide, pH, and temperature on growth and survival of marine hyperthermophilic archaea. *Applied and Environmental Microbiology*, *71*(10), 6383–6387. https://doi.org/10.1128/AEM.71.10.6383

Logan, B. E., Hamelers, B., Rozendal, R., Schröder, U., Keller, J., Freguia, S., et al. (2006). Microbial fuel cells: Methodology and technology. *Environmental Science and Technology*, *40*(17), 5181–5192. https://doi.org/10.1021/es0605016

Lovell, C. R., & Leaphart, A. B. (2005). Community-level analysis: Key genes of CO_2-reductive acetogenesis. *Methods in Enzymology*, *397*(2004), 454–469. https://doi.org/10.1016/S0076-6879(05)97028-6

Lucile, F., Cézac, P., Contamine, F., Serin, J. P., Houssin, D., & Arpentinier, P. (2012). Solubility of carbon dioxide in water and aqueous solution containing sodium hydroxide at temperatures

from (293.15 to 393.15) K and pressure up to 5 MPa: Experimental measurements. *Journal of Chemical and Engineering Data*, *57*(3), 784–789. https://doi.org/10.1021/je200991x

Lv, Z., Leite, A. F., Harms, H., Glaser, K., Liebetrau, J., Kleinsteuber, S., & Nikolausz, M. (2019). Microbial community shifts in biogas reactors upon complete or partial ammonia inhibition. *Applied Microbiology and Biotechnology*, *103*(1), 519–533. https://doi.org/10.1007/s00253-018-9444-0

Mamrosh, D., McIntush, K., & Fisher, K. (2014). Caustic scrubber designs for H_2S removal from refinery gas streams. *American Fuel and Petrochemical Manufacturers, AFPM - AFPM Annual Meeting 2014*, (January 2014), 671–698.

Mandal, B. P., Biswas, A. K., & Bandyopadhyay, S. S. (2004). Selective absorption of H_2S from gas streams containing H_2S and CO_2 into aqueous solutions of N-methyldiethanolamine and 2-amino-2-methyl-1-propanol. *Separation and Purification Technology*, *35*, 191–202. https://doi.org/10.1016/S1383-5866(03)00139-4

Mao, Z., Anani, A., White, R. E., A, S., & Appleby, A. J. (1991). A modified electrochemical process for the decomposition of hydrogen sulfide in an aqueous alkaline solution. *Journal of The Electrochemical Society*, *138*(5), 1299–1303. https://doi.org/10.1149/1.2085775

Marshall, C. W., Ross, D. E., Handley, K. M., Weisenhorn, P. B., Edirisinghe, J. N., Henry, C. S., et al. (2017). Metabolic reconstruction and modeling microbial electrosynthesis. *Scientific Reports*, *7*(1), 8391. https://doi.org/10.1038/s41598-017-08877-z

Martelli, G. N., Ornelas, R., & Faita, G. (1994). Deactivation mechanisms of oxygen evolving anodes at high current densities. *Electrochimica Acta*, *39*, 1551–1558.

Martinez-Fernandez, G., Denman, S. E., Yang, C., Cheung, J., Mitsumori, M., & McSweeney, C. S. (2016). Methane inhibition alters the microbial community, hydrogen flow, and fermentation response in the rumen of cattle. *Frontiers in Microbiology*, *7*(JUL), 1122. https://doi.org/10.3389/fmicb.2016.01122

May, P. M., Batka, D., Hefter, G., Königsberger, E., & Rowland, D. (2018). Goodbye to S^{2-} in aqueous solution. *Chemical Communications*, *54*, 1980–1983. https://doi.org/10.1039/c8cc00187a

McCartney, D. M., & Oleszkiewicz, J. A. (1991). Sulfide inhibition of anaerobic degradation of lactate and acetate. *Water Research*, *25*(2), 203–209.

McCrory, C. C. L., Jung, S., Peters, J. C., & Jaramillo, T. F. (2013). Benchmarking heterogeneous electrocatalysts for the oxygen evolution reaction. *J. Am. Chem. Soc.*, *135*, 16977–16987.

Mcintush, K. E., Fisher, K., & Beitler, C. A. M. (2013). Caustic scrubber designs for refinery fuel gas ,

sour water stripper gas , and other refinery applications. *LRGCC Conference Proceedings*, (September), 215–240.

McMurdie, P. J., & Holmes, S. (2013). Phyloseq: An R package for reproducible interactive analysis and graphics of microbiome census data. *PLoS ONE*, *8*(4), e61217. https://doi.org/10.1371/journal.pone.0061217

McMurdie, P. J., & Holmes, S. (2014). Waste not, want not: Why rarefying microbiome data is inadmissible. *PLoS Comput Biol*, *10*(4), e1003531.

Mendoza, P. G., Moshtarikhah, S., Langenhan, A. S., Groot, M. T. de, Keurentjes, J. T. F., Schouten, J. C., & Schaaf, J. van der. (2017). Intensification of the chlor-alkali process by using a spinning disc membrane electrolyzer. *Chemical Engineering Research and Design*, *128*(2017), 120–129. https://doi.org/10.1016/j.cherd.2017.10.001

Merino, N., Kawai, M., Boyd, E. S., Colman, D. R., McGlynn, S. E., Nealson, K. H., et al. (2020). Single-cell genomics of novel *Actinobacteria* with the Wood–Ljungdahl pathway discovered in a serpentinizing system. *Frontiers in Microbiology*, *11*(June), 1–21. https://doi.org/10.3389/fmicb.2020.01031

Miller, B., & Chen, A. (2005). Effect of concentration and temperature on electrochemical oscillations during sulfide oxidation on Ti/Ta_2O_5–IrO_2 electrodes. *Electrochimica Acta*, *50*, 2203–2212.

Miller, B., & Chen, A. (2006). Oscillatory instabilities during the electrochemical oxidation of sulfide on a Pt electrode. *Journal of electroanalytical chemistry*, *588*, 314–323. https://doi.org/10.1016/j.jelechem.2006.01.006

Mirzoyan, N., & Schreier, H. J. (2014). Effect of sulfide on growth of marine bacteria. *Archives of Microbiology*, *196*(4), 279–287. https://doi.org/10.1007/s00203-014-0968-0

Mochizuki, Y., & Tsubouchi, N. (2017). Removal of hydrogen sulfide in simulated coke oven gas with low-grade iron ore. *Energy Fuels*, *31*, 8087–8094.

Moioli, S., & Pellegrini, L. A. (2013). Regeneration section of CO_2 capture plant by MEA scrubbing with a rate-based model. *Chemical Engineering Transactions*, *32*, 1849–1854. https://doi.org/10.3303/CET1332309

Moioli, S., Pellegrini, L. A., Picutti, B., & Vergani, P. (2013). Improved rate-based modeling of H_2S and CO_2 removal by methyldiethanolamine scrubbing. *Industrial and Engineering Chemistry Research*, *52*(5), 2056–2065. https://doi.org/10.1021/ie301967t

Molitor, B., Richter, H., Martin, M. E., Jensen, R. O., Juminaga, A., Mihalcea, C., & Angenent, L. T. (2016). Carbon recovery by fermentation of CO-rich off gases - Turning steel mills into

biorefineries. *Bioresource Technology*, *215*, 386–396. https://doi.org/10.1016/j.biortech.2016.03.094

Monaco, G., Chen, H., Poidinger, M., Chen, J., De Magalhães, J. P., & Larbi, A. (2016). FlowAI: Automatic and interactive anomaly discerning tools for flow cytometry data. *Bioinformatics*, *32*(16), 2473–2480. https://doi.org/10.1093/bioinformatics/btw191

Moo, J. G. S., Omar, A., Jaumann, T., Oswald, S., Balach, J., Maletti, S., & Giebeler, L. (2018). One-pot synthesis of graphene-sulfur composites for Li-S batteries: Influence of sulfur precursors. *Journal of Carbon Research*, *4*, 1–17.

Moussa, D. T., El-Naas, M. H., Nasser, M., & Al-Marri, M. J. (2017). A comprehensive review of electrocoagulation for water treatment: Potentials and challenges. *Journal of Environmental Management*, *186*, 24–41. https://doi.org/10.1016/j.jenvman.2016.10.032

Mukherjee, A., Lordan, C., Ross, R. P., & Cotter, P. D. (2020). Gut microbes from the phylogenetically diverse genus *Eubacterium* and their various contributions to gut health. *Gut Microbes*, *12*(1), e1802866-28. https://doi.org/10.1080/19490976.2020.1802866

Müller, V. (2019). New horizons in acetogenic conversion of one-carbon substrates and biological hydrogen storage. *Trends in Biotechnology*, *37*(12), 1344–1354. https://doi.org/10.1016/j.tibtech.2019.05.008

Müller, V., Chowdhury, N. P., & Basen, M. (2018). Electron bifurcation: A long-hidden energy-coupling mechanism. *Annual Review of Microbiology*, *72*, 331–353. https://doi.org/10.1146/annurev-micro-090816-093440

Myers, J. A., Curtis, B. S., & Curtis, W. R. (2013). Improving accuracy of cell and chromophore concentration measurements using optical density. *BMC Biophysics*, *6*(1), 4. https://doi.org/10.1186/2046-1682-6-4

Niknam, P. H., Talluri, L., Fiaschi, D., & Manfrida, G. (2020). Gas purification process in a geothermal power plant with total reinjection designed for the Larderello area. *Geothermics*, *88*(January), 101882. https://doi.org/10.1016/j.geothermics.2020.101882

NIOSH. (2011). Hydrogen Sulfide. *Centers for Disease Control and Prevention*. https://www.cdc.gov/niosh/pel88/7783-06.html#:~:text=OSHA has accordingly established an,Poda and Aiken 1966%2F Ex. Accessed 19 January 2021

North-CCU-Hub. (2021). North-C-methanol. https://northccuhub.eu/north-c-methanol/. Accessed 6 January 2021

Nozaki, K. (1982). Fuel cell.

Nuñez, P., Hansen, H. K., Rodriguez, N., Guzman, J., & Gutierrez, C. (2009). Electrochemical

generation of Fenton's reagent to treat spent caustic wastewater. *Separation Science and Technology*, *44*, 2223–2233. https://doi.org/10.1080/01496390902979545

O'Flaherty, V, Lens, P., Leahy, B., & Colleran, E. (1998). Long-term competition between sulphate-reducing and methane-producing bacteria during full-scale anaerobic treatment of citric acid production wastewater. *Water Research*, *32*(3), 815–825.

O'Flaherty, Vincent, Mahony, T., O'Kennedy, R., & Colleran, E. (1998). Effect of pH on growth kinetics and sulphide toxicity thresholds of a range of methanogenic , syntrophic and sulphate-reducing bacteria. *Process Biochemistry*, *33*(5), 555–569.

Olivier, J. G. J., & J.A.H.W, P. (2020). *Trends in global CO_2 and total greenhouse gas emissions* (Vol. 2020). https://www.pbl.nl/sites/default/files/downloads/pbl-2020-trends-in-global-co2-and-total-greenhouse-gas-emissions-2019-report_4068.pdf

Osorio, F., & Torres, J. C. (2009). Biogas purification from anaerobic digestion in a wastewater treatment plant for biofuel production. *Renewable Energy*, *34*(10), 2164–2171. https://doi.org/10.1016/j.renene.2009.02.023

Ottesen, E. A., & Leadbetter, J. R. (2010). Diversity of formyltetrahydrofolate synthetases in the guts of the wood-feeding cockroach *Cryptocercus punctulatus* and the omnivorous cockroach *Periplaneta americana*. *Applied and Environmental Microbiology*, *76*(14), 4909–4913. https://doi.org/10.1128/AEM.00299-10

Pan, Y., Ye, L., & Yuan, Z. (2013). Effect of H_2S on N_2O reduction and accumulation during denitrification by methanol utilizing denitrifiers. *Environmental Science & Technology*, *47*, 8408–8415. https://doi.org/10.1021/es401632r

Parameswaran, P., Zhang, H., Torres, C. I., Rittmann, B. E., & Krajmalnik-Brown, R. (2010). Microbial community structure in a biofilm anode fed with a fermentable substrate : The significance of hydrogen scavengers. *Biotechnology and Bioengineering*, *105*(1), 69–78. https://doi.org/10.1002/bit.22508

Park, S., Yasin, M., Jeong, J., Cha, M., Kang, H., Jang, N., et al. (2017). Acetate-assisted increase of butyrate production by *Eubacterium limosum* KIST612 during carbon monoxide fermentation. *Bioresource Technology*, *245*(June), 560–566. https://doi.org/10.1016/j.biortech.2017.08.132

Patil, S. A., Arends, J. B. A., Vanwonterghem, I., Meerbergen, J. Van, Guo, K., Tyson, G. W., & Rabaey, K. (2015). Selective enrichment establishes a stable performing community for microbial electrosynthesis of acetate from CO_2. *Environmental Science and Technology*, *49*(14), 8833–8843. https://doi.org/10.1021/es506149d

Pedizzi, C., Regueiro, L., Rodriguez-Verde, I., Lema, J. M., & Carballa, M. (2016). Effect of oxygen on the microbial activities of thermophilic anaerobic biomass. *Bioresource Technology*, *211*,

765–768. https://doi.org/10.1016/j.biortech.2016.03.085

Perez, T. E. (2013). Corrosion in the oil and gas industry: An increasing challenge for materials. *JOM*, *65*(8), 1033–1042. https://doi.org/10.1007/s11837-013-0675-3

Perrin, D. (1982). *Ionisation constants of inorganic acids and bases in aqueous solution* (2nd editio.). Pergamon Press.

Petrov, K., & Srinivasan, S. (1996). Low temperature removal of hydrogen sulfide from sour gas and its utilization for hydrogen and sulfur production. *International Journal of Hydrogen Energy*, *21*(3), 163–169. https://doi.org/10.1016/0360-3199(95)00003-8

Philips, J. (2020). Extracellular electron uptake by acetogenic bacteria: Does H_2 consumption favor the H_2 evolution reaction on a cathode or metallic iron? *Frontiers in Microbiology*, *10*(January), 1–13. https://doi.org/10.3389/fmicb.2019.02997

Pikaar, I., Li, E., Rozendal, R. A., Yuan, Z., Keller, J., & Rabaey, K. (2012). Long-term field test of an electrochemical method for sulfide removal from sewage. *Water Research*, *46*(9), 3085–3093. https://doi.org/10.1016/j.watres.2012.03.013

Pikaar, I., Likosova, E. M., Freguia, S., Keller, J., Rabaey, K., & Yuan, Z. (2015). Electrochemical abatement of hydrogen sulfide from waste streams. *Critical Reviews in Environmental Science and Technology*, *45*(November), 1555–1578. https://doi.org/10.1080/10643389.2014.966419

Pikaar, I., Rozendal, R. A., Rabaey, K., & Yuan, Z. (2013). In-situ caustic generation from sewage: The impact of caustic strength and sewage composition. *Water Research*, *47*(15), 5828–5835. https://doi.org/10.1016/j.watres.2013.07.007

Pikaar, I., Rozendal, R. A., Yuan, Z., Keller, J., & Rabaey, K. (2011a). Electrochemical sulfide removal from synthetic and real domestic wastewater at high current densities. *Water Research*, *45*(6), 2281–2289. https://doi.org/10.1016/j.watres.2010.12.025

Pikaar, I., Rozendal, R. A., Yuan, Z., Keller, J., & Rabaey, K. (2011b). Electrochemical sulfide oxidation from domestic wastewater using mixed metal-coated titanium electrodes. *Water Research*, *45*, 5381–5388. https://doi.org/10.1016/j.watres.2011.07.033

Pokhrel, D., & Viraraghavan, T. (2004). Treatment of pulp and paper mill wastewater — a review. *Science of the Total Environment*, *333*, 37–58. https://doi.org/10.1016/j.scitotenv.2004.05.017

Pourbaix, M. (1966). *Atlas of electrochemical equilibria in aqueous solutions*. Pergamon, Oxford.

Prest, E. I., Hammes, F., Kötzsch, S., Loosdrecht, M. C. M. Van, & Vrouwenvelder, J. S. (2013). Monitoring microbiological changes in drinking water systems using a fast and reproducible

flow cytometric method. *Water Research*, *47*, 7131–7142. https://doi.org/10.1016/j.watres.2013.07.051

Prévoteau, A., Carvajal-Arroyo, J. M., Ganigué, R., & Rabaey, K. (2020). Microbial electrosynthesis from CO_2: forever a promise? *Current Opinion in Biotechnology*, *62*, 48–57. https://doi.org/10.1016/j.copbio.2019.08.014

Props, R., Monsieurs, P., Mysara, M., Clement, L., & Boon, N. (2016). Measuring the biodiversity of microbial communities by flow cytometry. *Methods in Ecology and Evolution*, *7*, 1376–1385. https://doi.org/10.1111/2041-210X.12607

Pulidindi, K., & Pandey, H. (2019). Global Acetic Acid Market Size worth $17.9bn by 2024. *Global Market Insights*. https://www.gminsights.com/pressrelease/acetic-acid-market. Accessed 31 July 2020

R Core Team. (2012). R: A language and environment for statistical computing. R Foundation for Statistical Computing, Vienna, Austria. *ISBN 3-900051-07-0*. https://www.r-project.org/

Rabaey, K., Van de Sompel, K., Maignien, L., Boon, N., Aelterman, P., Clauwaert, P., et al. (2006). Microbial fuel cells for sulfide. *Environmental Science & Technology*, *40*, 5218–5224. https://doi.org/10.1021/es060382u

Radjenovic, J., & Sedlak, D. L. (2015). Challenges and opportunities for electrochemical processes as next- generation technologies for the treatment of contaminated water. *Environmental Science and Technology*, *49*(49), 11292–11302. https://doi.org/10.1021/acs.est.5b02414

Rafferty, J. P. (2020). What happened to Acid Rain? *Encyclopedia Britannica*. https://www.britannica.com/story/what-happened-to-acid-rain. Accessed 17 December 2020

Ragsdale, S. W., & Pierce, E. (2008). Acetogenesis and the Wood-Ljungdahl pathway of CO_2 fixation. *Biochimica et Biophysica Acta - Proteins and Proteomics*, *1784*(12), 1873–1898. https://doi.org/10.1016/j.bbapap.2008.08.012

Rajalo, G., & Petrovskaya, T. (1996). Selective electrochemical oxidation of sulphides in tannery wastewater. *Environmental Technology*, *17*, 605–612.

Ramasubramanian, N. (1975). Anodic behavior of platinum electrodes in sulfide solutions and the formation of platinum sulfide. *Journal of Electroanalytical Chemistry*, *64*, 21–37.

Ramos-Suarez, M., Zhang, Y., & Outram, V. (2021). *Current perspectives on acidogenic fermentation to produce volatile fatty acids from waste*. *Reviews in Environmental Science and Biotechnology* (Vol. 0). Springer Netherlands. https://doi.org/10.1007/s11157-021-09566-0

Rankin, K., Bejan, D., & Bunce, N. J. (2010). Electrochemical oxidation of the sulfide ion in synthetic geothermal brines in batch cells using coke electrodes. *Industrial and Engineering Chemistry*

Research, (49), 6261–6266.

Rehim, S. S. A. El, Ali, L. I., Amin, N. H., & Mohamed, N. F. (1997). Potentiodynamic and cyclic voltammetric behaviour of a lead electrode in NaOH solution. *Monatshefte für Chemie*, *128*, 245–254.

Rehim, S. S. A. El, & Mohamed, N. F. (1998). Passivity breakdown of lead anode in alkaline nitrate solutions. *Corrosion Science*, *40*(11), 1883–1896.

Reis, M. A. M., Almeida, J. S., Lemos, P. C., & Carrondo, M. J. T. (1992). Effect of hydrogen sulfide on growth of sulfate reducing bacteria. *Biotechnology and Bioengineering*, *40*, 593–600.

Richter, H., Martin, M. E., & Angenent, L. T. (2013). A two-stage continuous fermentation system for conversion of syngas into ethanol. *Energies*, *6*(8), 3987–4000. https://doi.org/10.3390/en6083987

Riegler, P., Bieringer, E., Chrusciel, T., Stärz, M., Löwe, H., & Weuster-Botz, D. (2019). Continuous conversion of CO_2/H_2 with *Clostridium aceticum* in biofilm reactors. *Bioresource Technology*, *291*(May), 121760. https://doi.org/10.1016/j.biortech.2019.121760

Ringel, M., Gross, R., Krafft, T., Kröger, A., & Schauder, R. (1996). Growth of *Wolinella succinogenes* with elemental sulfur in the absence of polysulfide. *Archives of Microbiology Microbiol*, *165*, 62–64.

Ritchie, H., & Roser, M. (2016). CO_2 and GHG emissions by sector. *https://ourworldindata.org/emissions-by-sector#energy-electricity-heat-and-transport-73-2*.

Rode, L. M., Genthner, B. R. S. S., Bryant, M. P., Church, L. B., Voordouw, G., Armstrong, S. M., et al. (1981). Gut microbes from the phylogenetically diverse genus *Eubacterium* and their various contributions to gut health. *Applied and Environmental Microbiology*, *62*(1), 314–314. https://doi.org/10.1080/19490976.2020.1802866

Rodríguez, E., Harvey, W. S., & Ásbjörnsson, E. J. (2014). Review of H_2S abatement methods in geothermal plants. In *Thirty-Eighth Workshop on Geothermal Reservoir Engineering, Stanford University* (pp. 1–9).

Rubright, S. L. M., Pearce, L. L., & Peterson, J. (2017). Environmental toxicology of hydrogen sulfide. *Nitric Oxide*, *71*(412), 1–13. https://doi.org/10.1016/j.niox.2017.09.011

S&P Global Platts. (2020). Green hydrogen costs need to fall over 50% to be viable: S&P Global Ratings. https://www.spglobal.com/platts/en/market-insights/latest-news/electric-power/112020-green-hydrogen-costs-need-to-fall-over-50-to-be-viable-sampp-global-ratings. Accessed 7 January 2021

Saad, S. A., Welles, L., Lopez-Vazquez, C. M., Loosdrecht, M. C. M. Van, & Brdjanovic, D. (2017).

Sulfide effects on the anaerobic metabolism of polyphosphate-accumulating organisms. *Chemical Engineering Journal*, *326*, 68–77. https://doi.org/10.1016/j.cej.2017.05.074

Sakarika, M., Candry, P., Depoortere, M., Ganigué, R., & Rabaey, K. (2020). Impact of substrate and growth conditions on microbial protein production and composition. *Bioresource Technology*, *317*(July), 124021. https://doi.org/10.1016/j.biortech.2020.124021

Sander, R. (2015). Compilation of Henry's law constants (version 4.0) for water as solvent. *Atmospheric Chemistry and Physics*, *15*, 4399–4981.

Santos, G. O. S., Silva, L. R. A., Alves, Y. G. S., Silva, R. S., Eguiluz, K. I. B., & Salazar-Banda, G. R. (2019). Enhanced stability and electrocatalytic properties of $Ti/RuxIr_1-xO_2$ anodes produced by a new laser process. *Chemical Engineering Journal*, *355*(July 2018), 439–447. https://doi.org/10.1016/j.cej.2018.08.145

Saxe, M., & Alvfors, P. (2007). Advantages of integration with industry for electrolytic hydrogen production. *Energy*, *32*(1), 42–50. https://doi.org/10.1016/j.energy.2006.01.021

Schievano, A., Pant, D., & Puig, S. (2019). Editorial: Microbial synthesis, gas-fermentation and bioelectroconversion of CO_2 and other gaseous streams. *Frontiers in Energy Research*, *7*(October), 1–4. https://doi.org/10.3389/fenrg.2019.00110

Schloss, P. D., Gevers, D., & Westcott, S. L. (2011). Reducing the effects of PCR amplification and sequencing artifacts on 16S rRNA-based studies. *PLoS ONE*, *6*(12), e27310. https://doi.org/10.1371/journal.pone.0027310

Sekine, M., Akizuki, S., Kishi, M., Kurosawa, N., & Toda, T. (2020). Simultaneous biological nitrification and desulfurization treatment of ammonium and sulfide-rich wastewater: Effectiveness of a sequential batch operation. *Chemosphere*, *244*, 125381. https://doi.org/10.1016/j.chemosphere.2019.125381

Selvaraj, H., Chandrasekaran, K., & Gopalkrishnan, R. (2016). Recovery of solid sulfur from hydrogen sulfide gas by an electrochemical membrane cell. *RSC Advances*, *6*, 3735–3741. https://doi.org/10.1039/C5RA19116E

Sercu, B., Núñez, D., Van Langenhove, H., Aroca, G., & Verstraete, W. (2005). Operational and microbiological aspects of a bioaugmented two-stage biotrickling filter removing hydrogen sulfide and dimethyl sulfide. *Biotechnology and Bioengineering*, *90*(2), 259–269. https://doi.org/10.1002/bit.20443

Sergienko, N., & Radjenovic, J. (2020). Manganese oxide-based porous electrodes for rapid and selective (electro)catalytic removal and recovery of sulfide from wastewater. *Applied Catalysis B: Environmental*, *267*(February), 118608. https://doi.org/10.1016/j.apcatb.2020.118608

Seuntjens, D., Van Tendeloo, M., Chatzigiannidou, I., Carvajal-Arroyo, J. M., Vandendriessche, S., Vlaeminck, S. E., & Boon, N. (2018). Synergistic exposure of return-sludge to anaerobic starvation, sulfide, and free ammonia to suppress nitrite oxidizing bacteria. *Environmental Science and Technology*, *52*(15), 8725–8732. https://doi.org/10.1021/acs.est.7b06591

Shao, D., Li, X., Xu, H., & Yan, W. (2014). An improved stable Ti/Sb-SnO_2 electrode with high performance in electrochemical oxidation processes. *RSC Advances*, *4*, 21230–21237.

Sheu, S. H., & Weng, H. S. (2001). Treatment of olefin plant spent caustic by combination of neutralization and fenton reaction. *Water Research*, *35*(8), 2017–2021. https://doi.org/10.1016/S0043-1354(00)00466-8

Shutske, J., Larson, R., Schaefer, D., Binversie, L., Rifleman, S., & Skjolaas, C. (2017). *Notes from the Field: Death of a Farm Worker After Exposure to Manure Gas in an Open Air Environment — Wisconsin, August 2016*. *MMWR Morb Mortal Wkly Rep*. https://www.cdc.gov/mmwr/volumes/66/wr/mm6632a6.htm#suggestedcitation

Singh, A., & Lal, R. (2009). *Sphingobium ummariense* sp. nov., a hexachlorocyclohexane (HCH)-degrading bacterium, isolated from HCH-contaminated soil. *International Journal of Systematic and Evolutionary Microbiology*, *59*, 162–166. https://doi.org/10.1099/ijs.0.65712-0

Smith, T. J., & Stevenson, K. J. (2007). Reference electrodes. In C. G. Zoski (Ed.), *Handbook of Electrochemistry*. Elsevier.

Solvay S.A. (2018). Solvay to increase prices of hydrogen peroxide. https://www.solvay.com/sites/g/files/srpend221/files/tridion/documents/20180709 PR Solvay to increase prices of hydrogen peroxide.pdf

Song, F., Bai, L., Moysiadou, A., Lee, S., Hu, C., Liardet, L., & Hu, X. (2018). Transition metal oxides as electrocatalysts for the oxygen evolution reaction in alkaline solutions: An application-inspired renaissance. *Journal of the American Chemical Society*, *140*, 7748–7759.

Song, S., Zhang, H., Ma, X., Shao, Z., Baker, R. T., & Yi, B. (2008). Electrochemical investigation of electrocatalysts for the oxygen evolution reaction in PEM water electrolyzers. *International Journal of Hydrogen Energy*, *33*, 4955–4961.

Spöri, C., Kwan, J. T. H., Bonakdarpour, A., Wilkinson, D. P., & Strasser, P. (2017). The stability challenges of oxygen evolving catalysts: Towards a common fundamental understanding and mitigation of catalyst degradation. *Angewandte Chemie - International Edition*, *56*(22), 5994–6021. https://doi.org/10.1002/anie.201608601

Spurgeon, J. M., & Kumar, B. (2018). A comparative technoeconomic analysis of pathways for commercial electrochemical CO_2 reduction to liquid products. *Energy and Environmental Science*, *11*(6), 1536–1551. https://doi.org/10.1039/c8ee00097b

statista. (2020). Prices of electricity for the industry in Belgium from 2008 to 2019. © *Statista 2021*. https://doi.org/10.1787/eco_surveys-prt-2017-graph20-en

Statista. (2019). Price of sulfur in the United States from 2014 to 2019 (in U.S. dollars per ton). *Statista*. https://www.statista.com/statistics/1031180/us-sulfur-price/

Steger, F., Rachbauer, L., Windhagauer, M., Montgomery, L. F. R., & Bochmann, G. (2017). Optimisation of continuous gas fermentation by immobilisation of acetate-producing Acetobacterium woodii. *Anaerobe*, *46*(2017), 96–103. https://doi.org/10.1016/j.anaerobe.2017.06.010

Stephenson, R. L., & James B. Blackburn, J. (1997). *The industrial wastewater systems handbook* (1st ed.). CRC Press.

Steudel, R. (1996). Mechanism for the formation of elemental sulfur from aqueous sulfide in chemical and microbiological desulfurization processes. *Ind. Eng. Chem. Res.*, *35*(4), 1417–1423. https://doi.org/10.1021/ie950558t

Steudel, R. (2020). The chemical sulfur cycle. In Piet N.L. Lens (Ed.), *Environmental Technologies to Treat Sulfur Pollution: Principles and Engineering* (2nd ed., pp. 11–53). IWA Publishing.

Steudel, R., & Chivers, T. (2019). The role of polysulfide dianions and radical anions in the chemical, physical and biological sciences, including sulfur-based batteries. *Chemical Society Reviews*, *48*(12), 3279–3319. https://doi.org/10.1039/c8cs00826d

Straub, M., Demler, M., Weuster-Botz, D., & Dürre, P. (2014). Selective enhancement of autotrophic acetate production with genetically modified *Acetobacterium woodii*. *Journal of Biotechnology*, *178*, 67–72. https://doi.org/10.1016/j.jbiotec.2014.03.005

Sun, L., Toyonaga, M., Ohashi, A., Tourlousse, D. M., Matsuura, N., Meng, X. Y., et al. (2016). *Lentimicrobium saccharophilum* gen. nov., sp. nov., a strictly anaerobic bacterium representing a new family in the phylum bacteroidetes, and proposal of *Lentimicrobiaceae* fam. nov. *International Journal of Systematic and Evolutionary Microbiology*, *66*(7), 2635–2642. https://doi.org/10.1099/ijsem.0.001103

Sun, M., Zhai, L.-F., Li, W.-W., & Yu, H.-Q. (2016). Harvest and utilization of chemical energy in wastes by microbial fuel cells. *Chemical Society Reviews*, *45*, 2847–2870. https://doi.org/10.1039/c5cs00903k

Szpyrkowicz, L., Kaul, S. N., Neti, R. N., & Satyanarayan, S. (2005). Influence of anode material on electrochemical oxidation for the treatment of tannery wastewater. *Water Research*, *39*, 1601–1613. https://doi.org/10.1016/j.watres.2005.01.016

Takasu, Y., & Murakami, Y. (2000). Design of oxide electrodes with large surface area.

Electrochimica Acta, *45*, 4135–4141.

Takors, R., Kopf, M., Mampel, J., Bluemke, W., Blombach, B., Eikmanns, B., et al. (2018). Using gas mixtures of CO, CO_2 and H_2 as microbial substrates: the do's and don'ts of successful technology transfer from laboratory to production scale. *Microbial Biotechnology*, *11*(4), 606–625. https://doi.org/10.1111/1751-7915.13270

Teder, A. (1971). The equilibrium between elementary sulfur and aquesous polysulfide solutions. *Acta Chemica Scandinavica*, *25*, 1722–1728.

Thiel, G. P., Kumar, A., Gómez-González, A., & John H. Lienhard, V. (2017). Utilization of desalination brine for sodium hydroxide production: technologies, engineering principles, recovery limits, and future directions. *ACS Sustainable Chem. Eng.*, *5*, 11147–11162. https://doi.org/10.1021/acssuschemeng.7b02276

Tomasini-Montenegro, C., Santoyo-Castelazo, E., Gujba, H., Romero, R. J., & Santoyo, E. (2017). Life cycle assessment of geothermal power generation technologies: An updated review. *Applied Thermal Engineering*, *114*(2017), 1119–1136. https://doi.org/10.1016/j.applthermaleng.2016.10.074

Ucar, D., Yilmaz, T., Di Capua, F., Esposito, G., & Sahinkaya, E. (2020). Comparison of biogenic and chemical sulfur as electron donors for autotrophic denitrification in sulfur-fed membrane bioreactor (SMBR). *Bioresource Technology*, *299*(December 2019), 122574. https://doi.org/10.1016/j.biortech.2019.122574

Uihlein, A. (2014). *2014 JRC Geothermal Energy Status Report*. https://doi.org/10.2790/460251

Ungerfeld, E. M. (2015). Shifts in metabolic hydrogen sinks in the methanogenesis-inhibited ruminal fermentation: A meta-analysis. *Frontiers in Microbiology*, *6*(FEB), 37. https://doi.org/10.3389/fmicb.2015.00037

Ushiba, Y., Takahara, Y., & Ohta, H. (2003). *Sphingobium amiense* sp. nov., a novel nonylphenol-degrading bacterium isolated from a river sediment. *International Journal of Systematic and Evolutionary Microbiology*, *53*, 2045–2048. https://doi.org/10.1099/ijs.0.02581-0

Vaiopoulou, E., Provijn, T., Prévoteau, A., Pikaar, I., & Rabaey, K. (2016). Electrochemical sulfide removal and caustic recovery from spent caustic streams. *Water Research*, *92*, 38–43. https://doi.org/https://doi.org/10.1016/j.watres.2016.01.039

Valdenaire, D., & Mennecier, S. (2020). *Producing low sulphur marine fuels in Europe – 2020-2025 vision*.

Valente, A., Iribarren, D., & Dufour, J. (2020). Comparative life cycle sustainability assessment of renewable and conventional hydrogen. *Science of The Total Environment*, (xxxx), 144132.

https://doi.org/10.1016/j.scitotenv.2020.144132

Van Hege, K., Verhaege, M., & Verstraete, W. (2004). Electro-oxidative abatement of low-salinity reverse osmosis membrane concentrates. *Water Research*, *38*, 1550–1558.

Vatistas, N., & Cristofaro, S. (2000). Lead dioxide coating obtained by pulsed current technique. *Electrochemistry Communications*, *2*, 334–337.

Vega, J. L., Klasson, K. T., Kimmel, D. E., Clausen, E. C., & Gaddy, J. L. (1990). Sulfur gas tolerance and toxicity of co-utilizing and methanogenic bacteria. *Applied Biochemistry and Biotechnology*, *24–25*(1), 329–340. https://doi.org/10.1007/BF02920257

Vilchez-Vargas, R., Geffers, R., Suárez-Diez, M., Conte, I., Waliczek, A., Kaser, V. S., et al. (2013). Analysis of the microbial gene landscape and transcriptome for aromatic pollutants and alkane degradation using a novel internally calibrated microarray system. *Environmental Microbiology*, *15*, 1016–1039. https://doi.org/10.1111/j.1462-2920.2012.02752.x

VITO/Infomil. (2009). *Fact sheets on air emission abatement techniques*. www.infomil.nl

Voordouw, G., Armstrong, S. M., Reimer, M. F., Fouts, B., Telang, A. J., Shen, Y., & Gevertz, D. (1996). Characterization of 16s rRNA genes from oil field microbial communities indicates the presence of a variety of sulfate-reducing, fermentative, and sulfide-oxidizing bacteria. *Applied and Environmental Microbiology*, *62*(5), 1623–1629. https://doi.org/10.1128/aem.62.5.1623-1629.1996

Vostrikov, A. A., Fedyaeva, O. N., Shishkin, A. V., & Sokol, M. Y. (2017). Oxidation of hydrogen sulfide and corrosion of stainless steel in gas mixtures containing H_2S, O_2, H_2O, and CO_2. *Journal of Engineering Thermophysics*, *26*(3), 314–324. https://doi.org/10.1134/S181023281703002X

Vrieze, J. De, Coma, M., Debeuckelaere, M., Meeren, P. Van Der, & Rabaey, K. (2016). High salinity in molasses wastewaters shifts anaerobic digestion to carboxylate production. *Water Research*, *98*, 293–301. https://doi.org/10.1016/j.watres.2016.04.035

Wainaina, S., Kisworini, A. D., Fanani, M., Wikandari, R., Millati, R., Niklasson, C., & Taherzadeh, M. J. (2020). Utilization of food waste-derived volatile fatty acids for production of edible *Rhizopus oligosporus* fungal biomass. *Bioresource Technology*, *310*(March), 123444. https://doi.org/10.1016/j.biortech.2020.123444

Wang, H.-Z., Yan, Y.-C., Gou, M., Yi, Y., Xia, Z.-Y., Nobu, M. K., et al. (2019). Response of propionate-degrading methanogenic microbial communities to inhibitory conditions. *Applied Biochemistry and Biotechnology*, *189*(1), 233–248. https://doi.org/10.1007/s12010-019-03005-1

Wang, Longyao, Lu, P., Liu, C., & Wang, L. (2015). Electro-oxidation of sulfide on Ti/RuO_2 electrode in an aqueous alkaline solution. *International Journal of Electrochemical Science*, *10*, 8374–8384.

Wang, Lu, Kan, A. T., Zhang, Z., Yan, F., Liu, Y., Dai, Z., & Tomson, M. B. (2014). Field method for determination of bicarbonate alkalinity. In *SPE International Oilfield Scale Conference and Exhibition* (pp. 1–13). https://doi.org/10.2118/169758-ms

Wang, Q., Garrity, G. M., Tiedje, J. M., & Cole, J. R. (2007). Naïve Bayesian classifier for rapid assignment of rRNA sequences into the new bacterial taxonomy. *Applied and Environmental Microbiology*, *73*(16), 5261–5267.

Wang, T., Zhang, D., Dai, L., Dong, B., & Dai, X. (2018). Magnetite triggering enhanced direct interspecies electron transfer: A scavenger for the blockage of electron transfer in anaerobic digestion of high-solids sewage sludge. *Environmental Science and Technology*, *52*(12), 7160–7169. https://doi.org/10.1021/acs.est.8b00891

Wang, Y., Li, M., Feng, C., & Zhang, Z. (2012). Electrochemical oxidation of sulfide in oil wastewater using Ti/IrO_2 anode. *Environmental Progress & Sustainable Energy*, *31*(4), 500–506. https://doi.org/10.1002/ep

Wang, Y. Q., Yu, S. J., Zhang, F., Xia, X. Y., & Zeng, R. J. (2017). Enhancement of acetate productivity in a thermophilic (55 °C) hollow-fiber membrane biofilm reactor with mixed culture syngas (H_2/CO_2) fermentation. *Applied Microbiology and Biotechnology*, *101*(6), 2619–2627. https://doi.org/10.1007/s00253-017-8124-9

Waterston, K., Bejan, D., & Bunce, N. J. (2007). Electrochemical oxidation of sulfide ion at a boron-doped diamond anode. *Journal of Applied Electrochemistry*, *37*(3), 367–373. https://doi.org/10.1007/s10800-006-9267-z

Wei, Y., Li, C., Wang, Y., Zhang, X., Li, Q., & Xu, T. (2012). Regenerating sodium hydroxide from the spent caustic by bipolar membrane electrodialysis (BMED). *Separation and Purification Technology*, *86*, 49–54. https://doi.org/10.1016/j.seppur.2011.10.019

Wei, Y., Wang, Y., Zhang, X., & Xu, T. (2013). Comparative study on regenerating sodium hydroxide from the spent caustic by bipolar membrane electrodialysis (BMED) and electro-electrodialysis (EED). *Separation and Purification Technology*, *118*, 1–5. https://doi.org/10.1016/j.seppur.2013.06.025

Weiss, M. (2012). Is Acid Rain a Thing of the Past? *American Association for the Advancement of Science*. http://news.sciencemag.org/2012/06/acid-rain-thing-past. Accessed 17 December 2020

Wieringa, K. T. (1939). The formation of acetic acid from carbon dioxide and hydrogen by

anaerobic spore-forming bacteria. *Antonie van Leeuwenhoek*, *6*(1), 251–262. https://doi.org/10.1007/BF02146190

Windels, E. M., Van Den Bergh, B., & Michiels, J. (2020). Bacteria under antibiotic attack: Different strategies for evolutionary adaptation. *PLoS Pathogens*, *16*(5), 1–8. https://doi.org/10.1371/journal.ppat.1008431

Winnick, J., Sather, N. F., & Huang, H. S. (1984). Electrochemical separation and concentration of hydrogen sulfide from gas mixtures.

Wolin, M. J., & Miller, T. L. (1980). Molybdate and sulfide inhibit H_2 and increase formate production from glucose by *Ruminococcus albus*. *Archives of Microbiology*, *142*, 137–142.

Wu, G., Wan, F., Fu, H., Li, N., & Gao, H. (2015). A matter of timing: Contrasting effects of hydrogen sulfide on oxidative stress response in *Shewanella oneidensis*. *Journal of Bacteriology*, *197*(22), 3563–3572. https://doi.org/10.1128/JB.00603-15.Editor

Xia, J., Pérez-Salado Kamps, Á., Rumpf, B., & Maurer, G. (2000). Solubility of hydrogen sulfide in aqueous solutions of single strong electrolytes sodium nitrate, ammonium nitrate, and sodium hydroxide at temperatures from 313 to 393 K and total pressures up to 10 MPa. *Fluid Phase Equilibria*, *167*(2), 263–284. https://doi.org/10.1016/S0378-3812(99)00324-6

Xia, Y., Lü, C., Hou, N., Xin, Y., Liu, J., Liu, H., & Xun, L. (2017). Sulfide production and oxidation by heterotrophic bacteria under aerobic conditions. *The ISME Journal*, *11*, 2754–2766. https://doi.org/10.1038/ismej.2017.125

Yang, N. J., & Hinner, M. J. (2015). Getting across the cell membrane: An overview for small molecules, peptides and proteins. *Methods in Molecular Biology*, *1266*, 29–53. https://doi.org/10.1007/978-1-4939-2272-7

Yang, Y., & Hoffmann, M. R. (2016). Multi-layer anode for saline wastewater treatment: Manipulating oxidant generation pathway by TiO_2 thin film deposition. In *251st American Chemical Society National Meeting & Exposition*.

Yang, Y., Shin, J., Jasper, J. T., & Hoffmann, M. R. (2016). Multilayer heterojunction anodes for saline wastewater treatment: Design strategies and reactive species generation mechanisms. *Environmental Science & Technology*, *50*, 8780–8787.

Yi, Y., Weinberg, G., Prenzel, M., Greiner, M., Becker, S., Schlögl, R., & Heumann, S. (2017). Electrochemical corrosion of a glassy carbon electrode. *Catalysis Today*, *295*, 32–40.

Yin, Q., Gu, M., & Wu, G. (2020). Inhibition mitigation of methanogenesis processes by conductive materials: A critical review. *Bioresource Technology*, *317*(August). https://doi.org/10.1016/j.biortech.2020.123977

Yuan, Y., Cheng, H., Chen, F., Zhang, Y., Xu, X., Huang, C., et al. (2020). Enhanced methane production by alleviating sulfide inhibition with a microbial electrolysis coupled anaerobic digestion reactor. *Environment International*, *136*(January). https://doi.org/10.1016/j.envint.2020.105503

Zermeño-Montante, I., Nieto-Delgado, C., Sagredo-Puente, R. D., Cárdenas-Galindo, M. G., & Handy, B. E. (2011). Catalytic wet air oxidation of sodium sulfide solutions. Effect of the metal-support and acidity of the catalysts. *Top Catal*, *54*, 579–586. https://doi.org/10.1007/s11244-011-9623-z

Zhai, L.-F., Song, W., Tong, Z.-H., & Sun, M. (2012). A fuel-cell-assisted iron redox process for simultaneous sulfur recovery and electricity production from synthetic sulfide wastewater. *Journal of Hazardous Materials*, *243*, 350–356. https://doi.org/10.1016/j.jhazmat.2012.10.046

Zhang, F., Ding, J., Shen, N., & Zhang, Y. (2013). In situ hydrogen utilization for high fraction acetate production in mixed culture hollow-fiber membrane biofilm reactor. *Applied Microbiology and Biotechnology*, *97*, 10233–10240. https://doi.org/10.1007/s00253-013-5281-3

Zhang, L., De Schryver, P., De Gusseme, B., De Muynck, W., Boon, N., & Verstraete, W. (2008). Chemical and biological technologies for hydrogen sulfide emission control in sewer systems: A review. *Water Research*, *42*, 1–12. https://doi.org/10.1016/j.watres.2007.07.013

Zhang, X., Philips, J., Roume, H., Guo, K., Rabaey, K., & Pre, A. (2017). Rapid and quantitative assessment of redox conduction across electroactive biofilms by using double potential step chronoamperometry. *ChemElectroChem*, 1026–1036.

Βάρβογλης, Α. (2014). Ετυμολογικό Λεξικό Χημικών Όρων. http://www.chem.uoa.gr/?p=6979&lang=el. Accessed 23 December 2020

CURRICULUM VITAE

Eleftheria Ntagia

Center of Microbial Ecology and Technology (CMET)

Faculty of Bioscience Engineering, Department of Biochemical and microbial technology, Coupure Links 653 (A0.092), 9000 Ghent, BELGIUM

Email address: Eleftheria.Ntagia@UGent.be

CURRENT POSITION:

01/2016 – 01/2022 **AAP/PhD candidate in Center of Microbial Ecology and Technology (CMET), Ghent University**

My current position in CMET as an Assisant Academic Staff (AAP), comprises of doctoral research as well as teaching activities. My activities in this position include teaching of wastewater treatment design courses and research on:

- Electrochemical treatment of sulfide containing industrial wastewater streams
- Electrode materials suitable for electrochemical sulfide oxidation
- Sulfide resistant bioproduction from waste gas streams

EDUCATION:

2013/09 – 2015/09 Wetsus Academy, Master programme in Water Technology (Joint degree of Wageningen University, University of Groningen, University of Twente) (MSc)

2006/09 – 2012/09 Democritus University of Thrace (DUTH), Department of Environmental Engineering (Engineering Diploma, MSc equivalent)

EMPLOYMENT:

2015/04 – 2015/08 Internship in the Luxembourg Institute of Science and Technology (LIST)on the "Value from Urine" project

PEER REVIEWED PUBLICATIONS:

Eleftheria Ntagia, Erika Fiset, Linh Truong Cong Hong, Eleni Vaiopoulou, Korneel Rabaey (2020). Electrochemical treatment of industrial sulfidic spent caustic streams for sulfide removal and caustic recovery. Journal of Hazardous Materials, Volume 388, 15 April 2020, 121770

Eleftheria Ntagia, Ioanna Chatzigiannidou, Adam J. Williamson, Jan B. A. Arends, Korneel Rabaey (2020). Homoacetogenesis and microbial community composition are shaped by pH and total sulfide concentration. Microbial Biotechnology. 13(4). p.1026-1038

Eleftheria Ntagia, Erika Fiset, Ligia da Silva Lima, Ilje Pikaar, Xu Zhang, Adriaan W. Jeremiasse, Antonin Prévoteau, Korneel Rabaey (2019). Anode materials for sulfide oxidation in alkaline wastewater: An activity and stability performance comparison. Water Res. 149, 111–119.

Eleftheria Ntagia, **Pau Rodenas**, Annemiek ter Heijne, Cees J.N. Buisman, Tom H.J.A. Sleutels (2016). Hydrogen as electron donor for copper removal in bioelectrochemical systems. International journal of hydrogen energy. 41: 5758 – 5764

BOOK CHAPTERS:

Eleftheria Ntagia, Antonin Prévoteau, Korneel Rabaey (2020). Electrochemical treatment of sulfur pollution: Environmental Technologies to Treat Sulfur Pollution: Principles and Engineering, 2nd Edition, Piet N.L. Lens (Ed.). p. 247 – 276

CONFERENCE CONTRIBUTIONS:

Eleftheria Ntagia, Wen Hao, Korneel Rabaey; Electrochemistry connects the petroleum refineries with the chemical industry: a case study to turn the waste of the first into feedstock for the second. 29th ISE topical meeting, 18 – 21 April 2021, virtual (Prague, Czech Republic)

Eleftheria Ntagia, Erika Fiset, Linh Truong Cong Hong, Eleni Vaiopoulou, Korneel Rabaey; Electrochemical sulfide removal and caustic recovery from real spent caustic streams. *Poster presentation*. 16th IWA Leading Edge Conference on Water and Wastewater Technologies, 10 – 14 June 2019, Edinburgh, United Kingdom

Eleftheria Ntagia, Erika Fiset, Linh Truong Cong Hong, Eleni Vaiopoulou, Korneel Rabaey; Electrochemical sulfide removal and caustic recovery from real spent caustic streams: A case study with Ir MMO and Ru MMO electrodes. *Oral presentation*. 25th ISE topical meeting, 12 – 15 May 2019, Toledo, Spain

Eleftheria Ntagia, Erika Fiset, Ligia da Silva Lima, Ilje Pikaar, Xu Zhang, Adriaan W. Jeremiasse, Antonin Prévoteau, Korneel Rabaey; Anode Materials For Sulfide Oxidation In Alkaline Wastewater: An Activity and Stability Performance Comparison. *Oral presentation*. 233rd ECS meeting, 13 – 17 May, Seattle, WA, USA

Inka Vanwonterghem, Guruprasad V Talekar, Peter Clauwaert, **Eleftheria Ntagia**, Pankaj Sharma, Jan Arends, Srikanth Mutnuri, Korneel Rabaey; Empowered septic tanks : vertical flow

constructed wetlands combined with electrochemical disinfection to treat septic tank effluent and provide safe water for reuse. *Poster contribution*. 2018 Gordon Research Conference on Environmental Sciences: Water , 24 – 29 June 2018, Holderness, NH, USA

Eleftheria Ntagia, Jan B. A. Arends, Korneel Rabaey; Towards sulfide resistant bioproduction; understanding sulfide toxicity during homoacetogenic fermentation. *Poster contribution*. 5th International Symposium on Microbial Metabolism (ISMSM-5), 16 – 18 April 2018, Vienna, Austria

Eleftheria Ntagia, Louis Demasure, Evans M. Tembo, Stephen J. Andersen, Guruprasad Gupta, Jan B.A. Arends, Peter Clauwaert, Srikanth Mutnuri, Korneel Rabaey; Electrochemical Sanitation: Anodic and Cathodic Electrolysis to Treat Septic Tank Effluent in Goa, India and Ghent, Belgium. *Poster contribution*. 1st Symposium on Microbiological Methods for Waste and Water Resource Recovery (MMWWRR 2017), 18 – 19 May 2017, Delft, The Netherlands

Eleftheria Ntagia, Pau Rodenas, Annemiek ter Heijne, Cees J.N. Buisman, Tom H.J.A. Sleutels. Hydrogen as electron donor for copper removal in bioelectrochemical systems. *Poster contribution*. 7th European Summer School Electrochemical Engineering, 22 – 26 June 2015, Leeuwarden, The Netherlands

TEACHING EXPERIENCE:

2016/01 – present	Teaching asisstant at the Faculty of Bioscience Engineering, Ghent University for the courses: Biotechnological Processes for Environmental Sanitation, Microbial Technology for Reuse, Microbial Technology and Environmental Sanitation
2019/04	Teaching assistant at Ghent University Global Campus, Incheon, Korea for the courses: Water Treatment, Renewable Resources Technology

ADMINISTRATIVE EXPERIENCE:

2019/10	Co-organization of the 1st CAPTURE Conference, Ghent, Belgium
2019 and 2020/02	Co-organization of the 1st and 2nd Women in Science Day, at the Faculty of Bioscience Engineering, UGent, Ghent, Belgium

ACKNOWLEDGEMENTS

The journey of writing this book lasted 5 years for me, which can be considered a long time, but yet again: ''Time is nothing but a social contract''. There has been a great number of people and circumstances that have led me to this point of my life, which constitutes the completion of my biggest mental effort. However, I will only thank here the people that were pivotal to the writing of this book, and my personal development, during these 5 years.

I would like to thank Korneel Rabaey first, for giving me the opportunity to work alongside him, which was actually my motivation to apply for this position at CMET. I would like to acknowledge him for urging me, intentionally or not, to always be sharp at our meetings and up to the game. This was the greatest lesson I have been given so far in CMET. I would also like to thank him for entrusting me with the task of teaching in the Korea campus, which was one of the most incredible, work and life, experiences.

I would like to thank Erika Fiset and Jan Arends for taking up the responsibility of being my co-promotors, somewhere in the middle of this journey. I would like to thank both of them for teaching me how to be a more organized and focused researcher and how to be a better writer. And also for always backing up my efforts, my experiments, my manuscripts and for taking the extra effort with me to bring them to a better state. I would like to explicitly thank Jan for teaching me how to be bold and claim the recognition of my work and how to also be proud of my work.

I would like to thank Antonin Prévoteau for urging me to always question my work and for the continuous scientific support that I have received, without him being an official promotor of mine. I also thank him for teaching me everything – the little – I know about electrochemistry and for lending his ears to my working frustrations a thousand times.

I would like to thank Ioanna Chatzigiannidou, my most dearest friend and colleague in CMET. I thank her for trying, unsuccessfully, to teach me some of the wonders of molecular biology and for all the work that she has done with me on that aspect for this book. I also thank her deeply for being my comrade in the organization of the Women in Science Day, that we have started together and completed with the support of the rest of the Be4Diversiy team members. Ιωαννάκι μου γλυκό σε ευχαριστώ πολύ για τη φιλία σου, είναι ό,τι πολυτιμότερο βρήκα στο CMET, hands down.

I would like to thank Eleni Vaiopoulou, for leading me through my first steps in CMET and for guiding me through the world of spent caustic streams. I also thank her, for guiding me through the first psychostruggles of the PhD life and for an excellent, memorable, drinking session in t'Velootje.

I would like to acknowledge Ilje Pikaar, Josè M. Carvajal Arroyo, Adam J. Williamson and Xu Zhang for their support and for their extensive work on my manuscripts and Stephen J. Andersen for the most motivating and enjoyable English proof-reading. I would also like to acknowledge Karel Folens for turning successfully my abstract into a samenvatting.

I would like to acknowledge my friend Ioanna Florou for this amazing piece of art that I managed to diminish to a PhD thesis cover and my friend Adrià Pàez Forteza for digitalising it.

I would like to thank the over 200 students with whom I have interacted during these 5 years as an assistant here, and also my thesis students. Next to them I have learned unaccountable things, from wastewater treatment practices around the world to how to deal with haunted houses in Lusaka. I would like to thank them for being patient with me in my first steps as a tutor and for training me into becoming a teacher. I specifically and deeply thank my students Ligia da Silva Lima and Lin Truong Cong Hong for working closely with me and contributing to my two first PhD papers. I would like to acknowledge their smarts and their hard work with the tedious sulfur samples and also their adorable shyness. I would like to acknowledge Evans Tembo, Louis Demasure and Pankaj Sharma for being very curious students and for the excellent time that we have spent together working in the electrochemical disinfection project.

I would like to thank some of the CMET stuff members. Mike Taghon, for helping me out in the lab so many times and for getting angry at me as many times as I got angry at him. Equality is everything. Annick Beyaert, Siska Maertens, Jana De Bodt and Renée Graveel for helping me out a couple of times needed and for the nice chit-chat here and there. Tim Lacoere, for dealing with my Illumina and reactor scheme ventures and for the authentic beeropolitical debates. I would explicitly like to acknowledge my dearest Greet Van de Velde for dealing with my annoying sulfur samples again and again. I thank Sarah Steenbeke for making CMET easy, for continuously poking me to tally and I would like to praise her amazingly cheerful character.

I would like to thank my dearests Christine Graveel and Regine Haspeslagh for the warmest welcome in the beginning and the immense support that I have received all these years as a PhD student and as an assistant in CMET. Christine and Regine, you have made my working and personal life in Belgium as smooth as the Belgian praline.

I would like to thank my lovely colleagues, Myrsini, Barbara, Lotte, Soup, Arjen, Florian, Xiaofei, Luiza, Rui, Funda, Professor Ramon and everyone else in the MECAT team and in the lab, whom I have missed so much this last year of the pandemic. I would also like to thank my lovely former colleagues (and also Gio and Nina), Curro, Steve, Erika, Amanda, Kun, Melanie, Dries, Hugo, Pieter C., Tyler, Jeet, Naya, the Cristinas, Charlotte, whom I have missed even before the pandemic started. I am thanking them for the scientific and emotional support, for all the great times in Techhall, for showing me their tricks with reactors and their favourite glue, for showing me how to climb, for teaching me

English, for the dishes cooked with duck fat, for introducing me to the Belgian music scene, for the most awkward lunch discussions, for suffering together with me in Rotonde, for willingly speaking with me in Dutch, for inviting me to their homes, for teaching me that Americans are not bad, for celebrating easter with me, my parents and a group of Bulgarians, for the uplifting beer sessions in Koepuur, for the almost professional Fatboy Slim dancing improvisations, for showing up for my first birthday without my family. I would like to explicitly thank Myrsini for taking care of my reactor in December 2019 and in the day of the ''big crash'', the 29th of February 2020.

I would like to thank all the members of the Be4Diversity team, for giving me the opportunity to work alongside them towards achieving what I consider as a progressive university. I would like to acknowledge the journalist Lamprini Thoma for her podcast ''Ράδιο Venceremos'', that kept me sane the first three months of the pandemic while I was totally alone in the lab. I would also like to acknowledge Ruben Props for dealing twice with my FCM samples during this scary period.

I would like to acknowledge Agathi Naka for being my friend for 15 consecutive years, for being my comrade in exile, and in the dancefloor, and for her immense psychological support during my PhD years. Νάκα μου σου χρωστάω τα χιλιάρικα του ψυχολόγου. I would like to thank my friends back at home, and the ones I made here, for continuously teaching me how to be a proper friend and for continuously showing me that reality still goes on, outside the Faculty of Bioscience Engineering, Ghent, Belgium. I will not mention everyone here, but they all know that they are very much loved by me and their emotional support to me is explicitly acknowledged. Παρ'όλα αυτά, θα ευχαριστήσω εδώ εσάς, τους φίλους μου, που με παίρνατε και τα λέγαμε και που με στηρίξατε τόσο πολύ, όσο έγραφα αλλά και προηγουμένως. Τη Χριστινιώ μου και τη Σωτηρούλα μου, το Κατερινάκι μου και τη Φαχουρίδου μου, τον αγαπημένο μου φίλο Χριστόφορο, το Μιρελλάκι και τον Αγγελέτο μου.

I would like to acknowledge my sister, Panagiota Ntagia, for proof-reading all my cover letters and PhD applications and for providing me with shelter, before getting my position at CMET. I would also like to thank her for buying me a coin purse to fit my first PhD salary in January 2016 and for sending me by post a bottle of Champagne when I submitted this book for the first time, in February 2021.

I would like to acknowledge my family, my sister and my parents, Stelios Ntagias and Vaso Tzivi, for backing up all my efforts and for cheering for me, every single moment since the day I was born. Αδερφή, Μάνα, Πατέρα, σας ευχαριστώ και τους τρεις για την ευκαιρία που μου δώσατε να ολοκληρώσω ένα διδακτορικό, μαθαίνοντας μου την αγάπη για τη γνώση και την ανάγκη να κοπιάζεις γι' αυτά που ονειρεύεσαι και πιστεύεις. Και φυσικά στηρίζοντας με οικονομικά, σε βάρος πολλές φορές των δικών σας επιθυμιών. Σας αφιερώνω αυτό το βιβλίο και σας το χαρίζω για να εμπλουτίσει τις βιβλιοθλήκες σας. Σας αγαπώ πάρα πολύ και σας κουβαλάω μαζί μου πάντα. Την αγάπη σας, τα τραγούδια σας, τα φαγητά σας, τις αγκαλιές σας.